TURNIP MOSAIC VIRUS GENOME-LINKED PROTEIN (VPg) INHIBITS POKEWEED ANTIVIRAL PROTEIN (PAP)-MEDIATED DEPURINATION OF RNA

BY

ARTEM V. DOMASHEVSKIY

A dissertation submitted to the Graduate Faculty in Biochemistry in partial fulfillment of the requirements for the degree of Doctor of Philosophy, The City University of New York

2011

This manuscript has been read and accepted for the Graduate Faculty in Biochemistry in satisfaction of the dissertation requirements for the degree of Doctor of Philosophy.

DIXIE J. GOSS

Date — Chair of Examining Committee

EDWARD J. KENNELLY

Date — Executive Officer

FRIDA KLEIMAN

DERRICK BRAZILL

LAWRENCE KOBILINSKY

VERN L. SCHRAMM

Supervisory Committee

THE CITY UNIVERSITY OF NEW YORK

Abstract

TURNIP MOSAIC VIRUS GENOME-LINKED PROTEIN (VPg) INHIBITS POKEWEED ANTIVIRAL PROTEIN (PAP)-MEDIATED DEPURINATION OF RNA

by

Artem V. Domashevskiy

Adviser: Professor Dixie J. Goss

Pokeweed antiviral protein (PAP) from *Phytolacca americana* is a ribosome inactivating protein (RIP) and is an RNA *N*-glycosidase that removes specific purine residues from the sarcin/ricin (S/R) loop of large rRNA, arresting protein synthesis at the translocation step. PAP is a cap-binding protein, and it was suggested that it inhibits translation of RNA by binding to the 5' m^7G cap structure of eukaryotic mRNA, and depurinating the mRNA at sites downstream of the cap structure. PAP is a potent antiviral agent against many plant, animal, and human viruses. Depurination of capped viral RNA may be the primary mechanism for PAP's antiviral activity. However, the above mechanism does not clarify the inhibitory effect of PAP on the replication of uncapped viruses. To elucidate the mechanism of RNA depurination, and to understand how PAP recognizes and targets various RNAs, the interactions between PAP and Turnip mosaic virus (TuMV) genome linked protein (VPg) were investigated. VPg is important in the initiation of protein synthesis, functioning as a cap analog. VPg stimulates the *in vitro* translation of uncapped IRES-containing RNA and inhibits capped RNA translation in wheat germ extracts. In this work, fluorescence spectroscopy and HPLC techniques were used to quantitatively describe PAP-VPg interactions. PAP interacts strongly with VPg, thus the effect of VPg on the PAP

catalyzed depurination of several different RNA molecules was determined to investigate whether VPg binding to PAP influences selectivity of depurination. PAP binds to and depurinates both m^7GpppG-capped and uncapped S/R oligo nucleotide and TEV RNAs, supporting previous conclusions that the cap structure is not the only determinant for PAP depurination of RNA. VPg decreases depurination of the above capped and uncapped RNAs and competes with TEV RNA for PAP binding. VPg may confer an evolutionary advantage by suppressing one of the defense mechanisms of the plant. Depurination inhibition of PAP by VPg also suggests the possible use of this protein against cytotoxic activity of RIPs and inhibition of their biological potency.

In memory of my mentor and dearest friend Dr. Diana E. Friedland

AKNOWLEDGEMENTS

There was a time in which I thought this project would never be complete. There are many people to whom I must give credit and the utmost gratitude. Your encouragement and genuine concern carried me through this process.

First and foremost I would like to take this opportunity to express my deepest gratitude to my mentor Professor Dixie J. Goss; I could not have imagined having a better adviser and mentor for my PhD research, who has given me a big part of her wisdom, patience, and generosity. Prof. Goss, I owe you my greatest debt and appreciation for providing me with endless support during my quest for a doctoral degree. It is my honor to work under your supervision.

Professor Diana E. Friedland, much of the heart of this research stems from you, your encouragement, and your inspiration. This dissertation has benefited greatly from your knowledge, kindness, and help. You were the true ambassador between my knowledge and the field of Science. I wish you were still here to witness my success, and to award me my diploma. I am forever thankful for your aid. I dedicate this work to you. Your strength, integrity, and unconditional love continue to inspire me.

I would like to acknowledge my committee members Professors Frida Kleiman (Hunter College, the Department of Chemistry), Derrick Brazill (Hunter College, the Department of Biology), Lawrence Kobilinsky (John Jay College of Criminal Justice, the Department of Science), and Vern Schramm (Albert Einstein College of Medicine, the Department of Biochemistry), for their guidance and encouragement; it has been invaluable in this task. Teachers who love their subject have students who love the subject. Passion sparks interest, and

interest produces a genuine desire to learn and strive for excellence. I am forever grateful for your contribution to my academic growth.

I would like to thank the Department of Chemistry at Hunter College (Drs. Dixie Goss, Frida Kleiman, Pamela Mills, Klaus Grohmann, C. Michael Drain, Nancy Greenbaum, Lynn Francescini, Cliff Soll, Gabriela Smeureanu, Derrick Brazill from the Biology Department, as well as Nicole Popa, Mirela Settenhofer, Nala Fernando, Gabriela Solotchi, Rodica Nyerges, Tomoko Hagane-Mullins), the Department of Science at John Jay College (Dr. Diana Friedland, Lawrence Kobilinsky, Shu-Yuan Cheng, Francis Sheehan, as well as Nikolay Azar, Natalya Kotsek, Suzanne Sherbell, Azinia Brooks, Argeliz Pomales, and Kiezia Lawrence), Prof. Lynne Maquat from Rochester University, the Department of Biochemistry, Prof. Susan Rotenberg from Queens College, the Department of Chemistry, and the secretary of the Biochemistry Department at the Graduate Center, Judy Li, for allowing me to perform my research, and to work with students that have motivated me to continue my educational pursuits. “In order to keep it, one must give it away,” and teaching Science is a passion that maintains my desire for knowledge.

I am grateful to the Goss (Drs. John Trujillo, Mateen Khan, Shemaila Sultana, Anamika Banerjee, Ozgur Ecevit, Hasan and Sumeyra Yumak, as well as Sohani Das Sharma, Bidisha Banerjee, and Jia Ma) and Friedland Laboratories (Allie Toney, Kana Noro, Jeannine DeGrazia, Amy Baldwin, Jacqueline Chaparro, Shari Maltz, Janelle Freyea, Samantha Iverson, Konrad Ornatowski, Christopher Shaw) members for constructing supporting surroundings, for sharing your knowledge, and providing your help. Kana thank you for your help in protein purifications; you are invaluable. I have gained many excellent friends and colleagues during my doctoral pursuit.

Dad, you have inspired me to be all I could be and told me from my earliest childhood that I would someday get my doctorate. You envisioned this day coming over twenty five years ago – and now it's finally here. I wish you were still alive to see all my accomplishments. Thank you from the bottom of my heart.

Mom, and my dearest friend, I wouldn't be the person I am today without your love, acceptance, and encouragement. You've been my constant and greatest cheerleader. Your belief in me has inspired me to keep pursuing my visions and my goals through both the ups and downs of my life. Thank you.

I would like to convey my colossal gratitude to the Dynamite Youth Foundation (William Fusco, Karen Carlini, Nick Sarerno, Barbara Sarnelli, Sarah Lewis-Fernandez, James Schneider, Ed Kenny, Jennifer Reinhardt, Scott Lynch, Peter Mitro, Ronna Podber, Dawne Marro, Yolanda Valle, Lucille Henry, Jennifer Kilbride-Walters, Nikki Schleninger, and Debra Rubowitz) for your patience, endurance; constant encouragement, wisdom, and support that have helped me keep going and believing in myself. I am grateful beyond words. Much of the heart of my goals I owe to you. You are my role models and my friends alike. Without your love and support I would be nowhere near where I am today.

The past few years would not be possible without the incredible support of ALL MY FAMILY and friends (Alla and Anna Abidor, Alex and Alla Eidelstein, Alfredo Murga Jr., Peter Broniewicz, Mehgan McFadden, Foster A. Reisz, Monica Kwasnika, and Natalia Zayachkivska). Thank you for your love, encouragement, and direction to carry me through all of life's challenges. You have been the foundation of my sanity and spirit. You fill my life with joy and laughter; you carry me through the worst and the best of days. Thank you for teaching me how to balance meaningful work and meaningful personal life. I am unreasonably lucky. I love you all,

and I am forever grateful for your support and friendship. Thank you for always having faith in me.

TABLE OF CONTENTS

LIST OF TABLES

LIST OF FIGURES

GLOSSARY OF ABBREVIATIONS, ACRONYMS, FORMULAS, AND SYMBOLS

A	Absorbance
Amp	Ampicillin
Ant-m^{7}GTP	Anthranoyl 7-Methylguanosine Triphosphate
ATP	Adenosine 5'-Triphosphate
BSA	Bovine Serum Albumin
CA	Chloroacetaldehyde
CF	Correction Factor
Cm	Chroloamphenicol
conc.	Concentrated
ddH_2O	Deionized Distilled Water
DEAE	Diethylaminoethyl
DEPC	Diethylpyrocarbonate
DF	Dilution Factor
dil.	Dilute
DTT	Dithiothreitol
Δ	Change in Quantity
EDTA	Ethylenediaminetetraacetic Acid
eIF	Eukaryotic Initiation Factor
em.	Emission
EtBr	Ethidium Bromide
EtOH	Ethyl Alcohol

ex.	Excitation
Et_2O	Diethyl Ether
ε	Extinction Coefficient
F	Fluorescence
g	Gram or Gravitational Force (when multiplied by a factor)
G^o	Gibbs Free Energy
GTP	Guanosine 5'-Triphosphate
h.	Hour(s)
H^o	Standard Enthalpy
HCl	Hydrochloric Acid
HEPES	4-(2-Hydroxyehtyl)-1-piperazineethanesulfonic Acid
HPLC	High Pressure Liquid Chromatography
IPTG	Isopropyl β-D-thiogalactopyranoside
IRES	Internal Ribosome Entry Site
K_a	Association Constant
KCl	Potassium Chloride
K_d	Dissociation Constant
K_{eq}	Equilibrium Constant
KOH	Potassium Hydroxide
Km	Kanamycin
LB	Luria-Bertani Medium
λ	Wavelength
m	Maximal Quench (when italicized)

max.	Maximum
M	Molar Concentration
ME	β-Mercaptoethanol
MES	2-(*N*-Morpholino)ethanesulfonic Acid
MeOH	Methyl Alcohol
$MgCl_2$	Magnesium Chloride
m^7G	7-Methylguanosine
min.	Minute(s)
mol	Mole, quantity of a substance
NaAc	Sodium Acetate
NaCl	Sodium Chloride
NaOH	Sodium Hydroxide
NH_4Cl	Ammonium Chloride
NH_4OH	Ammonium Hydroxide
$(NH_4)_2SO_4$	Ammonium Sulfate
NHS	*N*-Hydroxysuccinimide
OD	Optical Density
PAGE	Polyacrylamide Gel Electrophoresis
PAP	Pokeweed Antiviral Protein
PEG	Poly(ethylene glycol)
PBS	Phosphate Buffered Saline
PK	Pseudoknot
PMSF	Phenylmethylsulfonyl Fluoride

PrOH	n-Propyl Alcohol
PVP	Polyvinylpyrrolidone
Q	Fractional Quench
RIP(s)	Ribosome Inactivating Protein(s)
rpm	Revolutions per Minute
S	Sedimentation Coefficient
S^o	Standard Entropy
SDS	Sodium Dodecyl Sulfate
sec.	Second(s)
S/R	Sarcin-Ricin
STI	Soybean Trypsin Inhibitor
TEMED	*N,N,N',N'*-Tetramethylenediamine
TEV	Tobacco Etch Virus
TLC	Thin Layer Chromatography
Tris-HCl	Tris(hydroxymethyl)aminomethane Hydrochloride
TuMV	Turnip Mosaic Virus
UTR(s)	Untranslated Region(s)
UV	Ultraviolet
VPg	Viral Protein Linked to Genome
v/v	Volume to Volume
W	Watt
WT	Wild Type

I INTRODUCTION

I-1 POKEWEED ANTIVIRAL PROTEIN AND OTHER RIPs

I-1-A Introduction to Ribosome Inactivating Proteins

Various plants produce proteins that are thought to play an important role in their defense mechanism against foreign pathogenic invaders. These proteins are widely found throughout the plant kingdom as well as in many species of fungi and bacteria. Biological effects credited to these proteins go back to ancient times owing to the high toxicity possessed by castor bean – *Ricinus communis* L. and jequirity bean – *Abrus precatorius* L. (*1*). Stillmark while working on his doctoral thesis realized that the castor bean toxin was a protein and suggested the name ricin (*1*). Such poisons possess selective toxicity that has been explored by biologists to create transgenic plants resistant to viral and fungal infections *(2, 3),* cancer researchers to investigate immuno-conjugate therapeutics (*4-6*), political and military groups to create biological weaponry (*7-9*), and by mystery writers to engage the readers (*10*). These, so called ribosome inactivating proteins (RIPs) are RNA *N*-glycosidases that selectively modify large rRNA molecules and render them incompetent to sustain advanced stages of translation (*11*). Yet other plants, like common pokeweed – *Phytolacca Americana* L. (Figure 1.1 and 1.2) (*12*) and common soapwart – *Saponaria officinalis* L., produce pokeweed antiviral protein (PAP) and saporin, respectively, that impose lower toxicity on biological systems. In fact, evidence for the lack of RIPs has been obtained only for *Arabidopsis thaliana* L., as this plant does not express detectible amounts of RIPs nor contains a sequence encoding a putative RIP in its genome (*13*). Commonly, RIPs being potent cellular toxins are exported out of the cell once they are synthesized, and localized within the cell wall matrix (*14*). It is hypothesized that they gain access into the cytoplasm as the pathogen enters the cell, thus promoting their antiviral activity by impairing host ribosomes (*15*).

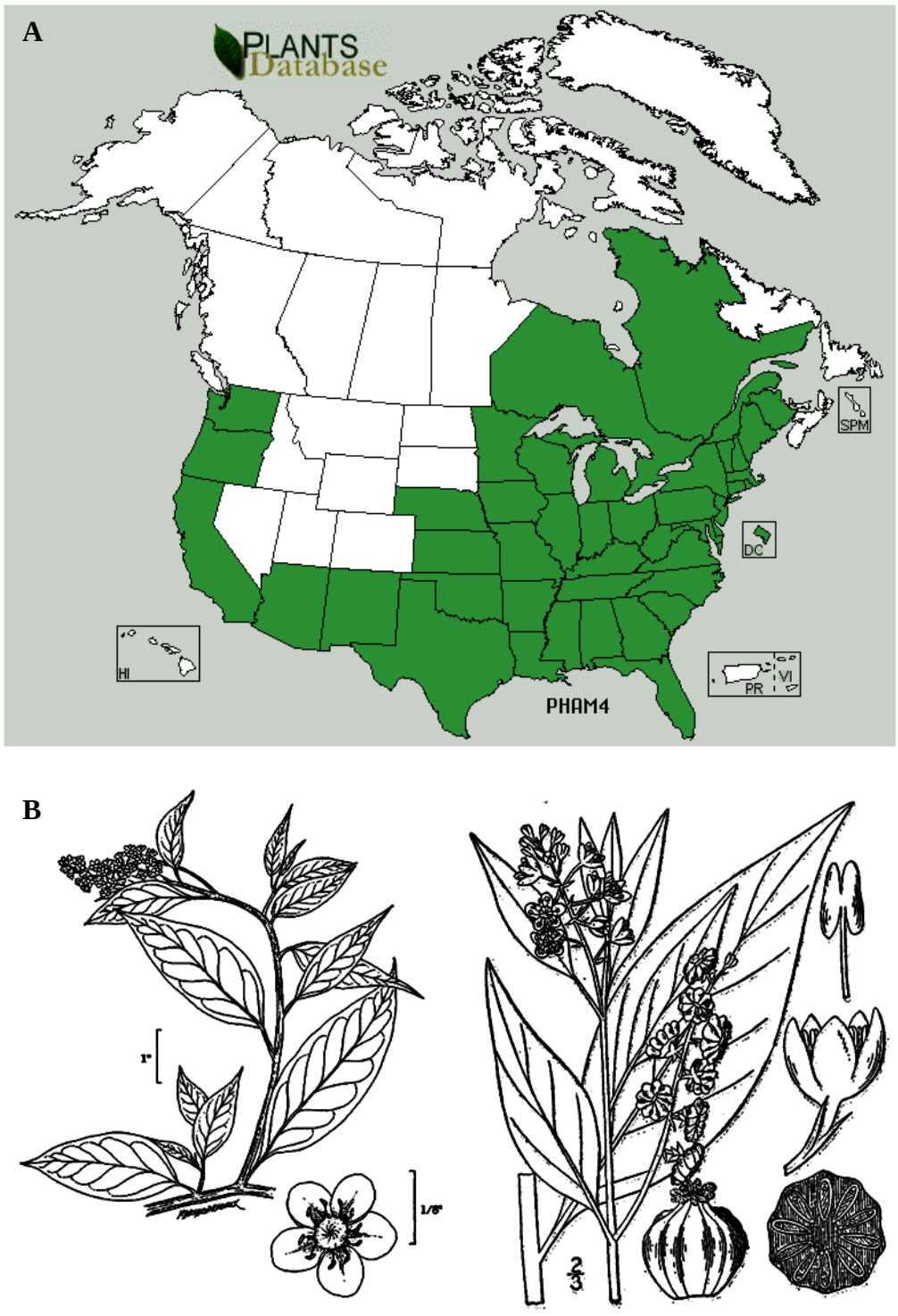

Figure 1.1 *Phytolacca americana* L. (PHAM4): (A) Distribution within United States and Canada (*16*); (B) Plant sketches (*17, 18*).

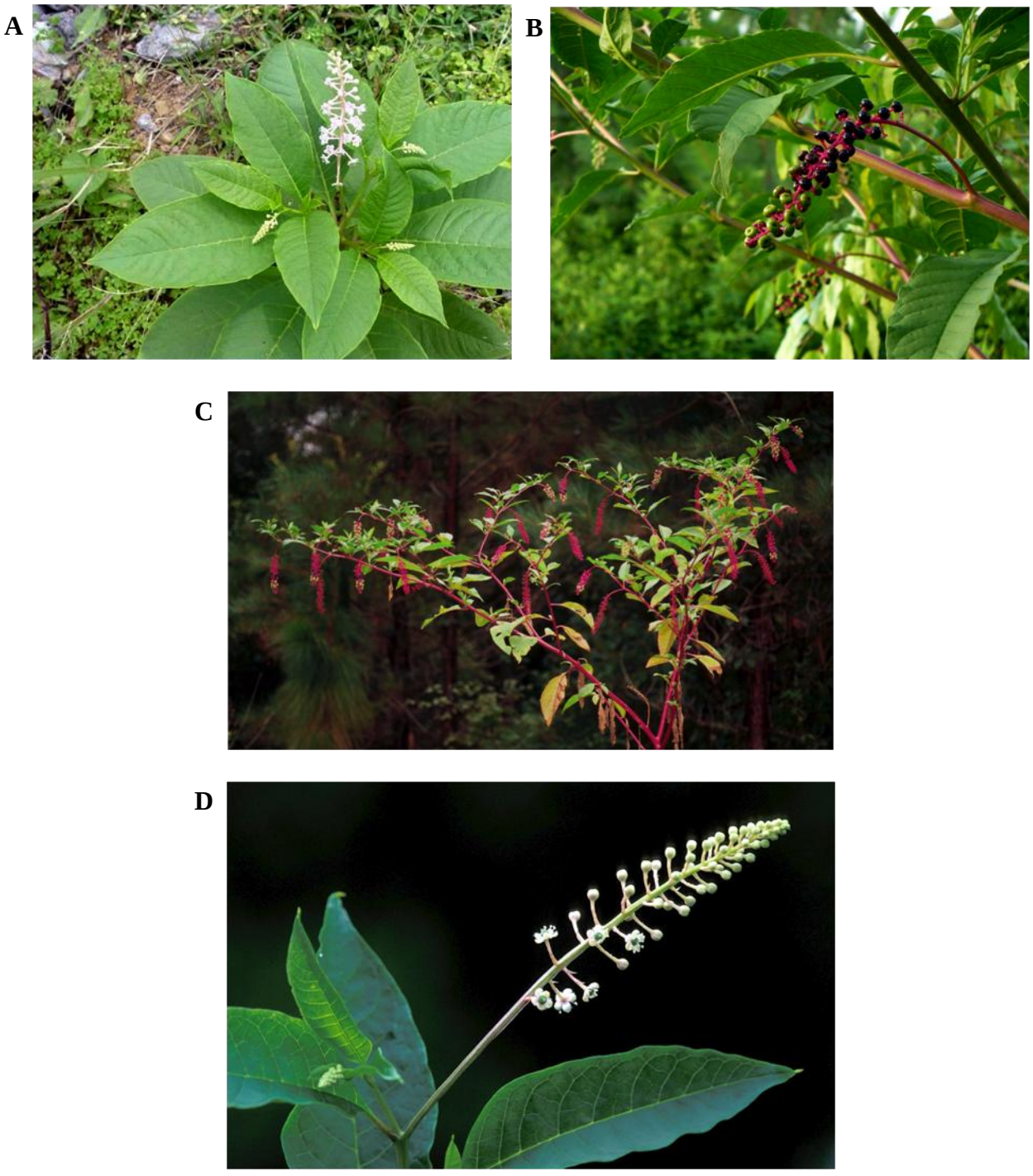

Figure 1.2 *Phytolacca americana* L.: (A) Pokeweed plant (*19*); (B) Poke berries (*20*); (C) Pokeweed bush (*21*); (D) Flowering plant (*19*, *22*).

I-1-B Classification of Ribosome Inactivating Proteins

Historically, the term "ribosome inactivating protein" was introduced to designate proteins isolated from various plant materials and so named because they irreversibly inactivate ribosomes. This name was suggested before the structure and enzymatic activity of RIPs were realized. After the mechanism of action of RIPs on ribosomes became clear, the name was used entirely for these *N*-glycosidases [EC 3.2.2.22]. This is critical because other types of proteins that inactivate or damage ribosomes by different maneuvers (e.g., RNases or proteases) are not classified as RIPs. Ad interim, the term RIP is retained exclusively for proteins embodying an RNA *N*-glycosidase domain that is structurally affiliated with the traditional RIPs. The first recognized RIPs were ricin and abrin from castor bean (*Ricinus communis* L.) and jequirity bean (*Abrus precatorius* L.) respectively, two potent toxins studied by Paul Ehrlich (*23, 24*). However, only in 1971 it was discovered that ricin inhibits eukaryotic protein synthesis (*25*) and then that it exerts its action by impairing ribosomes (*26*). Concurrently, it was announced that a pokeweed antiviral protein (PAP) from *Phytolacca americana* L. leaves (common pokeweed, Figure 1.1) impeded protein synthesis through a related mechanism (*27*). Ultimately many other proteins with similar properties were reported, which were categorized into two major classes based on their physical properties: holo-RIPs and chimero-RIPs (Figure 1.3) (*28*). Holo-RIPs consist exclusively of a single RNA *N*-glycosidase domain. Most holo-RIPs consist of a single, intact polypeptide of approximately 30 kDa and are primarily referred to as type 1 RIPs (*12, 29*). These are strongly basic proteins that share several conserved active site residues and secondary structure (*30-32*) yet are clearly distinct in global sequence homology and posttranslational alterations. Examples include pokeweed antiviral protein (PAP) (Figure 1.4), saporin (from soapwart, *Saponaria officialis* L.), and barley (*Hordeum vulgare* L.) translational inhibitor.

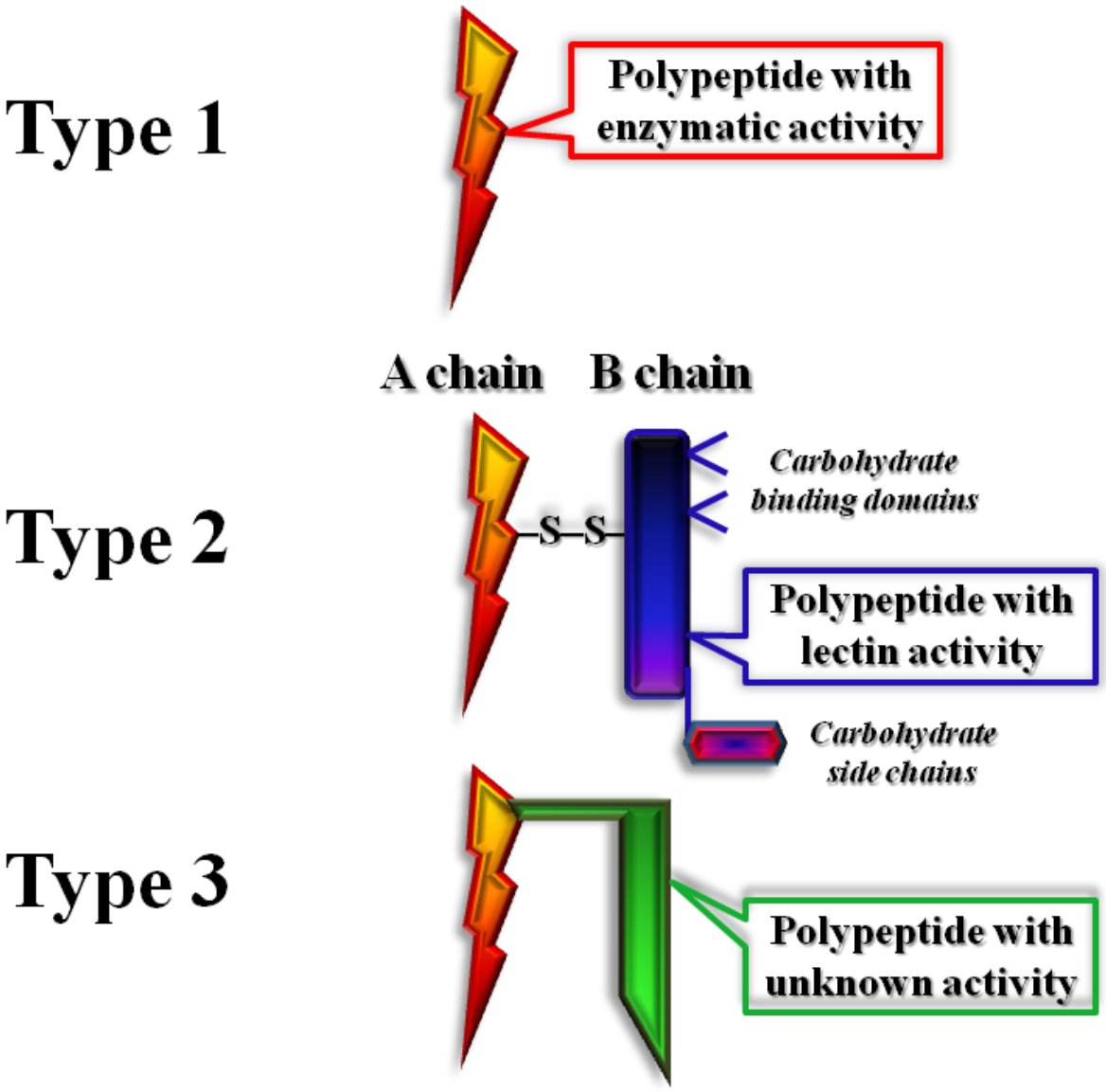

Figure 1.3 Schematic representation of the structure of ribosome inactivating proteins (RIPs). This figure was a courtesy of Dr. Tomas Girbes, and was adapted from Girbes *et al.* (*33*).

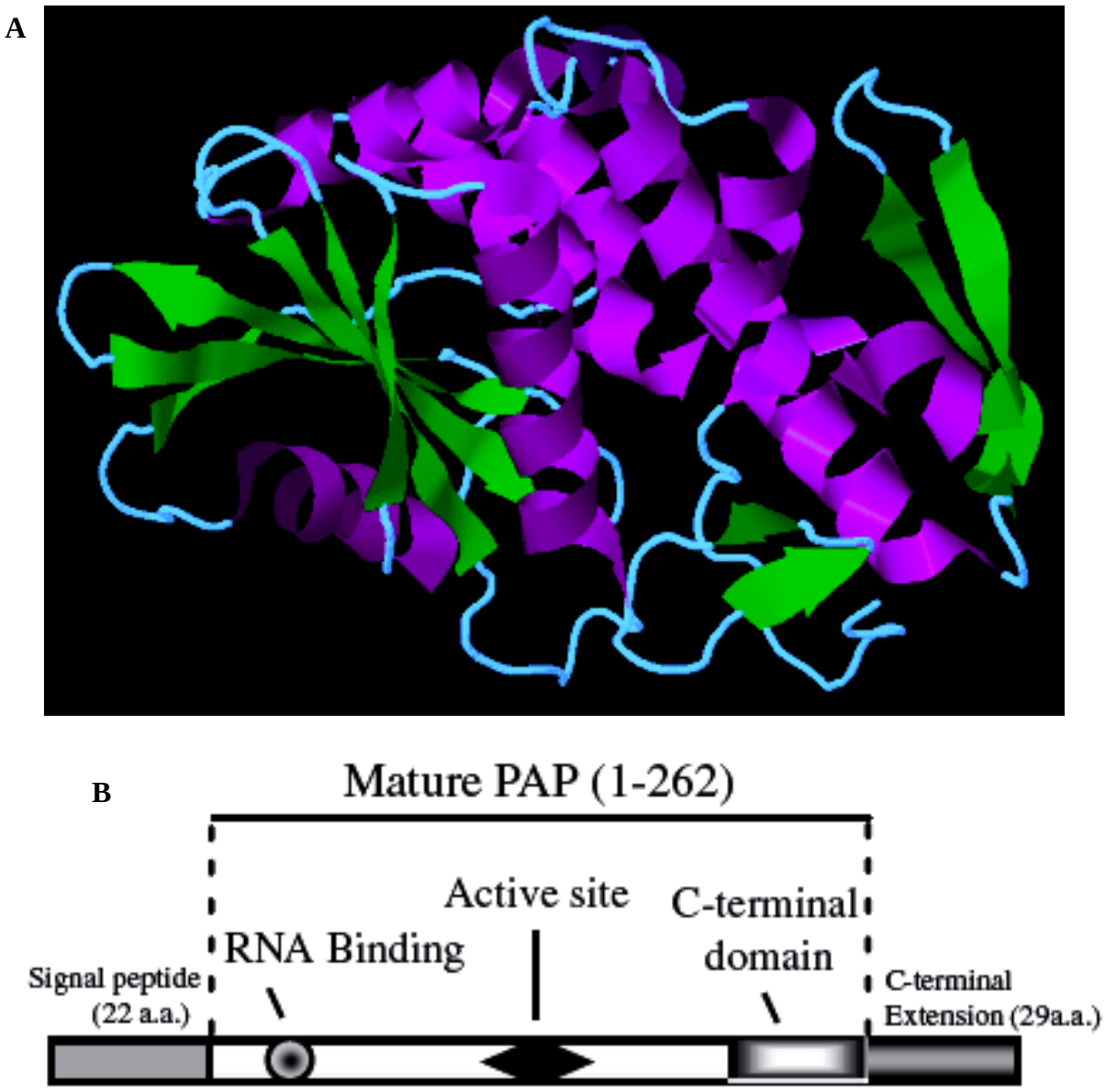

Figure 1.4 **(A)** Low temperature structure of pokeweed antiviral protein, PDB ID is 1QCI. This image was downloaded from protein data bank (*34*). **(B)** Diagram of wild-type PAP. A precursor PAP (313 amino acids) contains a 22-amino-acid signal sequence and its *N*-terminus and a 29-amino-acid *C*-terminal extension. The mature protein is 262 amino acids in length (1-262).
This figure was a courtesy of Dr. Nilgun E. Tumer (*35*).

The majority of characterized RIPs fall into the type 1 class (*29*). Type 1 RIPs inhibit cell-free protein synthesis and are only mildly toxic to cells and animals.

Chimero-RIPs are constructed of one or more protomers consisting of an *N*-glycosidase domain linked to a structurally and functionally distinct domain. Most chimero-RIPs are also known as type 2 RIPs. Type 2 RIPs, like ricin and abrin, are acutely toxic heterodimeric proteins with an amino-terminal domain equivalent to type 1 RIPs (enzymatic domain with RIP activity) joined by a disulfide bond to a divergent carboxyl-terminal domain with lectin properties (carbohydrate binding domain), each of approximate M_r of 30,000 (*36-38*). Both domains are assembled from a single precursor that is post-translationally modified by the excision of a linker sequence between the two domains. The amino-terminal RNA *N*-glycosidase domain and the carboxyl-terminal sugar binding domain are referred to as the A- and B-chains, respectively (*37*). The lectin chain is able to bind to galactosyl moieties of glycoproteins and/or glycolipids that are located on the exterior of eukaryotic cells (*39-41*) and promote reverse transport of the A-chain to the cytosol (*42-44*). The RIP accesses translational machinery and depurinates ribosomes after it enters the cytosol. The extracellular location prevents contact between RIP and ribosomes of healthy cells, yet provides an immediate source of the toxin when a pathogen vector disrupts the cell. The type 2 RIPs have been quite valuable for studies of endocytosis and intracellular transport in mammalian cells (*45-47*).

Type 3 RIPs are synthesized as inert precursors (proRIPs) that must undergo proteolytic modifications to in order to acquire their full enzymatic activity (*28*). These RIPs are much less common than type 1 or type 2 RIPs. Presently, type 3 RIPs have been identified only from maize (*Zea mays* L.) and barley (from *Hordem vulgare* L.) (*48-51*). In maize, proRIPs are acidic peptides that are cleaved *in vivo* to release amino acids from an internal portion as well as short

segments at both amino- and carboxyl-termini. These proteolytic cleavages result in proteins with tightly associated polypeptide subunits of 16,500 and 8,500 kDa (*51*). Both proteins identified in maize are type 3 RIPs (*48, 51, 52*). Barley, in contrast, has one type 1 RIP and one type 3 RIP. The latter, called JIP60, is induced by jasmonic acid and its activity is initiated after proteolytic cleavage to remove internal and carboxyl-terminal domains (*49*). The inner portions of JIP60 appear at relatively identical position within the primary amino acid sequence as in the maize RIPs. The purpose of these additional domains in the type 3 RIPs is not known. After its cleavage, the processed functioning peptide is similar in charge and enzymatic activity to type 1 RIPs (*51, 53, 54*).

I-1-C Distribution of RIPs among Plants, Fungi, Algae, and Bacteria

Research performed in the past twenty years disclosed that RIPs are broadly dispensed among plants, fungi, alga, and bacteria (*29, 55, 56*), and new findings show that a RIP-type activity has been reported in animal tissues as well (*57*). Studies described by Girbés *et al.*, show a comprehensive group of type 1 and type 2 RIPs belonging to a rather wide range of families seemingly unrelated from a Phylogenetic perspective (*33*). A large number of RIPs has been identified in a small group of families, namely *Caryophyllaceae*, *Cucurbitaceae*, *Euphorbiaceae*, *Sambucaceae*, *Phytolaccaceae* and *Poaceae*. Although, this is probably an outcome of the screening procedure which Girbés *et al.* used to describe plants with elevated concentrations of RIP, rather than to determine their distribution in the plant kingdom (*33*). Moreover, a large number of RIPs have been isolated from only one tissue of the plant. Some RIPs could be induced by different factors like senescence (*58*), viral infection (*59*), development (*50*) and stress (*60*).

The molecular weight of type 1 RIPs fall in the range from 21 to 38 kDa. As for type 2 RIPs, the molecular weights of the two-chain peptide range from 56 to 69 kDa (*33*). Bacterial RIPs examined included Stx1 and Stx2 from *Escherichia coli*; these RIPs promote their enzymatic activity as their plant analogues (*61-63*). Research reveals that RIPs are found in several fungi species (*64-67*). At least one RIP has been isolated from alga, *Laminaria japonica* A. (*68*). All of the above discoveries favor the generally acknowledged hypothesis that RIPs are enzymes widely distributed and therefore they must play pivotal and as yet undefined biological roles.

The majority of plants producing RIPs synthesize several isoforms that may be extant together in the same organ of the plant, or restricted to specific organs. These isoforms can arise either from the expression of distinct members of a gene family, or from differences in the processing and/or glycosylation of a primary gene product. In addition, accumulation of type 1 RIPs in several species is believed to be enhanced by stress and a diverse group of signaling molecules. The activity of RIPs in *Phytolacca americana* leaves, for instance, increases up to 15-fold following heat treatment and osmotic stress (*58*). For detailed description of pokeweed antiviral protein isoforms isolated from *Phytolacca americana* refer to Section I-1-D.

I-1-D Phylogenetic Relationship among Ribosome Inactivating Proteins; Isoforms of Pokeweed Antiviral Protein

The cDNAs encoding for an ample collection of types 1 and 2 RIPs have been entirely sequenced. A phylogenetic tree that discloses the type 1 RIPs and the type 2 RIPs A-chains produced by comparing the sequences of a number of RIPs listed in Table 1.1 is illustrated in Figure 1.5 (*33*). Chiefly, a significant RIP of each one of the identified RIP-containing species was chosen because the RIPs obtained from the same species, essentially, show a higher

Table 1.1 RIPs used to construct the phylogenetic tree of Figure 1.5. This table was a courtesy of Dr. Tomas Girbes. (*33*).

Bacteria							
Class	**Subclass**	**Order**	**Family**	**Species**	**RIP**	**Type RIP**	**Swiss-Prot/TrEMBL accession number**
Proteobacteria	Gammaproteo-bacteria	Enteroba-cteriales	Enterobacte-riaceae	*Eschericia coli*	Stx 1 A subunit	bacterial	Q8VV64
Proteobacteria	Gammaproteo-bacteria	Enteroba-cteriales	Enterobacte-riaceae	*Shigella dysenteriae*	Stx A subunit	bacterial	P10149
Magloliophyta							
Class	**Subclass**	**Order**	**Family**	**Species**	**RIP**	**Type RIP**	**Swiss-Prot/TrEMBL accession number**
Magnoliopsida	Magnoliidae	Laurales	Lauraceae	*Cinnamonin camphora*	Cinnamomin I	2	Q94BW5
	Rosidae	Cucurbitales	Cucurbitaceae	*Bryonia dioca*	Bryodin I	1	P33185
				Trichosanthes kirilowii	alpha-Trichosanthin	1	P09989
				Trichosanthes cucumerina	Trichoanguin	1	P56626
				Cucurbita moschata	Moschatin II	1	Q8S2R5
				Cucumis figarei	RIP 1	1	Q9FRX4
				Luffa cylindrica	Luffin-alpha	1	Q00465
				Momordica charantia	Momordin I	1	P16094
				Momordica balsamina	Momordin II	1	P29339
		Euphorbiales	Euphorbiaceae	*Ricinus communis*	Ricin	2	P02879
				Gelonium multiflorum	Gelonin	1	P33186
				Jatropha curcas	Curcin	1	Q8S452
		Santalales	Viscaceae	*Viscum album*	Mistletoe lectin	2	Q8RXH6
		Fabales	Fabaceae	*Abrus precatorius*	Abrin c*, APA**	2	P28590, Q9M6E9
	Caryophyllidae	Caryophyllales	Amaranthaceae	*Amaranthus viridis*	Amarandin-S	1	Q96322
			Chenopodiaceae	*Spinacia oleracea*	RIP	1	Q8VWY2
				Beta vulgaris	Betavulgin	1	Q39418
				Chenopodium album	RIP CAP30B	1	Q9AUE3
			Nyctaginaceae	*Mirabilis jalapa*	MAP	1	P21326
				Bougainvillea spertabilis	Bouganin	1	Q8W4U4
			Phytolaccaceae	*Phytolacca americana*	PAP-S	1	P93444
				Phytolacca acinosa	PAP	1	Q941G8
				Phytolacca insularis	RIP 2	1	Q9XFF8

Table 1.1 …continued (*33*).

Class	Subclass	Order	Family	Species	RIPs	Type RIP	Swiss-Prot/TrEMBL accession number
			Caryophyllaceae	*Dianthus caryophyllus*	Dianthin 30	1	P24476
				Dianthus chinensis	RIP 1	1	Q93Y66
				Saponaria officinalis	Saporin 6	1	P20656
			Aizoaceae	*Mesembryanthemum crystallinum*	RIP1	1	P93261
	Asteridae	Dipsacales	Sambucaceae	*Sambucus nigra*	Nigrin b*, SNAI**	2	P33183, Q41358
				Sambucus sieboldiana	Sieboldin b*, SSA**	2	Ref., D25317 (GenBank)
				Sambucus ebulus	Ebulin 1	2	Q9AVR2
		Lamiales	Lamiaceae	*Clerodendrum aculeatum*	CA-SRI protein	1	P93077
Liliopsida	Commelinidae	Poales	Poaceae	*Zea mays*	proRIP-alpha chain	1	P28522
				Oryza sativa	RIP 1	1	Q9AS85
				Triticum aestivum	Tritin	1	Q07810
				Secale cereal	Protein synthes. inhibit.	1	JC5848 (GenBank)
				Hordeum vulgare	RIP 1	1	P22244
	Liliidae	Liliales	Liliaceae	*Muscari armeniacum*	Musarmin 3	1	Q8L5M4
				Polygonatum multiflorum	PMRIPm	2	Q9M654
			Iridaceae	*Iris hollandica*	IrisRIPA3*, IRAb**, IRAr***	1	O04358, Q8W2E7, Q8W2E8

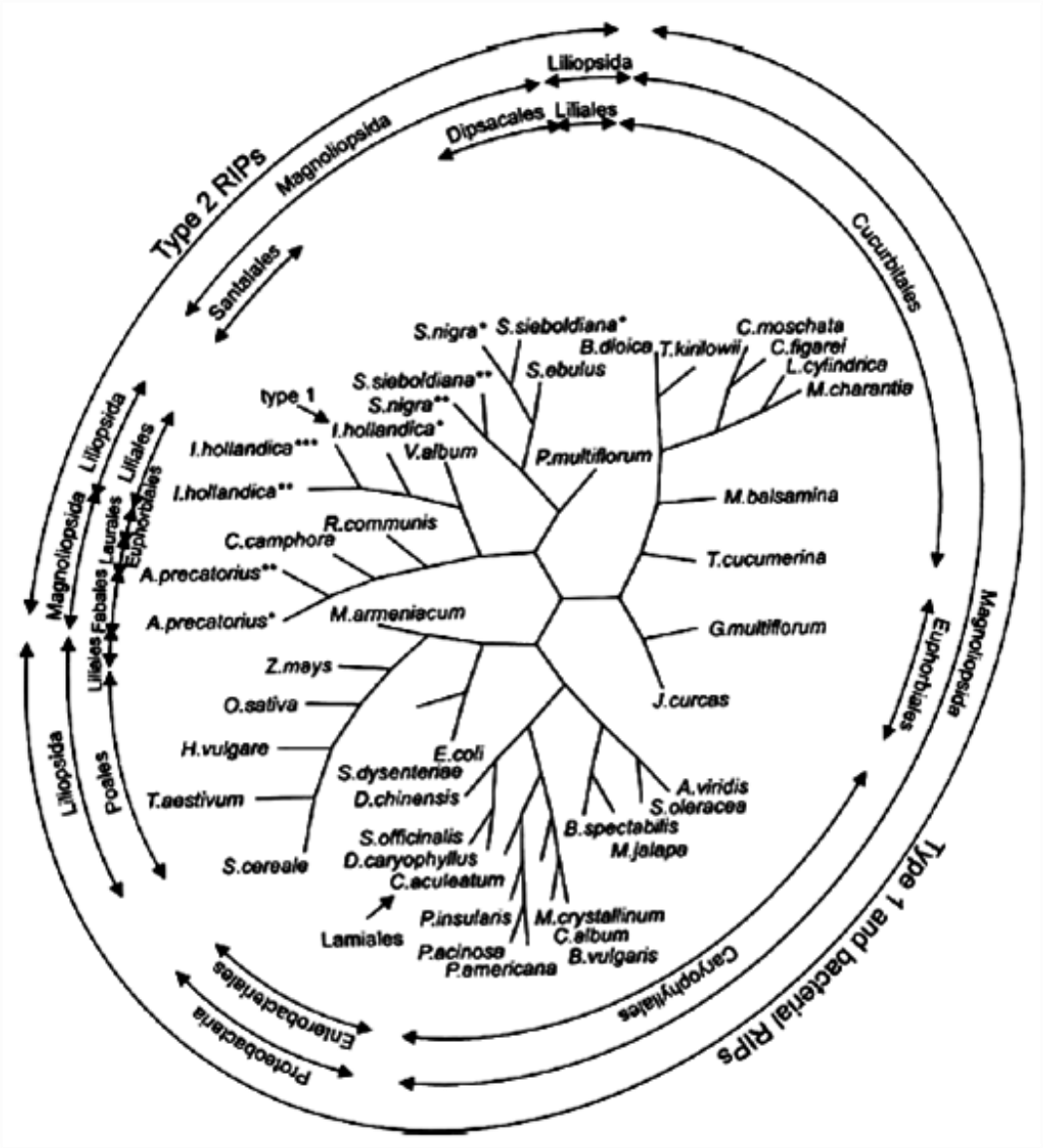

Figure 1.5 Dendrogram of the phylogenetic relationship of type 1 RIPs and the A chain of type 2 RIPs. Amino acid sequences of type 1 RIPs, the A chain of type 2 RIPs and the A chains of bacterial RIPs were aligned using CLUSTAL W (*69*) and the phylogenetic tree was generated using the neighbor-joining method (*70*). Asterisks refer to the proteins listed in Table 1.1.
This figure was a courtesy of Dr. Tomas Girbes (*33*).

homology among them than with RIPs of other species. For the most part, RIPs of the same taxon have analogous amino acid sequences, which is indicative of their presence in parent species and that they have evolved in parallel to the differentiation of the corresponding plants. The RIPs of the families Aizoaceae, Chenopodiaceae, and Phytolaccaceae appear related with amino acid homologies in the range of 32 – 76% (*33*).

Commonly, it is believed that the A- and B-chains of type 2 RIPs have appeared by means of fusion of an ancestral type I RIP and a lectin. No close analogue of the *N*-glycosidase domain has been identified in other proteins, however, elements of the three domain structure of type 1 RIPs are encountered in other RNA-binding proteins like RNase H from *E. coli* and the retroviral reverse transcriptases (*71*). Because of the occurrence of this domain in organisms as divergent as bacteria and angiosperms, the question arises as to where it originated. It was proposed that horizontal gene transfer had occurred between pro- and eukaryotes and *vice versa (72)*, to account for the fact that sequence comparisons between the A-chain of the bacterial toxins and higher plants reveal a maximum identity of only 14%.

The B-chain of type 2 RIPs and affiliated lectins is comprised of duplicate copies of a ternary galactose-binding peptide, termed α, β and γ subdomains, each of which is made of ~40 amino acid residues. The docking site for galactose is brought about by the sugar binding pockets that are constructed by a sharp bend in the backbone formed by a sequence Asp, Val and Arg, followed by a variable aromatic amino acid residue (*73*). The B-chain of type 2 RIPs is thought to be derived from an ancestral lectin of ~40 amino acid residues by two duplication/in tandem insertion events, which resulted before its fusion with the ancestral *N*-glycosidase domain (*74*). On the other hand, the *N*-glycosidase domain of the A-chain is widely distributed and extremely ancient. The A-chain was identified in discoidin II, from the slime mold *Dictyostelium*

discoideum, in human interleukins, human fibroblast growth factor, β-xynalase of *Streptomyces olivacoviridis* and in the marine mannose receptor, mCys-MR (*75*). All of these are now considered to be representatives of the ricin B family.

Most of type 1 RIPs are encoded by intron-less genes that define proRIPs with N- and C-terminal extensions with respect to the mature forms. For instance, several isoforms of pokeweed antiviral protein from *Phytolacca americana* L. have been described (Table 1.2) (refer to Table 1.3 for complete phylogenetic lineage of *Phytolacca americana*) (*12, 33, 76-78*). All of them possess pronounced antiviral properties and high enzymatic activity on ribosomes from diverse phyla. These isoforms are encoded by a gene family composed of approximately nine members (*76*). PAP-I (or simply PAP), PAP-II and PAP-III are leaf isoforms that appear in spring, early summer and late summer respectively (*12, 76-80*), whereas PAP-S1 and PAP-S2 are isoforms isolated from seeds that exhibit the highest activity *in vitro* of all the isoforms (*81-83*). PAP and PAP-S1 share 76% sequence identity, PAP-S1 and PAP-S2 have 83%, whereas PAP and PAP-II are only 33% identical (*83, 84*). A further isoform, α-PAP, is similar in sequence to PAP-S1, and essentially expressed in all organs (*83-85*); it shares 74% identity with PAP. Figure 1.6 illustrates an alignment of deduced amino acid sequences of several mature PAP isoforms (*83*). PAP-R has been isolated from the roots of pokeweed plant (*33, 86*) and PAP-H is from hairy roots (*33, 87*). It is intriguing to note that RIP-free callus and suspension cultures of *P. americana* have been acquired (*33, 88*). A gene-silencing event must have occurred during the establishment of the cultures because RIP-isoforms are ubiquitously expressed in all organs of the plant (*84*).

Table 1.2 Isoforms of pokeweed antiviral protein (*12, 33, 76-87*).

Isoform	Source	Number of aminoacyl residues			MW (kDa) Mature protein	Intron	% identity to PAP
		Mature Protein	N-terminal extension	C-terminal extension			
PAP (PAP-I)	Spring leaves	262	22	29	29	No	—
PAP-II	Early summer leaves	285	25	ND	30	Yes	33
PAP-III	Late summer leaves	285	ND	ND	30	ND	ND
PAP-S1	Seeds	262	ND	ND	29		76
PAP-S2	Seeds	262	24	28	29	No	83% to PAP-S2
α-PAP	Expressed in all organs	261	24	9		No	74
PAP-R	Roots	271	ND	ND	29.8	ND	ND
PAP-H	Hairy roots	268	ND	ND	29.5	ND	ND
PAP-C	Tissue culture	262	ND	ND	29	ND	ND

Table 1.3 Complete phylogenetic lineage of *Phytolacca americana* L. (*89, 90*).

Rank	Scientific name	Taxon identifier	Mnemonic	Common name	Synonym	Other names
---	Cellular organism	131567	---	---	---	biota
Superkingdom	Eukaryota	2759	9EUKA	---	---	Eucarya Eucaryotae Eukarya Eukaryotae eucaryotes eukaryotes
Kingdom	Viridiplantae	33090	9VIRI	---	---	Plantae Chlorobionta Chlorophyta/Embryophyta group green plants
Subkingdom	Tracheobionta	58023	9TRAC	---	---	Tracheophyta vascular plants
Phylum	Streptophyta	35493	---	---	---	Streptophyta Bremer 1985
---	Streptophytina	131221	---	---	---	Charophyta/Embryophyta group
---	Embryophyta	3193	9EMBR	---	---	higher plants land plants plants
---	Euphyllophyta	78536	---	---	---	---
Superdivision	Spermatophyta	58024	9SPER	---	---	seed plants
Division	Magnoliophyta	3398	9MAGN	---	---	Angiospermae angiosperms flowering plants
Class	eudicotyledons	71240	---	---	---	Dicotyledoneae Magnoliopsida dicots dicotyledons eudicots
Subclass	Caryophyllidae	3570	---	---	---	---
---	core eudicotyledons	91827	---	---	---	core eudicots
Order	Caryophyllales	3524	9CARY	---	---	Centrospermae Nepenthineae Physenales Polygonales
Family	Phytolaccaceae	3525	---	---	---	pokeweed family
Genus	Phytolacca	3526	---	---	---	---
Species	Phytolacca americana	3527	PHYAM	American pokeweed	Phytolacca decandra	Phytolacca americana L. Virginia poke common pokeberry common pokeweed red stem pokeweed

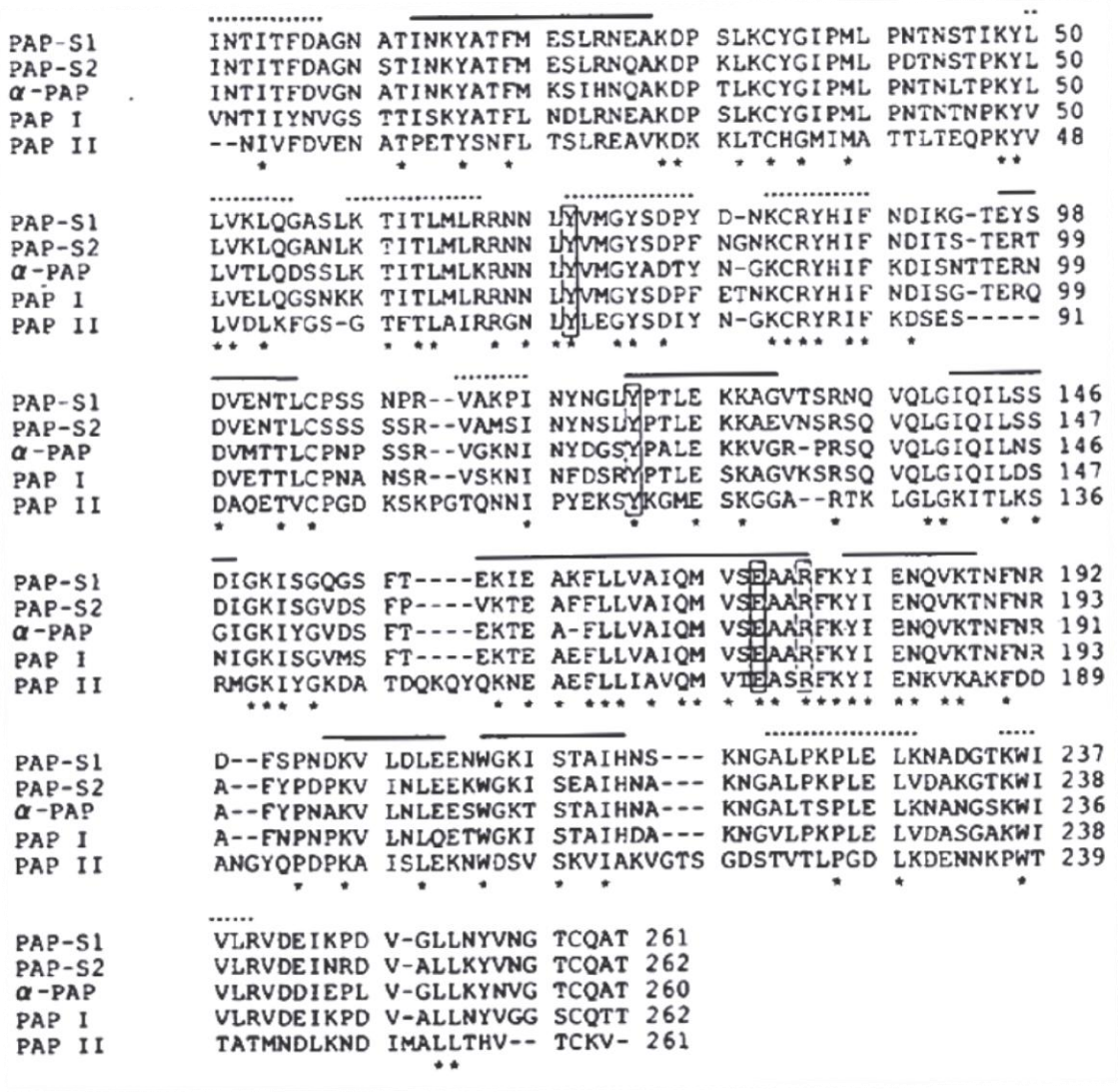

Figure 1.6 Alignment of deduced amino acid sequences of mature PAP isoforms.
The sequences of five PAP isoforms were aligned and gaps (─) were introduced to maximize homology using the ClustalX program (*91*). Identical amino acids are marked by asterisks (*). Amino acid residues possibly involved in catalytic activity are boxed. Regions of α helix (▬) and β strands (- - -) are indicated above the sequences.
This figure was a courtesy of Dr. Keiichi Watanabe (*83*).

I-1-E Biological and Enzymatic Activities of Ribosome Inactivating Proteins

I-1-E-i Biological Activities

Distinct biological activity of both type 1 and type 2 RIPs has served as the basis for their identification. Ricin, type 2 RIP, was isolated by Stillmark (*1*) over a century ago as the toxic essence of castor bean seeds. Ricin's high toxicity was attributed to its agglutinating activity, meaning that the carbohydrate binding activity of type 2 RIPs was distinguished long before their enzymatic activities and their inhibitory activity on protein synthesis. Carbohydrate binding ability of type 2 RIPs is attributed to the B-chain that embodies two or possibly three binding sites (*41, 85*). Sugar binding specificities of B-chains vary among individual RIPs, even though they possess high sequence similarity and essentially identical three-dimensional structures. Type 2 RIPs owe their toxicity and cytotoxicity to the deviations in the lectin activity and specificity, and is determined, in part, by the binding ability of the B-chain to interact with a sugar-containing receptor on the cell surface. Ricin and abrin are highly toxic proteins; however, type 2 RIPs present with remarkable differences in their cytotoxicity. Ricin, for instance, is known to induce 50% apoptosis in cells at concentrations below 1 ng/ml, while some elderberry type 2 RIPs display no significant effects at 1 mg/ml (*86*).

Duggar and Armstrong (*87*) are credited with the discovery of type 1 RIPs when they observed that a protein isolated from *Phytolacca americana*, bore an antiviral activity, and inhibited transmission of tobacco mosaic virus (TMV) in plants. Yet, not until 1978 was PAP acknowledged as a protein synthesis inhibitor (*88*). Myriad, but surely not all, type 1 RIPs are antiviral proteins. Type 1 RIPs are not as cytotoxic as type 2 RIPs, since they are not capable of crossing the cell membrane on their own. A number of specialized animal cells, nevertheless, are able to import type 1 RIPs by endocytosis and consequently are susceptible to the RIP activity.

Not until the discovery of the inhibitory activity on protein synthesis, the molecular basis for the biological activities of RIPs continued to be poorly understood. Only after it was realized that monomeric protein synthesis inhibitors share a significant sequence identity with ricin's A-chain, the first central link amid type 1 and type 2 RIPs became evident and the exploration for a general mechanism started. Soon enough, it was declared that ricin, abrin, and PAP inhibit cell-free protein synthesis by permanent inactivation of the ribosomes by means of arresting the function of elongation factors EF-1 and EF-2 (*29, 92*). Despite the fact that the 'victim' of RIPs was diagnosed, the question endured as to how RIPs deactivate ribosomes.

I-1-E-ii Classical Enzymatic Activities

Presently, it is acknowledged that all ribosome inactivating proteins are enzymes, some of which possess multiple enzymatic activities. Several classical enzymatic activities are discussed below, including site-specific RNA *N*-glycosidase activity (Figure 1.7) toward ribosomes and rRNA, polynucleotide:adenosine/guanosine activity, and depurination of capped mRNA.

Site-specific RNA *N*-glycosidase activity toward ribosomes and naked ribosomal RNA

It was first established by Endo *et al.* (*93*) that RIPs are enzymes, and that ricin is able to recognize a specific and highly conserved region within the large 28*S* rRNA and cleave a distinct glycosidic bond between an adenine and the nucleotide on the RNA. For rat liver ribosome, this distinct site is A4324 and positioned within a single-stranded loop, referred to as the sarcin/ricin (S/R) loop of the 28*S* rRNA (Figure 1.8) (*29*). The S/R loop is positioned in domain VII of the rRNA. After the adenine is removed, the depurinated site is unstable and becomes subject to

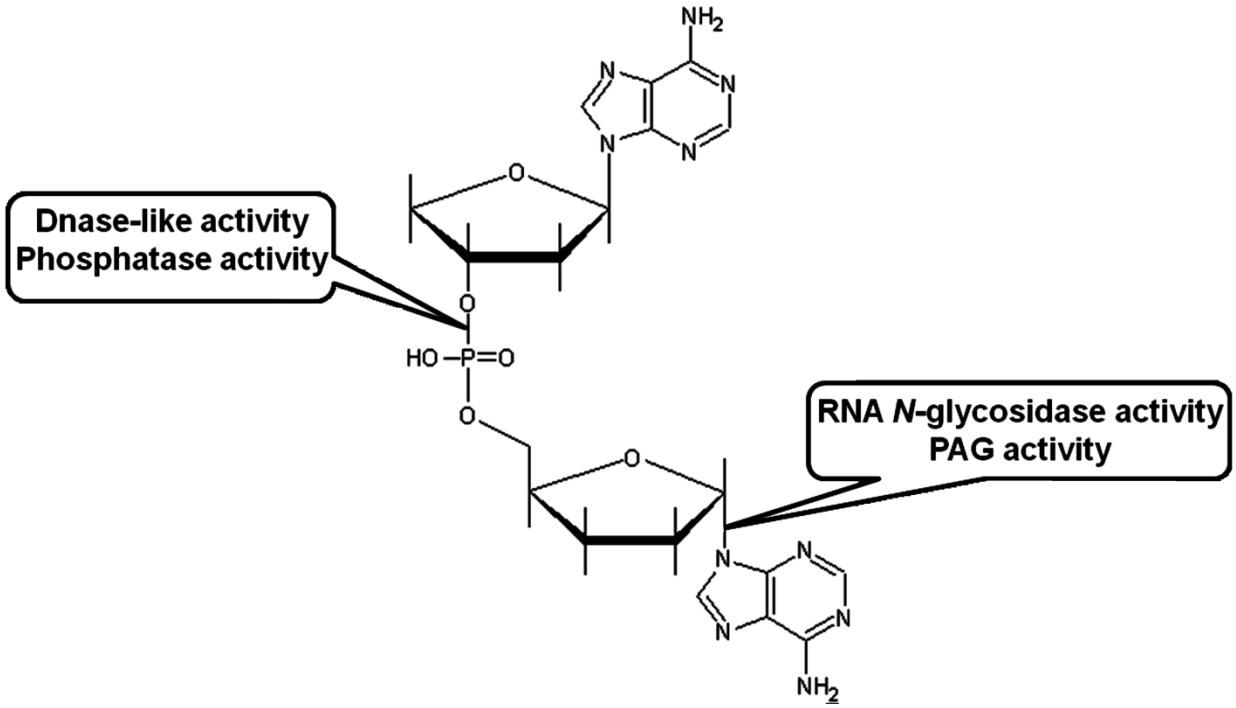

Figure 1.7 Schematic representation of the action sites for RNA *N*-glycosidase activity, polynucleotide:adenosine glycosidase (PAG) activity, and presumed DNase-like and phosphatase activity of RIPs.

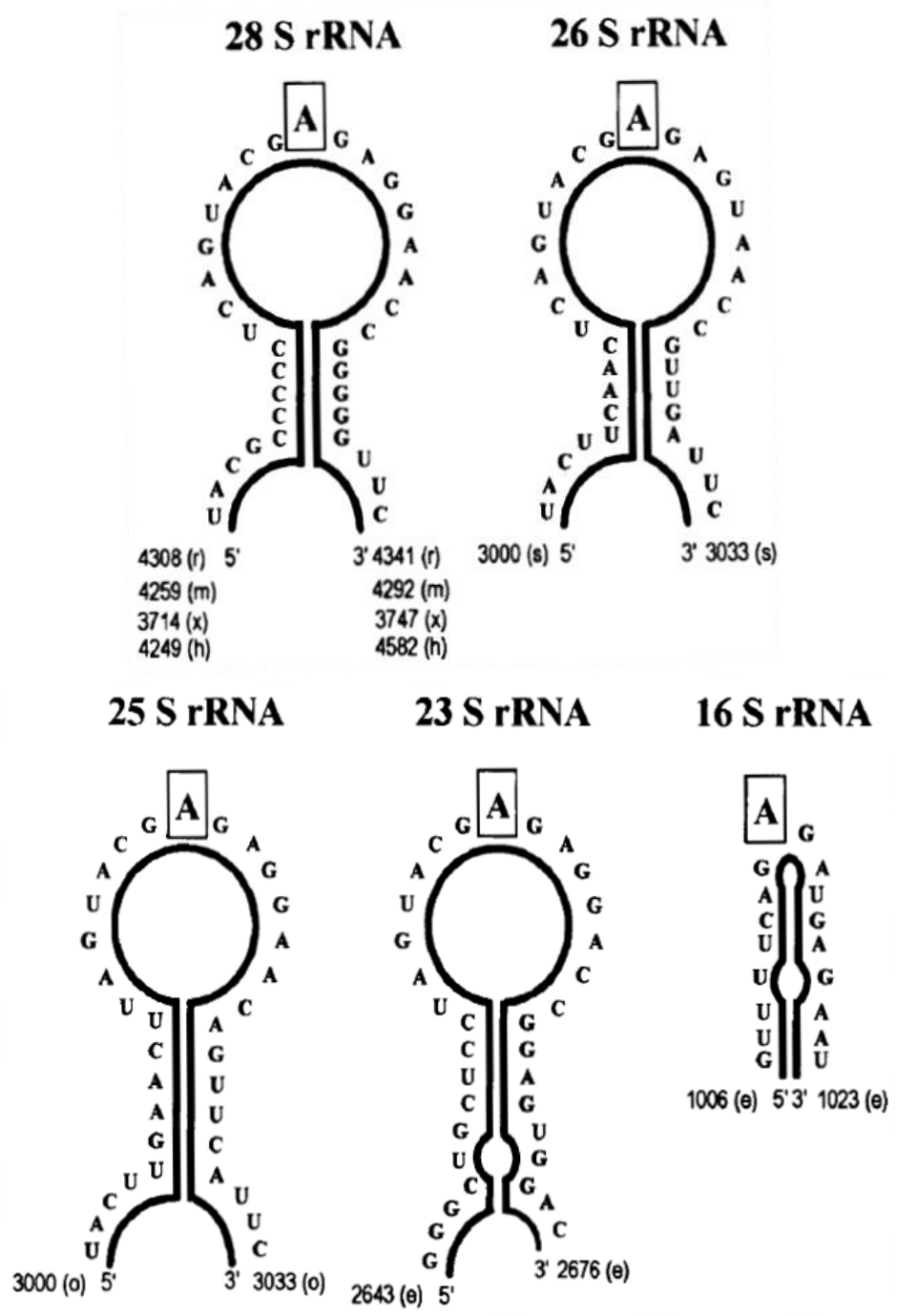

Figure 1.8 Structure of rRNA substrates for *N*-glycosidase activity of RIPs. Secondary structures are as compiled by Gutell and Fox. (e) *E. coli*, (h) *Homo sapiens*, (m) mouse, (o) *Oryza sativa*, (r) rat, (s) *S. cerevisiae*, (x) *X. laevis*. These structures were a courtesy of Dr. Robin Gutell. (*94*).

a β-elimination reaction when the RNA is treated with acidic aniline. This cleaves the 3'-end of the rRNA and the depurination product can be detected by electrophoresis. This site-specific RNA *N*-glycosidase activity is a common characteristic attributed to all RIPs.

During the elongation cycle of translation, the elongation factor eEF1A (EF-Tu in prokaryotes), with GTP, brings an aminoacyl-tRNA to the A-site of the ribosome. GTPase activity is stimulated by aminoacyl-tRNA anticodon recognition of the mRNA codon and hydrolysis of GTP, then releases eEF1A following delivery of the aminoacyl-tRNA (*95*). Peptide bond formation is catalyzed by the rRNA (*96, 97*) and causes the transfer of the peptide from the peptidyl-tRNA in the P-site of the ribosome to the A-site, thereby extending the peptide chain by one amino acid. The nascent chain, located now at the A-site, is translocated to the P-site, and this movement is mediated by elongation factor eEF-2 (EF-G in prokaryotes) at the expense of GTP hydrolysis (*98*). The deacylated tRNA leaves the ribosome via the E-site, a new aminoacyl-tRNA is brought to the A-site, and the cycle repeated (*99-101*)

The understanding that RIPs inhibit translation elongation and that depurination of the S/R loop hinders the binding of elongation factor 2 is well documented (*102, 103*). The role of this factor is to mediate translocation of the peptide chain from the A-site to the P-site of the ribosome. Hence, PAP and other RIPs inhibit the translocation step of elongation (Figure 1.9) (*104*). Evidence presented by Mansouri *et al.* (*104*) shows that PAP depurinates the ribosome when the A-site of the peptidyl-transferase center is empty; therefore, the conformation of the ribosome that is susceptible to depurination is different from the conformation at which the defective ribosome is stalled due to depurination by PAP. PAP specifically inhibits Ty*1*-directed +1 ribosomal frameshifting and retrotransposition (*105, 106*).

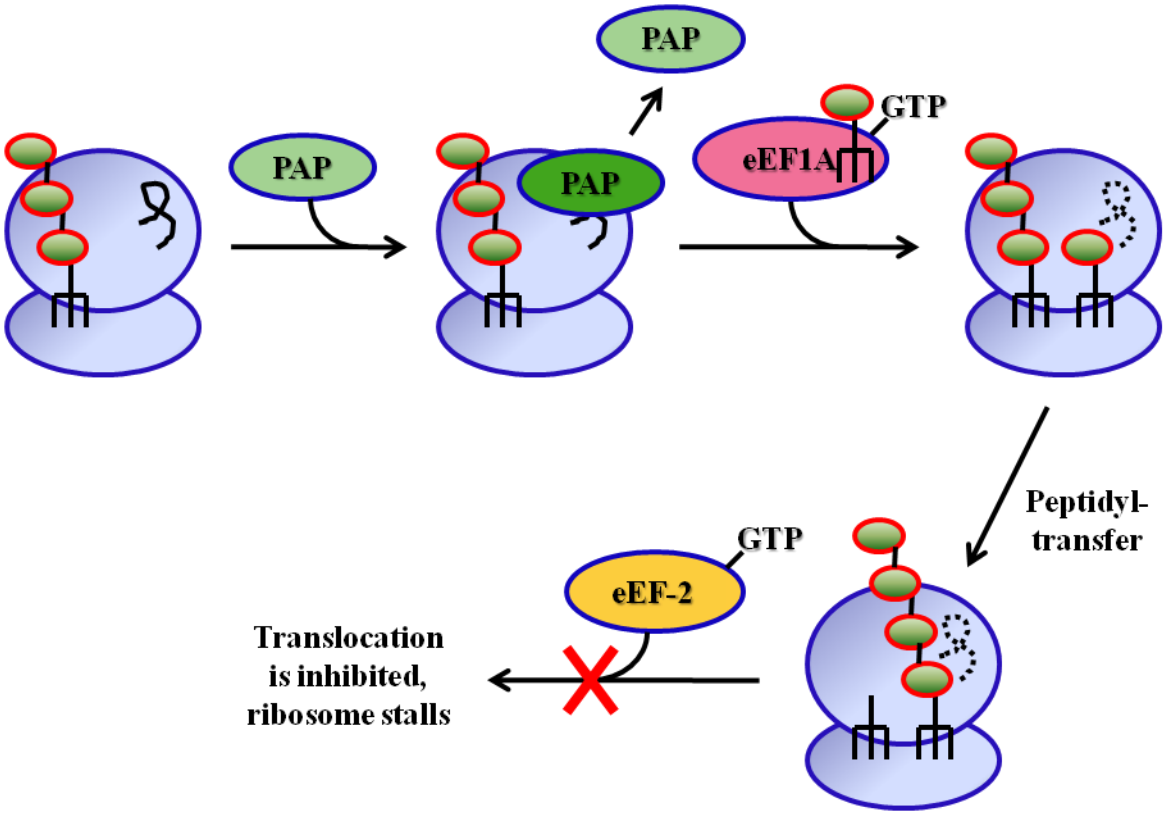

Figure 1.9 Model illustrating the step of the elongation cycle at which PAP depurinates the ribosome. Following the translocation step of the peptidyl-tRNA from the A-site to the P-site and prior to the arrival of a new aminoacyl-tRNA to the A-site, PAP binds to the ribosome and depurinates the sarcin/ricin loop. PAP then dissociates from the ribosome. The dashed line represents the depurinated sarcin/ricin loop. The eEF1A ternary complex binds to the ribosome and delivers the aminoacyl-tRNA to the A-site. Peptidyl transfer occurs, mediated by the rRNA. Binding of the eEF-2 GTP binary complex required for translocation of the peptidyl-tRNA from the A-site to the P-site is inhibited by depurination (indicated by the X), and the ribosome stalls with the peptidyl-tRNA at the A-site (*104*).
This figure was a courtesy of Dr. Kathi Hudak, and was adapted from Mansouri *et al.* (*104*).

A plausible mechanism for ricin and the entire class of RIPs is shown in Figure 1.10 (*107*). As the C1'-N9 bond breaks, negative charge accumulates in the adenine ring and positive charge in the ribose ring. The former is stabilized by partial, or complete, protonation of N3 by Arg180. This purely structural finding was surprising since acid/base depurination in organic media is thought to proceed by protonation at N7. However, studies by Schramm *et al.* confirmed that ricin depurination does not involve N7 protonation (*108*). Those studies also showed that the ricin reaction transition state has oxocarbenium character on the ribose. This was further confirmed by the synthesis of novel compounds that incorporated the cationic character, as amines, into a ribose analog. As expected for true transition state analogs, these were potent, tightly binding, ricin inhibitors (*109*). The exact role of the invariant Glu177 is still unclear. It may act to polarize water, as suggested in Figure 1.10, or it may simply pair with, and electrostatically stabilize, the transition state oxocarbenium (*107*).

While all RIPs possess RNA *N*-glycosidase activity toward ribosomes, their substrate specificity is greatly diversified. For instance, ricin exhibits vigorous activity toward yeast and mammalian ribosomes but has low activity on plant and *Escherichia coli* ribosomes (*29*), whereas PAP depurinates ribosomes from plants, bacteria, yeasts, and lower and higher animals (*29*). The majority of type 1 RIPs possess quite wide specificity toward ribosomes from a variety of species, while type 2 RIPs have a preference for animal ribosomes. Contribution to the substrate specificity comes from both RIPs and ribosomes alike. The S/R loop within the rRNA is universally conserved, therefore deviations in sensitivity between different ribosomes is most likely to come from the ribosomal proteins. These proteins may either permit or restrict access of the RIPs to the target structure. It was reported that the binding targets of the ricin A chain are rat liver ribosomal proteins L9 and L10e (*110*), but protein L3 serves as the binding partner for PAP

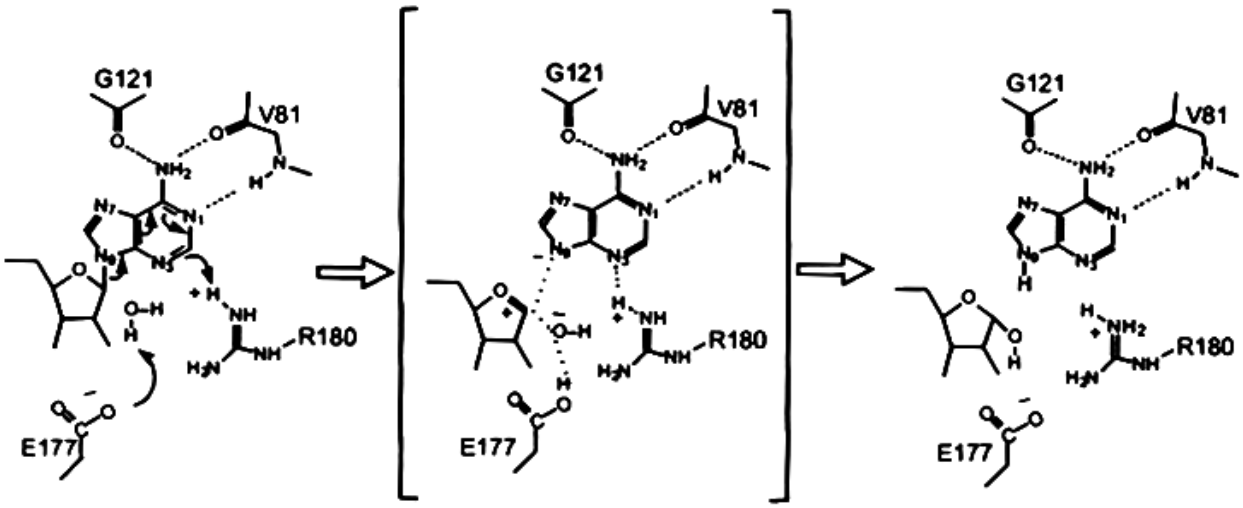

Figure 1.10 A plausible mechanism for ricin and the RIP family. The susceptible adenine binds in a specificity pocket and contacts the side chain of two invariant tyrosines that are not shown in the figure. Y80 lies above the adenine and is stacked on it, while Y123 lies below. A possible transition state structure is indicated in brackets as panel B. C1'-N9 bond breaking is catalyzed and the polarization is aided by partial, or possibly complete, protonation of N3 by Arg180. The putative transition state, panel B, shows negative charge developing on the leaving adenine and positive change on the ribose in the form of an oxocarbenium cation. Water is the ultimate nucleophile and in this figure it is shown being polarized by the basic side chain of E177. Alternatively, the E177 carboxylate may serve to stabilize the oxocarbenium ion.
This figure was adapted from Robertus *et al.* (*107*), and used with the permission of Bentham Science Publishers Ltd ©.

docking to yeast ribosomes (*111*), and expression of a truncated form of L3 ribosomal protein confers resistance to PAP in transgenic plants (*112*). L3 protein is an extremely conserved protein in ribosomes, which probably accounts for PAP's broad-spectrum activity toward ribosomes from different taxonomic groups. Structural differences of RIPs themselves may also account for their diversified activities. An important query concerning substrate specificity is whether RIPs act on conspecific (belonging to the same species) ribosomes. Previously, it was suggested that RIPs do not affect ribosomes of the plant in which they are expressed; however, recent studies have shown that RIPs are fully capable of depurinating and inactivating conspecific ribosomes. Bonness *et al.* (*15*) have shown that pokeweed ribosomes are inactivated by treatment with PAP and are nearly as sensitive to attack as are wheat ribosomes.

While the rRNA in native ribosomes is the ideal substrate for RIPs, naked rRNA (*113*) and a synthetic oligoribonucleotides that mimic the S/R domain (*114*), serve as the substrate for RIP activity as well. All RIPs are able to depurinate the equivalent adenine residue from naked rRNA as from native ribosomes, but many of them depurinate naked rRNA at multiple sites. In addition, several RIPs are able to depurinate naked rRNA from nonsubstrate ribosomes. For instance, ricin is able to act on naked *E. coli* 23*S* rRNA, however possesses no activity against the intact *E. coli* ribosomes.

Polynucleotide:adenosine and polynucleotide:guanosine glycosidase activity

Only with the advances in high-performance liquid chromatography (HPLC) that was coupled to fluorescence detectors, researchers were able to detect, identify, and quantify possible reaction products of RIPs and the amount of free adenine released from different substrates by RIPs (*115*). This technique allowed for direct measurement of ribosomal depurination, and also

identified some unusual activities of RIPs. Some RIPs acted on rRNA at specific single sites (*116*); yet others were shown to depurinate multiple adenines from various nucleic acid substrates such as herring sperm DNA, poly(A), tRNA, and even TMV RNA (*117*). A matter that is worthy of attention is the depurination of viral RNA by RIPs (Figure 1.11). Various RIPs serve as effective inhibitors of animal and/or plant viruses. The mode of action for the antiviral activity of RIPs is poorly understood, however there is indication that this activity does not depend solely on the ribosomal inactivation. It has been postulated that a direct interaction of RIPs with viral RNA or DNA might be an alternative mechanism. Recent studies showed that the pokeweed antiviral proteins PAP-I, PAP-II, and PAP-III cause a concentration-dependent depurination of genomic HIV-1 RNA (*118-120*), TMV RNA (*121*), poliovirus (*122*), herpes simplex virus (*123*), influenza virus (*124*), BMV RNA (*125*), and LCMV (*126*). In contrast, the A chain of ricin does not depurinate same viral RNAs to produce detectable quantities of adenine. Figure 1.11 illustrates a molecular model of PAP-rRNA and PAP-viral RNA interactions (*120*).

Some RIPs are also able to remove specific guanine residues from both eukaryotic and prokaryotic rRNA. Treatment of rat ribosomes with ricin causes the removal of G4323 from the S/R loop (*93*). An analogous activity has been described for PAP. Using a quantitative HPLC technique, it was shown that recombinant PAP releases a guanine residue from *E. coli* rRNA (*119*). Likewise, it was reported, that by using a highly sensitive primer extension assay, wild-type PAP removes G4323 from rabbit reticulocyte, tobacco, and yeast ribosomes (*127*). Modeling studies and X-ray crystallographic analysis confirmed that a guanine base fits into the active site pocket of PAP without disturbing the geometry and is sandwiched between the side groups of Y72 and Y123 in the same manner as an adenine base (*34, 128*). Thus far, no

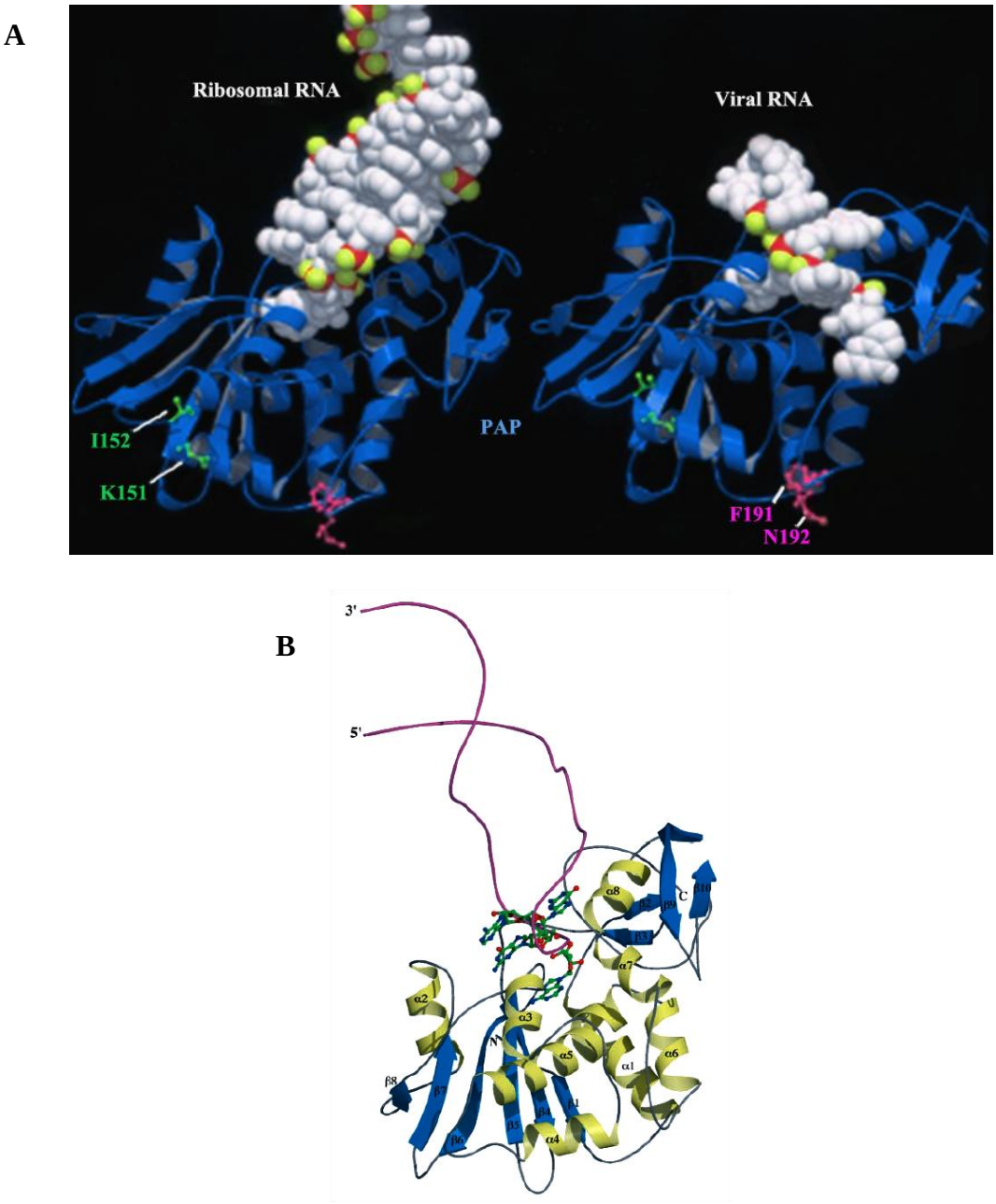

Figure 1.11 Molecular model of PAP-RNA interactions. (A) Ribbon and space-filling representation of PAP (blue) complex models with rRNA (left, in white) and viral RNA (right, in white) molecules. This figure was adapted from Uckun *et al.* (*120*), Copyright Clearance Center (conf. # 10364940).
(B) Molecular model of PAP-RNA stem loop model indicating the four nucleotides that make up the targeted tetra-loop (GAGA) of the conserved S/R loop sequence. The β strands of PAP are blue and are labeled β1-β10. The α helices are green and are labeled α1-α8. The phosphate backbone of the RNA fragment is violet, and the GAGA nucleotides are shown in ball-and-stick models. This figure was adapted from Rajamohan *et al.* (*129*) © The American Society of Biochemistry and Molecular Biology.

evidence has been reported for a possible deguanylating activity of other RIPs. This indicates that such deguanylating activity cannot be attributed to all RIPs.

Depurination of capped and uncapped mRNA; Mechanism for antiviral action of PAP

Recent findings have put forward a novel mechanism for the inhibition of translation by PAP (*127*). This inhibition of translation is based on a specific depurination of capped mRNA. Hudak *et al.* used WT PAP and three different PAP mutants (PAPx, an active site mutant (E176V); PAPn, a mutant with a substitution (G75D) in the amino-terminal sequence; PAPc, a mutant lacking the carboxyl-terminal 25 amino acid residues) that do not depurinate tobacco or rabbit ribosomes, and have shown that PAP inhibits the in vitro translation of BMV and potato virus X RNAs without ribosomal depurination (*127*). These studies have shown that PAP is able to differentiate between capped and uncapped mRNAs, since PAP and some of its mutants inhibit the translation of capped (but not uncapped) luciferase transcripts. Presence of m^7GTP analog has lowered translational inactivation activity of PAP and PAP mutants, implying that these RIPs are able to recognize the cap structure on the mRNAs. Examination of the PAP-treated luciferase transcripts revealed that the capped but not the uncapped RNAs were subject to degradation by acidic aniline, and therefore were depurinated in vitro. Based to these findings, Hudak *et al.* have concluded that PAP may inhibit translation by binding to the cap structure and depurinating the RNA and that depurination of capped viral RNA may be the primary mechanism for the antiviral activity of PAP (*130*). Baldwin *et al.* (*131*) have characterized the interactions of PAP with m^7GTP cap analog (Figure 1.12) using fluorescence spectroscopy.

These results depict a promising mechanism to explain the antiviral activity of PAP, however, some queries remain. For instance, the above proposed mechanism does not clarify the

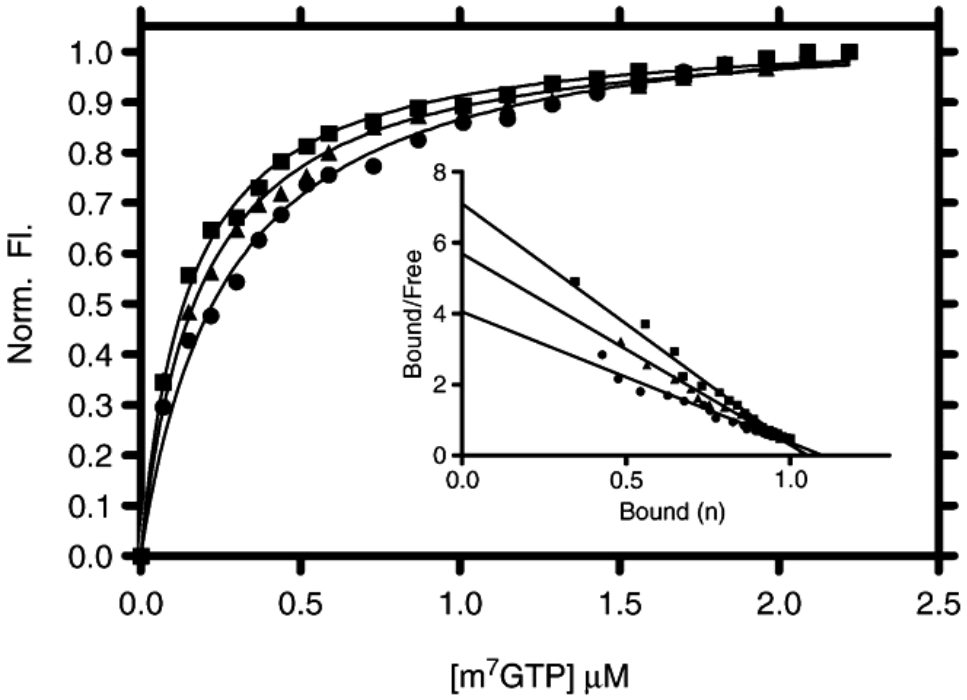

Figure 1.12 Titration of constant concentrations of PAP with m^7GTP at varying temperatures. Curves show increasing binding at various temperatures (■ 12 ^oC, ▲ 19 ^oC, ● 25 ^oC). The titration buffer was B20 (20 mM HEPES, 100 mM KCl, 1 mM DTT, pH 6.5). The inset depicts the corresponding Scatchard analyses of the titration data. Lines were plotted using V_{max} and K_d calculated by Prism 4.03 using nonlinear regression (*131*).
This figure was a courtesy of Amy Baldwin (*131*), and reprinted with the permission from Elsevier provided by Copyright Clearance Center (Licence # 2639460892176).

inhibitory effect of PAP on the replication of uncapped viruses such as influenza (*124*) and poliovirus (*122*). Vivanco *et al.* (*132*) have examined the activity of PAP against a variety of capped and uncapped viral RNAs, and demonstrated that PAP does not depurinate every capped RNA and that it can inhibit translation of uncapped viral RNAs *in vitro* without causing detectable depurination at multiple sites. PAP depurinated the capped Tobacco mosaic virus (TMV) and Brome mosaic virus (BMV) RNAs, but did not depurinate the uncapped luciferase RNA, indicating that PAP can distinguish between capped and uncapped RNAs, but no detectable depurination of capped Alfalfa mosaic virus (AMV) RNA was recorded. This implies that recognition of the cap structure alone is not sufficient for depurination of RNAs at multiple sites (*132*). Moreover, PAP did not cause detectable depurination of uncapped RNAs from Tomato bushy stunt virus (TBSV), Satellite panicum mosaic virus (SPMV), and uncapped RNA containing poliovirus IRES; however, *in vitro* translation experiments showed that PAP inhibited translation of the above viral RNAs (*132*). The overall mechanism of PAP antiviral activity remains to be elucidated.

Recent work published by Wang *et al.* (*133*) presents evidence that PAP binds to eIF4G and its isoform eIF*iso*4G. In wheat, two forms of eIF4G exist, which differ in size, 180 (eIF4G) and 86 kDa (eIF*iso*4G), and they bear only 30% identity at the amino acid level (*134, 135*). Studies show that PAP binds specifically to each form, and genetic and biochemical analyses present evidence that a region of the protein, between amino acids 511 and 624, is required for PAP binding activity (*133*). PAP binds to m^7GTP-Sepharose and this interaction does not diminish the binding of PAP to purified eIF*iso*4G, indicating that a complex can form between the cap structure, PAP and eIF*iso*4G. In the presence of wheat germ lysate, PAP depurinated uncapped transcripts containing a functional WT 3’ translational enhancer sequence (3’TE), but

did not depurinate messages containing a non-functional mutant 3'TE (*133*). This result supports earlier hypothesis that binding of PAP to eIF4G and eIF*iso*4G can provide a mechanism for PAP to access both uncapped and capped viral RNAs for depurination. In support to the above findings, Baldwin *et al.* (*131*) have shown that PAP not only binds to the initiation factor scaffolding protein eIF*iso*4G, but that binding of cap analog to PAP is increased by this protein-protein interaction, suggesting a model (Figure 1.13) where PAP interacts with eIF*iso*4G/eIF4G (as part of the eIF*iso*4F/eIF4F complex) and binds to the cap region of mRNA. Furthermore, addition of eIF*iso*4E/eIF4E (as part of the eIF*iso*4F/eIF4F complex) lowers the binding affinity of PAP for the cap competitively because both are specific cap-binding proteins. These PAP-eIF interactions possibly unfold the active site of PAP thus recognizing purine residues for depurination (*131*).

I-1-E-iii Regulators of enzymatic activity of RIPs

Ribosome inactivating proteins display their RNA N-glycosidase activity at a very low concentration. A given IC_{50} value for an individual RIP sometimes deviates between different laboratories because of the diversity in plant sources or activity assay systems; commonly it is affirmed that the minimal quantity necessary for type 1 RIPs depurination of animal ribosomes is at picomolar concentrations, while that for plant or microbial ribosomes is at nanomolar concentrations. Type 2 and 3 RIPs are ordinarily less active than type 1 RIPs. Consequently, it is useful to identify molecules that can regulate enzymatic activity of RIPs and how these activities are controlled. Several type 1 RIPs have a notable ATP requirement and supernatant factors for activity (*136-138*). These requirements are aimed at the ribosome, meaning that preincubation of the ribosome with the cofactors boosts the rate of successive depurination by the RIP.

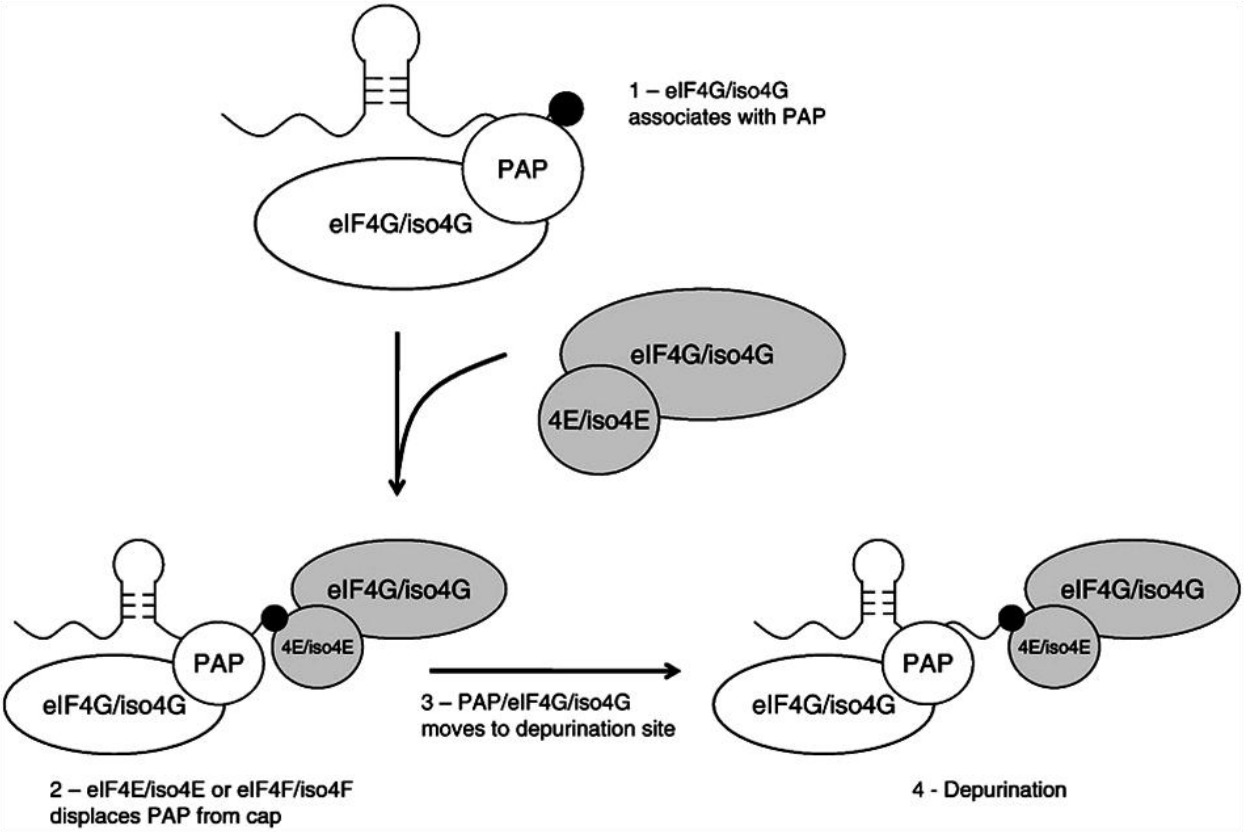

Figure 1.13 Schematic diagram of the proposed model for PAP interaction with initiation factors and capped mRNA. Step 1: PAP/eIF4G/iso4G* binds to capped mRNA. Whether PAP binds to mRNA as a complex with eIF4G/iso4G has not been determined. In Step 2, eIF4E/iso4E binds to the complex and releases the cap from PAP. It is likely eIF4E/iso4E* binds as the eIF4F/iso4F complex. PAP and eIF4G/iso4G are then free to move (Step 3) to the depurination site where enzymatic activity occurs (Step 4). *eIF4G/iso4G and eIF4E/iso4E are part of the eIF4F/iso4F complex and are shown in partial subunit form for clarity (*131*). This figure was a courtesy of Amy Baldwin (*131*), and reprinted with the permission from Elsevier provided by Copyright Clearance Center (Licence # 2639460892176).

Phosphorylation of ribosomal proteins is not required even though ATP is hydrolyzed in the process. Individual RIPs require different cofactors (*139*). Why some RIPs show cofactor requirements and others do not is unclear. Adenine, the reaction product released by RIPs, acts as an uncompetitive down regulator of RIPs activity, and binds to the enzyme-substrate complex (*140*).

I-1-F Physiological Role, Extracellular Localization, Entry, and Intracellular Routing of RIPs

RIPs possess a set of unique biological activities toward human and animal cells that could be exploited in therapeutical studies against viral infections, as well as enormous prospective they offer for antitumor activities. However, it is doubtful that plants synthesize RIPs just to meet the requirements of humans for antitumor and antiviral drugs. Presently, there is no unequivocal and agreeable answer to why plants produce and accumulate RIPs, despite the comprehensive knowledge on their structure, activity, and action mechanism.

RIPs are synthesized in many, but surely not all, plant species. Sequencing of the genome of *Arabidopsis thaliana* provided evidence that this plant that does not produce any detectable amounts of RIPs nor does it contain a sequence encoding a putative RIP in its whole genome (*13*). This means that RIPs are not ubiquitous among plant species, and do not play a universal role in their growth, development, or defense. Nevertheless, some facts support the notion that RIPs play a defense function in plants. Only type 2 RIPs are able to gain entree to the cytoplasm of intact cells via a receptor-lectin-mediated uptake process (*29, 141*). Toxicity of type 2 RIPs is restricted to animal cells because bacteria and fungi are protected by a cell wall, for type 2 RIPs must bind glycan receptors on the cell surface to ensure their entry. Ricin and abrin are thought to protect the seeds of these plants against plant-eating animals (*142*). There is no documented

oral toxicity of Type 1 and type 3 RIPs toward higher animals and invertebrates, meaning that these RIPs do not play the same role against plant consuming organisms. However, there is evidence that type 1 RIPs have direct effect on yeast and plant pathogenic fungi (*143*). The antiviral activity of type 1 RIPs is well documented (*144*), although the underlying mechanism has not been elucidated.

Founded on the extracellular localization of PAP, a model for its antiviral action has been postulated (*14*): when virus infects the cell, PAP also gains entrance, and disrupts cellular protein synthesis, hence killing virus-infected cells and thus averting viral replication. The extracellular location prevents contact between PAP and ribosomes of healthy cells, yet provides an immediate source of the toxin when a pathogen vector disrupts the cell. This is so called "local suicide hypothesis." This model also implies that viral infection is accompanied by severe cell damage. Now, since protein synthesis will stop almost immediately once the cells lose their structural integrity, depurination of the ribosomes by RIPs could hardly have any direct effect (*11*). In addition, it is observed that RIP-containing plants are not resistant against viruses. For instance, even pokeweed plants, which express up to 5% of PAP of the total protein in the cell (*145*), are susceptible to plant viruses. The antiviral activity of RIPs, therefore, probably relies on a circuitous mechanism that activates the defense system of the plant. Proof for such an indirect mechanism has not yet been obtained from plants that normally express RIPs, but only from transgenic tobacco plants expressing recombinant RIPs.

Persuasive evidence for antiviral action of RIPs *in planta* was supported by experiments with transgenic plants. Expression of PAP allowed the tobacco plant resistance against infection by mechanically and aphid-transmitted viruses including potato virus X, potato virus Y, and cucumber mosaic virus (*2, 146*). Regrettably, RIPs caused serious phenotype changes because of

their toxicity for the transgenic plants, so antiviral RIPs with a lower toxicity toward host plants were used, like a low-toxic isoform of PAP from leaves (PAP II) (*147*) and a mutant of PAP (PAPc) that exhibits full antiviral activity *in planta* but is not cytotoxic. Because of the separation of antiviral activity and ribosome-inactivating activity of PAPc, virus-resistant tobacco lines with a normal phenotype could be obtained (*147, 148*).

It should be noted that, in addition to having a defense role against plant pathogens, RIPs may also provide a regulatory role in cell metabolism. It has been observed that RIP activity appears to emerge, or elevate when seeds reach maturation (*149*), as well as in senescent or stressed leaves (*58*), in association with events accompanying inhibition of plant cell metabolism. Enzymatic action of RIPs on DNA (not discussed here) may certainly contribute to this regulation, because depurination may be adequate to disrupt transcription. Enzymatic activity on various RNA templates and on poly(A) tails point toward regulation of expression and cell metabolism. Age of the plant and the environmental conditions of its residence surely affect the activity of PAP. During senescence or when subjected to heat or osmotic stress, it was noted that the translational inhibitory action and DNA deadenylation have considerably increased in pokeweed's leaves (*58*).

Ready *et al. (14)* have treated pokeweed mesophyll cells with rabbit anti-pokeweed antiviral protein IgGs, followed by ferritin-conjugated goat anti-rabbit IgGs, and used electron microscopy to visualize the PAP localization within the pokeweed plant cells (Figure 1.13 A). Usually, the mesophyll cell wall has a natural granular appearance under the electron microscope in the absence of ferritin binding (Figure 1.13 B). PAP, as measured by ferritin binding, is densely concentrated outside the cytoplasmic membrane in the cell wall, and none was visualized on the inside, in the cytoplasm. Based on these micrographs, PAP is synthesized in the cytoplasm

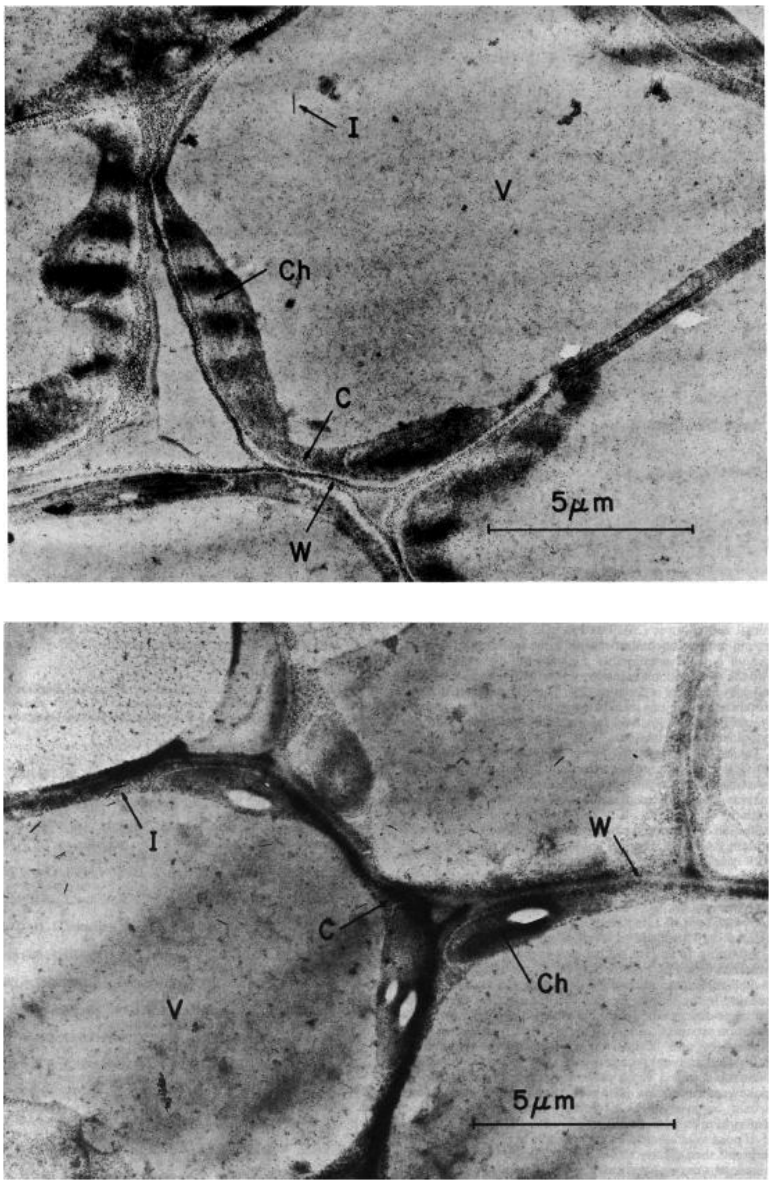

Figure 1.14 Localization of pokeweed antiviral protein in thin sections of pokeweed mesophyll cells. (A) Sections of cells were stained with rabbit anti-pokeweed antiviral protein, followed by ferritin-conjugated goat anti-rabbit IgG. V, vacuole; C, cytoplasm; Ch, chloroplast; W, cell wall; I, calcium oxalate inclusion. Note heavy ferritin binding in the wall matrix. The low contrast seen in these sections is a result of the fact that these tissues were not treated with osmium tetroxide prior to embedding and are not poststained with lead or uranium salts. (B) Control micrograph. Pokeweed mesophyll cells were stained with ferritin-conjugated goat anti-rabbit IgG without prior exposure to rabbit anti-pokeweed antiviral protein. Note the absence of ferritin binding in the cell wall.
This figure was a courtesy of Dr. Michael Ready, and adapted from Ready *et al. (14)*.

and extruded across the cellular membrane into the cell wall matrix (*14*). PAP was found in high density along the entire circumference of the wall, surrounding each cell in a pokeweed's cell envelope. The thickness of the enzyme-containing band was found to be at least 1600 nm wide, suggesting that the protein is not attached to the cell wall but is trapped within the cell wall matrix (*14*). There was no evidence how PAP was held within the cell wall matrix. This association is most likely weak because PAP can readily be obtained from water extracts of macerated leaf tissue. There is evidence that the protein binds weakly to some virus proteins, perhaps by salt bridges (*122*), and may actually be carried into the cytoplasm by the invader.

Type 2 RIPs follow a retrograde transport pathway through endosomes or Golgi to the ER and then the cytosol. This retrograde movement has been studied extensively for type 2 RIPs as well as for the ricin A-chain alone which has often been taken to be a model for the single chain type 1 RIPs. Initially it was thought that the single chain toxins might enter cells via passive mechanisms such as fluid uptake (*150*). However, different cell types vary considerably in their sensitivities to particular type 1 RIPs, even though fluid phase endocytosis should be occurring in all cell types. This observation, couples to the organ-specific toxicity of type 1 RIPs, suggests that specific mechanism(s) occur to permit their uptake. Overall, and in contrast with ricin, little is known about the intracellular pathways followed by type 1 RIPs and the compartment(s) from which they enter the cytosol has not been elucidated. While the precise details of the cellular entry pathway of most type 1 RIP into mammalian cells remain unknown, it seems that the absence of a cell-binding B polypeptide does not constitute an obligatory block on entry: type 1 possibly exploit normal endocytic uptake processes, even though their scope is considerably less than type 2 RIP counterparts (*151*). Recently, Baykal and Tumer have demonstrated that the *C*-terminus of PAP has distinct roles in transport to the cytosol, ribosome

depurination and cytotoxicity (*35*). Based on their experimental data, the authors have concluded that the *C*-terminal processing of the PAP precursor is necessary for export of PAP to the cytosol, and that the *C*-terminal residues 250-262 of the mature PAP are critical for its accumulation in the cytosol (*35*).

I-1-G Toxicity of RIPs and Bioterrorism

Reports about the use of ricin and abrin for homicidal purposes go back to ancient times. Nevertheless, usage of these toxins as regular weapons is a quite recent idea. The ease to acquire large amount of ricin, for example, made this toxin a good candidate for bioterrorism.

The US Chemical Warfare Service explored ricin as a feasible weapon during World War I. During World War II the British military developed, but never used, a ricin bomb termed the W-bomb (Compound W = ricin). In 1952 the US Army filed a patent on how to prepare ricin for weapon purposes (*152*). Later, this idea was given up, most likely because of the problems of delivery of high enough amount in aerosol form to make it an efficient weapon (*1*).

Certainly the extent to which ricin was collected for military purposes is not known, however it was intended to be employed in assassination of Georgi Markov, an exiled journalist who published incriminate information about the corrupt life of the Bulgarian communist leadership. On September 7th, 1978 Markov was poked with an umbrella carried by a man belonging to the Bulgarian secret police. “The man excused himself and rapidly left in a taxi” (*8*). Shortly after, Markov became ill and died. Autopsy of Markov’s body revealed that in the muscle beneath the site where he was poked by the umbrella a 90% platinum and 10% iridium alloy capsule of 1.52 mm in diameter containing two small holes was found containing 0.2 mg of

what is believed to have been ricin (*8*). The capsule must have been shot into the right thigh of Markov by a devise in the umbrella (*1*).

A month prior to Markov's assassination, another Bulgarian, Vladimir Kostov, obtained a small wound at a Paris subway station and shortly after became ill with fewer, but recovered. Examination led to the discovery of a similar platinum bullet. It contained ricin, and luckily for Kostov, the poison had not fully dissolved as the bullet had only penetrated the subcutaneous fat layer. Five more instances were identified where this assassination technique was used. It is probable that there were more cases as the uncharacteristic symptoms did not rise suspicions of poisoning (*1*). In the past decade ricin has been associated with terrorist organizations in several countries. The availability of improved anti-ricin vaccine (*153*) and better ability to trace and identify toxin in the body should make the toxin a less tempting compound for use in bioterrorism (*1, 154*).

Type 1 RIPs are certainly not as cytotoxic to higher animals, since they cannot cross the cell membrane on their own (*15*). Pokeweed plant synthesizes its toxin as a precursor and compartmentalizes it, as mentioned previously, within cell wall matrix. This ensures that the pokeweed's ribosomes never encounter its own toxin, leaving overall protein synthesis unaffected. In contrast to the healthy appearance of pokeweed, the expression of PAP in transgenic *N. tabacum* plants leads to various physiological changes (*2*). Transgenic tobacco plants producing high levels (more than 10 ng/mg protein) of PAP are sterile with a stunted, molted phenotype, which was correlated with the level of PAP expressed, whereas plants producing less than 1-5 ng PAP/mg protein are fertile and normal in appearance (*2, 143*).

The genes of PAP (*76*), PAP-II (*79*) and PAP-S (*155*) have been isolated from tissue specific cDNA libraries and sequenced. The PAP gene carries an open reading frame of 939 nt

coding for the mature PAP protein (262 amino acids) plus an *N*-terminal signal peptide of 22 amino acids (*76*) and a *C*-terminal extra peptide of 29 amino acids (*156*). This gene has been expressed in *E. coli* cells under an inducible (*lac*) promoter with an extremely low yield (0.13-0.16% of the total bacterial protein) (*157*). It was found that even the low level of gene expression slowed down significantly bacterial growth. Chen *et al.* also found that elimination of *N*-terminal signal peptide codons (22 amino acids) from the PAP gene led to an immediate cell death (*157*). The authors have concluded that PAP is highly toxic (*in vivo*) for prokaryotic cells (*158*).

I-1-H Immunotoxins and Other Conjugates of RIPs

In the late 1800s, it was found that when different dyes were injected into animals they specifically stained differential tissues. In 1906, Paul Ehrlich speculated (*159*) that this tissue specific affinity of dyes could be coupled with the toxicity of certain metals to generate a new class of tissue- and pathogen-specific drugs (*160*). This idea has been broadened and applied in the past years in augmentation of cell-specific reagents that have found their widest application in the elimination of unwanted target cells, particularly in the domain of cancer therapy. The construction of such cytotoxic agents is a theoretically simple task: attach a toxic substance or a mediator of toxicity to an appropriate vehicle molecule and you have a "magic bullet" that can find and eliminate the one-in-a-billion cells that have the requisite marker. The vehicle molecule directs recognition and binding capacity, while the associated toxic component effects cellular alterations leading to cell death (*160*).

The first carrier-toxin heteroconjugates of RIPs were prepared using polyclonal and later monoclonal antibodies with toxins that were able to block protein synthesis at the ribosome level. Biospecific agents other than monoclonal antibodies (hormones, growth factors, antigens,

cytokines, etc.) have also been employed in developing cell-targeting conjugates (*161*). Toxins of different types can be used to construct effective immunotoxin (IT) conjugates, including plant, bacterial and fungal toxins. RIPs (*56*) have been extensively used in preparation of such ITs. These chimeric ITs can be made with either type 1 or type 2 RIPs (*162*). The linkage of the carrier molecule to the toxin can be attained by chemical cross-linking, indirect linking, or gene fusion (*163*).

Several lines of research have effectively used PAP as component of IT, conjugated to a variety of monoclonal antibodies. Jansen *et al.* (*164*) have used B43-PAP immunotoxin plus cyclophosphamide to successfully treat human leukemia in mice with severe combined immunodeficiency (SCID). Uckun *et al.* have used B43 (anti-CD19)-PAP ITs in treatment of human pre-B acute lymphoblastic and other types of leukemia in mice (*165-168*). Erice *et al.* (*169*) have found that PAP conjugated to monoclonal antibodies recognizing CD4, CD5, or CD7 antigens effectively inhibited HIV-1 replication in normal $CD4^+$ T cells infected with HIV-1 strain LAV_{BRU}, as well as in activated T cells from two asymptomatic HIV-1-seropositive individuals (*170*). All of the above and many other lines of evidence point toward potential therapeutic PAP-immunoconjugate applications of this protein against a variety of cancer lines as well as HIV-1.

I-2 REGULATIONS AND CONTROL OF RNA TRANSLATION

I-2-A Initiation of Cellular mRNA Translation

Protein synthesis is divided into three steps: initiation, elongation and termination. Initiation refers to the assembly of a translation-competent ribosome at the AUG start codon on an mRNA. Translation elongation is the codon-dependent assembly of a polypeptide. Termination involves release of the completed protein when the ribosome reaches a termination

codon. These three steps are facilitated by *trans*-acting proteins that are referred to, respectively, as eukaryotic initiation factors (eIF), elongation factors (eEF) and release factors (eRF) (*171*). The initiation phase of protein synthesis can be further divided into three steps (Figure 1.15). First, the specific initiator methionyl–transfer RNA (Met–$tRNA_i^{Met}$) binds to the small (40*S*) ribosomal subunit to form a 43*S* pre-initiation complex. Then, the 43*S* complex binds to an mRNA to form a 48*S* pre-initiation complex that scans the AUG start codon. Finally, the large (60*S*) ribosomal subunit joins this complex to form an 80*S* ribosome (*172*). As might be expected for a complex biochemical process, the initiation phase of translation is a common target for regulation.

External cues are transduced to regulate protein synthesis by several diverse mechanisms, including posttranslational modification of translation factors or binding of regulatory proteins to the 5′- or 3′-untranslated regions (UTRs) of specific mRNAs (*173*). To understand translational regulatory strategies, here, we briefly review the translation pathway and the roles of the translation factors (*174, 175*). The translation factor eIF2, which is a G protein, binds to Met–$tRNA_i^{Met}$ in a GTP-dependent manner. This ternary complex associates with the 40*S* subunit and other initiation factors, including eIF1, eIF1A, eIF3 and possibly eIF5, to form the 43*S* preinitiation complex. The binding of the 43S complex to an mRNA is facilitated by the eIF4 family of translation factors (*176*). In addition to the AUG start codon, the 5′-7-methyl-GTP (m^7GTP) cap and the 3′-poly(A) tail on mRNAs are also important in translation initiation. The cap-binding complex eIF4F consists of the m^7GTP cap-binding protein eIF4E, the DEAD-box RNA helicase eIF4A and the scaffolding protein eIF4G (*177, 178*). Interestingly, eIF4G also binds to the poly(A)-binding protein (PABP) and the 43*S* component eIF3. Through its interactions with both eIF4E (binding to the mRNA cap) and PABP (binding to the mRNA

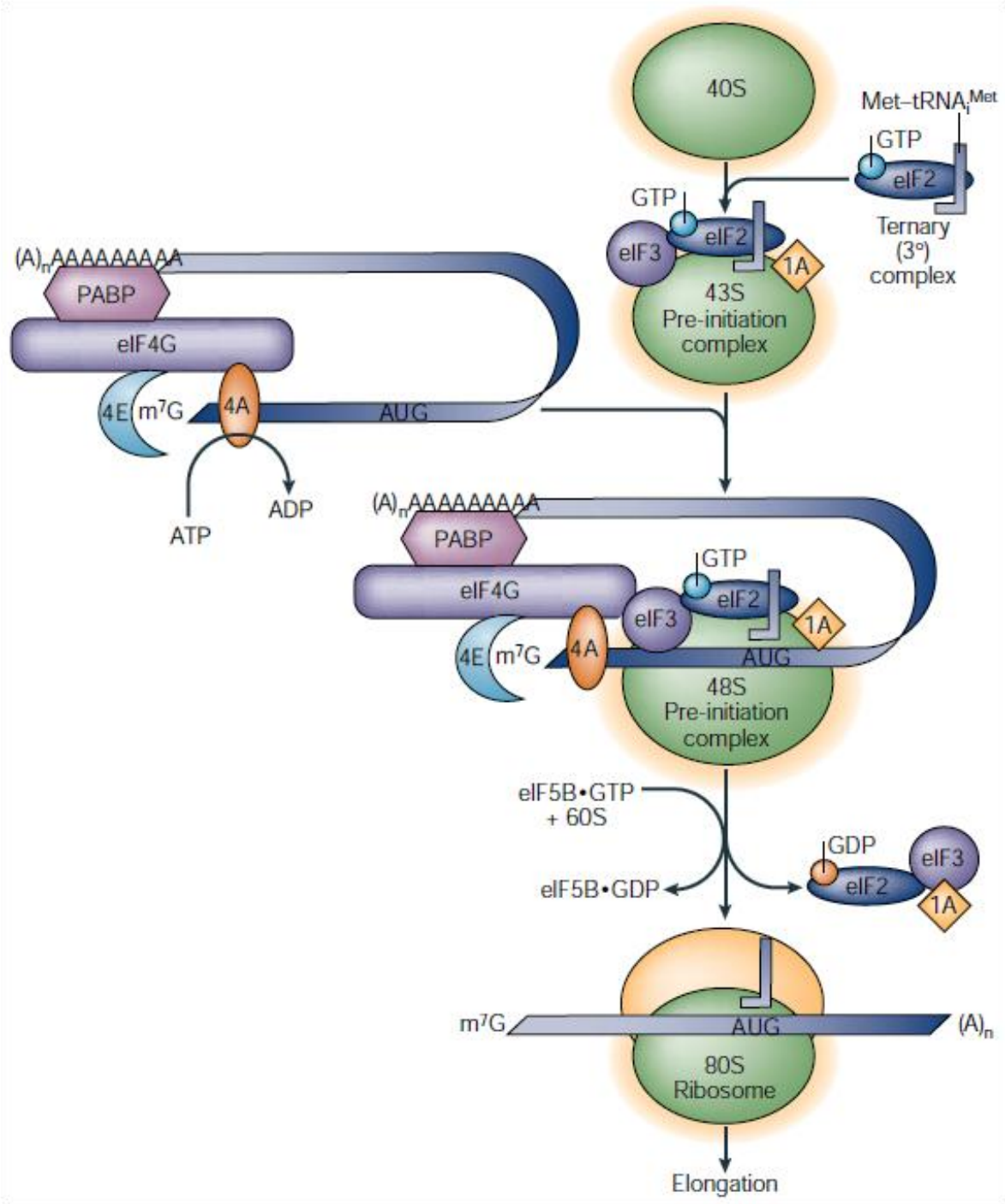

Figure 1.15 Pathway of translation initiation in eukaryotes. See text for detailed explanation. This figure was adapted from Klann *et al. (172)* and reprinted with the permission from Elsevier provided by Copyright Clearance Center (Licence # 2639710560291).

poly(A) tail), eIF4G effectively circularizes mRNAs. This mRNA circularization might similarly enhance eIF4F binding and 48*S* complex formation, providing a mechanism for the synergistic enhancement of translation by these modifications (*179*). The eIF4A component of eIF4F, with the initiation factor eIF4B, is thought to unwind secondary structures at the 5′ end of mRNAs. These mRNA-remodeling activities, in combination with the eIF4G–eIF3 interaction, are thought to promote the binding of the 43*S* complex to the mRNA, which forms the 48*S* pre-initiation complex (*176*).

After binding close to the 5′ end of the mRNA, the ribosomal complex migrates or scans down the mRNA and usually stops at the first AUG codon it encounters. Stable secondary RNA structures in the 5′ UTR or proteins that are bound to the 5′ UTR impede ribosome binding and scanning, thereby inhibiting translation (*173*). eIF4A or other helicase activities might remodel the 5′ UTR to facilitate ribosomal binding and scanning (*180*). Recognition of the start codon triggers hydrolysis of GTP by eIF2, which leads to the release of factors from the 48S complex and allows the eIF5B- and GTP-dependent joining of the large ribosomal subunit. eIF2, which is now bound to GDP, is then released from the 48*S* complex. Similar to many G proteins, eIF2 has a higher affinity for GDP than for GTP, and the guaninenucleotide exchange factor (GEF) eIF2B catalyses the exchange of GTP for GDP on eIF2, thereby recycling eIF2 for further rounds of translation initiation (*172*).

Translation factors and translational control mechanisms are downstream targets of several signaling pathways and are crucial during development and cellular stress responses. Many forms of translational control are homeostatic responses that alter general protein synthesis. However, reduced nutrient availability, oxidative stress, viral infection and misfolded proteins trigger inhibition of general protein synthesis, but stimulate translation of specific

mRNAs. This gene-specific translational control depends on regulatory elements in the mRNA, such as upstream open reading frames (uORFs), RNA secondary structures or regulatory protein-binding sites (*174*). So, mRNA specificity in translational control can be achieved through mRNA-specific binding proteins or through alterations to the general translational machinery. Downregulation of general protein synthesis has been linked to several forms of mRNA-specific translational control. For example, mRNAs that compete poorly for initiation factors and ribosomes are hypersensitive to small reductions in translational activity and their translation is preferentially inhibited (*172*).

I-2-B Cap-Independent Translation of Plant Viral RNAs Containing Genome-Linked Proteins (VPg)

As described in the preceding section, efficient translation of eukaryotic mRNAs is thought to occur in a closed loop format, in which the 5'- and 3'-termini are brought into close proximity through the mediation of interactions involving translation initiation factors (*175, 179*). The key interactions involve PABP bound to the 3'-poly(A) tail and initiation factor eIF4E bound to the 5' cap, and the interactions of both proteins with scaffolding eIF4G protein. The isoforms eIF*iso*4G and eIF*iso*4E found in plants participate in similar interactions. These simultaneous interactions mutually increase binding affinities, stabilizing the closed loop. The 40*S* small ribosomal subunit associates with the 5'-end of the mRNA via its interaction with eIF3, which simultaneously binds eIF4G, and then initiates scanning towards the 3'-end (*181*).

Systemic infection of plants occurs when a virus establishes genome amplification, then cell-to-cell movement (*182*). In many cases these factors involve one or more proteins involved in virus replication and/or transport. Translation of viral RNAs by the host machinery is a crucial

event in the virus cell cycle and proceeds essentially as for cellular mRNAs (*183*). However, members of less than 20% of plant positive strand RNA viral genera have genomic and subgenomic mRNAs structured like host mRNAs, with a 5'-cap and poly(A) tail (*184*). The majority lacks one or both of these features. The evidence indicates that the closed loop model of the mRNA is applicable in these cases, with a variety of novel interactions substituting for the molecular bridging contacts that occur in normal cellular mRNAs.

Animal viruses have elaborate strategies that allow the preferential translation of viral mRNAs (*185*), with the consequence that host protein synthesis is usually blocked. This phenomenon is known as host translation shutdown. The most studied example of a block in translation involves the animal picornaviruses. The genus *Potyvirus* contains more than 200 members and belongs to the largest plant virus family, *Potyviridae* (*184*), similar to those of picornaviruses. Potyviruses have flexuous filamentous particles that contain an approximately 10 kilobases positive-sense single-stranded RNA that is covalently linked to a virus genome-linked protein (VPg) at the 5' end via a tyrosine residue (*186*) (Figure 1.16) and polyadenylated at the 3' end (*187-189*). The RNA has a single open reading frame that is translated into a large polyprotein, which is proteolyticaly processed into mature proteins by dedicated virus-encoded proteases (*190*). Potyviruses differ from picornaviruses in that their VPgs are several fold larger and the 5' UTRs are several fold shorter (~150 nt for potyviruses versus 600-1200 nt for picornaviruses), less structured than those of picornaviruses and do not contain more than one upstream AUGs (*191*). Highly structured 5' UTRs with embedded AUG triplets are typical of the well-characterized picornaviral IRES elements that confer cap-independent translation (*191*). Below is a brief description of two potyviral representatives – *Turnip Mosaic Virus* (TuMV) and *Tobacco Etch Virus* (TEV).

5`- GCGAAAGGCAAGAGGCAAAGACAGAAACTAAAGTTTCGCAATGCCCGAGAT
AACAAGATGGGTAGAGAAGTATATGGAGATGATGAAACCATAGAGCATTTCT
TTGGTGATGCCTACACAAAGAAAGGGAAGAGCAAGGGCAGGACACGTGGTA
TCGGACACAAAAACAGGAAGTTCATCAACATGTATGGGTTCGATCCTGAAGA
TTTCTCTGCTGTTCGTTTTGTGGATCCACTCACAGGAGCGACGTTGGATGA
CAACCCGCTCACAGACATCACCCTTGTGCAAGAGCACTTTGGCAACATAAGA
ATGAACTTACTCGGGGAAGATGAGCTGGACCCAAATGAAATACGTGTGAATAA
GACAATTCAGGCATACTACATGAACAATAAAACAGGCAAGGCTTTGAAAGTGG
ATCTGACACCACACATACCTCTCAAGGTGTGTGATCTTCACGCAACCATTGCT
GGATTCCCAGAGCGAGAAAACGAACTGAGGCAGACCGGAAAGGCTCAGCCCA
TTAACATAGATGAAGTGCCAAGAGCTAATAATGAACTCGTTCCGGTGGACCAC
GAG **- 3`**

H_2N – akgkrqrqkl kfrnardnkm grevygdddt iehffgdayt kkgkskgrtr gighknrkfi
nmygfdpedf savrfvdplt gatlddnplt ditlvqehfg nirmdllged eldsneirvn
ktiqayymnn ktgkalkvdl tphiplkvcd lhatiagfpe renelrqtgk aqpinidevp
rannelvpvd he hhhhhh – COOH

Figure 1.16 **(A)** cDNA sequence of the VPg gene. pETVPg1 vector and the sequence of VPg is a curtsey of Professor H. Miyoshi, Department of Mictobiology, St. Marianna University School of Medicine, Japan. **(B)** Amino acid sequence of VPg-His_6.

***Turnip Mosaic Virus* (TuMV) and *Tobacco Etch Virus* (TEV)**

Turnip mosaic virus (TuMV) is a member of the genus *Potyvirus* (*184*) and infects cruciferous plants throughout the world (*192*) (Figure 1.17). Cruciferous plants include a large variety of economically important crops belonging to different genera like horseradish, cabbage, broccoli, cauliflower, mustard seeds, and many others. Many TuMV isolates in the world have been classified into several strains or pathotypes (*193*). These classifications were based on host range, but the factors affecting the virus host range in cruciferous plants are not clear. The genome of TuMV encodes one large polyprotein, which is cleaved into at least ten mature proteins by three viral proteases (Pro) (*194*). In our research we have used VPg from TuMV. The potyviral VPg is 21.1 kDa.

Several functions have been attributed to Potyvirus VPg. First, the viral protein and its precursor form, VPg-Pro, interact with, and have stimulating effect on the activity of, the viral RNA-dependent RNA polymerase (RdRp), suggesting participation in virus replication (*195-198*). Moreover, interaction between VPg with eIF4E has been reported (*188, 199, 200*). The importance of this factor for TuMV replication has been shown in mutant *Arabidopsis thaliana* plants that do not express eIF*iso*4E (*201, 202*). Although these plants had a normal phenotype, they were immune to TuMV. VPg has also been shown to have a role in overcoming viral resistance in plants (*203-209*). Leonard *et al. (210)* have shown that eIF4E isomers and PABP are able to interact with VPg-Pro of TuMV *in planta*, suggesting a role for this viral protein in translation initiation recruitment. Myoshi *et al.* (*211*) have used surface plasmon resonance (SPR) and shown that the binding affinity of VPg for eIF*iso*4E is stronger than that of capped RNA, suggesting that viral VPg is able to interfere with formation of a translational initiation complex on host plant cellular mRNA by sequestering eIF*iso*4E. Experiments with affinity

A

B

Figure 1.17 **(A)** Uninfected cabbage of Cruciferous family. **(B)** Cabbage infected with Turnip mosaic virus. This figure was a courtesy of Dr. Tom Zitter (*212*).

affinity chromatography showed that VPg forms a ternary complex with eIF*iso*4E and eIF*iso*4G, suggesting that VPg may participate in viral translation initiation by functioning as an alternative cap-like structure (*211*) (Figure 1.18). Khan *et al.* (*213*) have used fluorescence stopped-flow studies and have shown that eIF*iso*4E and eIF*iso*4F rapidly bind to VPg, suggesting kinetic competition between VPg and m^7G cap because VPg bound to eIFs much faster than cap analogs. Also, Goss laboratory has shown that there was an enhancement of eIF*iso*4F-VPg binding with the addition of a structured RNA derived from TEV (see below), thus suggesting that translation initiation involving VPg occurs at an internal ribosome entry site (*213*), and possibly direct participation of VPg in the translation of the viral genome. Later, Khan *et al*. have shown that VPg stimulates the *in vitro* translation of uncapped IRES-containing RNA and inhibits capped RNA translation in *Triticum aestivum* (wheat germ) extract (*214*) (Figure 1.19). Stimulation of an *in vitro* translation of uncapped IRES-containing RNA and inhibition of capped RNA translation appear to depend on VPg-eIF/*iso*4E interactions.

Tobacco mosaic virus (TEV) is a plant pathogenic virus in the genus *Potyvirus* and the family *Potyviridae (215).* Like other members of the *Potyvirus* genus, TEV is a monopartite strand of positive-sense, single-stranded RNA surrounded by a capsid made of a single viral protein. The virus is a filamentous particle that measures about 730 nm in length. It is transmissible in a non-persistent manner by more than ten species of aphids including *Myzus persicae*. It also is easily transmitted by mechanical means but is not known to be transmitted by seeds. The virus infects many species of *Solanaceae*. *Solanaceae* is a family of flowering plants that contains a number of important agricultural crops as well as many toxic plants. The family is also informally known as nightshade – or potato family. The family includes *Datura* (Jimson weed), *Mandragora* (mandrake), *belladonna* (deadly nightshade), *Capsicum* (paprika, chili

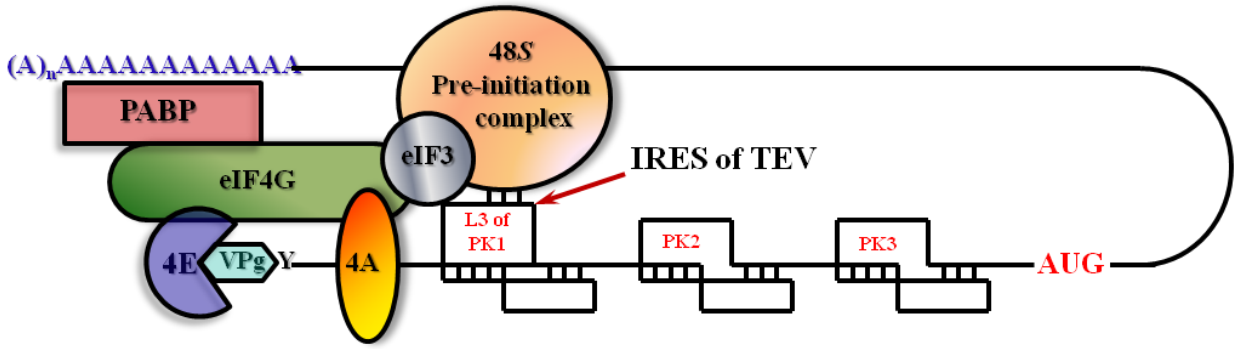

Figure 1.18 Depiction of VPg functioning as an alternative cap-structure in initiation in translation of uncapped Tobacco Etch virus (TEV) RNA that has a poly(A) tail and a 5' VPg covalently linked via a tyrosine residue (Y). VPg interacts with the cap-binding translation initiation factors 4E/*iso*4E which, in turn, interacts with the scaffolding protein eIF4G/*iso*4G. Poly(A) binding protein (PABP) binds to the poly(A) and simultaneously to eIF4G/*iso*4G, thus completing circularization of TEV RNA. 5' leader of TEV RNA contains three pseuknots (PK) within its secondary structure. PK1 is sufficient to confer cap-independent translation and loop 3 (L3) within PK1 contains an internal ribosome entry site (IRES) that is complementary to the ribosomal sequence (*213*, *216-218*).

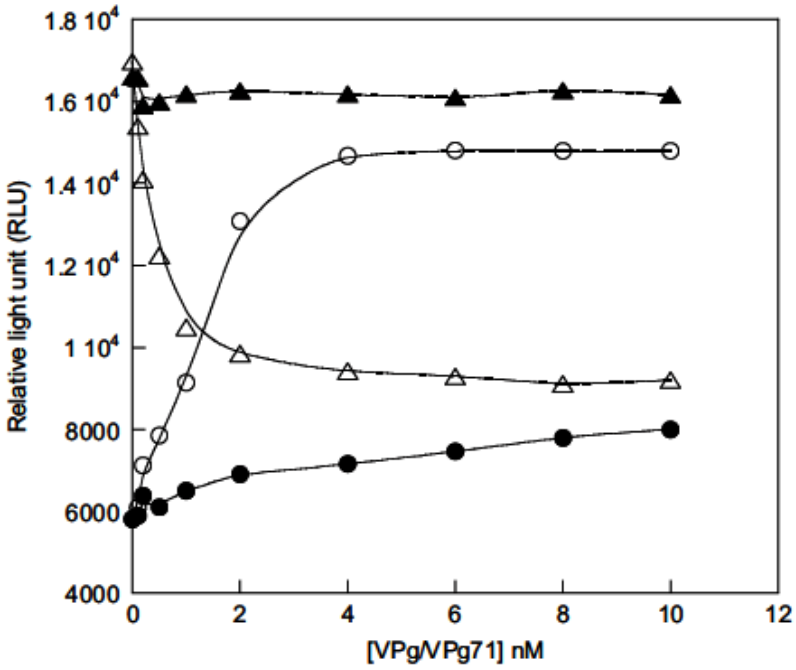

Figure 1.19 Translation of luciferase reporter TEV RNA constructs in wheat germ extracts. Luciferase relative light units were measured for capped $TEV^{1\text{-}143}$-*luc*-A_{50} RNA + wt VPg (Δ), capped $TEV^{1\text{-}143}$-*luc*-A_{50} RNA + VPg71 (▲), uncapped $TEV^{1\text{-}143}$-*luc*-A_{50} RNA + wt VPg (○), and $TEV^{1\text{-}143}$-*luc*-A_{50} RNA + VPg71 (●) in wheat germ translation extract. The reactions were incubated at 22 ^{o}C for 2 h with varying concentrations of VPg (0 – 10 nM) in the presence of 1.0 μM $TEV^{1\text{-}143}$-*luc*-A_{50} RNA, and light emission was measured after the addition of 0.5 mM of luciferase substrate.
This figure was a courtesy of Dr. Mateen Kahn, and was adapted from Khan *et al.* (*214*).

pepper) (*219*) (Figure 1.20), *Solanum* (potato, tomato, aubergine or eggplant), *Nicotiana* (tobacco), and *Petunia* (petunia).

The genomic RNA of TEV is polyadenylated and naturally lacks a 5'-cap but is nevertheless efficiently translated. The 143-nt TEV 5'-leader is sufficient to confer cap-independent translation (*220, 221*). Niepel and Gallie (*222*) have identified two regions within the TEV 5' leader that are necessary to direct cap-independent translation. The TEV 5'-leader is known to functionally interact with the poly(A) tail to promote optimal cap-independent translation and requires eIF4G and PABP (*222, 223*). Zeenko and Gallie (*217*) have shown that the pseudoknot 1 (PK1) within the structure of TEV 5'-leader is able to confer cap-independent translation, and contains an internal ribosome entry site (IRES) (Figure 1.21). Cap-independent translation supported by TEV IRES is eIF4G-dependent (*223*), raising the possibility that this initiation factor is directly or indirectly recruited to the IRES, stabilizing the closed loop format of translation. Furthermore, it has been shown that PK1 of TEV 5'-leader preferentially binds to eIF4G rather than eIF*iso*4G (*218*), and these interactions were quantified by fluorescence spectroscopy. It was also shown that the binding interactions between eIF4F and eIF4B are increased in the presence of PABP (*224*), further supporting these findings.

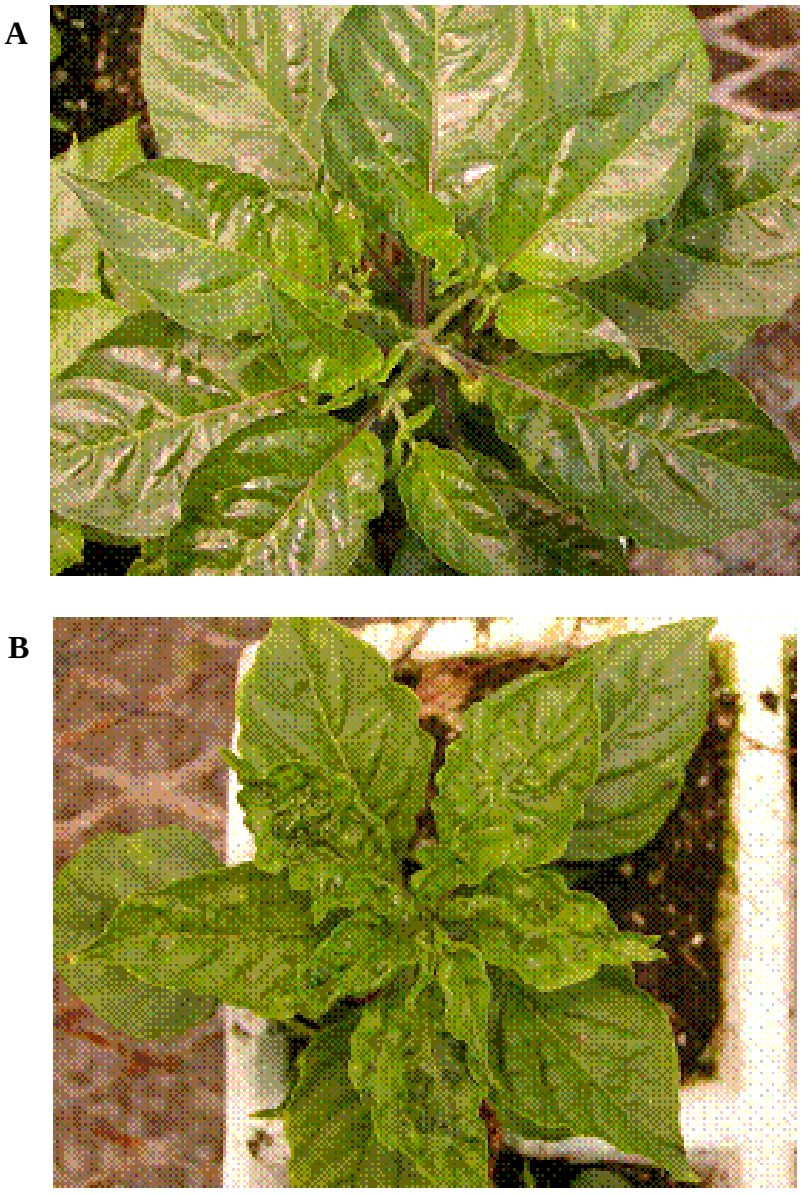

Figure 1.20 **(A)** Uninfected pepper plant of Piperaceae family. **(B)** Pepper plant infected with Tobacco Etch Virus.
These figures were a courtesy of Dr. Molly Jahn (*225*).

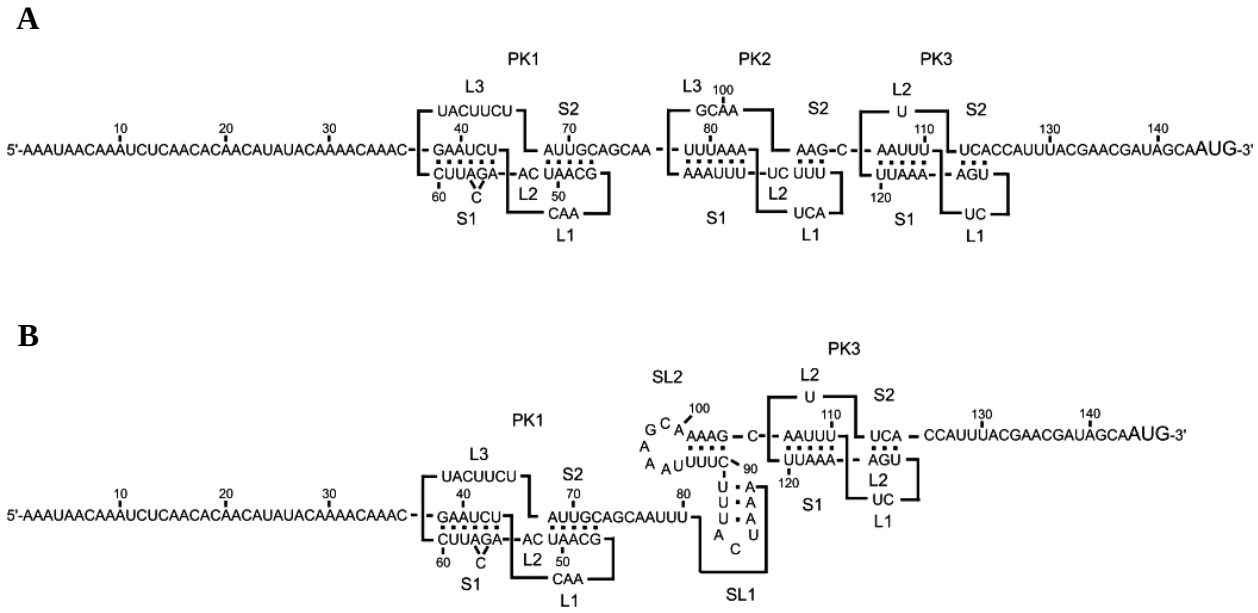

Figure 1.21 The predicted structure of the TEV 5'-leader. **(A)** The entire TEV 5'-leader (nt 1-143) is displayed with the predicted structure of the three pseudoknots, *i.e.* PK1, PK2, and PK3. The stems (*e.i.* S1 or S2) and loops (*e.g.* L1, L3, or L3) for each pseudoknot are indicated. **(B)** The TEV 5'-leader containing an alternative structure, *i.e.* SL1 and SL2, in place of PK2 is shown. This alternative structure is also consistent with the enzymatic and chemical probing data. The AUG at the 3' terminus represents the initiation codon of the TEV polyprotein-coding region (*217*).

This figure was a courtesy of Dr. Daniel Gallie, and was adapted from Zeenko and Gallie (*217*) (*129*) © The American Society of Biochemistry and Molecular Biology.

I-3 RATIONALE OF THE PRESENT RESEARCH

PAP is a cap-binding protein and has been shown to preferentially bind to the m^7GpppG cap structure at the 5'-end of viral mRNA and, thus access it for depurination, reducing infectivity of plant and animal viruses. Despite this cap-dependent model for mRNA depurination, it does not clarify the inhibitory effect of PAP on the replication of uncapped viruses. VPg, on the other hand, is a viral protein that interacts with the translation initiation factors, suggesting that it is important in the initiation of protein synthesis, perhaps substituting for the cap structure in cap-independent translation. VPg has been shown to stimulate the *in vitro* translation of uncapped IRES-containing RNA and inhibit capped RNA translation in wheat germ extract. Our experiments indicate that PAP possesses high affinity for VPg, almost twice as high as for m^7GTP cap analog. This being said, we have hypothesized that binding of PAP to VPg will selectively direct the depurination of uncapped viral RNA to that of capped cellular RNA by targeting PAP to the IRES of viral RNA. We have used fluorescence spectroscopy and HPLC techniques to quantify the above interactions, and examine the effect of VPg on depurination of uncapped and m^7GpppG-capped RNAs.

Our experimental results indicate that VPg diminishes the depurination of both uncapped and m^7GpppG-capped RNAs. Moreover, our data indicate that VPg competes with TEV RNA for PAP binding. Several conclusions can be drawn from our findings. First of all, PAP binds to and depurinates both uncapped and m^7GpppG-capped RNA transcripts. This supports previous conclusions that the cap structure is not the only determinant for inhibition of translation by PAP. Secondly, VPg decreases depurination of uncapped and m^7GpppG-capped RNAs and competes with TEV RNA for PAP binding. This supports the notion that VPg is a pivotal factor in overcoming viral resistance by providing virus with an evolutionary advantage to propagate its

genes and proliferate inside the infected host by suppressing the defense mechanism of the plant. Depurination inhibition by VPg also suggests the possible use of this protein against cytotoxic activity of RIPs and inhibition of their biological activity.

II EXPERIMENTAL PROCEDURES

II-1 EXPERIMENTAL MATERIALS

All chemicals used, unless otherwise noted, were of molecular biology grade. All solvents, unless states otherwise, were of HPLC grade. Tris(hydroxymethyl)aminomethane hydrochloride (Tris-HCl), soybean trypsin inhibitor (STI), agarose, 4-(2-hydroxyehtyl)-1-piperazineethanesulfonic acid (HEPES), aprotinin, magnesium chloride ($MgCl_2$), potassium chloride (KCl), phenylmethylsulfonyl fluoridate (PMSF), ethidium bromide (EtBr), diethylpyrocarbonate (DEPC), ethylenediaminetetraecetic acid (EDTA), isatoic anhydride, chloroacetaldehyde (CA), ammonium chloride (NH_4Cl), diethylaminoethyl (DEAE), adenosine 5'-triphosphate (ATP), guanosine 5'-triphosphate (GTP), cellulose phosphate, dithiothreitol (DTT), *N,N,N',N'*-tetramethylenediamine (TEMED), *n*-butyl alcohol, bromphenol blue, sodium dodecylsulfate (SDS), 2-(*N*-morpholino)ethanesulfonic acid (MES), sodium chloride (NaCl), poly(ethylene glycol) (PEG), β-mercaptoethanol (β-ME), the m^7GTP cap analog, RnaseZAP™, Silver Staining Kit, ammonium persulfate ($(NH_4)_2S_2O_8$), ultrapure glycerol, and Sephadex® G-25 were purchased from Sigma-Aldrich Co. (St. Louis, MO, USA). Chloramphenicol (Cm), ampicillin (Amp), kanamycin (Km), regenerated cellulose dialysis tubing of varying MWCO, hydrochloric acid (HCl), potassium hydroxide (KOH), sodium hydroxide (NaOH), sodium acetate (CH_3COONa, or NaAc), *N*,*N*'-methylenebisacrylamide, ammonium hydroxide (NH_4OH), ammonium sulfate ($(NH_4)_2SO_4$), agar, peptone, and yeast extract were purchased from Fisher Scientific Co. (Pittsburg, PA, USA). Methyl alcohol (MeOH), ethyl alcohol (EtOH), *n*-propyl alcohol (PrOH), diethyl ether (Et_2O), acrylamide, and polyvinylpyrrolidone (PVP) were purchased from Spectrum Chemical Co. (New Brunswick, NJ, USA). RiboMAX™ large scale RNA Production System T7 and SP6 were used for *in vitro* RNA and S/R oligo synthesis, and

were purchased from Promega Co. (Madison, WI, USA), as well as RNA Purification Kits, dioxane-free isopropyl β-D-thiogalactopyranoside (IPTG), nuclease-free water, and Ribo m^7G cap analog. The *Sal*I and *Nco*I restriction endonucleases, λ DNA and RNA and microRNA markers were obtained from New England Biolabs, Inc. (Ipswich, MA, USA). Sephadex® LH-20, 7-methyl-GTP Sepharose™ 4B (Pharmacia Biotech), low, high, and broad range molecular weight protein calibration markers were acquired from Amersham Biosciences, part of GE Healthcare (Pittsburg, PA, USA), as well as HiTrap™ FF chromatography columns (Mono Q HP and SP HP ion exchange columns, and nickel-nitrilotriacetic acid Superflow or Ni Sepharose™). Plasmid Isolation, Purification, and Gel Extraction Kits were obtained from Qiagen Co. (Valencia, CA, USA). *E. coli* Subcloning Efficiency™ DH5α™, One Shot® BL21(DE3)pLysS™ Competent Cells, and SYBR® Gold nucleic acid gel stain were from Invitrogen Co. (Carlsbad, CA, USA). Pierce® NHS-Fluorescein Antibody Labeling Kit and Pierce® Coomassie Plus – The Better Bradford™ Assay Kit were procured from Thermo Scientific Co. (Rockford, IL, USA). Complete Protease Inhibitor Cocktail Tablets were obtained from Roche Molecular Biochemicals Inc. (Nutley, NJ, USA).

II-2 EXPERIMENTAL INSTRUMENTATION AND EQUIPMENT

A Horiba Jobin Yvon FluoroMax®-3 fluorometer (Edison, NJ, USA) at the Science Department of John Jay College of Criminal Justice, CUNY (Dr. Diana Friedland's Laboratory) (Figure 2.1) possesses a 150 W xenon lamp with photodiode array detectors was used to acquire steady state fluorescence spectra in UV region, and allowed to use intrinsic and extrinsic protein fluorophores. SPEX-Fluorolog-τ-2 spectrophotometer from BWTEK Inc. (Newarkm DE, USA) at the Chemistry Department of Hunter College, CUNY (Dr. Dixie Goss' Laboratory) was used

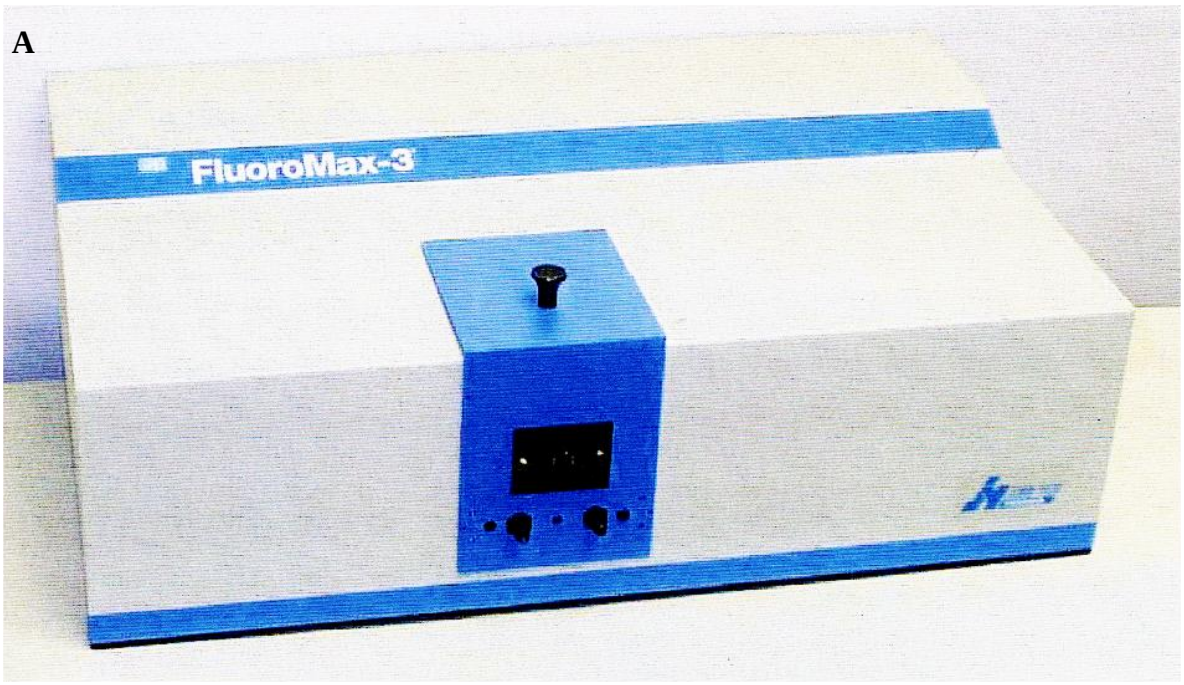

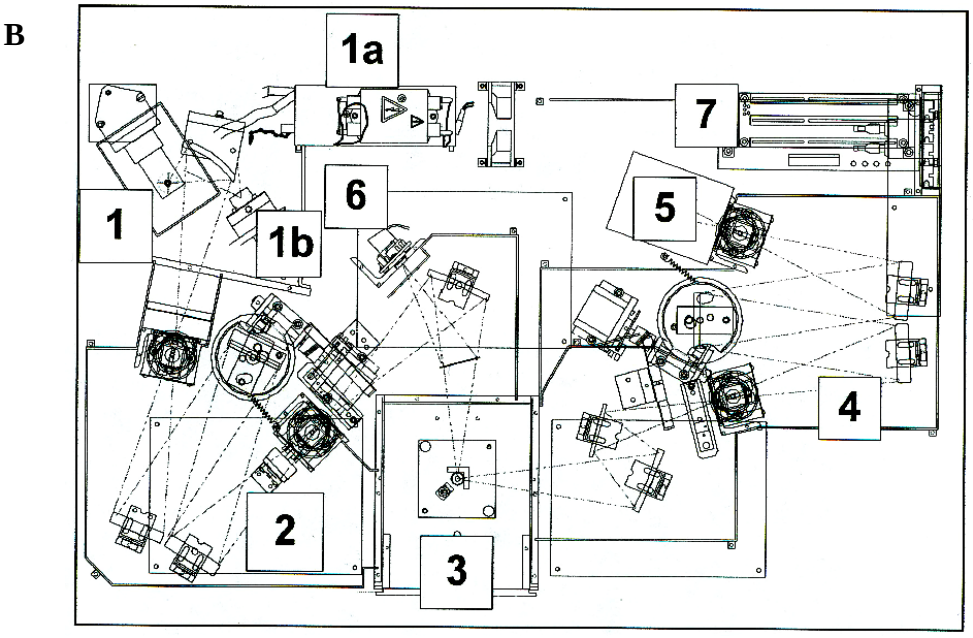

Figure 2.1 **(A)** A Horiba Jobin Yvon FluoroMax®-3 fluorometer (Edison, NJ, USA) at the Science Department of John Jay College of Criminal Justice, CUNY (Dr. Diana Friedland's Laboratory). **(B)** Schematic diagram of spectrofluorometer: 1, xenon arc-lamp and lamp housing; 1a, xenon lamp power supply; 1b, xenon flash lamp (FluoroMax®-P only); 2, excitation monochromator; 3, sample compartment; 4, emission monochromator; 5, signal detector (photomultiplier tube and housing); 6, reference detector (photodiode and current-acquisition module); 7, instrument controller.
This figure was adapted from FluoroMax®-3 fluorometer manual.

in experiments entailing high excitation intensity; it possesses a higher intensity (450 W) xenon arc lamp. Both fluorometers are equipped with FluorEssence Softwear from Horiba Scientific Co. which allowed for the analysis of the obtained data. All protein preparations and purifications were performed in an Isotemp Chromatography Refrigerator (+4^{o} C) from Fisher Scientific Co. Protein purification was accomplished using ÄKTApurifier system from GE Healthcare, equipped with Pump P-900, Monitor UV-900, Monitor UPC-900, Valve INV-907 and Mixer M-925 (Figure 2.2). All proteins, DNA and RNA samples, and temperature sensitive reagents were stored in either +4^{o} C Laboratory Refrigerator (Fisher Scientific Co.), in 70^{o} C REVCO Freezer from Cryostar Industries, Inc. (Westbury, NY, USA), or in 150^{o} C Cryogenic Preservation System, QUEUE Cryostar from Thermo Electron Co., part of Thermo Scientific. Distilled water used for all experiments, buffer and reagent preparations was deionized through a MILLI-Q^{TM} Water System equipped with Barnstead VWR Catridges from VWR$^{®}$ International (Bridgeport, NJ, USA). Enzymatic activity of PAP was measured and analyzed with a Waters high-pressure liquid chromatograph (HPLC) equipped with a Waters 2487 dual λ absorbance detector, a Waters 2475 multi λ fluorescence detector, Waters 600 controller and a Waters 717$_{plus}$ autosampler (Waters Co., Milford, MA, USA) (Figure 2.3). The column (4.6 x 150 mm) was reversed-phase XBridge^{TM} C_{18} (particle size 5 μm) purchased from Waters Associates. Empower 3 software (Waters Co.) was used to analyze the HPLC data. To disrupt cellular membranes of *E. coli* cells during protein purification, 60 Sonic Dismambrator equipped with Ultrasonic Converter and mini probe (Fisher Scientific Co.) was used. ACME^{TM} Supreme JUICERator$^{®}$, Model 6001, was used during homogenation of pokeweed plant cells. SORVALL$^{®}$ RC5C/Plus Centrifuge equipped with SOVRALL$^{®}$ SS-34 Rotor (Thermo Scientific) was used for cellular debris separation at speeds not exceeding 15,000 rpm. SORVALL$^{®}$ Discovery 100SE Centrifuge

A

B

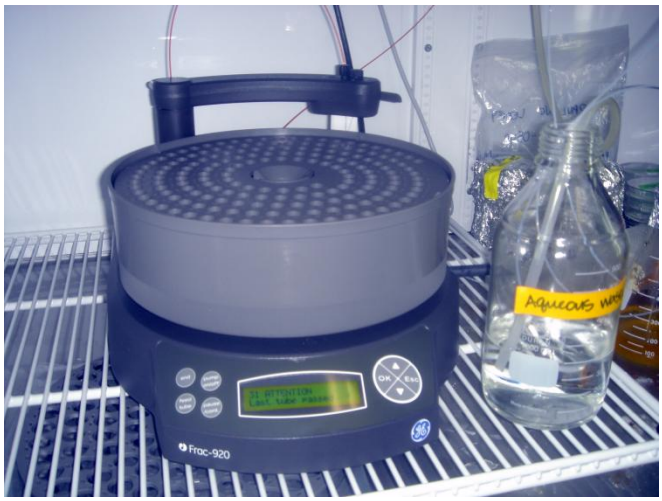

Figure 2.2 **(A)** ÄKTApurifier system from GE Healthcare, equipped with Pump P-900, Monitor UV-900, Monitor UPC-900, Valve INV-907 and Mixer M-925. **(B)** Automatic fraction collector, Frac 920.

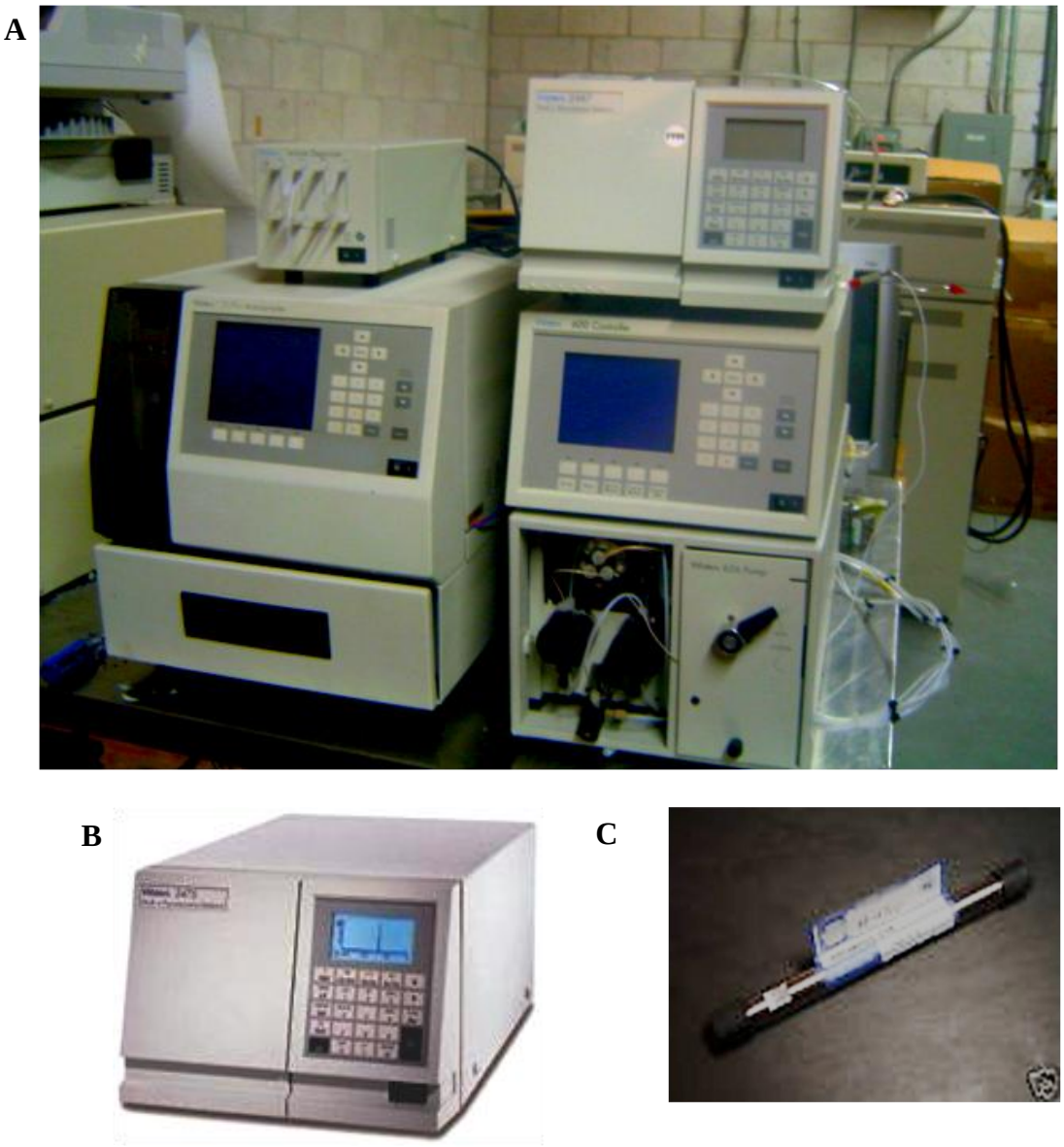

Figure 2.3 **(A)** Waters high-pressure liquid chromatograph equipped with a Waters 2487 dual λ absorbance detector (set at 254 nm), Waters 600 controller and a Waters 717_{plus} autosampler, and **(B)** a Waters 2475 multi λ fluorescence detector (excitation, 315 nm; emission, 415 nm). **(C)** The column (4.6 x 150 mm) was reversed-phase XBridge^{TM} C_{18} (particle size 5 μm) purchased from Waters Associates.

from Hitachi (Thermo Scientific) equipped with SORVALL® TV-850 Rotor was used for ultracentrifugation at speeds of approximately 45,000 rpm. SORVALL® 50 mL tubes from Kendro Laboratory Products (Thermo Scientific) were used for the above sample preparations. In addition, Eppendorf Centrifuge 5415D and temperature controlled Centrifuge 5415R were employed for small sample separations (Eppendorf International Co., Hauppauge, NY, USA). Centricone® Centrifugal Filter Devices from Millipore® (Fisher Scientific Co.) were used for sample separation, concentration, and buffer exchange. Excella E24 Incubator Shaker Series from New Brunswick Scientific (Edison, NJ, USA) was utilized for bacterial culture growth and induction, as well as stationary Lab-Line Incubator from Fisher Scientific. Ultraspec 1100 pro UV/visible spectrophotometer (Amersham Biosciences, part of GE Healthcare) equipped with DPU-414 Thermal Printer was employed for taking optical densities of protein and nucleic acid samples. Mettler Toledo (Columbus, OH, USA) PB602-S/FACT Balances and AB54-S/FACT Analytical Balances were used to determine the weight of samples in solution and buffer preparations. ISOTEMP 202S Water Bath and Dry Bath Incubator (Heating Block Incubator) were from Fisher Scientific Co., and were employed for sample incubations at various temperatures. Mini-PROTEIN® System containing Tetra Cell Single Core was purchased from BioRad Laboratories (Hercules, CA, USA), and used for protein separation and identification. PhastSystem (Amerasham Biosciences) was used for quick-check of proteins as they are eluted from the column. Mini-Horizontal Unit from FisherBiotech Electrophoresis Systems, series FB-SB-710 (Fisher Scientific Co.), was utilized for DNA and RNA separation and identification. PowerPac HC™ (BioRad Laboratories) was used as a power supply in protein/nucleic acid separations. SpectroLine UV Transilluminator, Slimline™ Series, was used to visualization of nucleic acid samples. PerkinElmer Geliance 600 Imaging System was used to visualize protein

and nucleic acid gels and take photographs using GeneSnap program from PerkinElmer. Gel Dryer, Model 583, was from BioRad, and allowed for protein gel drying for long term storage. Mettler Toledo SevenEasy pH Meter equipped with InLab® 413 pH Electrode was ideal for buffer preparations. Variety of Eppendorf Pipettman p-2, 10, 20, 100, 200, and 1000 were used in precise sample acquisition. Vortex-2 Genie® Scientific Industries were obtained from Fisher Scientific Co., and employed for sample mixing. Other equipment used included GAST non-lubricated vacuum pump (employed in drying of sample *in vacuo*), Kenmore Microwave (heating agarose solutions), etc.

II-3 EXPERIMENTAL METHODS

II-3-A Purification of Pokeweed Antiviral Protein

PAP used for these experiments was isolated from the spring leaves of the pokeweed plant (*Phytolacca Americana*) as previously described (*131*). Harvested leaves were frozen at -80 ^{o}C. The frozen leaves (100 g) were homogenized in an Acme juicer in 150 mL of cold grinding buffer (50 mM Tris-HCl, pH 7.5, 5 mM DTT, 0.2 mM EDTA, 1% PVP). The leaf slurry was filtered through several layers of cheesecloth and centrifuged at 8,000xg for 10 min at 4 ^{o}C. The supernatant was brought to 60% saturation with ammonium sulfate, and stirred for 3 h at 4 ^{o}C. The slurry was further centrifuged at 15,000xg for 15 min at 4 ^{o}C. The resulting supernatant was then brought to 100% saturation with $(NH_4)_2SO_4$ and allowed to stir over night at 4 ^{o}C. The slurry was centrifuged at 20,000xg for 20 min at 4 ^{o}C. The resulting pellet was then resuspended in Q buffer (20 mM Tris-HCl, pH 7.5, 1 mM DTT, 0.2 mM EDTA) and dialyzed against a total volume of 4 liters of Q buffer (buffer was changed every 6 to 12 hours). The dialyzed sample was loaded onto a Q-buffer equilibrated HiTrap Q FF column and purified using with ÄKTApurifier system from GE Healthcare (Figure 2.2), equipped with Pump P-900, Monitor UV-900, Monitor UPC-900, Valve INV-907 and Mixer M-925. The collected flow through was loaded onto a HiTrap SP FF column and washed with S buffer (10 mM MES, pH 5.2, 0.2 mM EDTA, 0.1 mM DTT) to remove any unbound sample and a stepwise gradient ranging from 100 mM NaCl to 500 mM NaCl (50 mM, 10 mL per each step) was used to elute proteins from the column (Figure 2.4). PAP eluded at approximately 250 mM NaCl. The fractions were analyzed by 12% SDS-PAGE for purity (Figure 2.5, A) and the protein concentration was determined using Pierce Coomassie Assay using standard BSA curve (Figure 2.6).

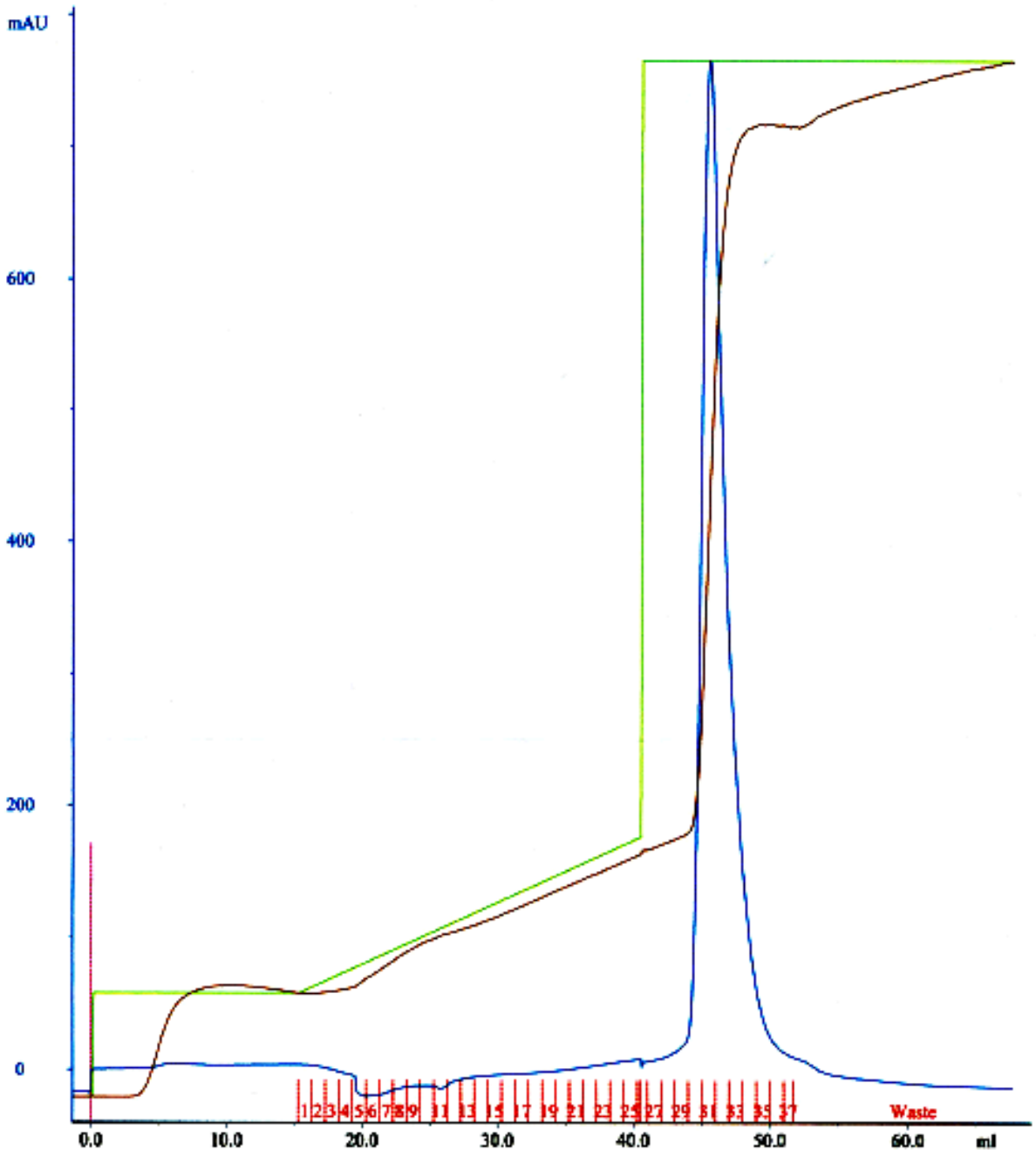

Figure 2.4 PAP elution profile from the SP column (——, injection; ——, fractions collected 1 through 27, 1 mL each; ——, UV absorption of the fractions at 280 nm; ——, NaCl concentration gradient; ——,conductivity of eluted fractions) using ÄKTApurifier system. PAP eluted at approximately 250 mM NaCl (fractions 29 through 35), as described in Section II-3-A.

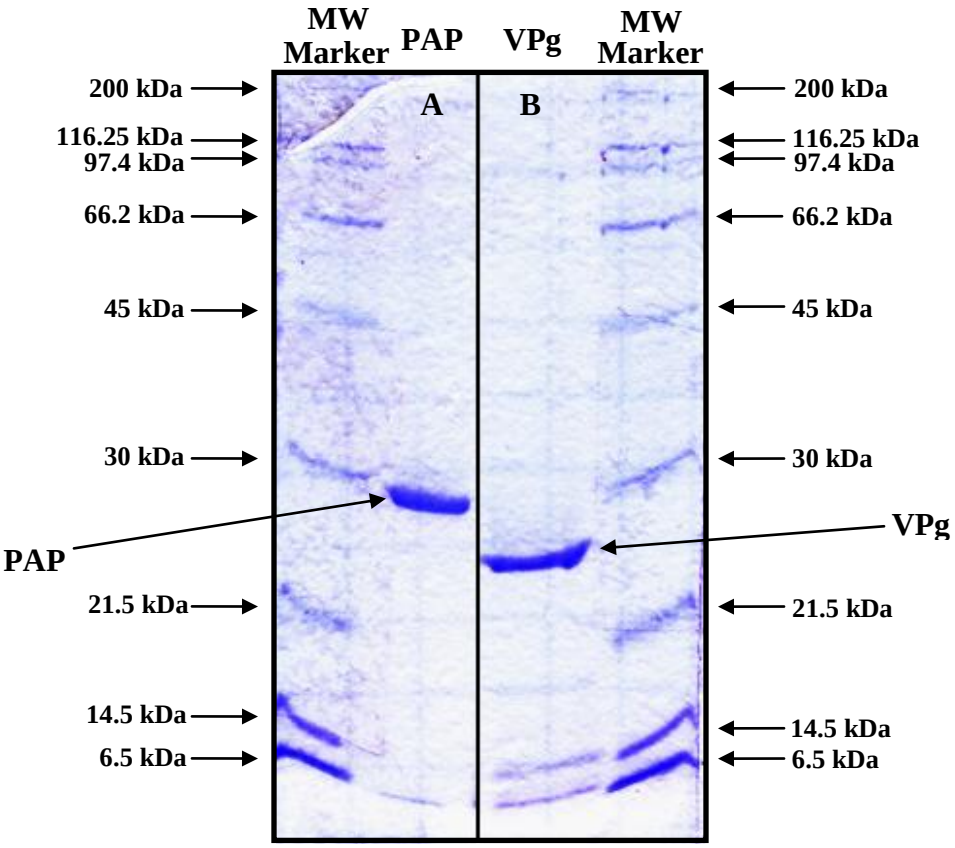

Figure 2.5 Sodium dodecyl sulfate polyacrylamide gel electrophoresis (SDS-PAGE, 12%) of **(A)** PAP and **(B)** VPg. Molecular weight (MW) marker lane is located on each site of the gel and contains the following protein standards: myosin from rabbit muscle, 200 kDa; β-galactosidase, from *E. coli*, 116.25 kDa; phosphorylase b, 97.4 kDa; albumin from bovine serum, 66.2 kDa; ovalbumin from chicken egg, 45 kDa; bovine carbonic anhydrase, 31 kDa; soybean trypsin inhibitor, 21.5 kDa; lysozyme from chicken egg white, 14.4 kDa, aprotinin from bovine milk, 6.5 kDa. The gel was prepared as described in Section VIII-3-I.

A

[BSA], mg/mL	A_{280}
0	0.000
100	0.072
200	0.144
300	0.232
400	0.294
500	0.390
600	0.411
700	0.520
800	0.578
900	0.599
1000	0.667

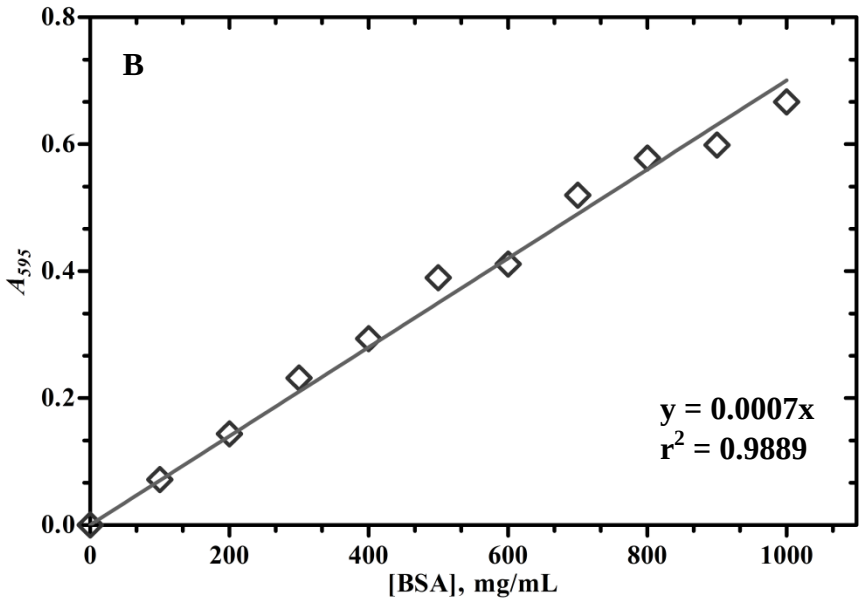

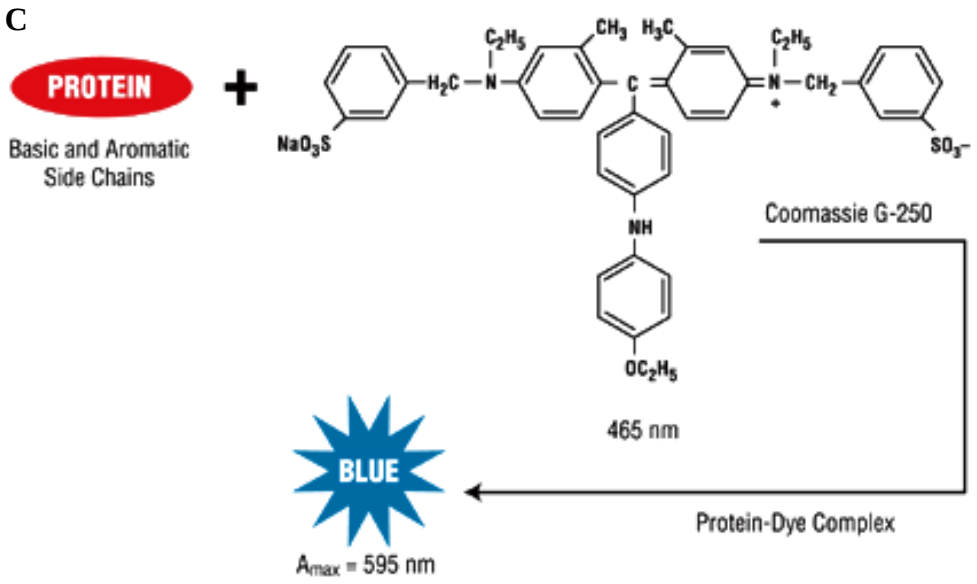

Figure 2.6 Bovine serum albumin (BSA) standard curve used in quantification of protein samples; prepared as described in Section VIII-3-E. **(A)** [BSA] standards in mg/mL in dH_2O. **(B)** BSA standard curve ($y = 0.0007x$, $r^2 = 0.9889$). **(C)** Schematic of the dye Coomassie® Brilliant Blue G-250 binding to proteins causes a shift in the absorption maximum of the dye from 465 nm (red) to 595 nm (blue) in acidic solutions (*226*). This dye forms strong, noncovalent complexes with proteins via electrostatic interactions with amino and carboxyl groups and via van der Waals forces.

II-3-B Expression and Purification of Wild Type (WT) VPg-His_6 and VPg-71-His_6

Purification of TuMV VPg was previously described (*211*). Briefly, *E. coli* BL21(DE3)pLysS cells were transformed with pETVPg1. Cells were cultured in Luria-Bertani (LB) Medium containing 100 µg/mL ampicillin and 20 µg/mL chloramphenicol at 25 ^{o}C. At an A_{600} of 0.5, protein expression was induced with 50 µM isopropyl 1-thio-β-D-galacropyranoside (IPTG) for 6 h, after which the cells were harvested by centrifugation (6,000xg at 4 ^{o}C). All subsequent steps were performed at 4 ^{o}C, in a cold-box. Cell pellets were resuspended into buffer A (20 mM Tris-HCl, pH 8.0, 300 mM NaCl, 10 mM imidazole), and disrupted by sonication. The lysates were centrifuged to remove the cell debris. The resulting supernatant was applied to a 5-mL nickel-nitrilo-triacetic acid Superflow column equilibrated with buffer A and connected to ÄKTApurifier system. The column was washed three times with 50 mL of buffer A, and the bound protein was eluted with 25 mL of buffer B (20 mM Tris-HCl, pH 8.0, 300 mM NaCl, 250 mM imidazole) (Figure 2.7). The protein was dialyzed against 1 liter of buffer C (20 mM Tris-HCl, pH 8.0, 10 mM NaCl, 1 mM DTT, 5% glycerol), further purified on Mono Q column and dialyzed against buffer D (20 mM Tris-HCl, pH 7.6, 150 mM NaCl, 5% glycerol). The purity of VPg-His_6 was confirmed by 12% SDS-PAGE and the protein concentration was determined using Pierce Coomassie Assay (Figure 2.5, B). Prior to spectroscopic measurements, all samples were dialyzed against buffer E (20 mM HEPES-KOH, pH 7.6, 100 mM KCl, 1.0 mM $MgCl_2$, 1.0 mM DTT, 1.0 mM EDTA), passed through a 0.22 µm Millipore filter, and concentrated with a Centricon 10 (Amicon Co.).

VPg-71-His_6 protein was provided by Professor Hiroshi Miyoshifrom the Department of Microbiology, St. Marianna University School of Medicine, Kawasaki, Japan.

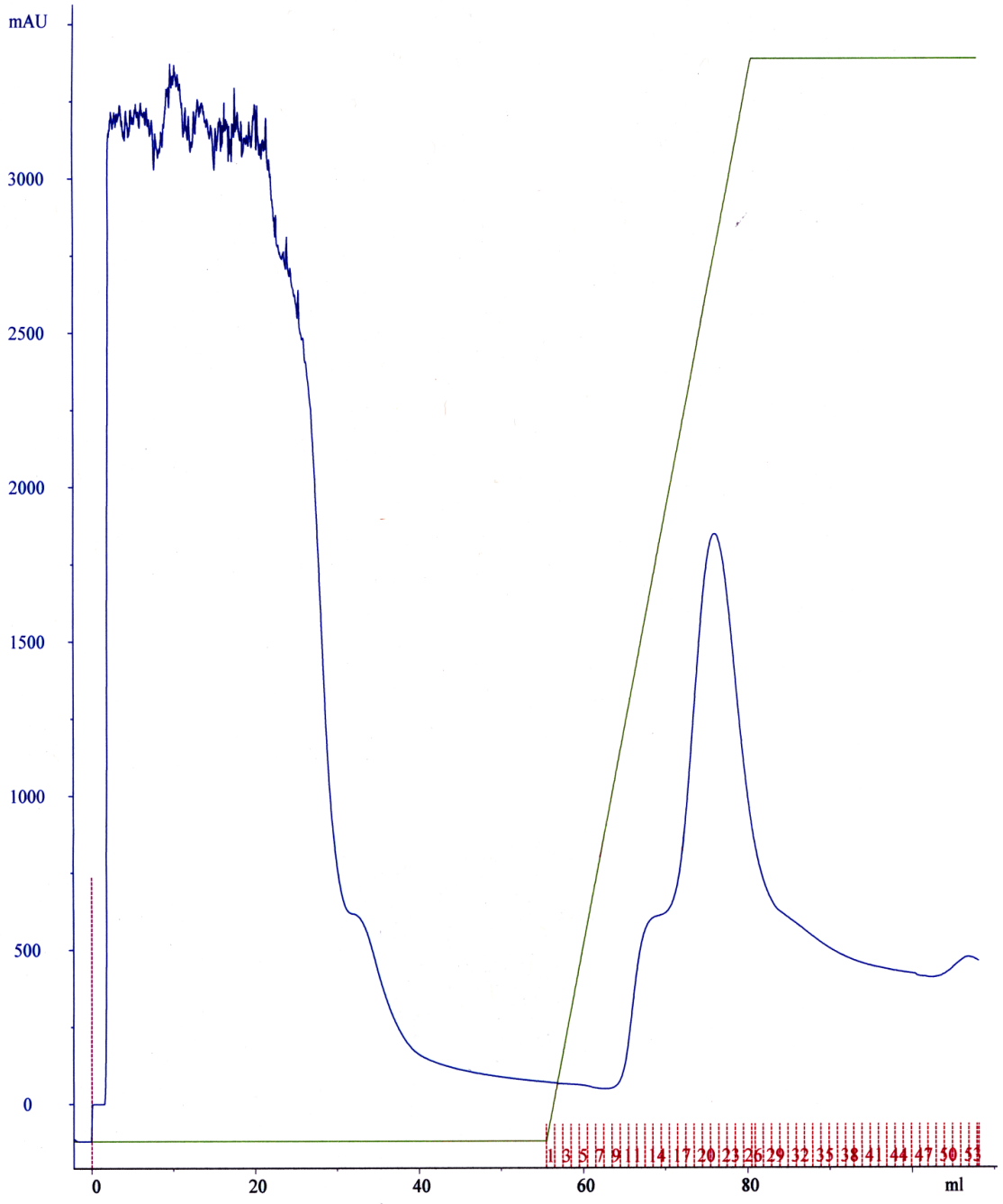

Figure 2.7 VPg elution profile from the nickel-nitrilo-triacetic acid Superflow column (——, injection; ——, fractions collected 1 through 53, 1 mL each; ——, UV absorption of the fractions at 280 nm; ——, NaCl concentration gradient) using ÄKTApurifier system. VPg eluted with Buffer B (fractions 15 through 28), as described in Section II-3-B.

II-3-C Expression and Purification of Eukaryotic Translation Initiation Factors (eIFs) *iso*4E and *iso*4G

The cap binding and scaffolding initiation factors (eIF*iso*4G and eIF*iso*4E) were expressed in *Escherichia coli* containing the constructed pET-3d vector in BL21(DE3)pLysS cells, as previously described (*213*, *227*). In brief, a Hi Trap Mono Q ion exchange column and an m^7GTP-Sepharose column were used for the purification of cap binding eIFs. *E. coli* cells bearing the above genes were disrupted by sonication, suspended in buffer B-600 (20 mM HEPES-KOH, pH 7.6, 1 mM DTT, 0.1 mM EDTA, 5% glycerol, 600 mM KCl) containing 0.5 mM PMSF, 0.5 mL of aprotinin, and 100 μg/mL of soybean trypsin inhibitor. The lysed cells were centrifuged at 15,000 rpm in a Sorvall SS-34 rotor for 30 min (S11 supernatant) to separate soluble proteins from the cell debris. The S11 supernatant was further centrifuged at 45,000 rpm in a Sorvall TV-850 rotor for 3 h (S175 supernatant) to remove ribosomes, mitochondria, and additional aggregates. The S175 supernatant was dialyzed against buffer B-50 (20 mM HEPES-KOH, pH 7.6, 1 mM DTT, 0.1 mM EDTA, 5% glycerol, 50 mM KCl). The dialyzed sample was applied to a 5-mL HiTrap Mono Q column equilibrated with buffer B-50 (10 bed volumes) with a flow rate of 2 mL/min. The column was washed at the same flow rate with buffer B-50 until optical density returned to base line. The expressed proteins were eluted with 50 – 400 mM KCl linear gradient at a flow rate of 2 mL/min. The peak was collected in 1.0-mL fractions. The sample was then subsequently applied to a 4-mL m^7GTP-Sepharose column equilibrated with buffer B-50. The column was washed with buffer B-50 containing 0.1 mM GTP to remove any GTP-binding proteins. Cap-binding proteins were eluted with buffer B-50 containing 100 mM GTP. HiTrap SP column was used to purify eIF*iso*4G by the following procedure (*228*). All

samples were analyzed by 12% SDS-PAGE and showed homogeneously pure proteins (Figure 2.8). All protein purification steps were carried out in a cold room, at 4 ^{o}C.

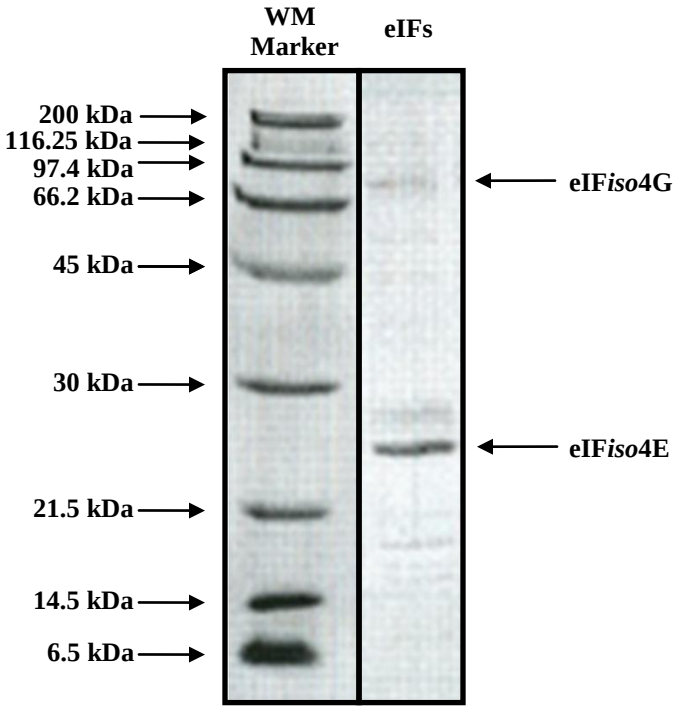

Figure 2.8 Sodium dodecyl sulfate polyacrylamide gel electrophoresis (SDS-PAGE, 12%) of eIF*iso*4G and eIF*iso*4E proteins. Molecular weight (MW) marker lane contains the following protein standards: myosin from rabbit muscle, 200 kDa; β-galactosidase, from *E. coli*, 116.25 kDa; phosphorylase b, 97.4 kDa; albumin from bovine serum, 66.2 kDa; ovalbumin from chicken egg, 45 kDa; bovine carbonic anhydrase, 31 kDa; soybean trypsin inhibitor, 21.5 kDa; lysozyme from chicken egg white, 14.4 kDa, aprotinin from bovine milk, 6.5 kDa. The gel was prepared as described in Section VIII-3-I.
The band at ~17 kDa is a degradation product, and comes from eIF*iso*4E purification.

II-3-D In Vitro Synthesis of S/R Oligo RNA and Tobacco Etch Virus (TEV) RNA

S/R oligo ds DNA template (5'-GGATCCTAATACGACTCACTATAGGGTGAACTT-AGTAC**GAGA**GGAACAGTTCA-3', 53 nucleotides) was purchased from Gene Link™ with the sequence corresponding to the universally conserved S/R loop of large rRNA. The linear DNA template was treated with proteinase K and purified by phenol:chloroform extraction as for TEV DNA. *In vitro* synthesis of the S/R oligo RNA used Promega RiboMAX™ large scale RNA production system T7 following the manufacturer's protocol. Cap analog, $m^7G(5')ppp(5')G$ was incorporated into the TEV transcript during the RiboMAX™ transcription reaction. Capped and uncapped transcripts were analyzed on 10% denaturing polyacrylamide/8M urea gels and the synthesized products were visualized by ethidium bromide staining (Sections VIII-2-A and VIII-3-H). Under the conditions of transcription more than 55% of RNA transcripts were capped, as determined by the fluorescence intensity of ethidium bromide (Figure 2.9, A). Capped RNA was sliced from the gels, redissolved in a buffer solution, precipitated with ethanol, and repurified. The concentration of TEV RNA was determined by measuring the optical density at 260 nm, and the purity of the synthesized RNA was confirmed by measuring the absorbance ratio $A_{260}/A_{280\ nm}$ in DEPC-treated water (Section VIII-3-D).

TEV DNA (Figure 2.8) constructs were kindly provided by Daniel R. Gallie, Department of Biochemistry, University of California, Riverside, California. The full length TEV construct was cloned as described previously (*217*). The TEV1-143 leader sequence was positioned next to the SP6 promoter of the PTL7SN.3 GUS vector. DNA was linearized with *Nco*I. The linearized DNA was treated with Proteinase K (100 μg/mL) and 0.5% SDS in 50 mM Tris-HCl, pH 7.5, 5 mM $CaCl_2$ for 30 min at 37 ^oC. DNA was further purified by extraction with phenol:chloroform:*iso*-amyl alcohol (25:24:1) at pH 8.0 followed by ethanol precipitation. Purity

of the resulted DNA was checked on a 1% agarose gel and the concentration was quantified spectrophotometrically and brought to 0.5 mg/mL. *In vitro* transcription of the TEV DNA used Promega RiboMAX^{TM} large scale RNA production system SP6 following the manufacturer's protocol. Cap analog, $m^7G(5')ppp(5')G$ was incorporated into the TEV transcript during the RiboMAX^{TM} transcription reaction. The ratio of cap analog:GTP was 5:1 to increase the efficiency of the transcription reaction. Capped and uncapped transcripts were analyzed on 6% denaturing polyacrylamide/8M urea gels and the synthesized products were visualized by ethidium bromide staining. Under the conditions of transcription more than 45% of RNA transcripts were capped, as determined by the fluorescence intensity of ethidium bromide (Figure 2.9, B). Capped RNA were sliced from the gels, redissolved in a buffer solution, precipitated with ethanol, and repurified. The concentration of TEV RNA was determined by measuring the optical density at 260 nm, and the purity of the synthesized RNA was confirmed by measuring the absorbance ratio $A_{260}/A_{280\ nm}$ in DEPC-treated water.

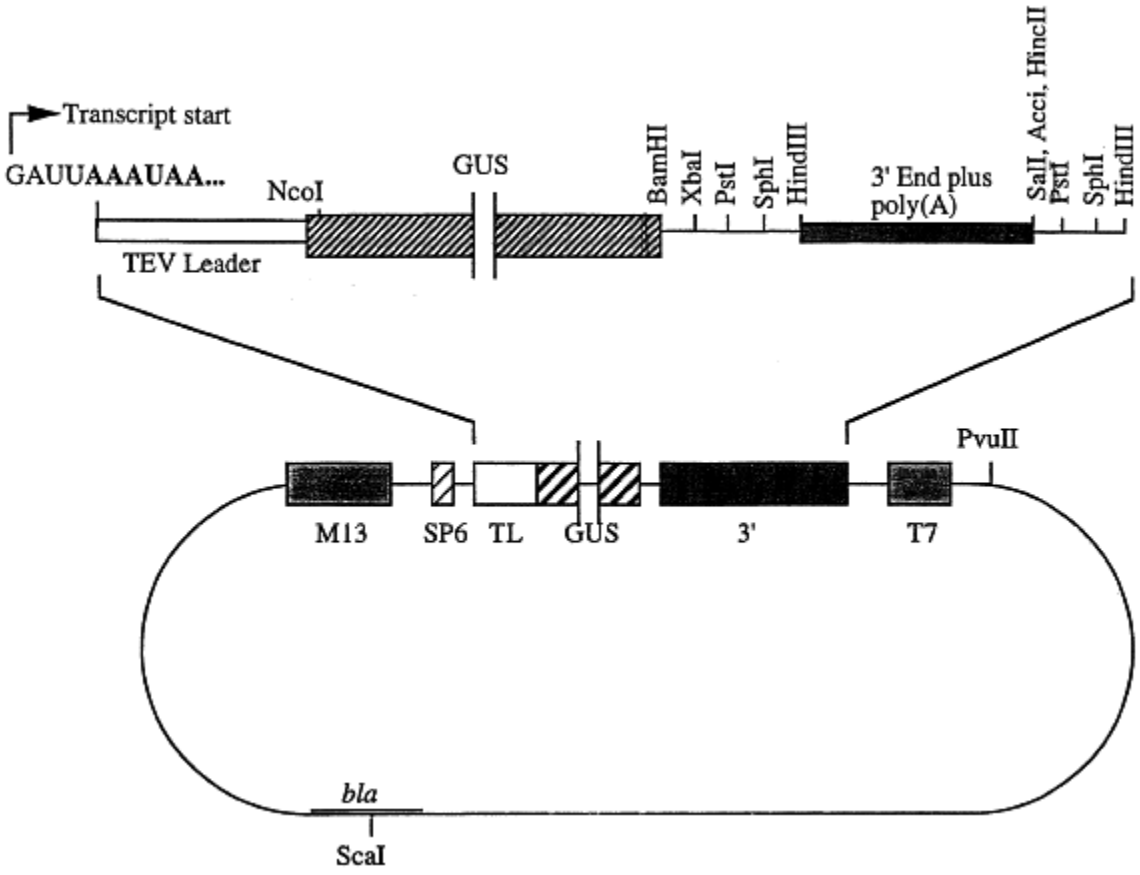

Figure 2.9 pTL7SN.3 GUS plasmid map (approx. 5500 bp). Plasmid DNA constructs were provided by Dr. Daniel R. Gallie, Department of Biochemistry, University of California, Riverside, California. The plasmid map was a courtesy of Dr. Jim Carrington from Center of Gene Research and Biotechnology, Oregon State University, OR, USA.

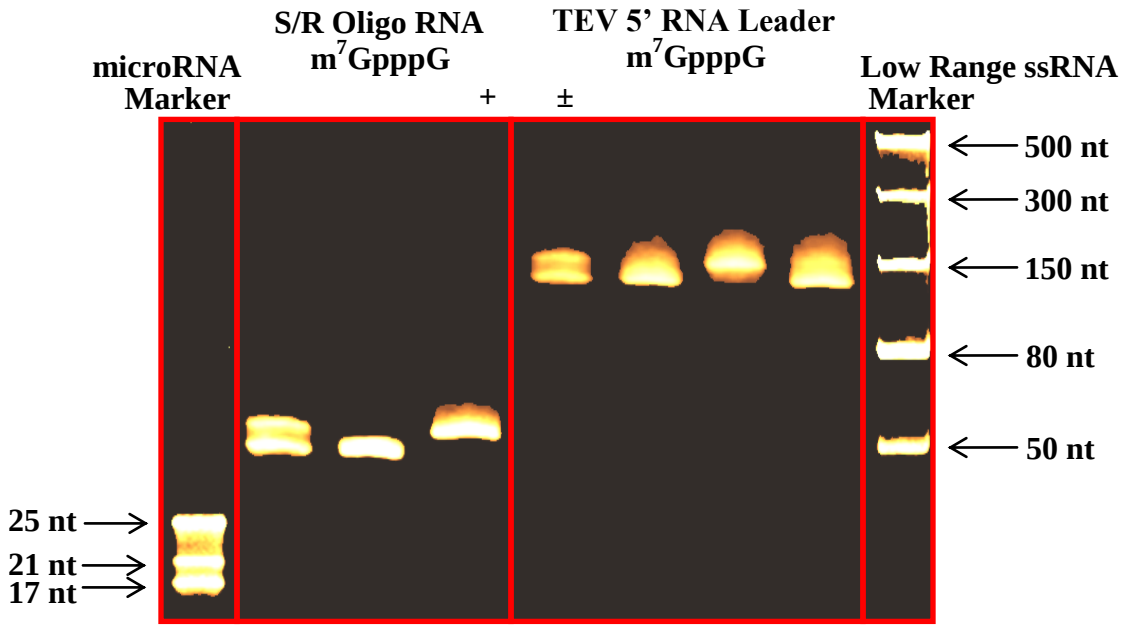

Figure 2.10 Denaturing polyacrylamide/8M urea gel electrophoresis of WT uncapped and m^7GpppG-capped S/R oligo RNA and TEV RNA (WT S/R oligo RNA is 53 nt; WT TEV RNA is 149 nt). The bands were stained with ethidium bromide. Capped RNAs were sliced from the gels, redissolved in a buffer solution, precipitated with ethanol, and repurified, as described in Section II-3-D. microRNA marker and low range ssRNA marker were purchased from New England BioLabs®, Inc. microRNA marker bands are as follows:
25-mer, 5'-AGAG**CAGUGGCUGGUUGAGAU**UUAA-3';
21-mer, AG**CAGUGGCUGGUUGAGAU**UU-3';
17-mer, 5'-**CAGUGGCUGGUUGAGAU**-3'.

II-3-E Fluorescence Assay for Adenine Released by PAP

Experiments were performed by incubating RNA (10 nmol/mL) in Depurination Buffer (20 mM Tris-HCl, pH 7.5, 100 mM NH_4Cl, 7 mM magnesium acetate, and 1 mM DTT) for 15 min at 37 ^oC in the absence and presence of PAP and VPg in 100 μL reaction volumes. At the end of incubations, 1 vol. of cold ethanol was added and, after 10 min at –80 ^oC, the ethanol-soluble fractions were recovered by centrifugation for 15 min at 14,000 rpm. Free adenine present in the ethanol-soluble fractions was converted into its etheno derivative (Figure 2.11) (*115*, *229*): 150 μL portions of the ethanol-soluble fractions were each diluted to 1 mL with DEPC water, and 0.4 mL of a mixture of 0.14 M chloroacetaldehyde and 0.1 M sodium acetate buffer, pH 5.1, was added to each. The samples were heated in a water bath at 80 ^oC for 40 min, extracted four times with 1 vol. of water-saturated diethyl ether, and passed through 0.45 μm pore-size filters. Fractions were analyzed with a Waters high-pressure liquid chromatograph equipped with a Waters 2487 dual λ absorbance detector (set at 254 nm), a Waters 2475 multi λ fluorescence detector (excitation, 315 nm; emission, 415 nm), Waters 600 controller and a Waters 717_{plus} autosampler (Figure 2.3). The column (4.6 x 150 mm) was reversed-phase XBridge^{TM} C_{18} (particle size 5 μm) purchased from Waters Associates. The column was eluted isocratically with 50 mM ammonium acetate buffer, pH 5.0/methanol (89:11, v/v) at room temperature. Elution profiles were analyzed by Waters Empower^{TM} chromatography software. Each experiment included a standard of N^6-ethenoadenine in the appropriate buffer and internal standards obtained by adding known amounts of N^6-ethenoadenine to the ethanol-soluble fractions from control and PAP-treated RNA. The amount of adenine released from PAP-treated RNA was calculated from the standards after subtraction of the fluorescence reading given by control RNA.

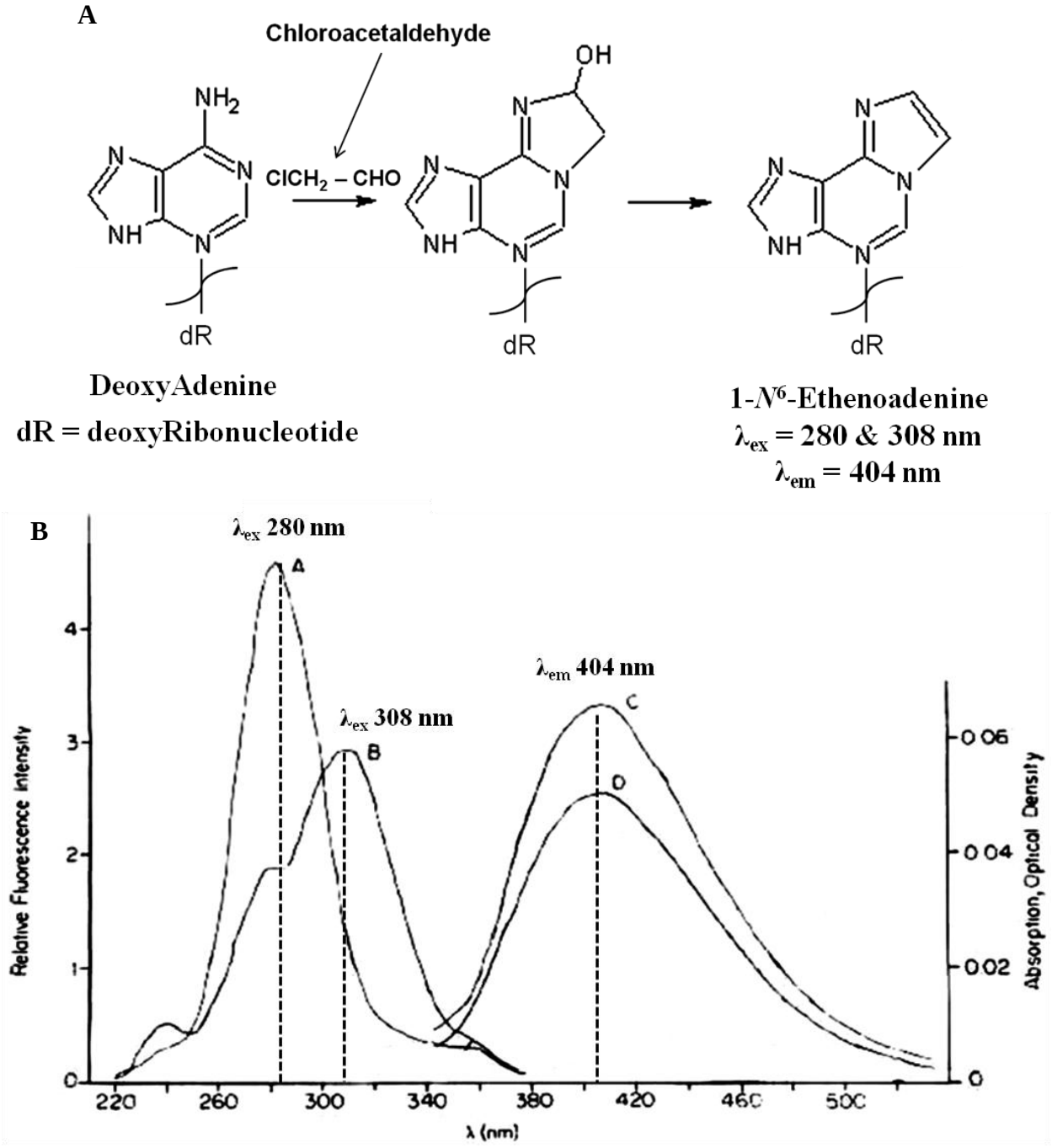

Figure 2.11 **(A)** The two-step reaction of adenosine with chloroacetaldehyde yielding fluorescent 1-N^6-ethenoadenine derivative. This figure was adapted from Krzyzoziak *et al.* (*230*) and remodeled. **(B)** Excitation and emission spectra of ethenoadenosine (A, pH 2.5, emission wavelength, 404 nm; B, pH 5.6, emission wavelength, 404 nm; C, pH 2.5, excitation wavelength, 280 nm; D, pH 5.6, excitation wavelength, 308 nm).
This figure was a courtesy of Dr. Jane Vanderkooi, and was adapted from Vanderkooi *et al.* (*231*).

II-3-F Synthesis of the Fluorescent Anthranoyl-m^{7}GTP Analog

The fluorescent anthranoyl-m^{7}GTP cap analog was synthesized as described previously (*232, 233*) with the following modifications (Figure 2.12). The m^{7}GTP cap (10 mg) was dissolved in 1 mL of distilled water at 37 ^{o}C. The pH of the resulting solution was adjusted to 9.6 with 2*N* NaOH. To this solution with continuous stirring crystalline isatoic anhydride (5 mg) was added. The pH of the mixture was maintained at 9.6 by titrating 2*N* NaOH during the 2 h reaction. After the reaction was complete, the pH of the reaction mixture was adjusted to 7.0 with 1*N* HCl solution. The reaction mixture containing the products and the unreacted materials was loaded onto a Sephadex LH-20 (2.4 x 56 cm) column equilibrated with autoclaved distilled water (Figure 2.13). The column was eluted with the same solvent at the flow rate of about 6 mL/h. Fractions of 1 mL were collected, and assayed by TLC on silica gel (Figure 2.14). The plates developed in system A (*n*-propyl alcohol:ammonia:water, 6:3:1, v/v containing 0.5 g/L EDTA). The ant-m^{7}GTP analog had brilliant blue fluorescence (monitored by UV lamp), while anthranilic acid (a byproduct of this reaction) showed dark violet fluorescence. Peak fractions of the fluorescent analog were pooled, combined, and lyophilized *in vacuo* at the temperature of liquid nitrogen to prevent degradation. The resulting residue was then dissolved in a minimum amount of water (0.5 mL), and an excess of cold ethanol was added to induce the precipitation of the compound. The fluorescent cap analog was then dried *in vacuo* over phosphoric anhydride at 4 ^{o}C giving an amorphous powder.

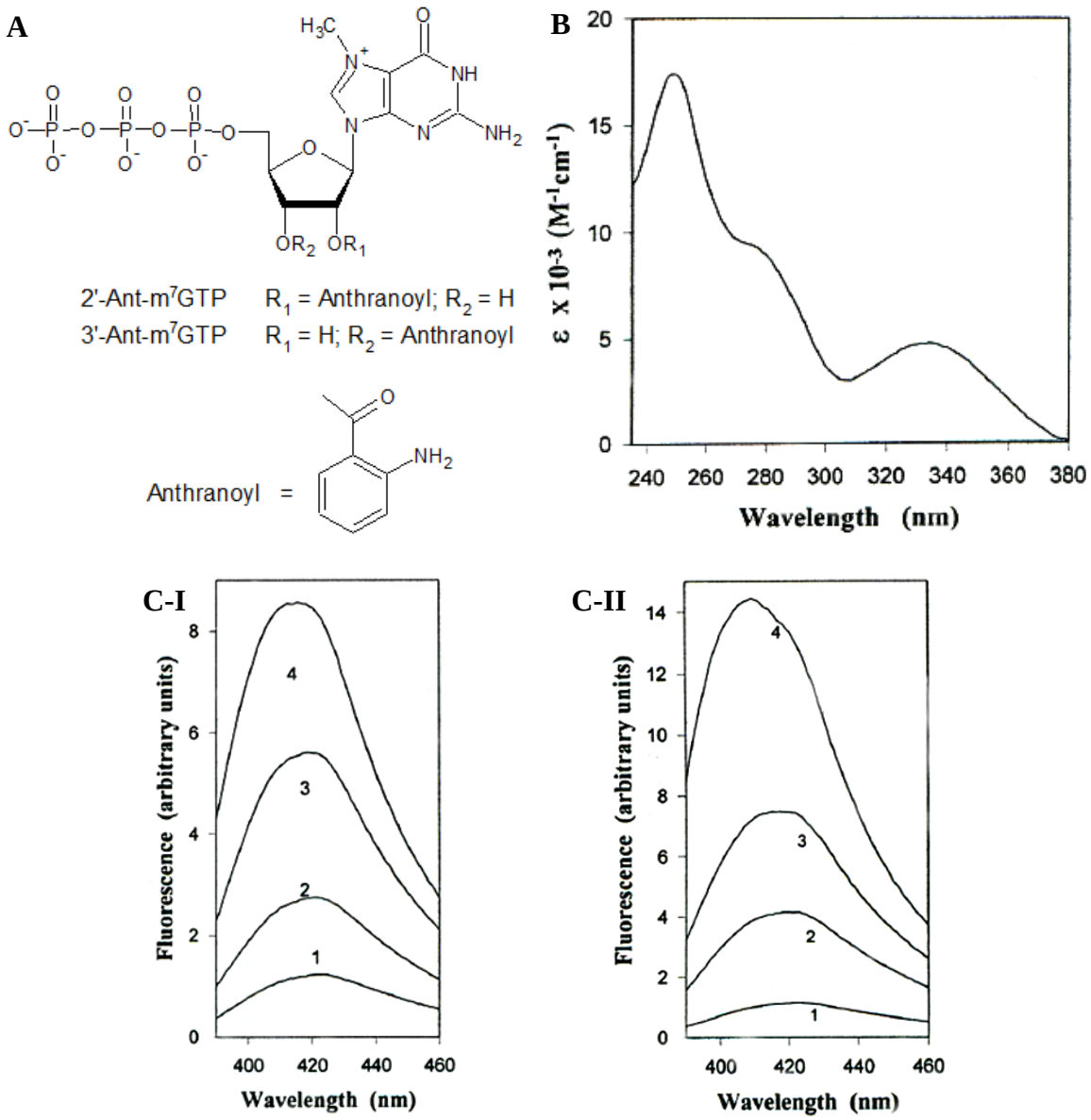

Figure 2.12 **(A)** structure of the anthranoyl (Ant) derivative of m^7GTP. **(B)** UV absorption spectrum of Ant-m^7GTP. The spectrum was measured in 20 mM HEPES, pH 7.6, 22 °C. **(C)** Fluorescence emission spectra of Ant-m^7GTP. All samples (1.5 μM Ant-m^7GTP) were in 20 mM HEPES, pH 7.6. Excitation was at 332 nm. **(C-I)** The spectra in water/ethanol at the ratio indicated: 1, aqueous solution (0% ethanol); 2, 20% (v/v) ethanol; 3, 40% (v/v) ethanol; 4, 80% (v/v) ethanol. **(C-II)** The spectra in water/DMF solution: 1, aqueous solution (0% DMF); 2, 20% (v/v) DMF; 3, 40% (v/v) DMF; 4, 80% (v/v) DMF.
These figures were a courtesy of Dr. Dixie J. Goss, and were adapted from Ren *et al.* (*232*).

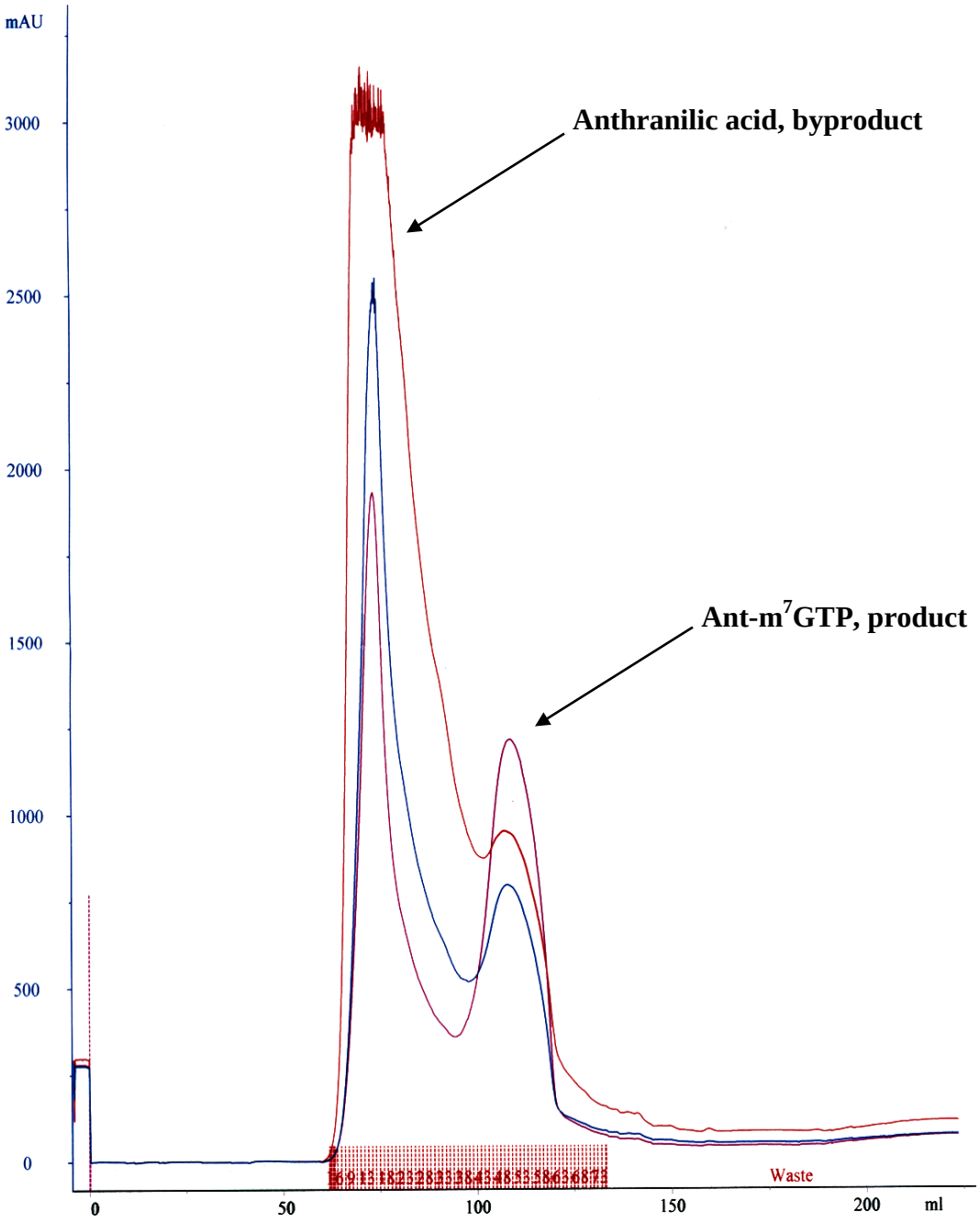

Figure 2.13 Anthranoyl (Ant)-m^7GTP elution profile from the Sephadex LH-20 (——, injection & UV3 absorption at 300 nm; ——, fractions collected 1 through 73, 1 mL each & UV2 absorption at 258 nm; ——, UV1 absorption of the fractions at 332 nm) using ÄKTApurifier system. Ant-m^7GTP eluted with ddH_2O (fractions 35 through 120), as described in Section II-3-F.

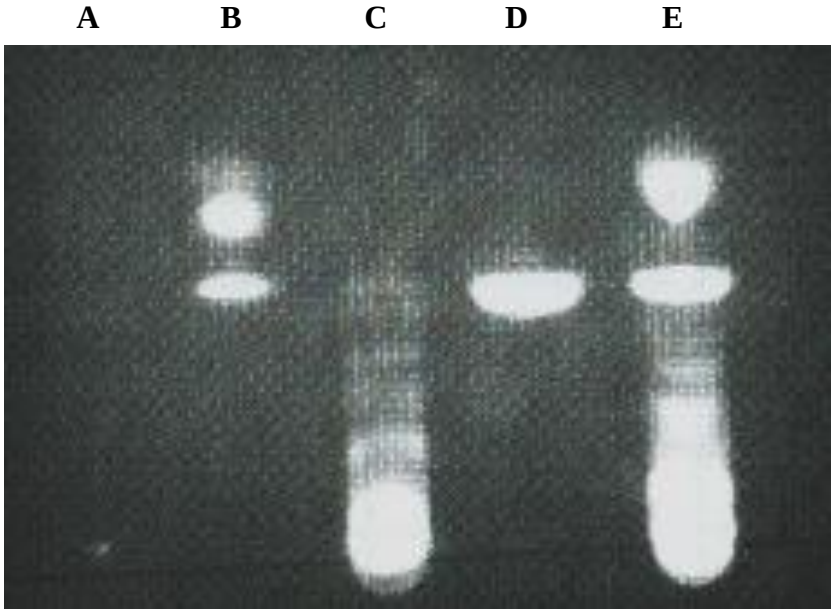

Figure 2.14 Silica gel TLC of **(A)** m^7GTP, **(B)** isatoic anhydride, **(C)** ant-m^7GTP, **(D)** anthranilic acid, and **(E)** reaction mixture, as monitored by UV absorbance at 366 nm. The solvent system was *n*-propyl alcohol:ammonia:water, 6:3:1, v/v containing 0.5 g/L EDTA Purification procedure is described in Section II-3-F. The R_f values were determined as follows: 0.1 for ant-m^7GTP, 0.68 for anthranilic acid, and 0.74 for isatoic anhydride.

II-3-G Labeling of PAP with NHS-Fluorescein

Pokeweed anti-viral protein was labeled with fluorescent *N*-hydroxysuccinimide (NHS)-fluorescein reagent using Pierce® NHS-Fluorescein Antibody Labeling Kit (Thermo Scientific) according to the manufacture's protocol. NHS-ester labeling reagents react efficiently with primary amines in the side chains of lysine (K) residues of PAP (Figure 2.15). PAP storage buffer S was replaced with 50 mM sodium borate, pH 8.5 buffer, containing 1 mM DTT using Microcon® centrifugal filters (Millipore). Fluorophore-to-protein ratio was estimated spectrophotometrically in phosphate-buffered saline (PBS) by measuring absorbance at 280 nm and 495 nm (i.e. A_{max} of NHS-Fluorescein), A_{280}/A_{max} = 0.3. The average amount of labeling was determined to be 65%. Protein concentration was calculated as follows (*234*):

$$\textbf{Moles Fluor per Mole Protein} = \frac{A_{max}\ \textbf{of the Labeled Protein}}{\varepsilon_{fluor} \times \textbf{[Protein], (M)}} \times \textbf{DF} \quad [1]$$

where A_{max} is maximum absorbance of the labeled protein, measured at 495 nm, ε_{fluor} = 70,000 (NHS-Fluorescein molar extinction coefficient), [Protein], (M) is the molar protein concentration, and DF is dilution factor. The degree of PAP labeling was calculated as follows (*234*):

$$\textbf{[Protein], (M)} = \frac{A_{280} - (A_{max} \times \textbf{CF})}{\varepsilon_{protein}} \times \textbf{DF} \quad [2]$$

where A_{280} is absorbance of the non-labeled protein, measured at 280 nm, A_{max} is maximum absorbance of the labeled protein, measured at 495 nm, $\varepsilon_{protein}$ is molar extinction coefficient of the non-labeled protein, CF is correction factor, and DF is dilution factor.

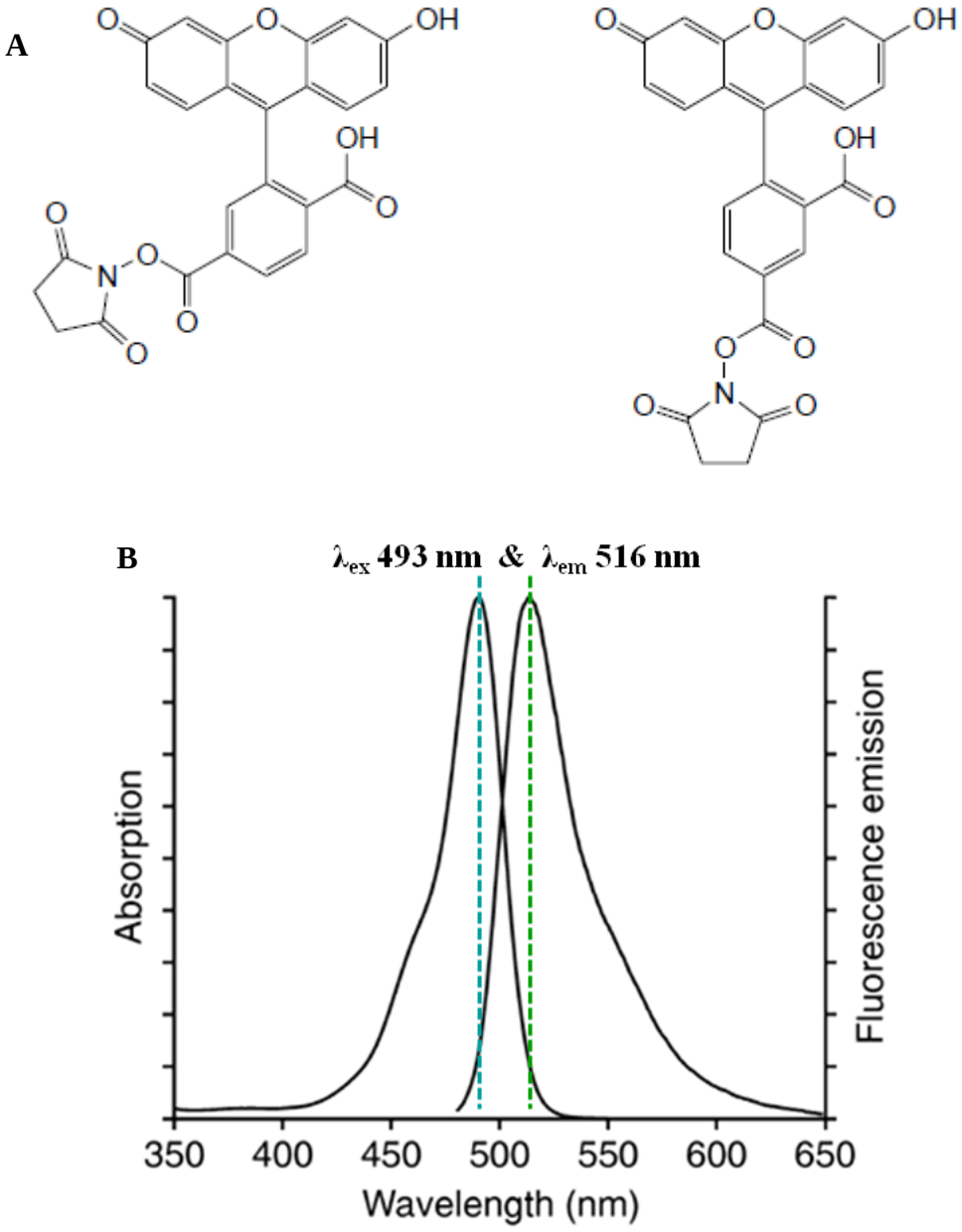

Figure 2.15 **(A)** Meta- and para-isomers of *N*-hydroxysuccinimide (NHS)-ester of fluorescein – the labeling reagents used in PAP labeling. **(B)** Excitation and emission spectra of fluorescein, pH 9.0.
These figures were adapted from Pierce Biotechnology NHS-Fluorescein Antibody Labeling Manual (*234*).

II-3-H Fluorescence Data Acquisition and Analysis

Steady state fluorescence was used to monitor protein-protein and protein-nucleic acid interactions (*235*). Acquisition of steady state fluorescence in the ultra violet region allows use of intrinsic protein fluorophores to determine equilibrium constants. A Horiba Jobin Yvon FluoroMax®-3 fluorometer (Figure 2.1) with a 150 W xenon lamp with photodiode array detectors was used for all fluorescence measurements. Fluorescence changes (quenching or enhancement, depending on the titrations) were monitored using excitation wavelength of 280 nm and emission wavelength of 332 nm (intrinsic protein fluorescence) or using excitation of 332 nm for Anthranoyl group and 493 nm for NHS-Fluorescein, and emission wavelength of 420 nm for Anthranoyl group and 516 nm for NHS-Fluorecein (for extrinsic fluorophores). All samples were thermo-regulated at different temperatures, *i.e.*, 5, 10, 15, 20, 25 ± 0.5 ^{o}C. The temperatures were monitored by a themocoupled chamber. All titrations were performed in a titration buffer (20 mM HEPES-KOH, pH 7.5, 100 mM KCl, 1 mM DTT). For each data point three samples were prepared. The fluorescence intensity of a protein (e.g., PAP) was measured in the first sample. A second sample containing specific amount of titrant protein (e.g., VPg) was also measured, and the corrected intensities of the two samples were summed together (F_s). A third sample containing the same amount of PAP and VPg proteins was mixed together, and the corrected fluorescence intensity for this complex was obtained (F_c). The difference in fluorescence intensity related to the complex was defined as $\Delta F = F_c - F_s$. Similar measurements were also performed for other titrations. The inner filter corrections for the RNA experiments were applied as described previously (*218*) using the following equation (*235*):

$$F_{corr} = F_{obs} \times \text{antilog}\left(\frac{A_{ex} + A_{em}}{2}\right) \quad [3]$$

where F_{corr} and F_{obs} are the corrected and observed fluorescence intensities, respectively. A_{ex} and A_{em} are the absorbance of the excitation and emission wavelengths, respectively. Corrections for the dilutions of the titrated samples were taken into consideration as well. The absorbance of the sample was measured using an Ultrospec 1100 Pro UV-visible absorption spectrophotometer. The normalized fluorescence difference (ΔF / ΔF_{max}) between the protein-protein and protein-RNA complexes and the sum of the individual fluorescence spectra were used to determine the equilibrium dissociation constant (K_d). A double reciprocal plot was used for determination of ΔF_{max}. The details of the data fitting are described elsewhere (*214, 236, 237*). Data were analyzed, plotted, and fit by PRISM®, version 5 using the Equation 6 (see below). Nonlinear least-squares fitting of plotted normalized data was used; one-site and two-site binding models were tested for. Briefly, the binding of VPg to PAP, for example, was assumed to proceed through the mechanism:

A + B ⇆ C, where A is the PAP, B is VPg, and C is PAP-VPg complex. Equation 4 defines the binding equilibrium constant:

$$K_{eq} = \frac{[C]}{[A]\,[B]} \qquad [4]$$

where [A] is the concentration of the uncomplexed PAP, [B] represents the free VPg, and [C] is the PAP-VPg complex. Normalized fluorescence is defined by Equation 5:

$$\overline{\Delta F} = \frac{F_t - F_0}{F_\infty - F_0} = \frac{\Delta F}{\Delta F_{max}} = \frac{[C]}{[A]_t} \qquad [5]$$

where F_∞ is the fluorescence end point and F_0 is the initial fluorescence point. The following conservation equations were used: $[A]_t = [C] + [A]$ and $[B]_t = [C] + [B]$. By making the appropriate substitutions into Equations 4 and 5 and converting the solved equation into quadratic form, Equation 6 results (*236*):

$$F_t = \left[\frac{(K[A]_t + K[B]_t + 1) - \sqrt{(K[A]_t + K[B]_t + 1)^2 - 4K^2[A]_t[B]_t}}{2\,K\,[A]_t}\right](F_\infty - F_0) + F_0 \qquad [6]$$

where K is the equilibrium binding constant, $[A]_t$ is the total PAP, and $[B]_t$ is the total VPg concentration after each addition. The data were fit by allowing K, F_∞, and $[A]_t$ to vary. The large errors in this experiment result partly from allowing the concentration of PAP to vary. Small differences in $[A]_t$ change K_{eq} (*236*).

II-3-I Evaluation of Thermodynamic Parameters

Thermodynamic parameters, ΔH (van't Hoff enthalpy), ΔS (entropy), and ΔG (free energy), were determined using the following equations:

$$-\ln K_{eq} = \frac{\Delta H^o}{RT} - \frac{\Delta S^o}{R} \qquad [7]$$

$$\Delta G^o = -R\,T \ln K_{eq} = \Delta H^o - T\Delta S^o \qquad [8]$$

R and T are the universal gas constant and absolute temperature, respectively. K_{eq} was determined at five different temperatures. ΔH and ΔS were determined from the slope and the intercept of a plot of ln K_a against 1/T. ΔG was determined from equation 8.

II-3-J Determining the Number of Binding Sites

The quenching of the native fluorescence emission maximum was monitored for the fluorescence change relative to untitrated PAP or eIF*iso*4F. The fractional quench, Q, was determined at each PAP/VPg or eIF*iso*4F/VPg molar ratio (R). For an observed fluorescence intensity F, the fractional quench, Q, was obtained from the equation (*238*):

$$Q = \frac{F_0 - F}{m} \quad [9]$$

here *m* is the maximal quench.

Fractional quench is linearly related to ligand binding,

$$\frac{[\text{Ligand} - \text{Protein}]}{[\text{Protein}]_T} = Q \quad [10]$$

where $[\text{Protein}]_T$ represents the total PAP or eIF*iso*4F protein concentration. The average number of binding sites (*n*) was determined from the *x* intercept of the Scatchard plot *Q versus* $Q / (R - Q)[\text{Protein}]_T$ (*238*).

III RESULTS

III-1 PAP Binds VPg with High Affinity

To determine the binding constants for PAP and VPg of TuMV, direct fluorescence titration studies were performed (Figure 3.1). The equilibrium binding constant was determined from the difference in fluorescence intensity between the protein-protein complex and the sum of the individual fluorescence intensities (Table 2.1). The equilibrium constant for PAP-VPg interactions was determined to be 29.5 ± 1.8 nM at 25 ^{o}C. This compares with VPg-eIF*iso*4F K_d of 81.3 nM (*213*), and PAP-m^{7}GTP binding of 43.3 nM (*131*). A control titration was performed of PAP with lysozyme to make sure that PAP is not just a sticky protein binding to other proteins indiscriminately (Figure 3.2).

III-2 PAP Binding to VPg is Enthalpically Driven and Entropically Favored

To establish the forces that drive PAP-VPg interactions, the thermodynamics of PAP-VPg binding were determined. Table 1 shows that the affinity of PAP for VPg increases with the decrease in temperature (K_d = 29.5 ± 1.8 nM at 25 ^{o}C versus 12.5 ± 0.6 nM at 5 ^{o}C). A van't Hoff plot of $-\ln K_{eq}$ *versus* the reciprocal of absolute temperature (T^{-1}) was used to calculate entropy (ΔS^{o}), and enthalpy (ΔH^{o}) (*inset* in Figure 3.1). The values of ΔH^{o} and ΔS^{o} were obtained from the intercept and the slope, respectively (correlation coefficient of >0.98). The van't Hoff analyses showed that the VPg binding to PAP is enthalpy-driven (ΔH^{o} = –29.2 ± 0.9 J/mol), and entropy favored (ΔS^{o} = +46.0 ± 3.0 J/Kmol), leading to a negative ΔG^{o} (–43.0 ± 1.8 kJ/mol) (Table 2.2). The $T\Delta S$ van't Hoff component contributes 32% overall to the value of ΔG^{o} at 25 ^{o}C. The relatively large, favorable, entropic contributions to the PAP-VPg binding suggest that hydrophobic residues are less solvent exposed in the combined structure.

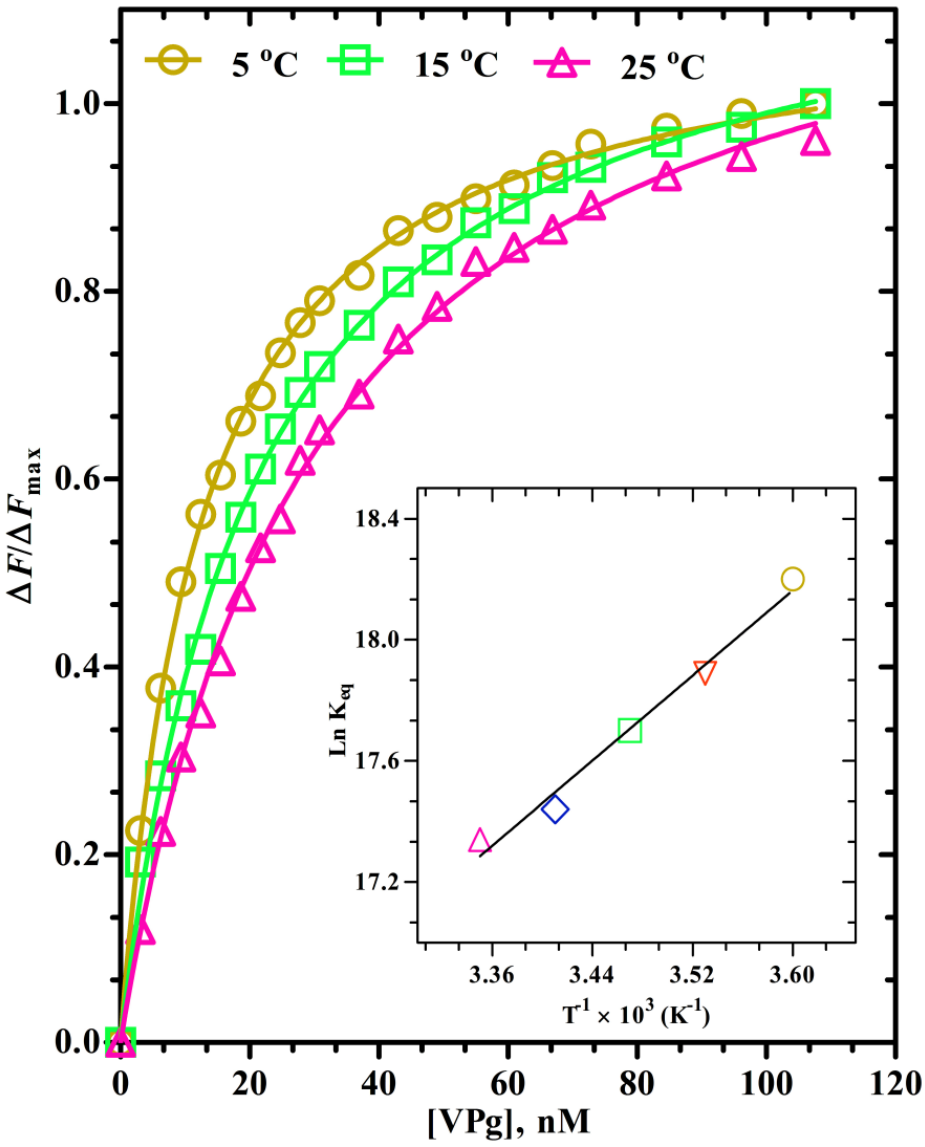

Figure 3.1 Temperature dependence of PAP-VPg interactions. The normalized fluorescence values (λ_{ex} = 280 nm and λ_{em} = 332 nm) for the fraction of the bound ligand ($\Delta F/\Delta F_{max}$) are plotted *versus* VPg concentration at 5 °C (—○—), 10 °C (—▽—), 15 °C (—□—), 20 °C (—◇—), and 25 °C (—△—). PAP concentration was 100 nM in titration buffer. The curves were fit to obtain dissociation constants (K_d) as described under "Experimental Procedures." The *inset* is van't Hoff plot for the interactions of PAP with VPg.

Table 2.1 Equilibrium dissociation constants for the interactions of PAP with VPg/VPg-71.

Complex	Equilibrium Dissociation Constant, K_d, [nM]				
	5 °C	10 °C	15 °C	20 °C	25 °C
PAP – VPg	12.5 ± 0.6	17.0 ± 0.7	20.9 ± 1.2	26.7 ± 1.3	29.5 ± 1.8
PAP – VPg-71	ND	ND	ND	ND	37.4 ± 3.0

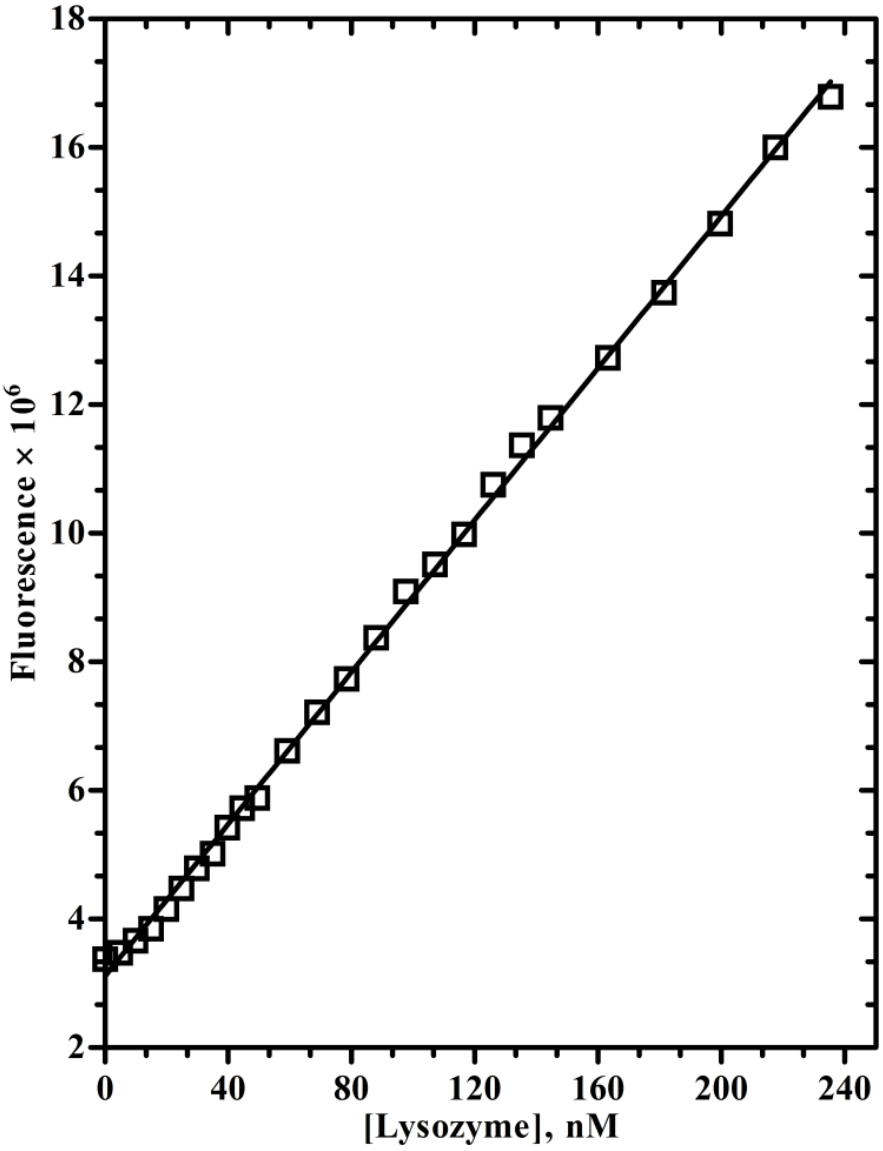

Figure 3.2 Titration of 100 nM PAP with Lysozyme. The titration buffer was 20 mM HEPES-KOH, pH 7.5, 100 mM KCl, 1 mM DTT. The excitation and emission wavelengths were 280 nm and 332 nm, respectively.

Table 2.2 Thermodynamic parameters for the interactions of PAP with VPg. ΔH^o and ΔS^o values were determined from van't Hoff plot and association constants. However, ΔG^o values were calculated at 25^o C using the equation $\Delta G^o = -$ RT ln K_{eq}.

Complex	Enthalpy, ΔH^o	Entropy, ΔS^o	Gibbs Free Energy, ΔG^o
	$kJ \cdot mol^{-1}$	$J \cdot K^{-1} \cdot mol^{-1}$	$kJ \cdot mol^{-1}$
PAP – VPg	– 29.2 ± 0.9	+ 46.0 ± 3.0	– 43.0 ± 1.8

III-3 PAP and VPg Bind in a 1:1 Ratio

To determine the stoichiometry of PAP-VPg binding, direct fluorescence titration studies of PAP with VPg were performed (Figure 3.3). The inset of Figure 3.3 shows the corresponding Scatchard plot (*inset* in Figure 3.3). The slope and intercept of the plot Q / [VPg] x 10^{-6} *versus* Q gave the binding constant (K_d = 29.5 ± 1.8 nM) and binding capacity (n = 0.99 ± 0.01) of PAP for VPg (*238*).

III-4 PAP and eIFiso4F Bind VPg at Different Sites

To investigate whether PAP binds at the same binding site on VPg as eIF*iso*4F, interactions of VPg-71 mutant with PAP were determined. VPg-71 is a truncated variant of wild type VPg where the *N*-terminal amino acids 1-70 are removed so it lacks eIF4F and eIF*iso*4F binding sites (*214*). PAP exhibits 2.8 times stronger binding affinity for VPg (29.5 ± 1.8 nM) than eIF*iso*4F (81.3 nM) (*213*). The equilibrium constant for PAP-VPg-71 was found to be 37.4 ± 3.0 nM at 25 ^{o}C (Figure 3.4, Table 2.1). Because VPg-71 has the eIF4F/*iso*4F binding sites removed yet still binds PAP with high affinity, we conclude that the PAP binding site on VPg differs from the eIF4F binding site on VPg.

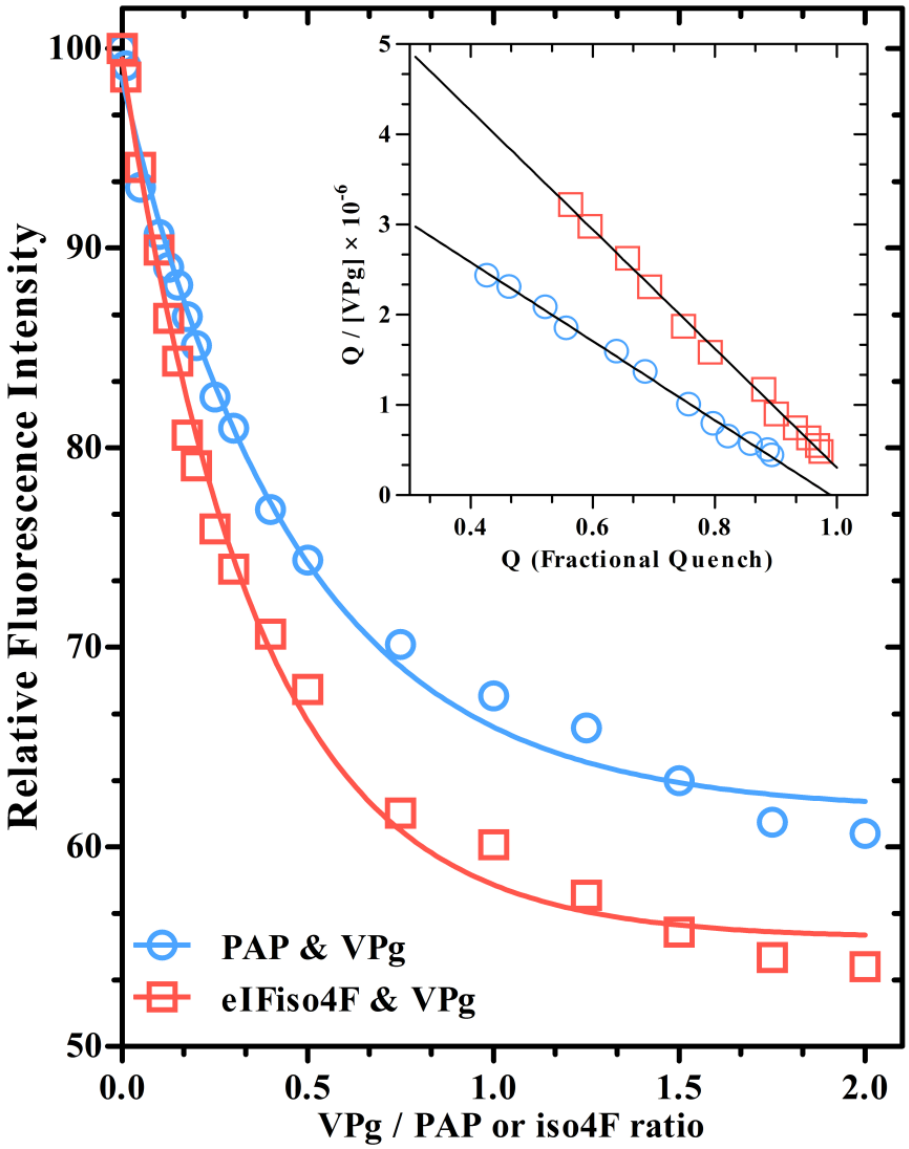

Figure 3.3 Competition of eIF*iso*4F (complex of eIF*iso*4E-eIF*iso*4G) (—□—) and PAP (—○—) binding with VPg. Intrinsic PAP or eIF*iso*4F fluorescence was monitored. VPg has negligible intrinsic fluorescence. The *solid lines* are the fitted theoretical curves. The *inset* illustrates Scatchard plots showing one binding site for eIF*iso*4F and PAP with VPg. The slope and intercept of the straight line obtained on the plot Q/[VPg] x 10^{-6} *versus* Q provided the binding constant (K_a) and binding capacity (n) of the above proteins with VPg. Q is the fractional quench of fluorescence in titration. n for the PAP-VPg was determined as 0.99 ± 0.01 and for eIF*iso*4F-VPg was 1.05 ± 0.01 (T = 25 ^{o}C, λ_{ex} = 280 nm, λ_{em} = 332 nm) (*213*).

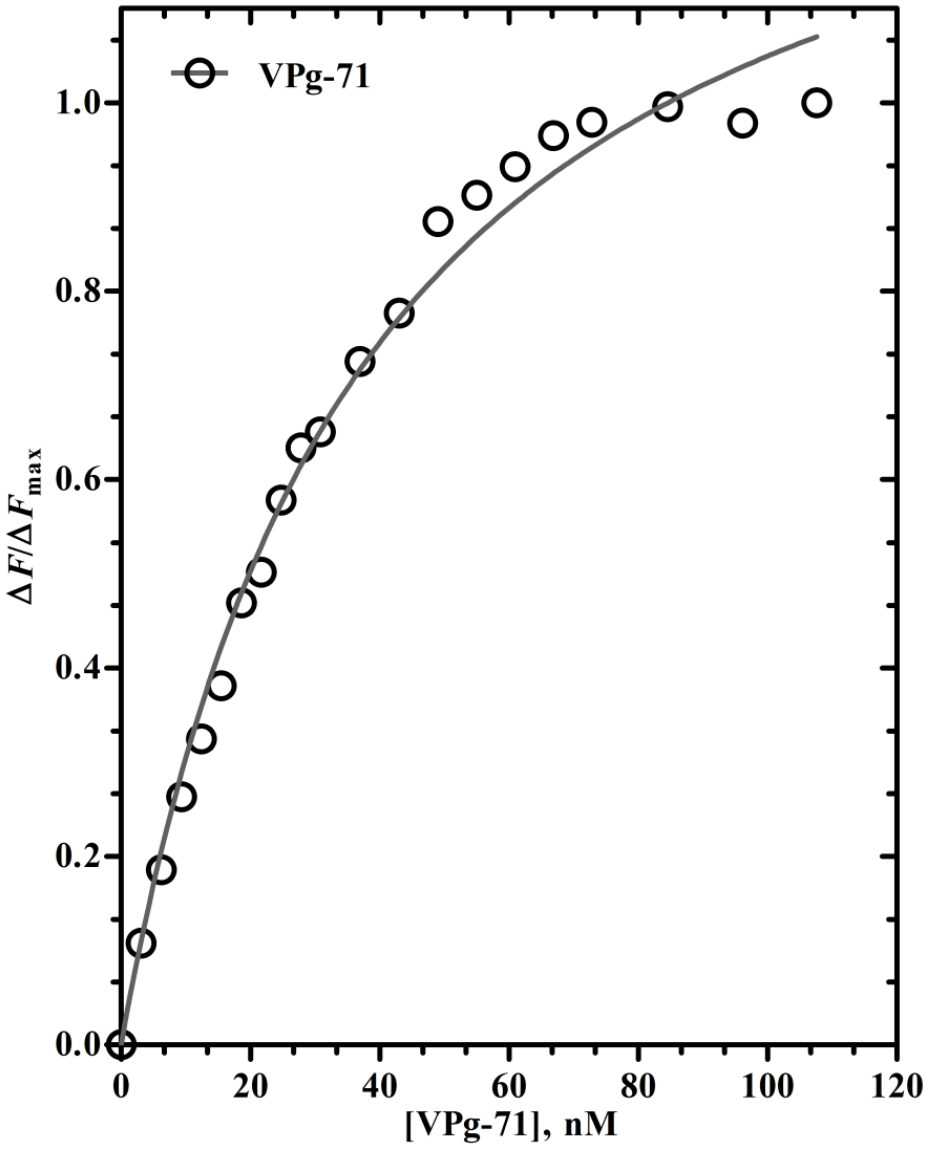

Figure 3.4 Titration of PAP with VPg-71 mutant. The normalized fluorescence values for the fraction of the bound ligand are plotted *versus* VPg-71 concentration at 25 ^{o}C. PAP concentration was 100 nM in titration buffer. The excitation and emission wavelengths were 280 nm and 332 nm, respectively. The curve was fit to obtain dissociation constants (K_d) as described under "Experimental Procedures."

III-5 VPg and Cap Analog Bind PAP in a Mixed Type Competition

To determine whether binding of VPg and cap to PAP is competitive or not, the fluorescent cap analog anthranoyl-(Ant)-m^7GTP was used (*232*, *233*). The competitive substitution reactions were performed at constant Ant-m^7GTP concentration (100 nM) monitoring the fluorescence change of the analog and increasing amounts of PAP in the absence and presence of VPg (Figure 3.5). Ant-m^7GTP was a suitable candidate to study these competition interactions because excitation (332 nm) and emission (420 nm) of this extrinsic fluorophore is far removed from the protein fluorescence, and K_d for the PAP-Ant-m^7GTP interactions was essentially the same as previously reported for m^7GTP interaction with PAP (K_d = 43.3 nM) (*131*). The apparent affinity of PAP for the fluorescent cap analog decreased from 41.7 ± 2.0 nM in the absence of VPg to 108 ± 35 nM in the presence of 90 nM VPg (Table 2.3). PAP binds to VPg with higher affinity (28.9 ± 0.8 nM) than to Ant-m^7GTP (41.7 ± 2.0 nM). Lineweaver-Burk plots (*inset* in Figure 3.5) meet at the left of the *y* axis intercept, indicative of mixed-type competitive ligand binding between Ant-m^7GTP and VPg, suggesting that VPg binds to PAP at a site distant from the cap binding site. Further, it binds to either free PAP or PAP-cap complex.

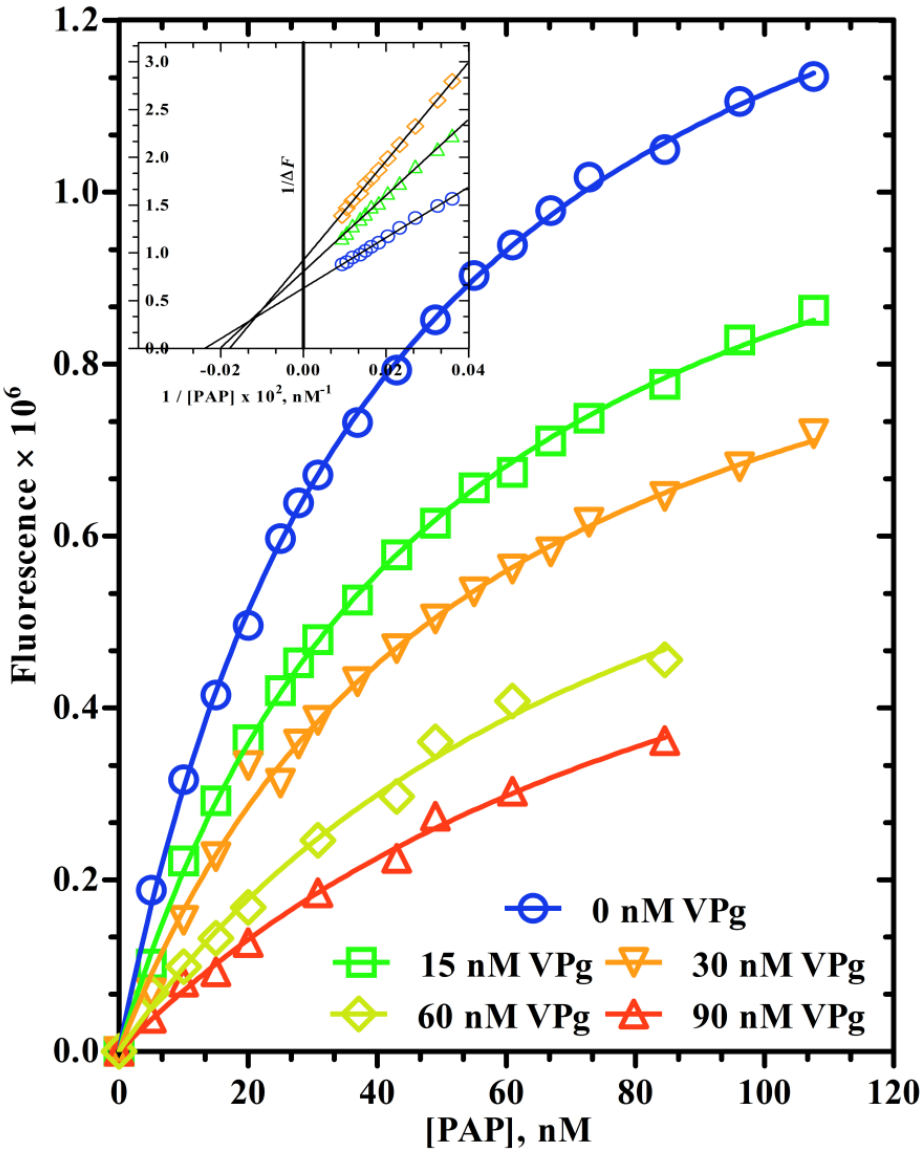

Figure 3.5 Ant-m^{7}GTP cap analog and VPg show mixed competition binding for PAP. The fluorescence change of Ant-m^{7}GTP cap analog was measured with increasing concentrations of PAP. VPg concentrations were 0 nM, —○—; 15 nM, —□—; 30 nM, —▽—; 60 nM, —◇—, and 90 nM, —△—. The excitation wavelength was 332 nm, and emission was 420 nm. The *solid lines* are the fitted curves. The *inset* shows a Lineweaver-Burk plot for competition of Ant-m^{7}GTP and VPg with PAP. The spectrum was measured in buffer containing 100 nM Ant-m^{7}GTP and VPg as indicated. Data points were fitted using least square analysis.

Table 2.3 Apparent Equilibrium inhibition constants, K_{app}, for the competition titrations of VPg and Ant-m^7GTP for PAP.

Complex	**Final Concentration of VPg Added**				
	0.0 nM	15 nM	30 nM	60 nM	90 nM
	Apparent Equilibrium Inhibition Constant, K_{app}, [nM]				
PAP – Ant-m^7GTP	41.7 ± 2.0	49.3 ± 2.7	55.8 ± 7.9	87.8 ± 32	108 ± 35

III-6 VPg and eIFiso4F Bind PAP Competitively

To determine if binding of VPg and eIF*iso*4F to PAP was competitive or noncompetitive, *N*-hydroxysuccinamide (NHS)-Fluorescein-labeled PAP was utilized. The competitive substitution reactions were performed at constant (NHS)-Fluorescein-labeled PAP concentration (200 nM) monitoring the fluorescence change of the extrinsic fluorophore (λ_{ex} = 493 nm and λ_{em} = 516 nm) with increasing amounts of VPg in the absence and presence of eIF*iso*4F (Figure 3.6). VPg has very low intrinsic fluorescence, and the K_d for the NHS-Fluorescein-labeled PAP-m^7GTP interactions (63.8 ± 7.9 nM at 25 ^oC, Figure 3.7) is in agreement with previously published WT PAP-m^7GTP value (*131*). This allowed us to use this extrinsic fluorophore to study changes that PAP undertakes as eIF*iso*4F substitutes for VPg from PAP-eIF*iso*4F complex. The apparent affinity of labeled PAP for VPg was found to decrease from 51.0 ± 6.9 nM in the absence of eIF*iso*4F to 95.4 ± 12.4 nM in the presence of 150 nM eIF*iso*4F (at 25^oC) (Table 2.4). Fluorescence data were also represented as a double-reciprocal plot (*inset* in Figure 3.6) where the lines meet on the *y*-axis, indicating a competitive-type ligand binding between VPg and eIF*iso*4F, suggesting that VPg is bound on or near the eIF*iso*4F binding site on PAP.

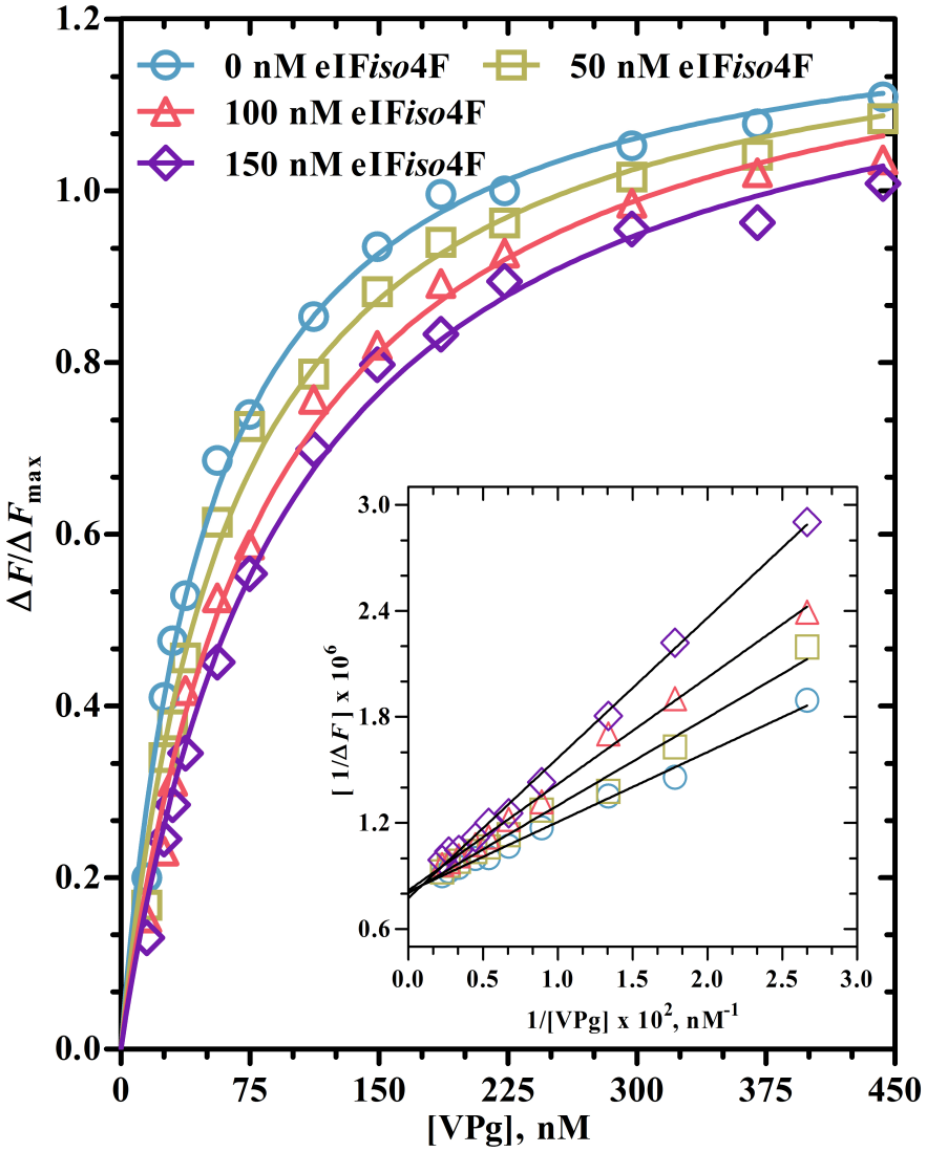

Figure 3.6 eIF*iso*4F and VPg bind competitively to NHS-Fluorescein-labeled PAP. The fluorescence change of NHS-Fluorescein-labeled PAP was monitored (λ_{ex} = 493 nm, λ_{em} = 516 nm) with increasing concentrations of VPg in the presence and absence of eIF*iso*4F (0 nM, —○—; 50 nM, —□—; 100 nM, —△—; 150 nM, —◇—). The *solid lines* are the fitted curves. The *inset* represents Lineweaver-Burk Plots competitive binding. Data points were fitted using least square analysis.

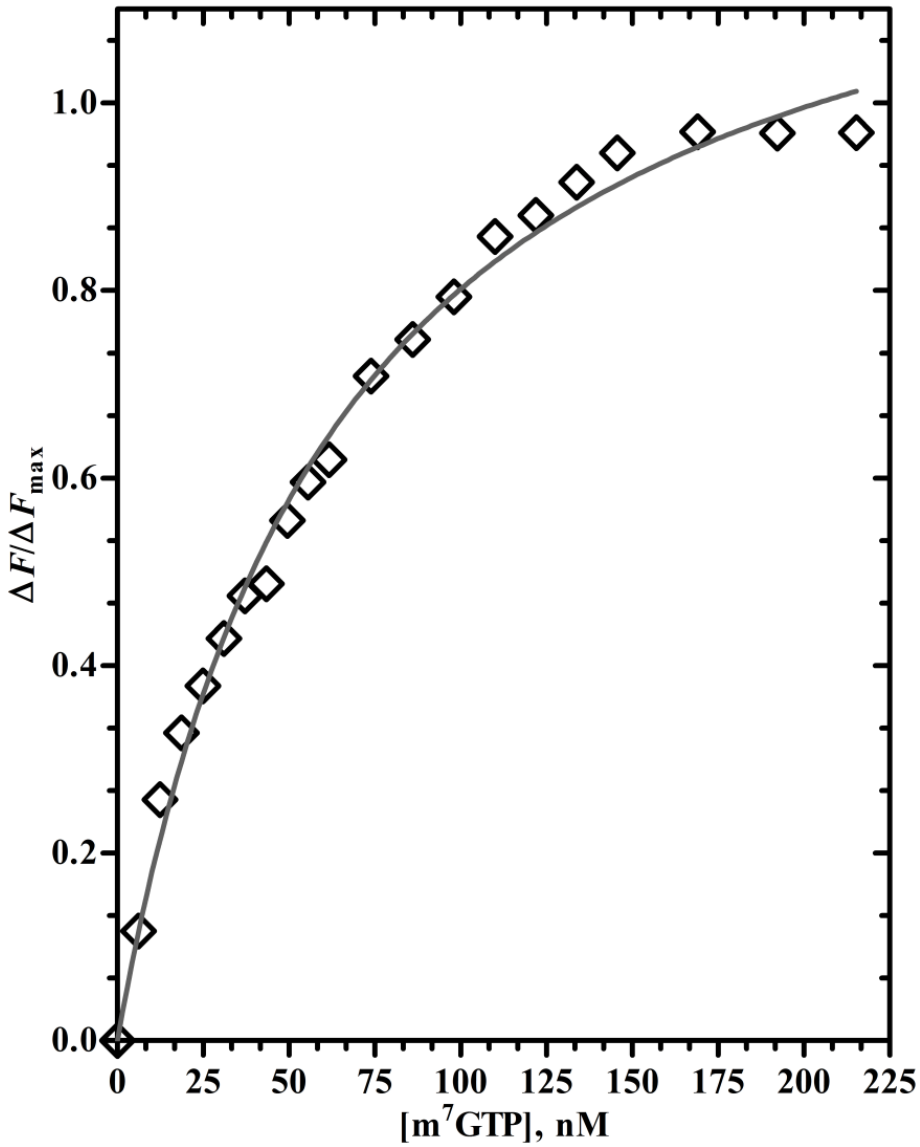

Figure 3.7 Fluorescence titration of 100 nM of NHS-Fluorescein-labeled PAP with m^{7}GTP. The fluorescence change of NHS-Fluorescein-labeled PAP was monitored (λ_{ex} = 493 nm, λ_{em} = 516 nm) with increasing concentrations of m^{7}GTP cap analog. Data points were fitted using least square analysis.

Table 2.4 Pseudo-apparent equilibrium inhibition constants, K_{app}, for the competition titrations of NHS-Fluorescein labeled PAP and eIF*iso*4F for VPg.

Complex	**Final Concentration of eIF*iso*4F Added**			
	0.0 nM	50 nM	100 nM	150 nM
	Apparent Equilibrium Inhibition Constant, K_{app}, [nM]			
NHS-Fluorescein-labeled PAP – VPg	51.0 ± 6.9	63.5 ± 9.5	84.1 ± 13	95.4 ± 12

III-7 VPg Competes with TEV RNA for PAP Binding

Zeenko and Gallie (*217*) have previously demonstrated that the uncapped 5' TEV (tobacco etch virus) UTR contains a pseudoknot 1 (PK1) within its structure that is sufficient to confer cap-independent translation. In order to determine if VPg interaction with PAP affected TEV binding, competition experiments were performed, where PAP binding to TEV in the presence of increasing amounts of VPg was determined. VPg had previously been shown to enhance TEV translation (*214*) by a mechanism where VPg enhances eIF4F binding to the TEV mRNA. The competitive reactions were performed at constant (NHS)-Fluorescein-labeled PAP concentration (100 nM) monitoring the fluorescence change of the extrinsic fluorophore (λ_{ex} = 493 nm and λ_{em} = 516 nm) with increasing amounts of TEV RNA in the absence and presence of VPg (Figure 3.8). The apparent affinity of labeled PAP for TEV RNA was found to decrease from 13.1 ± 1.3 nM in the absence of VPg to 27.6 ± 2.7 nM in the presence of 100 nM VPg (at 25 ^{o}C) (Table 2.5). A double-reciprocal plot (*inset* in Figure 3.8) shows that the lines meet on the *y*-axis, indicating a competitive-type ligand binding between VPg and TEV for PAP.

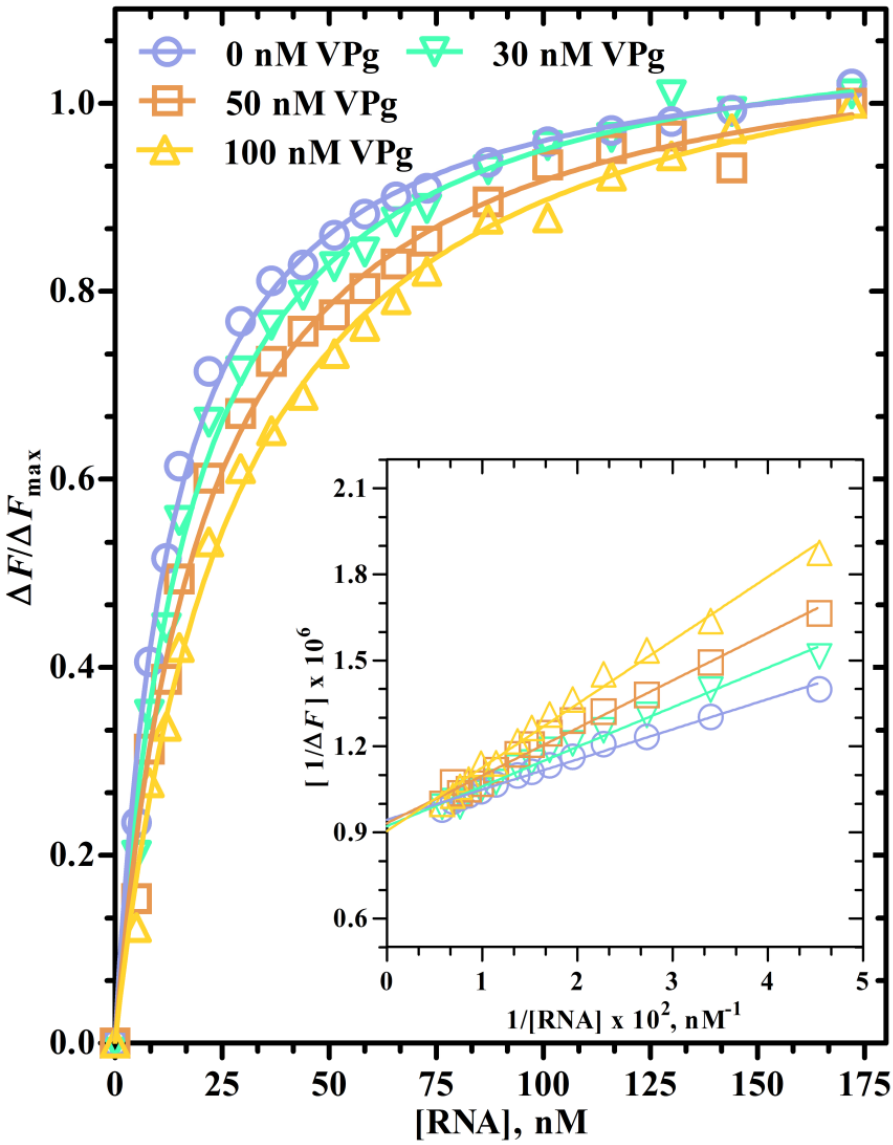

Figure 3.8 Fluorescence titrations for the competition experiments of VPg and WT TEV RNA for NHS-Fluorescein-labeled PAP. The fluorescence change of NHS-Fluorescein-labeled PAP was monitored (λ_{ex} = 493 nm, λ_{em} = 516 nm) with increasing concentrations of TEV RNA in the presence and absence of VPg (0 nM, —○—; 30 nM, —▽—; 50 nM, —□—; 100 nM, —△—), in order to establish the nature of competition between PAP and VPg for TEV RNA. The *solid lines* are the fitted curves. The *inset* represents Lineweaver-Burk Plots for the above interactions. Data points were fitted using least square analysis.

Table 2.5 Apparent equilibrium dissociation inhibition constants, K_{app}, for the competition titrations of NHS-Fluorescein labeled PAP and VPg for TEV RNA.

Complex	**Final Concentration of VPg Added**			
	0.0 nM	30 nM	50 nM	100 nM
	Apparent Equilibrium Inhibition Constant, K_{app}, [nM]			
NHS-Fluorescein-labeled PAP – TEV RNA	13.1 ± 1.3	17.1 ± 1.7	20.5 ± 2.4	27.6 ± 2.7

III-8 PAP Depurinates Both WT (Uncapped) and m^{7}GTP-capped S/R Oligo RNA and TEV RNA

To examine the extent to which PAP discriminates between capped and uncapped RNA transcripts and thus elucidate how PAP recognizes and targets various RNAs for depurination, a synthetic S/R oligonucleotide RNA and TEV RNA were used as substrates for PAP enzymatic activity. PAP recognized a specific and highly conserved region, the S/R loop within the large rRNA, and cleaves a distinct adenine residue (A4324) on the RNA (for the rat liver ribosome) (*29*). Previous reports showed that PAP was able to recognize the cap structure on RNA transcripts (*127*). It was postulated that PAP binding to the cap structure promotes the depurination of capped mRNAs (*130*). Other findings indicated that PAP is able to inhibit translation of uncapped RNAs without detectable levels in depurination (*132*). Both findings are not mutually exclusive, but in fact imply that the cap structure itself is not enough to promote the depurination of RNA or inhibition of RNA translation. To elucidate whether the cap structure has any effect on depurination of S/R oligo and TEV RNAs, the above RNAs were capped during run-off transcription reactions with an m^{7}GpppG cap analog. Using previously published quantification methods (*239-241*), the amount of adenine released upon RNA depurination by PAP was converted into a highly fluorescent 1-N^6-ethenoadenosine derivative by means of chloroacetaldehyde (CA) treatment. The previously reported limit of detection for 1-N^6-ethenoadenosine (0.02 pmol) and limit of quantification (0.05 pmol) (*239*), suggested that this is a suitable method to determine the amount of adenine released from S/R oligo and TEV RNAs. Zamboni *et al.* have employed this method to identify the amount of adenine released from ribosomes by ricin and gelonin (*115*). Separation using HPLC techniques and identification by means of fluorescence allowed for construction of a linear relationship between the amount of 1-

N^6-ethenoadenosine derived from the depurination of RNAs and the integrated peak area over a wide range of 1-N^6-ethenoadenosine concentrations (from 10 to 200 pmol) (Figure 3.9). The amount of adenine released from WT S/R oligo and WT TEV RNA versus m^7GpppG-capped S/R oligo and TEV RNAs with an addition of increasing amounts of PAP was determined. Under the conditions of HPLC, loaded fractions gave a single fluorescent peak with a retention time of 4.5 min (Figures 3.10 A and B). Our data indicate that both, WT and m^7GpppG-capped transcripts of S/R oligo and TEV RNA are subject to depurination by PAP. The amount of adenine released upon depurination of capped versus uncapped RNAs was of the same order of magnitude. PAP depurination did not discriminate between either capped or uncapped S/R oligo and capped or uncapped TEV RNAs (Figure 3.11). The amount of adenine released from capped and uncapped S/R oligo was 14.9 ± 0.8 nM and 13.7 ± 0.7 nM, respectively. The amount of adenine released from capped and uncapped TEV RNA was 6.0 ± 0.4 nM and 4.1 ± 0.1 nM, respectively.

The amount of adenine released upon depurination of identical quantities of TEV RNA is significantly lower than adenine released from S/R oligo RNA. As mentioned previously, PAP and other RIPs, depurinate specific purine residues in the S/R loop of the large rRNA molecule. It is not surprising that S/R oligonucleotide has a greater extend of depurination compared to TEV RNA. Nevertheless, the lesser extend of depurination of TEV RNA may be explained by the fact that TEV RNA is 143-nt 5'leader and is one of the most compact viral elements that can promote cap-independent translation (*221*). It contains secondary structure elements within its structure such as pseudoknots that are likely to hinder susceptible purine residues in otherwise linear RNA structure from being enzymatically cleaved by PAP.

III-9 VPg Decreases PAP Mediated Depurination of S/R Oligo RNA and TEV RNA

Having determined that PAP binds to VPg with a high affinity, and VPg stimulates the *in vitro* translation of uncapped IRES-containing RNA and inhibits capped RNA translation in wheat germ extracts (*214*), we investigated the extent to which the binding of VPg to PAP selectively targets PAP to the IRES of uncapped viral RNA, and increased its depurination compared to capped RNA. VPg in the depurination reactions decreased depurination of both WT (uncapped) and m^7GpppG-capped RNA constructs. Presence of equimolar VPg concentrations to that of PAP in the depurination reactions completely abolished PAP's enzymatic activity, indiscriminately whether the RNA transcripts were capped or not (Figures 10 BA and B). Figure 11 summarizes these findings. The results from our experiments show that VPg does not target PAP to IRES-containing RNA nor S/R oligo RNA, but rather acts as a potent inhibitor of PAP activity. VPg plays an important role in the viral infection cycle, replication, cell-to-cell movement, and also has been implicated in overcoming viral resistance in plants (*205*). Our findings further support the notion that VPg may play a role in overcoming viral resistance by suppressing the defense mechanism of the plant. Furthermore, depurination inhibition by VPg also suggests the possible use of this protein against cytotoxic activity of RIPs and inhibition of their biological potency.

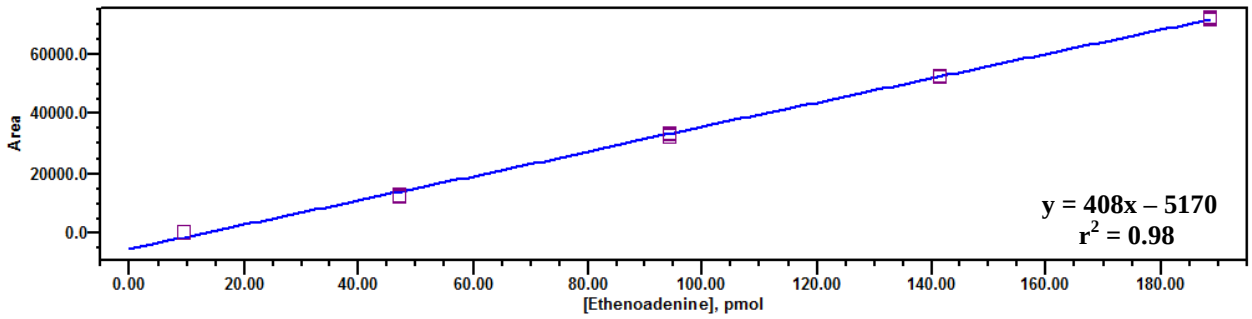

Figure 3.9 1-N^6-Ethenoadenine standard curve.

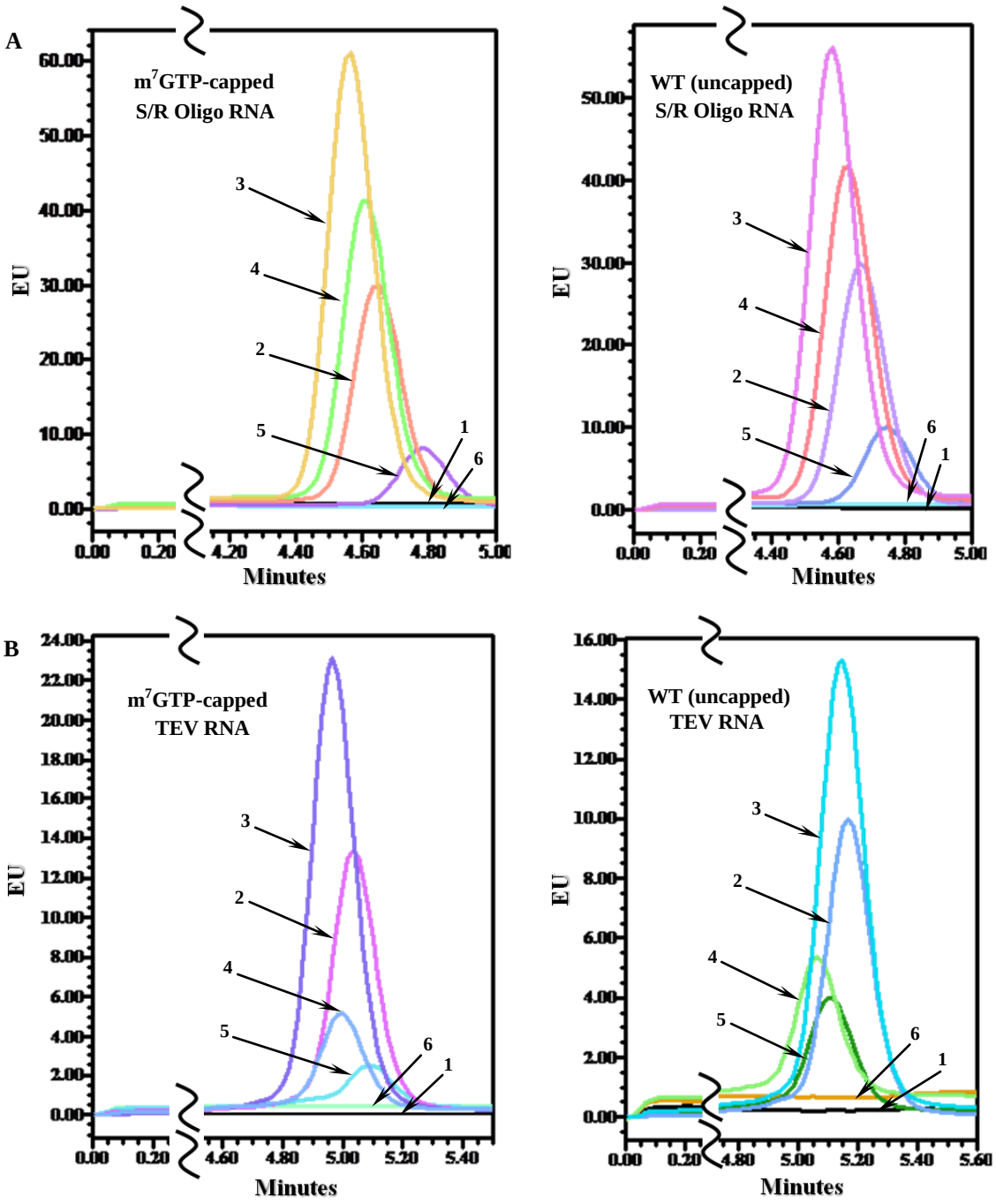

Figure 3.10 HPLC chromatogram of S/R oligo and TEV RNA depurination by PAP in the absence and presence of increasing amounts of VPg. **(A)** m^7GTP-capped and uncapped S/R oligo RNA; **(B)** m^7GTP-capped and uncapped TEV RNA. The amount of 1-N^6-ethenoadenine was monitored at the excitation wavelength of 315 nm and emission wavelength of 415 nm (1, 100 nM RNA; 2, 100 nM RNA + 50 nM PAP; 3, 100 nM RNA + 100 nM PAP; 4, 100 nM RNA + 100 nM PAP + 25 nM VPg; 5, 100 nM RNA + 100 nM PAP + 50 nM VPg; 6, 100 nM RNA + 100 nM PAP + 100 nM VPg).

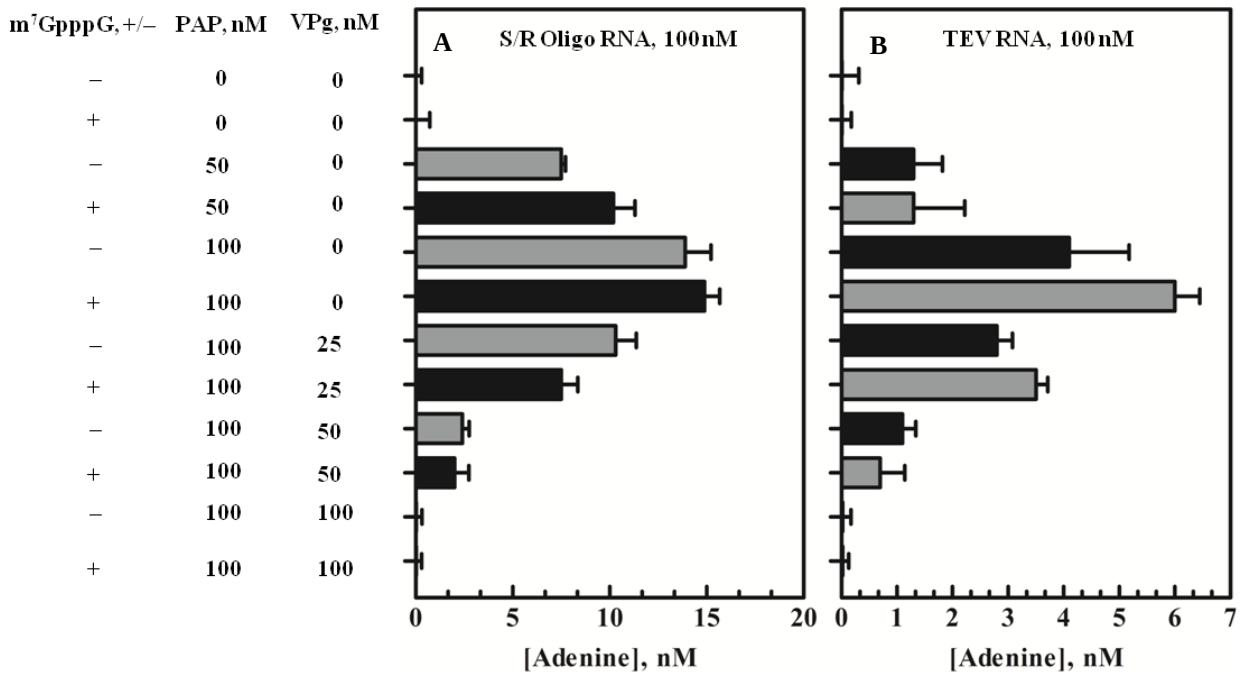

Figure 3.11 VPg inhibits PAP depurination of S/R oligo and TEV RNA. **(A)** Comparison of WT (uncapped) S/R oligo RNA depurination by PAP (black bars) to that of m^7GpppG-capped S/R oligo RNA (gray bars) in the presence and absence of VPg. **(B)** Comparison of WT (uncapped) TEV RNA depurination by PAP (black bars) to that of m^7GpppG-capped TEV RNA (gray bars) in the presence and absence of VPg. All depurination reactions were performed in triplicates.

III-10 PAP Depurinates TEV RNA at Relatively High Rates

To examine the rates at which PAP depurinates WT TEV RNA, standard quantification of adenine in the discontinuous assay format was performed. Samples with constant concentrations of RNA in the depurination buffer were incubated with PAP, and as described in Materials and Methods, fractions containing adenine released upon depurination were incubated with chloroacetaldehyde to convert adenine into its fluorescent derivative. Analysis of the fractions on the HPLC indicated that RNA depurination by PAP was virtually 80% complete after 3 minutes (Figure 3.12 A). To establish catalytic constants of TEV RNA depurination by PAP, the RNA concentrations were varied. The progress of the reaction was monitored by the appearance of a UV absorbent product, at the saturating conditions. Calculated depurination rates were plotted against the RNA concentrations resulting in a Michaelis-Menten type behavior (Figure 3.12 B). The catalytic constant, k_{cat} was calculated to be 2.5 min^{-1} (0.04167 s^{-1}). Fluorescence titrations of NHS-labeled PAP with RNA produced K_M of 15.6 nM. The specificity constant, k_{cat}/K_M was calculated to be 3.1 x 10^6 $M^{-1}s^{-1}$ (Table 2.6).

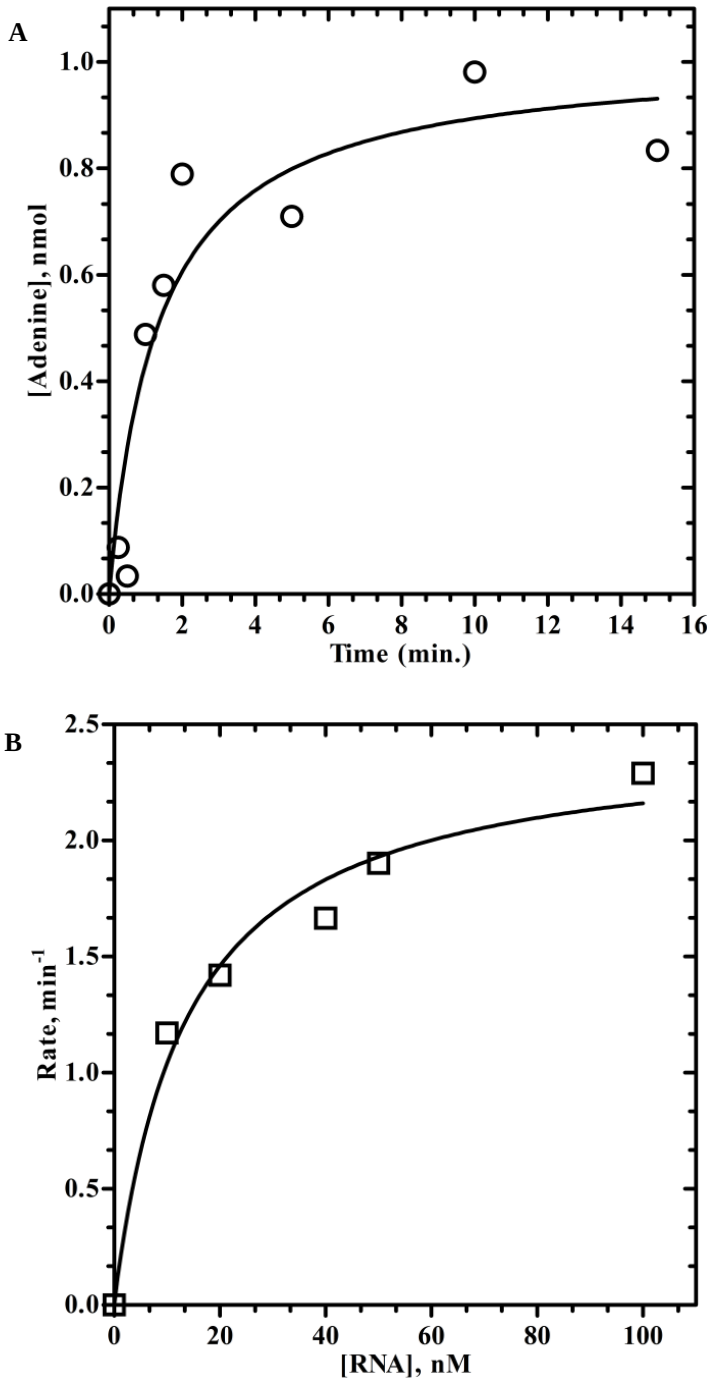

Figure 3.12 Kinetics of WT TEV RNA depurination by PAP. **(A)** Time course of adenine released during depurination of RNA by PAP as measured by the fluorescence of 1-N^6-ethenoadenine. Aliquots of PAP-RNA depurination mixtures were withdrawn at different times, and loaded directly onto the HPLC column. Excitation and emission wavelengths were 315 nm and 415 nm, respectively. **(B)** 1-N^6-ethenoadenine assay kinetic curve for depurination catalysis of RNA by PAP. 100 nM PAP was treated with increasing concentrations of rRNA, and the amount of released adenine was monitored as described in Experimental Section.

Table 2.6 PAP kinetic parameters.

Substrate	Michaelis Constant, K_m, [nM]	Turnover Number, k_{cat}, [min^{-1}]	Specificity Constant, k_{cat}/K_m, [$M^{-1} \cdot sec^{-1}$]
TEV RNA	13.6 ± 0.9	2.5 ± 0.3	$3.1 \pm 0.3 \times 10^6$

IV DISCUSSION

PAP depurinates a distinct adenine residue (A4324) from the sarcin/ricin (S/R) loop of the 28*S* rRNA (for the rat liver ribosome) (*29*). PAP is a cap-binding protein, and it was suggested that it inhibits translation of RNA by binding to the cap structure of eukaryotic mRNA, and depurinating the mRNA at sites downstream of the cap structure. PAP serves an effective inhibitor of animal and/or plant viruses. The mechanism of antiviral activity of PAP is poorly understood, however it is believed that this activity does not depend solely on the ribosomal depurination (*127*).

Khan *et al.* have characterized interactions between VPg, plant eIF*iso*4E/*iso*4F and TEV RNA (*213*), and concluded that VPg increases binding affinity of eIFs for TEV RNA. The requirement for eIF4G in cap-independent translation (*218*) has been demonstrated, and a mechanism was proposed where VPg substitutes for the cap analog and enhances formation of an eIF4F complex with viral IRES (*213*, *214*). We therefore hypothesized that VPg may interact with PAP and possibly target it to uncapped RNA.

The rationale of our investigation was that PAP, being a cap-binding protein will bind to VPg that functions as a cap analog, and these interactions would produce a greater depurination effect of uncapped viral RNA compared to that of capped cellular RNA, since VPg stimulates the *in vitro* translation of uncapped IRES-containing RNA and inhibits capped RNA translation. Our research indicated that PAP has a high affinity for VPg, and that this affinity is almost twice that of the m^7GTP analog (*131*). Greater affinity of PAP for VPg than for the cap structure would produce an advantage for the cell if VPg were to localize PAP to viral RNA for depurination. However, VPg inhibits PAP activity providing a means to avoid one of the potential host cell defense mechanisms.

It is interesting to note that thermodynamic parameters of PAP-VPg binding are similar in magnitude to those of eIF*iso*4E- or eIF*iso*4F-VPg binding. Both interactions are enthalpically driven and entropically favored. Nearly one-third $T\Delta S$ van't Hoff component to the overall value of ΔG^{o} (at 25 ^{o}C) suggests lesser dependence on electrostatic contributions and a greater conformational contribution in the PAP-VPg binding, suggesting hydrophobic residues are less solvent exposed in the combined structure. The fact that PAP-VPg interactions are enthalpically driven and entropically favored at biological temperatures supports previous observations by Baldwin *et al.* (*131*), that, since PAP is a plant defense protein, it should be able to perform under unpredictable temperature conditions given its accepted function as a ribosome depurinating agent (*131*).

Moreover, analysis of a primary structure of PAP by ProteinPredict (PHD) (*242*), a server for protein sequence analysis, structure, and function reveals that within the *C*-terminal domain a pattern was identified corresponding to an *N*-myristoyation site, as well as prokaryotic membrane lipoprotein lipid attachment site. Myristoylation is an irreversible, co-translational protein modification found in animals, plants, fungi and viruses. In this protein modification, a myristoyl group is covalently attached via an amine bond to the α-amino group of an *N*-terminal amino acid of nascent polypeptide. Identification of this pattern in PAP may clarify how PAP is localized within the extracellular spaces of pokeweed plant that until now remained unclear. Additional mass spectrometry experiments are required to confirm this hypothesis.

Different equilibrium dissociation constant, K_d, values for PAP-VPg compared to eIF*iso*4E- or eIF*iso*4F-VPg binding suggest differences between PAP's active site and eIFs' cap-binding sites. Leonard *et al*. (*188, 210*) have established previously the interactions between VPg and various isoforms of eIF4E, and Khan *et al*. (*213*) have quantified eIF4E/*iso*4E-VPg

interactions as competitive with the m^7GTP cap analog (*188*). Moreover, the binding domain on VPg was mapped to a stretch of 35 amino acids, and substitution of aspartic acid residue found within this region completely abolished interactions of VPg with eIF4E/*iso*4E (*188*). Plants infected with a TuMV infectious cDNA (p35Tunos) showed viral symptoms with p35Tunos, while plants infected with p35TuD77N, a mutant which contained the aspartic acid substitution in the VPg domain that abolished the interaction with eIF4E/*iso*4E, remained symptomless, suggesting that VPg-eIF4E/*iso*4E interaction is a critical element for virus production (*188*). VPg-71 lacks eIF4F/*iso*4F binding sites (*214*), however PAP was able to bind VPg-71, indicating PAP binding site still remains present in VPg-71 and does not include, at least partially, the amino-terminus of the protein.

Having determined the binary interactions between PAP and VPg, PAP and eIF*iso*4F, and eIF*iso*4F and VPg, we have examined the ternary interactions. A summary of directly measured binary and ternary complexes is shown in Table 3.1, and schematically presented in Figure 4.1. The equilibrium association constants K_1, K_2, K_4, and K_5 (*213*), were directly measured by fluorescence titration experiments. The PAP-eIF*iso*4F equilibrium is K_1; PAP-VPg is K_2; K_5 was from Khan *et al.* (*213*), reflects the interaction of eIF*iso*4F with VPg; K_4 was determined by titrating PAP-VPg complex with eIF*iso*4F. In Figure 4.1, K_3 and K_6 were chosen as the thermodynamically dependent equilibrium constants and were calculated from the relationships [11] and [12]:

$$K_3 = \frac{K_2 K_4}{K_1} \qquad [11]$$

$$K_6 = \frac{K_2 K_4}{K_5} \qquad [12]$$

A comparison of the cross-terms in Figure 4.1 shows that the binding of eIF*iso*4F to PAP diminishes the binding of VPg (comparing K_1 and K_4); similarly, the binding of eIF*iso*4F to VPg diminishes the binding of PAP (comparing K_5 and K_4).

In order to quantitate these interactions, coupling energies were calculated according to the method published by Weber (*243*) and as previously described in detail (*244*, *245*). The coupling energies reflect the overestimation and underestimation of the free energy of binding for the formation of ternary eIF*iso*4F-VPg-PAP complex, $\Delta G^{o}_{(\text{eIF}iso4\text{F}\cdot\text{VPg}\cdot\text{PAP})}$, calculated from the addition of the component binary energies for the interaction of eIF*iso*4F with PAP, $\Delta G^{o}_{(\text{eIF}iso4\text{F}\cdot\text{PAP})}$, or with VPg, $\Delta G^{o}_{(\text{eIF}iso4\text{F}\cdot\text{VPg})}$, and PAP with VPg, $\Delta G^{o}_{(\text{PAP}\cdot\text{VPg})}$. These coupling energies therefore represent different binding perspectives and are defined by the equations [13], [14], and [15]:

$$\Delta \boldsymbol{G}^{\boldsymbol{o}}_{(\textbf{eIF}\boldsymbol{iso}\textbf{4F, VPg}\cdot\textbf{PAP})} = \Delta \boldsymbol{G}^{\boldsymbol{o}}_{(\textbf{eIF}\boldsymbol{iso}\textbf{4F}\cdot\textbf{VPg}\cdot\textbf{PAP})} - \Delta \boldsymbol{G}^{\boldsymbol{o}}_{(\textbf{eIF}\boldsymbol{iso}\textbf{4F}\cdot\textbf{VPg})} - \Delta \boldsymbol{G}^{\boldsymbol{o}}_{(\textbf{eIF}\boldsymbol{iso}\textbf{4F}\cdot\textbf{PAP})} \quad [13]$$

$$\Delta \boldsymbol{G}^{\boldsymbol{o}}_{(\textbf{PAP, eIF}\boldsymbol{iso}\textbf{4F}\cdot\textbf{VPg})} = \Delta \boldsymbol{G}^{\boldsymbol{o}}_{(\textbf{eIF}\boldsymbol{iso}\textbf{4F, VPg}\cdot\textbf{PAP})} + \Delta \boldsymbol{G}^{\boldsymbol{o}}_{(\textbf{eIF}\boldsymbol{iso}\textbf{4F}\cdot\textbf{VPg})} - \Delta \boldsymbol{G}^{\boldsymbol{o}}_{(\textbf{PAP}\cdot\textbf{VPg})} \quad [14]$$

$$\Delta \boldsymbol{G}^{\boldsymbol{o}}_{(\textbf{VPg, eIF}\boldsymbol{iso}\textbf{4F}\cdot\textbf{PAP})} = \Delta \boldsymbol{G}^{\boldsymbol{o}}_{(\textbf{eIF}\boldsymbol{iso}\textbf{4F, VPg}\cdot\textbf{PAP})} + \Delta \boldsymbol{G}^{\boldsymbol{o}}_{(\textbf{eIF}\boldsymbol{iso}\textbf{4F}\cdot\textbf{PAP})} - \Delta \boldsymbol{G}^{\boldsymbol{o}}_{(\textbf{PAP}\cdot\textbf{VPg})} \quad [15]$$

The values for $\Delta G^{o}_{(\text{eIF}iso4\text{F}\cdot\text{PAP})}$, $\Delta G^{o}_{(\text{VPg}\cdot\text{PAP})}$, and $\Delta G^{o}_{(\text{eIF}iso4\text{F}\cdot\text{VPg})}$ were determined from K_1, K_2, and K_5 in Figure 4.1, respectively. The respective K_{eq} values are given in Table 3.1. $\Delta G^{o}_{(\text{eIF}iso4\text{F}\cdot\text{VPg}\cdot\text{PAP})}$ were determined from the addition of the ΔG^{o} values calculated from K_2 and K_4. These interaction energies indicate how the binding of one component to its site affects the binding of a second component to its site; thus each component (PAP, VPg, and eIF*iso*4F) is created as if it possesses two binding sites. For instance, $\Delta G^{o}_{(\text{PAP, eIF}iso4\text{F}\cdot\text{VPg})}$ shows how the binding of eIF*iso*4F to one site on PAP affects the affinity of the VPg for its binding site on PAP. The coupling energies may be positive, negative, or zero, depending on whether the interactions

are anticooperative, cooperative, or noncooperative due to the binding of the second component, respectively (*245*). The coupling energies calculated in this manner are presented in Table 3.2.

The binding of either PAP or VPg to eIF*iso*4F enhances the subsequent binding of the second factor to eIF*iso*4F, $\Delta G^{o}_{(\text{eIF}iso4\text{F, VPg}\cdot\text{PAP})}$ is – 1.5 kJ/mol, that is indicative of cooperative heterotropic interaction between these proteins. On the other hand, the binding of either VPg or eIF*iso*4F to PAP is anticooperative, $\Delta G^{o}_{(\text{PAP, eIF}iso4\text{F}\cdot\text{VPg})}$ is + 1.1 kJ/mol, and supports competitive type binding between VPg and eIF*iso*4F, as previously determined. This suggests that the eIF*iso*4F-VPg interaction may prevent VPg from interacting with structural features of the PAP. The binding of PAP or eIF*iso*4F to VPg, $\Delta G^{o}_{(\text{VPg, eIF}iso4\text{F}\cdot\text{PAP})}$ is + 0.1 kJ/mol, is relatively indifferent to the subsequent binding of the second component to VPg. From these data, a mechanism can be proposed for the sequence of events leading to the formation of PAP-VPg-eIF*iso*4F complex with subsequent inhibition of depurination of VPg-derived RNA. Two models are possible where PAP first forms a binary complex with eIF*iso*4F initiation factor, with the subsequent binding to VPg, or PAP binds to a preformed eIF*iso*4F-VPg binary complex. Both models lead to a ternary PAP-VPg-eIF*iso*4F complex formation, which brings PAP to close proximity with viral RNA. However, the above cooperative interactions hinder PAP's enzymatic site from the depurination of RNA, thus promoting inhibition of plant's defense mechanism.

Since cap binding proteins bind to VPg similarly to cap analogs, and VPg stimulates the *in vitro* translation of uncapped IRES-containing RNA and inhibits capped RNA translation in wheat germ extracts (*214*), we analyzed the extent to which VPg can selectively target PAP to uncapped IRES-containing viral RNA. Our findings show that interactions of VPg with PAP do not target PAP to viral RNA as does eIF*iso*4F (*218*), instead VPg inhibits depurination of both capped and uncapped S/R oligo and IRES-containing TEV transcripts. This inhibition of PAP's

depurinating activity is concentration-dependent – equimolar concentrations of VPg completely abolish enzymatic activity of PAP. However, VPg has more profound effect on the inhibition of depurination of S/R oligo RNA. This suggests that either the elements of secondary structure within the TEV hinder PAP from depurinating every adenine residue within the structure, or VPg may allosterically change PAP conformation in the way that S/R oligo and TEV sites may not be identical or available for depurination to the same extent. Fluorescence titrations showed that VPg competes with TEV for PAP binding. Depurination inhibition by VPg also suggests the possible use of this protein against cytotoxic activity of RIPs and inhibition of their biological potency.

Table 3.1 Equilibrium dissociation constants for the mutual interactions of PAP, m^7GTP, VPg, eIF*iso*4F, and TEV RNA (T = 25 ^oC, unless noted otherwise).

Complex	K_d, [nM]	Complex	K_d, [nM]
PAP·m^7GTP[a]	43.3 ± 0.1[a]	eIF*iso*4F·VPg[b]	81.3 ± 1.9[b] (K_5)[3]
PAP·m^7GTP[1]	41.7 ± 2.0	eIF*iso*4F·TEV[c]	178.0 ± 3.0[c]
PAP[2]·m^7GTP	63.8 ± 7.9	PAP·m^7GTP[1] + VPg	87.8 ± 32
PAP·VPg	29.5 ± 1.8 (K_2)[3]	PAP[2]·VPg + eIF*iso*4F	84.1 ± 13 (K_4)[3]
PAP·VPg-71	37.4 ± 3.0	PAP[2]·TEV + VPg	27.6 ± 2.7
PAP[2]·VPg	51.0 ± 6.9	eIF*iso*4F·TEV + VPg[d]	49.3 ± 3.1[d]
PAP[2]·eIF*iso*4F	56.2 ± 0.7 (K_1)[3]	eIF*iso*4F·VPg + TEV[d]	108[d]
PAP·TEV	13.1 ± 1.3	PAP[2]·eIF*iso*4F + VPg[e]	44.1 ± 1.1[e] (K_3)[3]
---	---	VPg·eIF*iso*4F + PAP[2][e]	30.5 ± 1.2[e] (K_6)[3]

(a) Values were adapted from Baldwin *et al.* (2009) *(131).*
(b) Values were adapted from Khan *et al.* (2004) *(213).*
(c) Values were adapted from Ray *et al.* (2006) *(218).*
(d) Values were adapted from Khan *et al.* (2008) *(214).*
(e) Values were calculated from the thermodynamic cycle (Figure 4.1).
(1) Anthranoyl-m^7GTP was employed.
(2) NHS-Fluorescein-labeled PAP was employed.
(3) K_1, K_2, K_3, K_4, K_5, and K_6 values pertain to Figure 4.1.

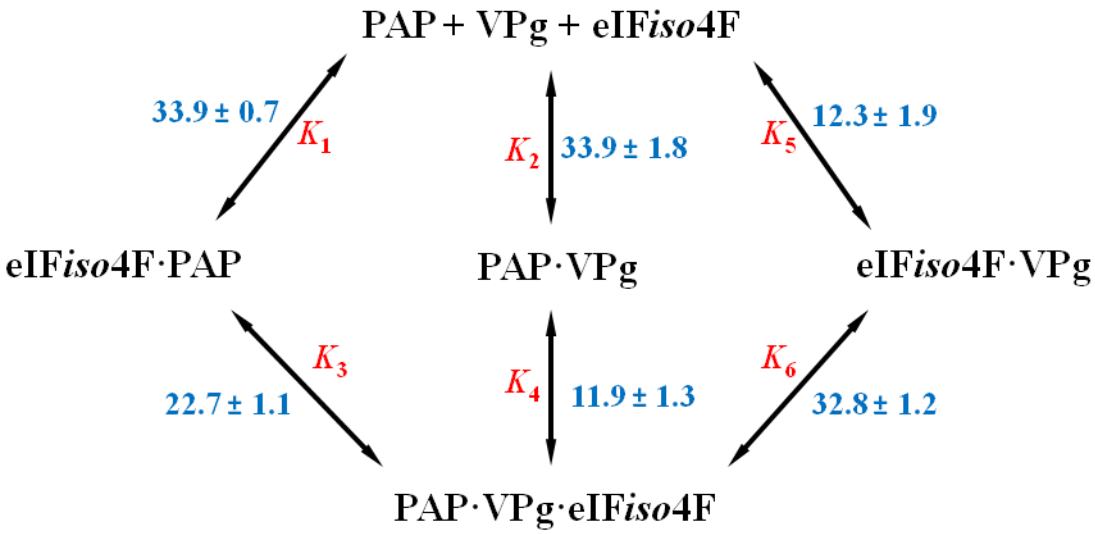

Figure 4.1 Schematic representations of the interactions between PAP, VPg, and eIF*iso*4F. K_1, K_2, K_4, and K_5 were determined experimentally; K_3 and K_6 were calculated as described in text. All equilibrium constants cited are 10^6 M^{-1}.

Table 3.2 Binding and coupling free energies (kJ/mol) for PAP, VPg, and eIF*iso*4F according to Figure 4.1 (T = 25 ^{o}C).

$\Delta G^{o}_{(PAP \cdot VPg)}$	$\Delta G^{o}_{(eIFiso4F \cdot PAP)}$	$\Delta G^{o}_{(VPg \cdot eIFiso4F)}$	$\Delta G^{o}_{(eIFiso4F,\ VPg \cdot PAP)}$	$\Delta G^{o}_{(PAP,\ eIFiso4F \cdot VPg)}$	$\Delta G^{o}_{(VPg,\ eIFiso4F \cdot PAP)}$
- 43.0	- 41.4	- 40.4	- 1.5	+ 1.1	+ 0.1

V FUTURE PERSPECTIVES

- Protein motions, particularly their conformational dynamics, regulate and often constitute protein function. Probing internal dynamics and structural determination of the PAP-VPg complexes requires complementary experiments that will allow for energetic and dynamic aspects of formation and stability of the PAP-VPg complex to be revealed. Fluorescence anisotropy studies will provide information or the binding mechanisms, and, hence, may lead to mechanistic models of PAP functioning and regulation on the molecular level.

- PAP depurinates the 5' UTR of TEV. TEV contains a pseudoknot 1 (PK1) element in the 5' UTR (*217*). This 5'leader promotes cap-independent translation and is preferentially bound by eIF4G (*223*). We have recently quantified this binding (*218*). To determine the mRNA structural elements necessary for PAP depurination and how their placement affects PAP activity, examination of the PAP binding to TEV constructs (PK1, S13, S23, CG) with different secondary structure is required. For those constructs with binding affinity, elucidation of the depurination site is essential. Also, investigation of the effects of m^7G cap and eIFs on RNA depurination is needed.

- Investigation of enzymatic activity of PAP mutants (PAPx, PAPc, and PAPn) on the depurination of TEV RNA will provide important information on the elements within the PAP primary structure that are required for depurination. PAPc is a nontoxic mutant of PAP with C-terminal deletion that does not depurinates host ribosomes, but exhibits antiviral activity when expressed in transgenic plants (*148*). PAPx is the active site mutant, and does

not confer viral resistance. PAPn is a mutant with N-terminal deletion that confers antiviral activity.

- To determine the affinity of cap binding protein interactions with PAP, and to see how this affects PAP association with mRNA cap and selection of mRNA depurination sites, quantification of PAP-eIF4E/*iso*4E is required. To determine if eIF4E and PAP are bound to eIF4G simultaneously, a pull down assay can be employed.

- Since VPg inhibits PAP enzymatic activity and thus may serve as a potent inhibitor of biological activity of other RIPs, the effect of VPg on the depurination of RNA by ricin, abrin (and other RIPs) is necessary. VPg may serve as a potent antidote against RIP poisoning, and could be therefore employed in biomedical research.

- Since VPg-71 (a mutant of VPg that lacks 71 amino acids in its N-terminus, and does not bind to eIFs) binds to PAP with high affinity, examination of other VPg mutants is required to map out the sequence on VPg necessary for PAP-binding.

VI APPENDIX

VI-1 BUFFERS AND SOLUTIONS USED IN THE EXPERIMENTS

☝ **IMPORTANT** Use distilled deionized H_2O in all recipes. Unless otherwise stated, sterile media can be stored at room temperature.

VI-1-A *E. coli* Cell Media and Solutions

- **LB Medium (Luria-Bertani Medium)**, a nutritionally rich medium, used for bacterial growth. Peptides and peptones are provided by tryptone. Vitamins and certain trace elements are provided by yeast extract. Sodium ions for transport and osmotic balance are provided by sodium chloride. Bacto-tryptone is used to provide essential amino acids to the growing bacteria, while the bacto-yeast extract is used to provide a plethora of organic compounds helpful for bacterial growth.

  Per 1 liter:

  To 950 mL of deionized H_2O, add:

tryptone	10 g
yeast extract	5 g
NaCl	10 g

  Shake until the solutes have dissolved. Adjust the pH to 7.0 with 5 *N* NaOH (~0.2 mL). Adjust the volume of the solution to 1 liter with deionized H_2O. Sterilize by autoclaving for 20 minutes at 15 psi (1.05 kg/cm^2) on liquid cycle.

- **LB Agar Medium**, LB medium containing agar in a final concentration of 1-2% for solidifying culture media. It is used as a culture medium for various microorganisms. Agar is a phycocolloid extracted from a group of red-purple marine algae (Class Rhodophyceae) particularly *Gelidium*.

  Per 100 mL:

tryptone	1 g
yeast extract	0.5 g
NaCl	1 g
Agar	1.5 g

1) Shake until the solutes have dissolved. Adjust the pH to 7.0 with 5 *N* NaOH (~0.2 mL). Adjust the volume of the solution to 1 liter with deionized H_2O. Sterilize by autoclaving for 20 minutes at 15 psi (1.05 kg/cm^2) on liquid cycle.
2) Pass the neck of the agar bottle through a flame to sterilize it. While pouring the agar, open the Petri dish lid as little as possible, hold at an angle, and keep the lid directly over the Petri dish. Pour enough melted agar into each sterile plastic Petri dish to cover 1/8" of the bottom. Cover the lid of the Petri dish immediately. Place the agar plates on a counter top to cool and set. Pass the neck of the agar bottle through flame again before applying the cap. After agar has solidified, stack the plates upside down in the refrigerator. Do Not Freeze! The purpose of placing the plates upside down is to prevent condensation from dripping down onto the agar surface which could then facilitate movement of organisms between colonies.

- **SOB Medium (Super Optimal Broth Medium)** is a nutrient-rich bacterial growth medium used for microbiological culture, generally of *E. coli*. Growth of *E. coli* in SOB or SOC (see below) medium results in higher transformation efficiencies of plasmids.

  Per 1 liter:

  To 950 mL of deionized H_2O, add:

tryptone	20 g
yeast extract	5 g
NaCl	0.5 g

  Shake until the solutes have dissolved. Add 10 mL of a 250 mM solution of KCl. (This solution is made by dissolving 1.86 g of KCl in 100 mL of deionized H_2O.) Adjust the pH of the medium to 7.0 with 5 *N* NaOH (~0.2 mL). Adjust the volume of the solution to 1 liter with deionized H_2O. Sterilize by autoclaving for 20 minutes at 15 psi (1.05 kg/cm^2) on liquid cycle. Just before use, add 5 mL of a sterile solution of 2 M $MgCl_2$. (This solution is made by dissolving 19 g of $MgCl_2$ in 90 mL of deionized H_2O. Adjust the volume of the solution to 100 mL with deionized H_2O and sterilize by autoclaving for 20 minutes at 15 psi [1.05 kg/cm^2] on liquid cycle.)

- **SOC Medium (Super Optimal broth with Catabolite repression)** is identical to SOB medium, except that it contains 20 mM glucose.

  After the SOB medium has been autoclaved, allow it to cool to 60^o C or less. Add 20 mL of a sterile 1 M solution of glucose. (This solution is made by dissolving 18 g of glucose in 90 mL of deionized H_2O. After the sugar has dissolved, adjust the volume of the solution to 100 mL with ddH_2O and sterilize by passing it through a 0.22-μm filter.)

- **Preparing Antibiotic-containing Media** - The following stock solutions are at a 1000× concentration, used to select for common Gram-negative or Gram-positive organisms that might carry resistance plasmids or other resistance genes (as opposed to susceptible strains that lack these genes). Solvent for antibiotics: distilled water, antibiotics such as tetracycline and chloramphenicol dissolve better in alcohols such as 70% ethanol or *iso*-propyl alcohol.

Antibiotic	Ampicillin	Chloramphenicol	Kanamycin
Amount for 10 mL Stock Solution	1 g	34 mg	500 mg
Final Concentration in agar media	100 μg/mL	34 μg/mL	50 μg/mL
Solvent	Water	70% EtOH	Water
Storage	-20^{o} C	-20^{o} C	-20^{o} C

1) Prepare and autoclave stock media as desired, such as LB Agar or minimal media.
2) The hot agar solution must cool before adding antibiotics as the heat may inactivate the drugs. Let the flask at room temperature, swirling every 15 minutes or so, until you can touch your fingers to the side of the flask for 2-3 seconds without removing them. At this point the agar should be warm enough that it won't soon solidify, but cool enough that it won't inactivate the antibiotics.
3) Add 1 mL of stock antibiotic per liter of agar. Use sterile pipette to add the solution.
4) Swirl the agar media containing antibiotic to mix it thorough. Try not to introduce air bubbles.
5) Pour the plates and let solidify. Cover the stack of plates with tinfoil, as light inactivates many antibiotics. Refrigerate until use.

Other Reagents and Solutions Used for Cell Cultivation

- **0.5 M Isopropyl β-D-Thiogalactopyranoside (IPTG)** – although lactose (and thus allolactose) is the natural inducer of *lac* operon, however, in the laboratory, an artificial inducer IPTG is always being used because it is not metabolized by the bacteria, and, thus it's concentration in bacterial culture remains relatively constant, thus allowing for the gene expression to be turned on. To prepare 0.5 M stock solution of IPTG, dissolve 1.62 g of IPTG in 12 mL of ddH_2O.

- **100 mM Phenylmethylsulfonyl Fluoride (PMSF)** – PMSF is a protease inhibitor. The action of proteases is blocked within the cell because of the presence of endosomes. When you lyse cell and membranes, various proteases are releases, thus digesting the proteins of interest. The action of proteases must be blocked during protein extraction and purification. To prepare 100 mM stock solution of PMSF, dissolve 440 mg of PMSF in 25 mL of *iso*-propyl alcohol. The use of PMSF in combination with protein inhibitor cocktail mix (see below) is ideal for every cell lysate. Addition of phosphatase inhibitor cocktails (see below) is also recommended to protect the phosphor-status of proteins. Dimethyl sulfoxide (DMSO) is a good stabilizing solvent for PMSF.

- **Complete Protease Inhibitor Cocktail Tables** – inhibit a broad spectrum of serine, cysteine and metalloproteases as well as calpains. They are very well suited for the protection of proteins isolated from animal tissues, plants, yeast and bacteria, and contain both irreversible and reversible protease inhibitors. One tablet is sufficient for the inhibition of the proteolytic activity in 50 mL extraction solution. Alternatively a stock

solution (25× conc.) can be prepared. Tables contain EDTA (18.5 mg/tablet yields 1 mM solution of EDTA in 50 mL).

- **100× Protease Inhibitor Stock Solution** – alternatively to the Complete Protease Inhibitor Cocktail Tablets, Protease Inhibitor stock solution can be prepared and used to inhibit the proteolytic activity of proteases.

  Per 10 mL Stock Solution:

Benzamidine HCl	16 mg
Phenanthroline	10 mg
Aprotinin	10 mg
Pepstatin A	10 mg
Leupeptin	10 mg
Soybean Trypsin Inhibitor (STI)	10 mg
1× HEPES-KOH, pH 7.6 Buffer	10 mL

  Use 1 mL of 100× Protease Inhibitor Stock Solution per 50 mL of lysis buffer.

- **Phosphatase Inhibitor Cocktail 1 and 2** – Crude cell extracts contain a number of endogeneous enzymes, such as proteases and phosphatases, which are capable of modifying the proteins present in the extract. The best way to improve the yield of intact proteins is to add inhibitors of these enzymes known to be present in the source material.

  1) Phosphatase Inhibitor Cocktail 1 has been optimized and tested for L-isozymes of alkaline phosphatase as well as serine/threonine protein phosphatases, such as protein phosphatases 1 and 2A. The cocktail is supplied as a clear solution in DMSO and

contains cantharidin (inhibits protein phosphatase A2), bromotetramisole (inhibits alkaline phosphatases), and microcystin LR (inhibits protein phosphatases 1 and 2A). Add 1 mL of cocktail solution per 100 mL of extraction buffer.

2) Phosphatase Inhibitor Cocktail 2 has been optimized and tested for tyrosine protein phosphatases, acid and alkaline phosphatases. The cocktail is supplied as a clear, faint yellow aqueous solution and contains sodium orthovanadate (inhibits a number of ATPases, protein tyrosine phosphatases, and other phosphate-transferring enzymes), sodium tartrate (inhibits acid phosphatases), and imidazole (inhibits alkaline phosphatases). Add 1 mL of cocktail solution per 100 mL of extraction buffer.

VI-1-B Buffers Used for Protein Purifications

- **10× HEPES-KOH, pH 7.6 Buffer**

Per 1 liter:

HEPES	59.6 g
KCl	74.6 g
$MgCl_2$	2.0 g
ddH_2O	900 mL

Mix, adjust pH to 7.6 by adding of 1*N* KOH then add ddH_2O to produce 1 L solution. DTT is added just before usage to produce 10 mM final concentration. Store at 4^o C. Dilution of 100 mL of 10× HEPES Buffer into 900 mL ddH_2O will produce 1 L of 1× Buffer containing 25 mM HEPES-KOH, pH 7.6, 100 mM KCl, and 10 mM $MgCl_2$.

- **Lysis Buffer**

Per 100 mL:

10× HEPES-KOH, pH 7.6 Buffer	10 mL
Glycerol, Ultrapure	10 mL
Complete Protease Inhibitor Cocktail	
Tablet or Stock Solution	1 Tablet or 1 mL Stock Solution
Phosphatase Inhibitor Cocktail 1	1 mL
Phosphoatase Inhibitor Cocktail 2	1 mL
100 mM PMSF Solution	1 mL
ddH_2O	76 mL

Do not store. Immediate usage of the buffer is recommended.

- **10× PBS Buffer (Phosphate-buffered Saline)**

Per 1 liter:

NaCl	80 g
KCl	2 g
Na_2HPO_4	14.4 g
K_2HPO_4	2.4 g

Mix thoroughly allowing reagents to dissolve. Adjust pH to 7.4 by addition of 1*N* HCl then add ddH_2O to produce 1 L solution. Store at 4^o C.

Dilution of 100 mL of 10× PBS Buffer into 900 mL ddH_2O will produce 1 L of 1× Buffer containing 1.37 M NaCl, 0.027 M KCl, and 0.119 M Phosphate Buffer, pH 7.4.

- **Grinding Buffer** (PAP purification; homogenation of pokeweed leaves)

  [50 mM Tris-HCl, pH 7.5, 0.2 mM EDTA, 5 mM DTT, 1% w/v PVP]

  Per 1 liter:

Tris base	6.1 g
EDTA, free acid	0.058 g
DTT *	0.77 g
PVP	1 g

  Mix thoroughly allowing reagents to dissolve. Adjust pH to 7.5 by addition of 1*N* HCl then add ddH_2O to produce 1 L solution. Store at 4^o C.

  * DTT is added fresh, prior to usage.

- **Q Buffer** (for PAP purification; Hi Trap Q FF column and dialysis)

  [20 mM Tris-HCl, pH 7.5, 0.2 mM EDTA, 1 mM DTT]

  Per 1 liter:

Tris base	2.4 g
EDTA, free acid	0.058 g
DTT *	0.15 g

  Mix thoroughly allowing reagents to dissolve. Adjust pH to 7.5 by addition of 1*N* HCl then add ddH_2O to produce 1 L solution. Store at 4^o C.

  * DTT is added fresh, prior to usage.

- **S Buffer** (for PAP purification; Hi Trap SP FF column)

  [10 mM MES, pH 5.2, 0.2 mM EDTA, 0.1 mM DTT]

  Per 1 liter:

MES	2.0 g
EDTA, free acid	0.058 g
DTT *	0.015 g

  Mix thoroughly allowing reagents to dissolve. Adjust pH to 5.2 by addition of 1*N* KOH then add ddH_2O to produce 1 L solution. Store at 4^o C.

  * DTT is added fresh, prior to usage.

- **Buffer A** (for VPg purification; sonication, equilibration, and washing buffer for His-tagged column)

  [20 mM Tris-HCl, pH 8.0, 300 mM NaCl, 10 mM imidazole]

  Per 1 liter:

Tris-HCl	3.2 g
NaCl	16.3 g
Imidazole	0.68 g

  Mix thoroughly allowing reagents to dissolve. Adjust pH to 8.0 by addition of 1*N* KOH then add ddH_2O to produce 1 L solution. Store at 4^o C.

- **Buffer B** (for VPg purification; elution buffer for His-tagged column)

  [20 mM Tris-HCl, pH 8.0, 300 mM NaCl, 250 mM imidazole]

  Per 1 liter:

Tris-HCl	3.2 g
NaCl	16.3 g
Imidazole	17 g

  Mix thoroughly allowing reagents to dissolve. Adjust pH to 8.0 by addition of 1*N* KOH then add ddH_2O to produce 1 L solution. Store at 4^o C.

- **Buffer C** (for VPg purification, dialysis buffer)

  [20 mM Tris-HCl, pH 8.0, 10 mM NaCl, 1 mM DTT, 5% v/v glycerol]

  Per 1 liter:

Tris-HCl	3.2 g
NaCl	0.54 g
DTT *	0.15 g
Glycerol, Ultrapure	50 mL

  Mix thoroughly allowing reagents to dissolve. Adjust pH to 8.0 by addition of 1*N* KOH then add ddH_2O to produce 1 L solution. Store at 4^o C.

  * DTT is added fresh, prior to usage.

- **Buffer D** (for VPg purification; HiTrap Mono Q column and dialysis buffer)

  [20 mM Tris-HCl, pH 7.6, 150 mM NaCl, 5% v/v glycerol]

  Per 1 liter:

Tris-HCl	3.2 g
NaCl	0.54 g
Glycerol, Ultrapure	50 mL

  Mix & adjust pH to 7.6 by addition of 1*N* KOH then add ddH_2O to produce 1 L solution. Store at 4^o C.

- **Buffer E** (for VPg purification; dialysis buffer and titration buffer)

[20 mM HEPES-KOH, pH 7.6, 100 mM KCl, 1.0 mM $MgCl_2$, 1.0 mM DTT, 1.0 mM EDTA]

  Per 1 liter:

HEPES	4.8 g
KCl	7.5 g
$MgCl_2$	0.2 g
DTT *	0.15 g
EDTA	0.29 g

  Mix & adjust pH to 7.6 by addition of 1*N* KOH then add ddH_2O to produce 1 L solution. Store at 4^o C. * DTT is added fresh, prior to usage.

- **Buffer B-50** (for eIFs purification; dialysis, Mono Q & m^7GTP Sepharose elution buffer)

[20 mM HEPES-KOH, pH 7.6, 0.1 mM EDTA, 1 mM DTT, 5% v/v glycerol, 50 mM KCl]

Per 1 liter:

HEPES	4.8 g
EDTA	0.029 g
DTT *	0.15 g
Glycerol, Ultrapure	50 mL
KCl	3.7 g

Mix thoroughly allowing reagents to dissolve. Adjust pH to 7.6 by addition of 1*N* KOH then add ddH_2O to produce 1 L solution. Store at 4^o C.

* DTT is added fresh, prior to usage.

- **Buffer B-400** (for eIFs purification; HiTrap Mono Q column elution buffer)

[20 mM HEPES-KOH, pH 7.6, 0.1 mM EDTA, 1 mM DTT, 5% v/v glycerol, 400 mM KCl]

Per 1 liter:

HEPES	4.8 g
EDTA	0.029 g
DTT *	0.015 g
Glycerol, Ultrapure	50 mL
KCl	30 g

Mix thoroughly allowing reagents to dissolve. Adjust pH to 7.6 by addition of 1*N* KOH then add ddH_2O to produce 1 L solution. Store at 4^o C.

* DTT is added fresh, prior to usage.

- **Buffer B-600** (for eIFs purification; lysis buffer containing 600 mM KCl)

  [20 mM HEPES-KOH, pH 7.6, 0.1 mM EDTA, 1 mM DTT, 5% v/v glycerol,

  600 mM KCl, protease and phosphatase inhibitors]

  Per 100 mL:

HEPES	0.48 g
EDTA	0.003 g
DTT	0.015 g
Glycerol, Ultrapure	5 mL
KCl	4.5 g
Tablet or Stock Solution	1 Tablet or 1 mL Stock Solution
Phosphatase Inhibitor Cocktail 1	1 mL
Phosphoatase Inhibitor Cocktail 2	1 mL
100 mM PMSF Solution	1 mL

  Mix thoroughly allowing reagents to dissolve. Adjust pH to 7.6 by addition of 1*N* KOH then add ddH_2O to produce 100 mL solution. Do not store. Immediate usage of the buffer is recommended.

VI-1-C Buffers and Solutions Used in Plasmid DNA Isolation and Purification

- **Buffer P1 (Resuspension Buffer)**

[50 mM Tris-HCl, pH 8.0, 10 mM EDTA, 100 μg/mL RNase A]

Per 250 mL:

Tris-HCl	1.97 g
EDTA, free acid	0.73 g
RNase A	25 mg

Dissolve the solutes in 200 mL dH_2O. Adjust pH with KOH to 8.0. Add RNase A. Adjust the volume to 250 mL. Store at 2-8 ^oC, after addition of RNase A.

- **Buffer P2 (Lysis Buffer)**

[200 mM NaOH, 1% SDS, w/v]

Per 250 mL:

NaOH	2.0 g
SDS	2.5 g

Dissolve the solutes in 250 mL dH_2O. Store at 15-25 ^oC.

- **Buffer P3 (Neutralization Buffer)**

[3.0 M CH_3COOK, pH 5.5]

Per 250 mL:

CH_3COOK	73.6 g

Dissolve the solute in 200 mL dH_2O. Adjust pH with glacial acetic acid to 5.5. Adjust the volume to 250 mL. Store at 15-25 ^oC or 2-8 ^oC.

- **Buffer FWB2 (QlAfilter Wash Buffer)**

[1 M CH_3COOK, pH 5.0]

Per 250 mL:

CH_3COOK	24.5 g

Dissolve the solute in 200 mL dH_2O. Adjust pH with glacial acetic acid to 5.0. Adjust the volume to 250 mL. Store at 15-25 ^oC.

- **Buffer QBT (Equilibration Buffer)**

[750 mM NaCl, 50 mM MOPS, pH 7.0, 15% isoPrOH, v/v, 0.15% Triton® X-100, v/v]

Per 250 mL:

NaCl	11.0 g
MOPS	2.62 g
isoPrOH	37.5 mL
Triton® X-100	375 µL

Dissolve the solute in 200 mL dH_2O. Adjust pH with glacial KOH to 7.0. Add isoPrOH and Triton® X-100. Adjust the volume to 250 mL. Store at 15-25 ^oC.

- **Buffer QC (Wash Buffer)**

[1.0 M NaCl, 50 mM MOPS, pH 7.0, 15% isoPrOH, v/v]

NaCl	14.6 g
MOPS	2.62 g
isoPrOH	37.5 mL

Dissolve the solute in 200 mL dH_2O. Adjust pH with glacial KOH to 7.0. Add isoPrOH. Adjust the volume to 250 mL. Store at 15-25 ^oC.

- **Buffer QF (Elution Buffer)**

[1.25 M NaCl, 50 mM Tris-HCl, pH 8.5, 15% isoPrOH, v/v]

Per 250 mL:

NaCl	18.3 g
Tris-HCl	1.97 g
isoPrOH	37.5 mL

Adjust pH with glacial KOH to 8.5. Add isoPrOH. Adjust the volume to 250 mL. Store at 15-25 ^{o}C.

- **Buffer QN (Elution Buffer)**

[1.6 M NaCl, 50 mM MOPS, pH 7.0, 15% isoPrOH, v/v]

Per 250 mL:

NaCl	23.4 g
MOPS	2.62 g
isoPrOH	37.5 mL

Dissolve the solute in 200 mL dH_2O. Adjust pH with glacial KOH to 7.0. Add isoPrOH. Adjust the volume to 250 mL. Store at 15-25 ^{o}C.

- **TE Buffer**

[10 mM Tris-HCl, pH 8.0, 1 mM EDTA]

Per 50 mL:

Tris-HCl	0.0788 g
EDTA, free acid	0.0146 g

Dissolve the solute in 40 mL dH_2O. Adjust pH with glacial KOH to 8.0. Adjust the volume to 50 mL. Store at 15-25 ^{o}C.

- **STE Buffer**

[100 mM NaCl, 10 mM Tris-HCl, 8.0, 1 mM EDTA]

Per 50 mL:

NaCl	0.2922 g
Tris-HCl	0.0788 g
EDTA, free acid	0.0146 g

Dissolve the solute in 40 mL dH_2O. Adjust pH with glacial KOH to 8.0. Adjust the volume to 50 mL. Store at 15-25 ^oC.

VI-1-D Buffers and Solutions Used for RNA Isolation and Purification

- **Restriction Endonuclease Buffers**

1) *Hind*III Endonuclease

1× NEBuffer 2:	**Storage Buffer:**
10 mM Tris-HCl, pH 7.9 @25^o C	10 mM Tris-HCl, pH 7.4 @ 25^o C
50 mM NaCl	250 mM NaCl
10 mM $MgCl_2$	1 mM DTT
1 mM DTT	0.1 mM EDTA
	500 μg/mL BSA
	50% Glycerol
	Storage Temperature: -20^o C

2) *Nco*I and *Sal*I Endonucleases

1× NEBuffer 3:	**Storage Buffer:**
50 mM Tris-HCl, pH 7.9 @ 25^{o} C	10 mM Tris-HCl, pH 7.4 @ 25^{o} C
100 mM NaCl	50 mM KCl
10 mM $MgCl_2$	1 mM DTT
1 mM DTT	0.1 mM EDTA
	200 μg/mL BSA (300 μg/mL for *Sal*I)
	50% Glycerol
	Storage Temperature: -20^{o} C

- **Ligation Buffers**

1× T4 DNA Ligase Reaction Buffer:	**Storage Buffer:**
50 mM Tris-HCl, pH 7.5 @ 25^{o} C	10 mM Tris-HCl, pH 7.4 @ 25^{o} C
10 mM $MgCl_2$	50 mM KCl
1 mM ATP	1 mM DTT
10 mM DTT	50% Glycerol
	Storage Temperature: -20^{o} C

- **RNase Buffer** – Proteinase K is a subtilisin-like endolytic serine protease that is isolated from the saprophytic fungus *Tritirachium album*. It has a high activity that is stable across a wide range of pH and temperature conditions and is suited to short digestion times. The activity of proteinase K is increased at elevated temperatures up to 65^{o} C. Calcium is not essential to the function of proteinase K. Therefore, EDTA and other

chelating agents do not interfere with the activity and may be used alongside proteinase K to inactivate calcium-dependent nucleases in DNA and RNA preparation. Proteinase K inactivates RNase and DNase during nucleic acid purification. Optimal RNA yields depend on a high-quantity DNA template. The DNA template must be free of RNase. If the presence of RNase is suspected, treat the DNA with Proteinase K (100 μg/mL) and SDS (0.5%) in 50 mM Tris-HCl (pH 7.5), 5 mM $CaCl_2$ for 30 minutes at 37^o C.

- **5× MOPS Buffer** (for RNA Sample Buffer Preparation)

  [0.2 M MOPS, pH 7.0, 50 mM sodium acetate, 5 mM EDTA]

  Per 10 mL:

MOPS	0.42 g
Sodium Acetate, Anhydrous	0.041 g
EDTA	0.015 g

  Mix thoroughly allowing reagents to dissolve. Adjust pH to 7.0 by addition of 1*N* KOH then add ddH_2O to produce 10 mL solution. Store at 4^o C.

- **TE Buffer** (for phenol:chloroform:*iso*-amyl alcohol saturation)

  [10 mM Tris-HCl, pH 8.0, 1 mM EDTA]

  Per 100 mL:

Tris-HCl	0.16 g
EDTA	0.029 g

  Mix thoroughly allowing reagents to dissolve. Adjust pH to 8.0 by addition of 1*N* KOH then add ddH_2O to produce 100 mL solution. Store at 4^o C.

- **TE-saturated Phenol:Chloroform:*iso*-Amyl Alcohol (25:24:1, v/v) (pH 8.0)**

  Mix equal parts of the TE buffer and phenol and allow the phases to separate. Then mix 1 part of the lower phenol phase with 1 part of the chloroform/*iso*-amyl alcohol (24:1, v/v).

- **Transcription 5× Buffer** (for the synthesis of RNA)

  [400 mM HEPES-KOH, pH 7.5, 160 mM $MgCl_2$ (for SP6) or 120 mM $MgCl_2$ (for T7), 10 mM Spermidine, 200 mM DTT]

  For 1 mL:

HEPES	0.095 g
$MgCl_2$	0.033 g (for SP6) or 0.024 g (for T7)
Spermidine base	16 μL
DTT	0.031 g

  Mix thoroughly allowing reagents to dissolve. Adjust pH to 7.5 by addition of 1*N* KOH then add ddH_2O to produce 1 mL solution. Store at -20^o C.

VI-1-E Buffers Used in PAP Labeling and PAP Titrations

- **0.67 M Borate Buffer, pH 8.5**

  [50 mM Sodium Borate, 17 mM H_3BO_3]

  Per 10 mL:

Borax, $Na_2B_4O_7 \times 10H_2O$	0.19 g

  Mix thoroughly allowing reagent to dissolve. Adjust pH to 8.5 by addition of boric acid, H_3BO_3 then add ddH_2O to produce 10 mL solution. Store at -20^o C.

- **1× PBS (Phosphate-buffered Saline)**

  [1.37 M NaCl, 0.027 M KCl, and 0.119 M Phosphate Buffer, pH 7.4]

  Per 10 mL:

NaCl	0.80 g
KCl	0.02 g
Na_2HPO_4	0.14 g
K_2HPO_4	0.024 g

  Mix thoroughly allowing reagents to dissolve. Adjust pH to 7.4 by addition of 1*N* HCl then add ddH_2O to produce 10 mL solution. Store at 4^o C.

- **PAP Titration Buffer**

  [20 mM HEPES-KOH, pH 7.5, 100 mM KCl, 1 mM DTT]

  Per 100 mL:

HEPES	0.48 g
KCl	0.67 g
DTT *	1.5 mg (per 10 mL)

  Mix thoroughly allowing reagents to dissolve. Adjust pH to 7.5 by addition of 1*N* KOH then add ddH_2O to produce 100 mL solution. Aliquot in 10 mL portions. Store at -20^o C.

  * DTT is added fresh, prior to usage.

VI-1-F Solutions Used in Anthranoyl-m^{7}GTP Synthesis

- **30% Ethanol Solution (v/v)** (for Ant-m^{7}GTP elution)

  Per 1 liter:

Ethyl Alcohol, Anhydrous	300 mL
ddH_2O	700 mL

  Mix reagents in a 1 L graduated cylinder. Add ddH_2O to the 1 L mark.

- **System A TLC Developing Solvent** (for silica gel plate development)

  [1-Propanol : NH_4OH : Water, 6:3:1, v/v, containing 0.5 g/L of EDTA]

  Per 100 mL:

1-Propanol	60 mL
NH_4OH	30 mL
Water	10 mL
EDTA, free acid	0.05 g

  Mix reagents in a 100 mL graduated cylinder. Add EDTA, and mix to dissolve.

- **System B TLC Developing Solvent** (for cellulose plate development)

  [2-Propanol : Water : HCl, 65:18.4:16.6, v/v]

  Per 100 mL:

2-Propanol	65 mL
Water	18.4 mL
HCl, conc.	16.6 mL

  In a 100 mL graduated cylinder add water to the concentrated HCl. Mix well, and add 1-propanol. Mix thoroughly.

VI-1-G Buffers Used to Measure Enzymatic Activity of PAP (Depurination)

- **Depurination Buffer**

[20 mM Tris-HCl, pH 7.5, 100 mM NH_4Cl, 7 mM Magnesium Acetate, 1 mM DTT]

Per 100 mL:

Tris, base	0.24 g
NH_4Cl	0.53 g
Magnesium Acetate	0.10 g
DTT *	0.015 g

Mix thoroughly allowing reagents to dissolve. Adjust pH to 7.5 by addition of 1*N* HCl then add ddH_2O to produce 100 mL solution. Store at -20° C.

* DTT is added fresh, prior to usage.

- **Chloroacetaldehyde/Sodium Acetate Buffer Mixture**

0.14 M Chloroacetaldehyde, 0.1 M Sodium Acetate, pH 5.1]

Prepare 100 mL of Sodium Acetate Buffer, pH 5.1 as follows: Take 0.82 g anhydrous sodium acetate and place into a 100 mL volumetric flask. Add ~ 90 mL ddH_2O. Mix well to dissolve. Adjust pH with 1 *N* acetic acid to acquire pH of 5.1.

Per 100 mL:

Chloroacetaldehyde, ~50 wt. % in H_2O	889 µL
Sodium Acetate Buffer, pH 5.1	99.1 mL

Take 99.1 mL of the above sodium acetate buffer, pH 5.1 and add 889 µL of ~50 wt. % chloroacetaldehyde in H_2O (MW 78.15 g/mol, d 1.236 g/mL). Mix well to dissolve. Store at 4° C.

- **Water-saturated Diethyl Ether**

  To prepare 1 L of water saturated diethyl ether, take 1 L of diethyl ether and mix with ~250 mL of ddH_2O. Mix well for 10 minutes. Allow two layers to separate. Use the lower, organic layer for extraction.

VI-1-H Solvents Used in HPLC Separation

- **HPLC Elution Buffer**

  [50 mM Ammonium Acetate Buffer, pH 5 / Methanol, 89:11, v/v]

  Prepare 1 L of Sodium Acetate Buffer, pH 5.1 as follows: Take 4.1 g anhydrous sodium acetate and place into a 1 L volumetric flask. Add ~ 950 mL ddH_2O. Mix well to dissolve. Adjust pH with 1 *N* acetic acid to acquire pH of 5.

  Per 1 liter:

Ammonium Acetate Buffer, pH 5	890 mL
Methanol, HPLC Grade	110 mL

  Mix well then filter through a 0.22 μm fiter. Try not to introduce air bubbles. Degas this solution using vacuum. Do not store. Use fresh to prevent bacterial accumulation.

VI-2 BUFFERS AND REAGENTS USED IN GEL ELECTROPHORESIS

VI-2-A DNA Agarose Gel Electrophoresis

- **50× TAE Buffer, pH 8.0 Stock Solution**

Per 1 liter:

Tris, free base	242 g
Acetic Acid, glacial	57.1 mL
0.5 M EDTA solution	100 mL

Dissolve Tris base in ~700 mL of ddH_2O; mix well to dissolve. Add acetic acid and EDTA solution; mix well. Adjust pH to ~ 8.3. Working solution is 1× TAE buffer is prepared by diluting 20 mL of 50× Stock Solution with ddH_2O to 1 L to produce 40 mM Tris-acetate and 1 mM EDTA. Store at room temperature for six months.

- **5× TBE Buffer, pH 8.0 Stock Solution**

Per 1 liter:

Tris, free base	54 g
Boric Acid	27.5 g
0.5 M EDTA solution	20 mL

Dissolve Tris base in ~800 mL of ddH_2O; mix well to dissolve. Add boric acid and EDTA solution; mix well. Adjust pH to ~ 8.3. Working solution is 0.5× TBE buffer is prepared by diluting 100 mL of 5× Stock Solution with ddH_2O to 1 L to produce 45 mM Tris-borate and 1 mM EDTA. Store at room temperature for six months.

TBE is usually made and stored as a 5× or 10× stock solution. The pH of the concentrated stock buffer should be ~8.3. Dilute the concentrated stock just before the

use and make the gel solution and the electrophoresis buffer from the same concentrated stock solution. Some investigators prefer to use more concentrated stock solutions of TBE (10× as opposed to 5×). However, 5× stock solution is more stable because the solutes do not precipitate during storage. Passing the concentrated buffer stocks through a 0.45-μm filter can prevent or delay formation of precipitates.

- **1.2% (w/v) Agarose in 1× TAE Buffer, pH 8.0 (or in 0.5× TBE Buffer, pH 8.0)**

  Use low EEO agarose of Molecular Biology Certified Grade with melting temperature of 90-95^{o} C and gelling temperature of 35-38^{o} C.

  Per 100 mL:

Agarose, low EEO	12 g

  Mix 1 g of powdered agarose with 100 mL of appropriate electrophoresis buffer (1× TAE or 0.5× TBE) in a 250-mL Erlenmeyer flask. Loosely plug the neck of the Erlenmeyer flask with Kimwipes. Heat the slurry in a microwave oven until the agarose dissolves. The agarose solution can become superheated and may boil violently if it is heated for too long in the microwave oven. Use insulated gloves or tongs to transfer the flask into a water bath at 55^{o} C. When the molten gel has cooled, add ethidium bromide to a final concentration of 0.5 μg/mL. Mix the gel solution thoroughly by gentle swirling. Poor the warm solution into the mold. Range of separation of liner DNA molecules in 1.2% (w/v) agarose gel is 0.4-6 kb.

- **6× DNA Sample Loading Buffer, Type III**

  [0.25% Bromphenol Blue, 0.25% Xylene Cyanol FF, 30% Glycerol in H_2O]

  Per 10 mL:

Bromphenol Blue	25 mg
Xylene Cyanol FF	25 mg
Glycerol, ultra pure	3 mL

  Dissolve bromphenol blue and xylene cyanol FF in ~6 mL of ddH_2O; mix well. Add 3 mL of ultra pure glycelor; mix well. Add ddH_2O to 10 mL. Aliquot and store at -20^o C for six months.

VI-2-B RNA Polyacrylamide/Urea Gel Electrophoresis

- **10% Acrylamide/8 M Urea gel** (for S/R oligo RNA)

  Per 500 mL:

Acrylamide:Bisacrylamide (40%:2%)	125 mL
10× TBE Buffer	50 mL
Urea	240 g
ddH_2O	to make to 500 mL

- **6% Acrylamide/8 M Urea gel** (for TEV RNA):

Acrylamide:Bisacrylamide (40%:2%)	75 mL
10× TBE Buffer	50 mL
Urea	240 g
ddH_2O	to make to 500 mL

Microwave the solution in an Erlenmeyer flask for about 10 sec. Swirl the flask to dissolve all the solids in the solution. Degas by hooking up the flask to a vacuum line and applying the vacuum for 1 to 2 min. Siliconize the gel casting plates. To the Acrylamide solution, add 125 μL of 10% Ammonium Persulfate and then add 25 μL of TEMED (per 10 mL gels). Pour the Acrylamide solution and insert a comb. Polymerize the gel for 20 min. The gel can be stored overnight at room temperature if the top of the gel is wetted with water and the whole gel is wrapped tightly in plastic wrap.

- **RNA Loading Buffer**

[50% Glycerol, 1 mM EDTA, 0.4% Bromphenol Blue, 1 mg/mL Ethidium Bromide]

Per 1 mL:

Glycerol, ultra pure	500 μL
0.5 M EDTA solution	2 μL
Bromphenol Blue	4 mg
Ethidium Bromide	1 mg

Mix bromphenol blue dye in ~ 500 μL of DEPC water and add 2 μL of 0.5 M EDTA solution. Add 1 mg of ethidium bromide and mix well to dissolve. Store at -20^{o} C.

- **RNA Sample Buffer**

Formamide, deionized	10.0 mL
37% Formaldehyde	3.5 mL
5× MOPS Buffer (final conc. 7%)	2.0 mL

Mix the reagents well. Dispense into aliquots and store at -20^{o} C for up to six months. Do not freeze-thaw more than twice.

VI-2-C Protein Electrophoresis

- **FILTER ALL SOLUTIONS**
- **CAUTION: Acrylamide is neurotoxic and should be handled with care!**
- **Note: The free base form of Tris and glycine were used when making these solutions. The term "Tris-HCl", used in these formulations, is an indication that the pH of the solution is adjusted with concentrated HCl.**

➢ Monomer Solution (30.8%T, 2.7%C_{bis})

Per 200 mL:

Acrylamide	60 g
N,N'-Methylenebis(acrylamide)	1.6 g
ddH_2O	to 200 mL

Dissolve the reagents in ~150 mL of ddH_2O; add water up to 200 mL mark.

Store up to 3 months at 4^o C in the dark.

➢ 4× Running Gel Buffer (1.5 M Tris-HCl, pH 8.8)

Per 200 mL:

Tris, free base	36.3 g

Dissolve the solute in ~150 mL of ddH_2O. Adjust to pH 8.8 with HCl, conc. Add ddH_2O to 200 mL. Store up to 3 months at 4^o C in the dark.

- **4× Stacking Gel Buffer (0.5 M Tris-HCl, pH 6.8)**

  Per 50 mL:

Tris, free base	3.0 g

  Dissolve the solute in ~40 mL of ddH_2O. Adjust to pH 6.8 with HCl, conc. Add ddH_2O to 50 mL. Store up to 3 months at 4^o C in the dark.

- **10% SDS Solution (Sodium Dodecyl Sulfate)**

  Per 100 mL:

SDS	10 g

  Dissolve the solute in ~70 mL ddH_2O; add water to a 100 mL mark. Store up to 6 months at room temperature.

- **10% Ammonium Persulfate Solution (Initiator)**

  Per 1.0 mL:

Ammonium Persulfate	0.1 g

  Dissolve the solute in 1.0 mL of ddH_2O; mix well. Use fresh; do not store.

- **Running Gel Overlay (0.375 M Tris-HCl, 0.1% SDS, pH 8.8)**

  Per 100 mL:

Running Gel Buffer	25 mL
10% SDS	1.0 mL

  Mix the solutions. Add ddH_2O to 100 mL. Store up to 3 months at 4^o C in the dark.

- **2× Treatment Buffer (0.125 M Tris-HCl, 4% SDS, 20% v/v Glycerol, 0.2 M DTT, 0.02% Bromphenol Blue, pH 6.8)**

  Per 10.0 mL:

4× Stacking Gel Buffer	2.5 mL
10% SDS	4.0 mL
Glycerol, Ultra Pure	2.0 mL
Bromphenol Blue	2.0 mg
Dithiothreitol	0.31 g

  Dissolve bromphenol blue and DTT in the 4× stacking gel buffer then add SDS; mix well for the solutes to dissolve. Add glycerol and mix well. Add ddH_2O to a 10 mL mark. Store 0.5-mL aliquots at -20^{o} C for up to 6 months.

- **1× Tank Buffer (Running Electrophoresis Buffer) (0.025 M Tris, 0.192 M Glycine, 0.1% SDS, pH 8.3)**

  Per 10 liters:

Tris, free base	30.28 g
Glycine	144.13 g
SDS	10 g

  Dissolve the solutes in 9.5 L ddH_2O; mix well to dissolve. Add ddH_2O up to 10 L mark. This solution can be made up directly in large reagent bottles because it is not necessary to check the pH. Store at room temperature for up to 1 month.

- **Water-saturated *n*-Butanol**

n-Butanol	50 mL
ddH_2O	5 mL

Combine in a bottle and shake. Use the top phase to overlay gels.

Store at room temperature indefinitely.

- **Standard Staining** (Always wear gloves and use distilled or deionized water)

  - **Staining Solution (0.025% Coomassie Brilliant Blue R-250, 40% Methanol, 7% Acetic Acid)**

    Per 2 liters:

Coomassie Brilliant Blue R-250	0.5 g
Methanol	800 mL

Stir the dye in methanol until dissolved. Then add:

Acetic Acid, glacial	140 mL

Mix well to ensure homogeneity. Add ddH_2O to 2 L mark. Filtering is not needed. Store at room temperature for up to 6 months.

  - **Destaining Solution I (40% Methanol, 7% Acetic Acid)**

    Per 1 liter:

Methanol	400 mL
Acetic Acid, glacial	70 mL

Mix the reagents and add ddH_2O to 1 L. Store at room temperature indefinitely.

- **Destaining Solution II (7% Acetic Acid, 5% Methanol)**

  Per 10 liters:

Acetic Acid, glacial	700 mL
Methanol	500 mL

  Mix the reagents and add ddH_2O to 10 L. Store at room temperature indefinitely.

- **Rapid Staining** (Always wear gloves and use distilled or deionized water)

  - **Rapid Stain Fixing Solution (25% *iso*-Propananol, 10% Acetic Acid)**

    Per 1 liter:

iso-Propanol	250 mL
Acetic Acid, glacial	100 mL

    Mix the reagents and bring to 1 L with ddH_2O.

  - **Rapid Coomassie Blue Stain (0.06% Coomassie Blue G-250, 10% Acetic Acid)**

    Per 1 liter:

Coomassie Blue G-250	0.6 g
Acetic Acid, glacial	100 mL

    Mix the reagents and bring to 1 L with ddH_2O.

- **Silver Staining for SDS-PAGE**

  - **Fixing Solution (50% MeOH, 12% HAc, 35% Formaldehyde)**

    Per 200 mL:

Methanol	100 mL
Acetic Acid, glacial	24 mL
Formaldehyde (35% in H_2O)	100 μL

    Mix the reagents and add 76 mL dH_2O to produce 200 mL Fixing Solution.

  - **Wash Solution (35% EtOH)**

    Per 200 mL:

Ethanol	73 mL
Water	127 mL

    Add water to the ethanol to produce 200 mL Washing Solution.

  - **Sensitizing Solution (0.02% $Na_2S_2O_3$)**

    Per 200 mL:

Sodium Thiosulfate	0.04 g
Water	200 mL

    Dissolve the solute in 200 mL of water to produce Sensitizing Solution.

- **Silver Equilibration Solution (0.2% $AgNO_3$, 0.076% Formalin)**

  Per 200 mL:

Silver Nitrate	0.4 g
Formalin (35% Formaldehyde)	152 μL
Water	200 mL

  Dissolve silver nitrate in water and add 35% folmaldehyde (v/v in H_2O) to produce 200 mL Silver Equilibration Solution.

- **Development Solution (6% Na_2CO_3, 0.05% Folmalin, 0.0004% $Na_2S_2O_3$)**

  Per 400 mL:

Sodium Carbonate	24 g
Formalin (35% Formaldehyde)	200 μL
0.02% Sodium Thiosulfate Solution	8 mL
Water	392 mL

  Mix the reagents and add water to 400 mL to produce Development Solution.

- **Stopping Solution (50% MeOH, 12% HAc)**

  Per 200 mL:

Methanol	100 mL
Acetic Acid, glacial	24 mL
Water	76 mL

  Mix the reagents and add water to 200 mL to produce Stopping Solution.

VI-3 MOLECULAR CLONING PROTOCOLS USED DURING EXPERIMENTS

VI-3-A Preparation of BL21(DE3) and DH5α *E.coli* Competent Cells (*246*)

☝ **All steps in this procedure should be carried out aseptically.**

1. Pick a single colony (2-3 mm in diameter) from a plate that has been incubated for 16-20 hours at 37 ^{o}C. Transfer the colony into 100 mL of LB broth or SOB medium in a 1 L flask. Incubate the culture for 3 hours at 37 ^{o}C with vigorous agitation, monitoring the growth of the culture. As a guideline, 1 OD_{600} of a culture of *E. coli* strain DH1 contains ~10^9 bacteira/mL. For efficient transformation, it is essential that the number of *viable* cells not exceed 10^8 cells/mL, which for most strains of *E. coli* is equivalent to an OD_{600} of ~0.4. To ensure that the culture does not grow to a higher density, measure the OD_{600} of the culture every 15-20 min. Plot a graph of the data so that the time when the OD_{600} of the culture approaches 0.4 can be predicted with some accuracy. Begin to harvest the culture when the OD_{600} reaches 0.35. Because the relationship between the OD_{600} and the number of viable cells/mL varies substantially from strain to strain, the spectrophotometer must be calibrated by measuring the OD_{600} of a growing culture of the particular strain of *E. coli* at different times in its growth cycle and determining the number of viable cells at each of these times by plating dilutions of the culture on LB agar plates in the absence of antibiotics.
2. Transfer the bacterial cells to sterile, disposable, ice-cold 50-mL polypropelene tubes. Cool the cultures to 0 ^{o}C by storing the tubes on ice for 10 min.
3. Recover the cells by centrifugation at 2700 x g (4100 rpm in a Sorvall GSA rotor) for 10 min at 4 ^{o}C.

4. Decant the medium from the cell pellets. Stand the tubes in an inverted position on a pad of paper towels for 1 min to allow the last traces of media to drain away.
5. Resuspend each pellet by swirling or gentle vortexing in 30 mL of ice-cold $MgCl_2$-$CaCl_2$ solution (80 mM $MgCl_2$, 20 mM $CaCl_2$).
6. Recover the cells by centrifugation at 2700 x g (4100 rpm in a Sorvall GSA rotor) for 10 min at 4 ^oC.
7. Decant the medium from the cell pellets. Stand the tubes in an inverted position on a pad of paper towels for 1 min to allow the last traces of media to drain away.
8. Resuspend the pellet by swirling or gentle vortexing in 2 mL of ice-cold $CaCl_2$ (or TFB) for each 50 mL of original culture.
9. At this point, either use the cells directly for transformation as described in Section VIII-3-B below or dispense into aliquots and freeze at -70 ^oC. For most strains of *E. coli* (except for MC1061), TFB may be used at this stage instead of $CaCl_2$ with equivalent or better results. The cells may be stored at 4 ^oC in $CaCl_2$ solution for 24-48 hours. The efficiency of transformation increases four- to sixfold during the first 12-24 hours of storage and thereafter decreases to the original level.

VI-3-B Transformation of *E.coli* Competent Cells with Plasmid DNA (*246*)

1. To transform the $CaCl_2$-treated cells directly, transfer 200 µL of each suspension of competent cells to a sterile, chilled 17 x 100-mm polypropylene tube using a chilled micropipette tip. Add DNA (no more than 50 ng in a volume of 10 µL or less) to each tube. Mix the contents of the tubes by swirling gently. Store the tubes on ice for 30 minutes.

2. Transfer the tubes to a rack placed in a preheated 42 ^{o}C circulating water bath. Store the tubes in the rack for exactly 90 seconds. Do not shake the tubes. Heat shock is a crucial step. It is very important that the cells be raised to exactly the right temperature at the correct rate.
3. Rapidly transfer the tubes to an ice bath. Allow the cells to chill for 1-2 min.
4. Add 800 µL of SOC medium to each tube. Incubate the cultures for 45 minutes in a water bath set at 37 ^{o}C to allow the bacteria to recover and to express the antibiotic resistance marker encoded by the plasmid. The cells may be gently agitated (50 cycles/minute or less in a rotary shaker) at 37 ^{o}C during the recovery period.
5. Transfer the appropriate volume (up to 200 µL per 90-mm plate) of transformed competent cells onto agar SOB medium containing 20 mM $MgSO_4$ and the appropriate antibiotic.
6. Store the plates at room temperature until the liquid has been absorbed.
7. Invert the plates and incubate at 37 ^{o}C. Transformed colonies should appear in 12-16 h.

VI-3-C DEPC-Treated Glassware (*246*)

Diethylpyrocarbonate (DEPC) is used in molecular cloning to inactivate trace amounts of RNases that may contaminate solutions, glassware, and plasticware that are to be used for the preparation of nuclear RNA or mRNA. DEPC is highly reactive alkylating agent that destroys the enzymatic activity of RNase chiefly by ethoxyformylation of histidyl groups.

Glassware and plasticware should be filled with solution of 0.1% DEPC in H_2O and allowed to stand for 1 hour at 37 ^{o}C or overnight at room temperature. Rinse the items several

times with DEPC-treated H_2O then autoclave them for 15 minutes at 15 psi (1.05 kg/cm^2) on liquid cycle.

In aqueous solution, DEPC hydrolyzes rapidly to CO_2 and ethanol, with a half-life in phosphate buffer of ~20 minutes at pH 6.0 and 10 minutes at pH 7.0. This hydrolysis is greatly accelerated by Tris and other amines, which themselves become consumed in the process. DEPC therefore cannot be used to treat solutions that contain these buffers. Samples of DEPC that are free of nucleophiles (e.g., H_2O and ethanol) are perfectly stable, but even small amounts of these solvents can cause complete conversion of DEPC to diethylcarbonate. For this reason, DEPC should be protected from moisture. Store it under small aliquots in dry conditions and always allow the bottle to reach ambient temperature before opening it.

VI-3-D Measuring Nucleic Acid Concentration

Concentration and quality of a sample of DNA or RNA are measured with UV spectrophotometer. The method requires a control (600 μL of solvent) and the sample (600 μL of the DNA or RNA dissolved in this solvent).

A solution containing 50 μg per mL of souble stranded DNA has an absorbancy (optical density) of 1.0 at a wavelength of 260 nm.

50/1.0 = (DNA)/OD read

(DNA) = 50 x OD read

Then, 600 μL of a solution of 5-10 μg/mL, with an absorbancy of 0.050 to 0.100 is what you should usually measure.

DNA quality measurement is based on the fact that OD at 260 nm is twice that at 280 nm if the solution contains pure DNA. If there is a contaminant, there is some additional OD which decreases the OD ratio between 260 and 280 nm.

Clean DNA has an OD-260/OD-280 between 1.8 and 2.0.

If the measured value is somewhat smaller, it indicates a contamination.

VI-3-E Measuring Protein Concentration

Typical protein assays are used to determine protein concentration by comparing the assay response of a sample to that of a standard whose concentration is known. Protein samples and protein standards are processed in the same manner by mixing them with assay reagent and using a spectrophotometer to measure the absorbances. Sample assay responses are directly comparable to each other if they are processed in exactly the same manner. Variance in protein quantity is the only possible cause for differences in final absorbance (color intensity) if samples are dissolved in the same buffer and the same stock solution of assay reagent is used for all samples.

The binding of the dye Coomassie® Brilliant Blue G-250 (Figure 2.5) to proteins causes a shift in the absorption maximum of the dye from 465 nm (red) to 595 nm (blue) in acidic solutions (*226*). This dye forms strong, noncovalent complexes with proteins via electrostatic interactions with amino and carboxyl groups and via van der Waals forces. Since the color response is nonlinear over a wide range of protein concentration, it is strongly recommended that a standard curve (Figure 2.5) be run with each assay. The dye is prepared as a stock solution in phosphoric acid. The method is a simple one-step procedure in which the dye reagent is added to the samples and the absorbance is determined at 595 nm. The method is quite sensitive and

accurate, but the reagent stains cuvettes and is somewhat difficult to remove. Dye-binding protein assays are compatible with most common buffers, chaotropic reagents (denaturants) such as 6 M guanidinium hydrochloride, 8 M urea, and preservatives such as sodium azide. However, high concentration of detergents can interfere with this assay. This assay uses commertially available reagents and is about four times as sensitive as the Folin-Ciocolteu (Lowry) assay.

1. Prepare the dye reagent by diluting 1 part Dye Reagent Concentrate with 4 parts distilled, deionized water (ddH_2O). Filter through Whatman #1 filter (or equivalent) to remove particulates. This diluted reagent may be used for approximately two weeks when kept at room temperature.
2. Dilute the BSA stock (~2 mg/mL) into small clean micro-centrifuge tubes with the appropriate diluents to prepare 0 to 1000 mg/mL concentrations in 100 mg/mL increments.
3. Transfer 20 µL of each standard to a clean dry test tube. Add 1.0 mL of dilute dye reagent to each tube and vortex. Incubate at least 5 min. Absorbance will increase over time; samples should incubate at room temperature for no more than 1 h.
4. Analyze standards and samples at least three times and use the means for analysis. Measure absorbance at 595 nm.

VI-3-F Plasmid DNA Purification Using QIAGEN Plasmid Midi Kit (*247*)

1. Pick a single colony from a freashly streaked selective plate and inoculate a starter culture of 2-5 mL LB medium containing the appropriate selective antibiotic. Incubate for ~8 h at 37 ^{o}C with vigorous shaking (~300 rpm). Use a tube or flask with a volume of at least 4 times the volume of the culture.

2. Dilute the starter culture 1/500 to 1/1000 into selective LB medium. For high-copy plasmids inoculate 25 mL medium. For low-copy plasmids, inoculate 100 mL medium. Grow at 37 ^{o}C for 12-16 h with vigorous shaking (~300 rpm). Use a flask or vessel with a volume of at least 4 times the volume of the culture. The culture should reach a cell density of approximately 3 g/L medium.
3. Harvest the bacterial cells by centrifugation at 6000 x g for 15 min at 4 ^{o}C. 6000 x g corresponds to 6000 rpm in Sorval® GSA or GS3 or Beckman™ JA-10 rotors. Remove all traces of supernatant by inverting the open centrifuge tube until all medium has been drained. You may stop protocol and continue later, freeze the cell pellets at -20 ^{o} C.
4. Resuspend the bacterial pellet in 4 mL Buffer P1. For efficient lysis it is important to use a vessel that is large enough to allow complete mixing of the lysis buffers. Ensure that RNase A has beed added to Buffer P1. The bacteria should be resuspended completely by vortexing or pipetting up and down until no cell clumps remain.
5. Add 4 mL Buffer P2, mix gently but thoroughly by inverting 4-6 times, and incubate at room temperature for 5 min. Do not vortex, as this will result in shearing of genomic DNA. The lysate should appear viscous. Do not allow the lysis reaction to proceed for more than 5 min. After use, the bottle containing Buffer P2 should be closed immediately to avoid acidification from CO_2 in the air.
6. Add 4 mL of chilled Buffer P3, mix immediately but gently by inverting 4-6 times, and incubate on ice for 15 min. Precipitation is enhanced by using chilled Buffer P3 and incubating on ice. After addition of Buffer P3, a fluffy white material forms and the lysate becomes less viscous. The precipitated material contains genomic DNA, proteins, cell debris, and SDS. The lysate should be mixed thoroughly to ensure even potassium

dodecyl sulfate precipitation. If the mixture still appears viscous and brownish, more mixing is required to completely neutralize the solution.

7. Centrifuge at ≥20,000 x g for 30 min at 4 ^{o}C. Remove supernatant containing plasmid DNA promptly. Before loading the centrifuge, the sample should be mixed again. Centrifugation should be performed in non-glass tubes (e.g., polypropylene).
8. Centrifuge the supernatant again at ≥20,000 x g for 15 min at 4 ^{o}C. Remove supernatant containing plasmid DNA promptly. This secondcentrifugation step should be carried out to avoid applying suspended or particulate material to the QIAGEN-tip. Suspended material (causing the sample to appear turbid) can clog the QIAGEN-tip and reduce or eliminate gravity flow.
9. Equilibrate a QIAGEN-tip by applying 4 mL Buffer QBT, and allow the column to empty by gravity flow. Flow of buffer will begin automatically by reduction in surface tension due to the presence of detergent in the equilibration buffer. Allow the QIAGEN-tip to drain completely. QIAGEN-tips can be left unattended, since the flow of buffer will stop when the meniscus reaches the upper frit in the column.
10. Apply the supernatant from step 8 to the QIAGEN-tip and allow it to ebter the resin by gravity flow. The supernatant should be loaded onto the QIAGEN-tip promptly. If it is left too long and becomes cloudy due to further precipitation of protein, it must be centrifuged again or filtered before loading to prevent clogging of the QIAGEN-tip.
11. Wash the QIAGEN-tip with 2 x 10 mL Buffer QC. Allow Buffer QC to move through the QIAGEN-tip by gravity flow. The first wash is sufficient to remove all contaminants in the majority of plasmid DNA preparations. The second wash is especially necessary

when large culture volumes or bacterial strains producing large amounts of carbohydrates are used.

12. Elute DNA with 5 mL Buffer QF. Collect the eluate in a 10 mL or 30 mL tube. Use of polycarbonate centrifuge tubes is not recommended as polycarbonate is not resistant to the alcohol used in subsequent steps. If you wish to stop the protocol and continue later, store the eluate at 4 ^{o}C. Storage periods longer than overnight are not recommended.
13. Precipitate DNA by adding 3.5 mL (0.7 volumes) room-temperature isopropanol to the eluted DNA. Mix and centrifuge immediately at ≥15,000 x g for 30 min at 4 ^{o}C. Carefully decant the supernatant. All solutions should be at room temperature in order to minimize salt precipitation, although centrifugation is carried out at 4 ^{o}C to prevent overheating of the sample. Isopropanol pellets have a glassy appearance and may be more difficult to see than the fluffy, salt-containing pellets that result from ethanol precipitation. Masking the outside of the tube before the centrifugation allows the pellet to be more easily located. Isopropanol pellets are also more loosely attached to the side of the tube, and care should be taken when removing the supernatant.
14. Wash DNA pellet with 2 mL of room temperature 70% ethanol, and centrifuge at ≥15,000 x g for 10 min. Carefully decant the supernatant without disturbing the pellet. The 70% ethanol removes precipitated salt and replaces isopropanol with more volatile ethanol, making DNA easier to redissolve.
15. Air-dry the pellet for 5-10 min, and redissolve the DNA in a suitable volume of buffer (e.g, TE Buffer, pH 8.0, or 10 mM Tris-HCl, pH 8.5. Redissolve the DNA pellet by rinsing the walls to recover all the DNA, especially if glass tubes have been used. Pipetting the DNA up and down to promote resuspension may cause shearing and should

be avoided. Overdrying the pellet will make the DNA difficult to redissolve. DNA dissolves best under slightly alkaline conditions; it does not easily dissolve in acidic buffers.

VI-3-G DNA Agarose Gel Electrophoresis (*246*)

Agarose is a linear polymer composed of alternating residues of D- and L-galactose joined by α-(1→3) and β-(1→4) glycosidic linkages. The following factors determine the rate of migration of DNA through agarose gels:

- The molecular size of the DNA. Molecules of double-stranded DNA migrate through gel matrices at rates that are inversely proportional to the $\log_{10}$ of the number of the base pairs. Larger molecules migrate more slowly because of greater frictional drag and because they worm their way through the pores of the gel less efficiently than smaller molecules.
- The concentration of agarose. A linear DNA fragment of a given size migrates at different rates through gels containing different concentrations of agarose. There is a linear relationship between the logarithm of electrophoretic mobility of the DNA and the gel concentration.
- The conformation of the DNA. Superhelical circular, nicked circular, and linear DNAs migrate through agarose gels at different rates. The relative mobilities of the three forms depend primarily on the concentration and type of agarose used to make the gel, but they are also influenced by the strength of the applied current, the ionic strength of the buffer, and the density of superhelical twists of the DNA.

- The presence of ethidium bromide in the gel and electrophoresis buffer. Intercalation of ethidium bromide causes a decrease in the negative charge of the double-stranded DNA and an increase in both its stiffness and length. The rate of migration of the linear DNA-dye complex through gels is consequently retarded by a factor of 15%.
- The applied voltage. At low voltages, the rate of migration of linear DNA fragments is proportional to the voltage applied. However, as the strength of the electric field is raised, the mobility of high-molecular-weight fragments increases differentially.
- The type of agarose. The two major classes of agarose are standard agaroses and low-melting-temperature agaroses. Within each class are various types of agaroses that are used for specialized applications.
- The electrophoresis buffer. The electrophoretic mobility of DNA is affected by the composition and ionic strength of the electrophoresis buffer. The absence of ions (e.g., if water is substituted for electrophoresis buffer in the gel or the reservoirs), electrical conductivity is minimal and DNA migrates slowly, if at all. In buffer of high ionic strength (e.g., if 10x electrophoresis buffer is mistakenly used), electrical conductance is very efficient and significant amounts of heat are generated, even when moderate voltages are applied. In the worst case, the gel melts and DNA denatures. (Refer to Section VI-2-A for electrophoresis buffer used in this research).

1. Seal the edges of a clean, dry glass plate (or the open ends of the plastic tray) with tape to form a mold. Set the mold on a horizontal section of the bench.
2. Prepare sufficient electrophoresis buffer (1x TAE or 0.5x TBE) to fill the electrophoresis tank and to cast the gel.

3. Prepare a solution of agarose in electrophoresis buffer at a concentration appropriate for separation of the particular size fragments expected in the DNA sample(s): Add the correct amount of powdered agarose to a measured quantity of electrophoresis buffer in an Erlenmeyer flask or a glass bottle.
4. Loosely plug the neck of the Erlenmeyer flask with Kimwipes. Heat the slurry in a microwave oven until the agarose dissolves.
5. Use insulated gloved or tongs to transfer the flask into a water bath at 55 ^{o}C. (Note: Ethidium bromide was not added directly into the gel, but the gels were stained with it after the electrophoresis has been completed).
6. While the agarose is cooling, choose an appropriate comb. Position the comb 0.5-1.0 mm above the plate so that the complete well is formed when the agarose id added to the mold.
7. Pour the warm agarose solution into the mold and allow the gel to set completely (~30-45 min at room temperature), then pour a small amount of electrophoresis buffer on the top of the gel, and carefully remove the comb. Pour off the electrophoresis buffer and remove the tape. Mount the gel in the electrophoresis tank.
8. Add just enough electrophoresis buffer to cover the gel to a depth of ~ 1 mm.
9. Mix the samples of DNA with 0.20 volumes of desired 6x gel-loading buffer (refer to Section VI-2-A).
10. Slowly load the sample mixture into the slots of the submerged gel using a disposable micropipette.
11. Close the lid of the gel tank and attach the electrical leads so that DNA will migrate toward the positive anode (red lead). Apply voltage of 1-5 V/cm.

12. When DNA samples or dyes have migrated a sufficient distance through the gel, turn off the electric current, remove the leads, and the lid from the gel tank.
13. Stain the gel in either ethidium bromide-electrophoresis buffer solution (0.5 μg/mL) or with SYBR Gold staining solution (1:10,000-fold).
14. Examine the gel by UV light.

VI-3-H RNA Polyacrylamide/Urea Gel Electrophoresis (*246*)

The electrophoretic analysis of single stranded nucleic acids is complicated by the secondary structures assumed by these molecules. Separation on the basis of molecular weight requires the inclusion of denaturing agents which unfold the DNA or RNA strands and remove the influence of shape on their mobility. Nucleic acids form structures stabilized by hydrogen bonds between bases. Denaturing requires disrupting these hydrogen bonds. The most commonly used DNA denaturants are urea and formamide. Each of these forms hydrogen bonds with the DNA bases, "saturating" H-bond sites and preventing the formation of inter-base bonds.

Both formamide and urea effectively lower the melting point of the DNA molecules, allowing the structures to fall apart at lower temperatures. Generally, concentrations of urea or formamide are chosen to give melting temperatures around 50 °C, and gels are run at that temperature. RNA is often denatured with harsher agents, because RNA tends to form stronger structures. RNA denaturation is discussed in RNA electrophoresis.

1. Clean glass plates thoroughly. Rinse with ethanol and wipe dry. Apply Glass Free to one plate to ensure release after electrophoresis.

2. Prepare the casting solutions (10% polyacrylamide/8 M urea for S/R oligo RNA separation and 6% polyacrylamide/8 M urea for TEV RNA separations were used) (refer to Section VI-2-B for solution preparation).
3. Degas the casting solution by applying vacuum. Degassing the casting solutions prior to initiation will improve reproducibility.
4. Add Ammonium Persulfate and TEMED and swirl gently to mix. Cast the gel. Insert the comb and allow to polymerize one to two hours.
5. Prerun the gel for 15-30 minutes before loading the samples. The gel temperature should be 45-50 ^{o}C.
6. Prepare RNA samples by mixing them with RNA loading buffer and RNA sample buffer.
7. Denature RNA samples by heat to disturb secondary structure.
8. Load the samples into the wells.
9. After completion of the run, allow the plates to cool 10-15 minutes before separation.
10. Stain the gels with SYBR Gold staining solution (1:10,000-fold).
11. Examine the gel by UV light (in a 10% gel, bromphenol blue runs as 10 nt and xylene cyanole as 55 nt; in a 6 % gel, promphenol blue runs as 25 nt and xylene cyanole as 110 nt).

VI-3-I Protein Electrophoresis – SDS-PAGE (*248*)

In SDS polyacrylamide gel electrophoresis (SDS-PAGE) separations, migration is determined not by intrinsic electrical charge of polypeptides but by molecular weight. Sodium dodecylsulfate (SDS) is an anionic detergent that denatures proteins by wrapping around the polypeptide backbone. In so doing, SDS confers a net negative charge to the polypeptide in

proportion to its length. When treated with SDS and a reducing agent, the polypeptides become rods of negative charges with equal "charge densities" or charge per unit length.

SDS-PAGE can resolve complex mixtures into hundreds of bands on a gel. The position of a protein along the lane gives a good approximation of its size, and, after staining, the band intensity is a rough indicator of the amount present in the sample. The ability to estimate size and amount of a protein leads to the various applications of SDS-PAGE; estimating purity and level of expression, immunoblotting, preparing for protein sequencing, and generating antibodies.

The dual gel caster holds glass or glass/alumina plate gel sandwiches allowing gels to be easily cast. The bottom of the sandwich is sealed against a rubber gasket with cam action. Once the gel is set, the sandwiches are transferred to gel electrophoresis unit.

1. For each sandwich, choose one notched alumina or glass plate, one rectangular glass plate, and two spacers. Use only unchipped plates. Assemble the gel sandwich, and insert it into gel electrophoresis unit.
2. Prepare 20 mL of the 12.5% Running gel in a 125-mL vacuum flask according to the following recipe (refer to Section VI-2-C for solution preparations):

Final gel concentration (20 mL):	12.5%
Monomer Solution	8.3 mL
4x Running Gel Buffer	5.0 mL
10% SDS	0.2 mL
ddH_2O	6.4 mL
Ammonium Persulfate[1]	100 µL
TEMED[1]	6.7 µL

[1]Added after deaeration.

3. Stopper the flask and apply vacuum for several minutes while stirring.
4. Add TEMED and Ammonium Persulfate and gently swirl the flask to mix, being careful not to generate bubbles.
5. Use a pipet to deliver the solution into one corner of the plate, taking care not to introduce any air pockets. Fill solution to 3 cm below the top of the gel. This height allows 1 cm of stacking gel below the wells. Add 100 µL of water-saturated *n*-butanol to overlay the gel and prevent its exposure to oxygen. Allow get to polymerize ≥1 hour. After the gel is set, prepare the stacking gel as described below.
6. Prepare the Stacking Gel solution in a 50-mL vacuum flask according to the following recipe (refer to Section VI-2-C for solution preparations):

Gel thickness:	0.75 mm	1.5 mm
Monomer Solution	0.44 mL	0.88 mL
4x Stacking Gel Buffer	0.83 mL	1.66 mL
10% SDS	33 µL	66 µL
ddH_2O	2.03 mL	4.06 mL
Ammonium Persulfate[1]	16.7 µL	33.4 µL
TEMED[1]	1.7 µL	3.3 µL

[1]Added after deaeration.

7. Rinse the overlay off the gel sandwich with ddH_2O.
8. Use a Pasteur pipet to apply the stacking gel over the resolving gel.
9. Introduce comb (at a slight angle) into the sandwich, taking care not to trap air under the teeth. Allow gel to polymerize ≥1 hour.

10. Remove the comb from the sandwich by carefully pulling on the comb while gently rocking it back and forth to break the suction.
11. Install the gel into the gel apparatus. Fill the buffer chambers with 1x running buffer.
12. Mix the protein samples with 2x Treatment Buffer, and denature for 5-10 min in a hot water bath. Load the samples into the wells.
13. Run the gel at constant voltage (150 V, 30 A, 12 Ω) for 45 min or until the dye front reaches the bottoms of the gel.
14. Stain and destain the gel.

VII RESULTED PUBLICATIONS / CONFERENCE PRESENTATIONS

VII-1 PUBLICATIONS

- Ray, S., Yumak, H., **Domashevskiy, A.,** Khan, M.A., Gallie, D.R., Goss, D.J. (2006) Tobacco Etch Virus mRNA Preferentially Binds Wheat Germ Eukaryotic Initiation Factor (eIF)4G rather than (eIF)iso4G. *J. Biol. Chem.* **281,** 35826-35834.
- **Domashevskiy, A.V.,** Friedland, D.E., Miyoshi, H., Gallie, D.R., Goss, D.J. (2011) Turnip Mosaic Virus Genome-Linked Protein (VPg) Inhibits Pokeweed Antiviral Protein (PAP)-Mediated Depurination of RNA. *Submitted for Publication to Biochemistry.*
- **Domashevskiy, A.V.,** Toney, A.E., DeGrazia, J., Noro, K. Gallie, D.R., Friedland, D.E. (2011) Binding of Pokeweed Antiviral Protein to Tobacco Etch mRNA Constructs: Structural Recognition and Affinity. *Manuscript in preparation*.

VII-2 CONFERENCE PRESENTATIONS

- Goss, D.J., Khan, M.A., **Domashevskiy, A.,** Yumak, H. (2008) Biophysical Insights into the Mechanism of Viral Synthesis. *MARM ACS J.* **40,** 254.
- Ray, S., **Domashevskiy, A.,** Yumak, H., Khan, M.A., Gallie, D.R., Goss, D.J. (2006) Tobacco Etch Virus mRNA Preferentially Binds Wheat Germ Eukaryotic Initiation Factor (eIF)4G rather than (eIF)iso4G. *FASEB J.* **20,** A108.
- **Domashevskiy, A.,** Friedland, D.E., Goss, D.J. (2010) Effects of Viral Genome-Linked Protein on Depurination of Viral RNA by Pokeweed Antiviral Protein. *FASEB J.* **24,** 499.3.
- Friedland, D.E., Toney, A.E., **Domashevskiy, A.,** DeGrazia, J. (2010) Binding of Pokeweed Antiviral Protein to Tobacco Etch mRNA Constructs: Structural Recognition and Affinity. *ASPB J.* In press.

- **Domashevskiy, A.V.,** Noro, K., Friedland, D.E., Goss, D.J. (2011) Turnip Mosaic Virus Genome-Linked Protein (VPg) Inhibits Pokeweed Antiviral Protein (PAP)-Mediated Depurination of RNA. *ACS Younger Chemists Committee (YCC) Symposium.* The Cooper Union.
- **Domashevskiy, A.V.,** Noro, K., Friedland, D.E., Goss, D.J. (2011) Turnip Mosaic Virus Genome-Linked Protein (VPg) Inhibits Pokeweed Antiviral Protein (PAP)-Mediated Depurination of RNA. *MARM ACS J*. In press.

X BIBLIOGRAPHY

1. Olsnes, S. (2004) The history of ricin, abrin and related toxins. *Toxicon* **44,** 361-370.

2. Lodge, J. K., Kaniewski, W. K., and Tumer, N. E. (1993) Broad-spectrum virus resistance in transgenic plants expressing pokeweed antiviral protein. *Proc. Natl. Acad. Sci. U S A* **90,** 7089-7093.

3. Jach, G., Görnhardt, B., Mundy, J., Logemann, J., Pinsdorf, E., Leah, R., Schell, J., and Maas, C. (1995) Enhanced quantitative resistance against fungal disease by combinatorial expression of different barley antifungal proteins in transgenic tobacco. *The Plant Journal* **8,** 97-109.

4. Frankel, A. E., FitzGerald, D., Siegall, C., and Press, O. W. (1996) Advances in Immunotoxin Biology and Therapy: A Summary of the Fourth International Symposium on Immunotoxins. *Cancer Research* **56,** 926-932.

5. Kreitman, R. J. (1999) Immunotoxins in cancer therapy. *Curr. Opin. Immunol.* **11,** 570-578.

6. Pastan, I., and FitzGerald, D. (1991) Recombinant toxins for cancer treatment. *Science* **254,** 1173-1177.

7. Christopher, G. W., Cieslak, T. J., Pavlin, J. A., and Eitzen, E. M., Jr. (1997) Biological warfare. A historical perspective. *JAMA* **278,** 412-417.

8. Knight, B. (1979) Ricin - a potent homicidal poison. *Br. Med. J.* **1,** 350-351.

9. Wiener, S. L. (1996) Strategies for the prevention of a successful biological warfare aerosol attack, *Mil. Med.* **161,** 251-256.

10. Christie, A. (1929) House of lurking death., In *Partners in Crime.* Dodd, Mead and Company, New York.

11. Peumans, W. J., Hao, Q., and Van Damme, E. J. (2001) Ribosome-inactivating proteins from plants: more than RNA N-glycosidases? *FASEB J.* **15,** 1493-1506.

12. Irvin, J. D. (1975) Purification and partial characterization of the antiviral protein from Phytolacca americana which inhibits eukaryotic protein synthesis. *Arch. Biochem. Biophys.* **169,** 522-528.

13. Arabidopsis Genome Initiative. (2000) Analysis of the genome sequence of the flowering plant Arabidopsis thaliana. *Nature* **408,** 796-815.

14. Ready, M. P., Brown, D. T., and Robertus, J. D. (1986) Extracellular localization of pokeweed antiviral protein. *Proc. Natl. Acad. Sci. U S A* **83,** 5053-5056.

15. Bonness, M. S., Ready, M. P., Irvin, J. D., and Mabry, T. J. (1994) Pokeweed antiviral protein inactivates pokeweed ribosomes; implications for the antiviral mechanism. *Plant J.* **5,** 173-183.

16. USDA, N. (2011) Distribution of Phytolacca americana L. The PLANTS Database.

17. NRCS., U.-N. P. D. U. (2011) Wetland flora: Field office illustrated guide to plant species. USDA Natural Resources Conservation Service.

18. Britton, N. L., and Brown, A. (1913) An illustrated flora of the northern United States, Canada and British Possessions. Charles Scribner's Sons, New York.

19. USDA, N. (2011) Phytolacca americana L. The PLANTS Database.

20. McMillian, J. (2011) Phytolacca americana L. USDA-NRCS PLANTS Database.

21. Bodner, T., Miller, J. H., and Miller, K. V. (2005) Forest plants of the southeast and their wildlife uses. USDA-NRCS PLANTS Database.

22. Barnes, T. G., and Francis, S. W. (2004) Wildflowers and ferns of Kentacky. Phytolacca americana L. USDA-NRCS PLANTS Database.

23. Ehrlich, P. (1891) Experimentelle Untersuchungenüber Immunität I. Ueber Ricin. *Dtsch. Med. Wochenschr.* **17,** 976-979.

24. Ehrlich, P. (1891) Experimentelle Untersuchungenüber Immunität I. Ueber Abrin. *Dtsch. Med. Wochenschr.* **17,** 1218-1219.

25. Lin, J. Y., Liu, K., Chen, C. C., and Tung, T. C. (1971) Effect of crystalline ricin on the biosynthesis of protein, RNA, and DNA in experimental tumor cells. *Cancer Res.* **31,** 921-924.

26. Montanaro, L., Sperti, S., and Stirpe, F. (1973) Inhibition by ricin of protein synthesis in vitro. Ribosomes as the target of the toxin. *Biochem. J.* **136,** 677-683.

27. Obrig, T. G., Irvin, J. D., and Hardesty, B. (1973) The effect of an antiviral peptide on the ribosomal reactions of the peptide elongation enzymes, EF-I and EF-II. *Arch. Biochem. Biophys.* **155,** 278-289.

28. Mundy, J., Leah, R., Boston, R., Endo, Y., and Stirpe, F. (1994) Genes encoding ribosome-inactivating proteins. *Plant Mol. Biol. Rep.* **12,** S60-S62.

29. Barbieri, L., Battelli, M. G., and Stirpe, F. (1993) Ribosome-inactivating proteins from plants. *Biochim. Biophys. Acta* **1154,** 237-282.

30. Husain, J., Tickle, I. J., and Wood, S. P. (1994) Crystal structure of momordin, a type I ribosome inactivating protein from the seeds of Momordica charantia. *FEBS Lett.* **342,** 154-158.

31. Mlsna, D., Monzingo, A. F., Katzin, B. J., Ernst, S., and Robertus, J. D. (1993) Structure of recombinant ricin A chain at 2.3 A. *Protein Sci.* **2,** 429-435.

32. Monzingo, A. F., and Robertus, J. D. (1992) X-ray analysis of substrate analogs in the ricin A-chain active site. *J. Mol. Biol.* **227,** 1136-1145.

33. Girbes, T., Ferreras, J. M., Arias, F. J., and Stirpe, F. (2004) Description, distribution, activity and phylogenetic relationship of ribosome-inactivating proteins in plants, fungi and bacteria. *Mini Rev. Med. Chem.* **4,** 461-476.

34. Kurinov, I. V., Myers, D. E., Irvin, J. D., and Uckun, F. M. (1999) X-ray crystallographic analysis of the structural basis for the interactions of pokeweed antiviral protein with its active site inhibitor and ribosomal RNA substrate analogs. *Protein Sci.* **8,** 1765-1772.

35. Baykal, U., and Tumer, N. E. (2007) The C-terminus of pokeweed antiviral protein has distinct roles in transport to the cytosol, ribosome depurination and cytotoxicity. *Plant J.* **49,** 995-1007.

36. Olsnes, S., and Pihl, A. (1973) Isolation and properties of abrin: a toxic protein inhibiting protein synthesis. Evidence for different biological functions of its two constituent-peptide chains. *Eur. J. Biochem.* **35,** 179-185.

37. Olsnes, S., and Pihl, A. (1981) Chimeric toxins. *Pharmacol. Ther.* **15,** 355-381.

38. Stirpe, F., Gasperi-Campani, A., Barbieri, L., Lorenzoni, E., Montanaro, L., Sperti, S., and Bonetti, E. (1977) Inhibition of protein synthesis by modeccin, the toxin of Modecca digitata. *FEBS Lett.* **85,** 65-67.

39. Sandvig, K., Olsnes, S., and Pihl, A. (1976) Kinetics of binding of the toxic lectins abrin and ricin to surface receptors of human cells. *J. Biol. Chem.* **251,** 3977-3984.

40. Olsnes, S., and Sandvig, K. (1988) How protein toxins enter and kill cells. *Cancer Treat. Res.* **37,** 39-73.

41. Steeves, R. M., Denton, M. E., Barnard, F. C., Henry, A., and Lambert, J. M. (1999) Identification of three oligosaccharide binding sites in ricin. *Biochemistry* **38,** 11677-11685.

42. van Deurs, B., Tonnessen, T. I., Petersen, O. W., Sandvig, K., and Olsnes, S. (1986) Routing of internalized ricin and ricin conjugates to the Golgi complex. *J. Cell Biol.* **102,** 37-47.

43. Beaumelle, B., Alami, M., and Hopkins, C. R. (1993) ATP-dependent translocation of ricin across the membrane of purified endosomes. *J. Biol. Chem.* **268,** 23661-23669.

44. Sandvig, K., and van Deurs, B. (1994) Endocytosis and intracellular sorting of ricin and Shiga toxin. *FEBS Lett.* **346,** 99-102.

45. Hazes, B., and Read, R. J. (1997) Accumulating evidence suggests that several AB-toxins subvert the endoplasmic reticulum-associated protein degradation pathway to enter target cells. *Biochemistry* **36,** 11051-11054.

46. Lord, J. M., and Roberts, L. M. (1998) Toxin entry: retrograde transport through the secretory pathway. *J. Cell Biol.* **140,** 733-736.

47. Sandvig, K., and van Deurs, B. (1999) Endocytosis and intracellular transport of ricin: recent discoveries. *FEBS Lett.* **452,** 67-70.

48. Bass, H. W., Webster, C., GR, O. B., Roberts, J. K., and Boston, R. S. (1992) A maize ribosome-inactivating protein is controlled by the transcriptional activator Opaque-2. *Plant Cell* **4,** 225-234.

49. Chaudhry, B., Muller-Uri, F., Cameron-Mills, V., Gough, S., Simpson, D., Skriver, K., and Mundy, J. (1994) The barley 60 kDa jasmonate-induced protein (JIP60) is a novel ribosome-inactivating protein. *Plant J.* **6,** 815-824.

50. Reinbothe, S., Reinbothe, C., Lehmann, J., Becker, W., Apel, K., and Parthier, B. (1994) JIP60, a methyl jasmonate-induced ribosome-inactivating protein involved in plant stress reactions. *Proc. Natl. Acad. Sci. U S A* **91,** 7012-7016.

51. Walsh, T. A., Morgan, A. E., and Hey, T. D. (1991) Characterization and molecular cloning of a proenzyme form of a ribosome-inactivating protein from maize. Novel mechanism of proenzyme activation by proteolytic removal of a 2.8-kilodalton internal peptide segment. *J. Biol. Chem.* **266,** 23422-23427.

52. Bass, H. W., GR, O. B., and Boston, R. S. (1995) Cloning and sequencing of a second ribosome-inactivating protein gene from maize (Zea mays L.). *Plant Physiol.* **107,** 661-662.

53. Hey, T. D., Hartley, M., and Walsh, T. A. (1995) Maize ribosome-inactivating protein (b-32). Homologs in related species, effects on maize ribosomes, and modulation of activity by pro-peptide deletions. *Plant Physiol.* **107,** 1323-1332.

54. Krawetz, J. E., and Boston, R. S. (2000) Substrate specificity of a maize ribosome-inactivating protein differs across diverse taxa. *Eur. J. Biochem.* **267,** 1966-1974.

55. Jimenez, A., and Vazquez, D. (1985) Plant and fungal protein and glycoprotein toxins inhibiting eukaryote protein synthesis. *Annu. Rev. Microbiol.* **39,** 649-672.

56. Stirpe, F., and Barbieri, L. (1986) Ribosome-inactivating proteins up to date. *FEBS Lett.* **195,** 1-8.

57. Barbieri, L., Valbonesi, P., Bondioli, M., Alvarez, M. L., Dal Monte, P., Landini, M. P., and Stirpe, F. (2001) Adenine glycosylase activity in mammalian tissues: an equivalent of ribosome-inactivating proteins. *FEBS Lett.* **505,** 196-197.

58. Stirpe, F., Barbieri, L., Gorini, P., Valbonesi, P., Bolognesi, A., and Polito, L. (1996) Activities associated with the presence of ribosome-inactivating proteins increase in senescent and stressed leaves. *FEBS Lett.* **382,** 309-312.

59. Girbés, T., de Torre, C., Iglesias, R., Ferreras, J. M., and Méndez, E. (1996) RIP for viruses. *Nature* **379,** 777-778.

60. Rippmann, J. F., Michalowski, C. B., Nelson, D. E., and Bohnert, H. J. (1997) Induction of a ribosome-inactivating protein upon environmental stress. *Plant Mol. Biol.* **35,** 701-709.

61. Hauf, N., and Chakraborty, T. (2003) Suppression of NF-κB Activation and Proinflammatory Cytokine Expression by Shiga Toxin-Producing Escherichia coli. *J. Immunol.* **170,** 2074-2082.

62. Brown, J. E., Ussery, M. A., Leppla, S. H., and Rothman, S. W. (1980) Inhibition of protein synthesis by Shiga toxin: activation of the toxin and inhibition of peptide elongation. *FEBS Lett.* **117,** 84-88.

63. Sandvig, K., and van Deurs, B. (2002) Transport of protein toxins into cells: pathways used by ricin, cholera toxin and Shiga toxin. *FEBS Lett.* **529,** 49-53.

64. Lam, S. K., and Ng, T. B. (2001) First simultaneous isolation of a ribosome inactivating protein and an antifungal protein from a mushroom (Lyophyllum shimeji) together with evidence for synergism of their antifungal effects. *Arch. Biochem. Biophys.* **393,** 271-280.

65. Lam, S. K., and Ng, T. B. (2001) Hypsin, a novel thermostable ribosome-inactivating protein with antifungal and antiproliferative activities from fruiting bodies of the edible mushroom Hypsizigus marmoreus. *Biochem. Biophys. Res. Commun.* **285,** 1071-1075.

66. Wang, H., and Ng, T. B. (2001) Isolation and characterization of velutin, a novel low-molecular-weight ribosome-inactivating protein from winter mushroom (Flammulina velutipes) fruiting bodies. *Life Sci.* **68,** 2151-2158.

67. Yao, Q. Z., Yu, M. M., Ooi, L. S., Ng, T. B., Chang, S. T., Sun, S. S., and Ooi, V. E. (1998) Isolation and Characterization of a Type 1 Ribosome-Inactivating Protein from Fruiting Bodies of the Edible Mushroom (Volvariella volvacea). *J. Agric. Food Chem.* **46,** 788-792.

68. Liu, R. S., Yang, J. H., and Liu, W. Y. (2002) Isolation and enzymatic characterization of lamjapin, the first ribosome-inactivating protein from cryptogamic algal plant (Laminaria japonica A). *Eur. J. Biochem.* **269,** 4746-4752.

69. Thompson, J. D., Higgins, D. G., and Gibson, T. J. (1994) CLUSTAL W: improving the sensitivity of progressive multiple sequence alignment through sequence weighting, position-specific gap penalties and weight matrix choice. *Nucleic Acids Res.* **22,** 4673-4680.

70. Saitou, N., and Nei, M. (1987) The neighbor-joining method: a new method for reconstructing phylogenetic trees. *Mol. Biol. Evol.* **4,** 406-425.

71. Ready, M. P., Katzin, B. J., and Robertus, J. D. (1988) Ribosome-inhibiting proteins, retroviral reverse transcriptases, and RNase H share common structural elements. *Proteins* **3,** 53-59.

72. Doolittle, R. F., Feng, D. F., Anderson, K. L., and Alberro, M. R. (1990) A naturally occurring horizontal gene transfer from a eukaryote to a prokaryote. *J. Mol. Evol.* **31,** 383-388.

73. Rutenber, E., Katzin, B. J., Ernst, S., Collins, E. J., Mlsna, D., Ready, M. P., and Robertus, J. D. (1991) Crystallographic refinement of ricin to 2.5 A. *Proteins* **10,** 240-250.

74. Rutenber, E., Ready, M., and Robertus, J. D. (1987) Structure and evolution of ricin B chain. *Nature* **326,** 624-626.

75. van Damme, E. J., Hao, Q., Chen, Y., Barre, A., Vandenbussche, F., Desmyter, S., Rouge, P., and Peumans, W. J. (2001) Ribosome-inactivating proteins: a family of plant proteins that do more than inactivate ribosomes. *Crit. Rev. Plant Sci.* **20,** 395-465.

76. Lin, Q., Chen, Z. C., Antoniw, J. F., and White, R. F. (1991) Isolation and characterization of a cDNA clone encoding the anti-viral protein from Phytolacca americana. *Plant Mol. Biol.* **17,** 609-614.

77. Irvin, J. D., and Uckun, F. M. (1992) Pokeweed antiviral protein: ribosome inactivation and therapeutic applications. *Pharmacol. Ther.* **55,** 279-302.

78. Myers, D. E., Irvin, J. D., Smith, R. S., Kuebelbeck, V. M., and Uckun, F. M. (1991) Production of a pokeweed antiviral protein (PAP)-containing immunotoxin, B43-PAP, directed against the CD19 human B lineage lymphoid differentiation antigen in highly purified form for human clinical trials. *J. Immunol. Methods* **136,** 221-237.

79. Poyet, J. L., Radom, J., and Hoeveler, A. (1994) Isolation and characterization of a cDNA clone encoding the pokeweed antiviral protein II from Phytolacca americana and its expression in E. coli. *FEBS Lett.* **347,** 268-272.

80. Rajamohan, F., Engstrom, C. R., Denton, T. J., Engen, L. A., Kourinov, I., and Uckun, F. M. (1999) High-level expression and purification of biologically active recombinant pokeweed antiviral protein. *Protein Expr. Purif.* **16,** 359-368.

81. Poyet, J. L., and Hoeveler, A. (1997) cDNA cloning and expression of pokeweed antiviral protein from seeds in Escherichia coli and its inhibition of protein synthesis in vitro. *FEBS Lett.* **406,** 97-100.

82. Barbieri, L., Aron, G. M., Irvin, J. D., and Stirpe, F. (1982) Purification and partial characterization of another form of the antiviral protein from the seeds of Phytolacca americana L. (pokeweed). *Biochem. J.* **203,** 55-59.

83. Honjo, E., Dong, D., Motoshima, H., and Watanabe, K. (2002) Genomic clones encoding two isoforms of pokeweed antiviral protein in seeds (PAP-S1 and S2) and the N-glycosidase activities of their recombinant proteins on ribosomes and DNA in comparison with other isoforms. *J. Biochem.* **131,** 225-231.

84. Hartley, M. R., and Lord, J. M. (2004) Genetics of ribosome-inactivating proteins. *Mini Rev. Med. Chem.* **4,** 487-492.

85. Frankel, A. E., Burbage, C., Fu, T., Tagge, E., Chandler, J., and Willingham, M. C. (1996) Ricin toxin contains at least three galactose-binding sites located in B chain subdomains 1 alpha, 1 beta, and 2 gamma. *Biochemistry* **35,** 14749-14756.

86. Battelli, M. G., Citores, L., Buonamici, L., Ferreras, J. M., de Benito, F. M., Stirpe, F., and Girbes, T. (1997) Toxicity and cytotoxicity of nigrin b, a two-chain ribosome-inactivating protein from Sambucus nigra: comparison with ricin. *Arch. Toxicol.* **71,** 360-364.

87. Duggar, B. M., and Armstrong, J. K. (1925) The effect of treating virus of tobacco mosaic with juice of various plants. *Ann. Mol. Bot. Gard.* **12,** 359-365.

88. Dallal, J. A., and Irvin, J. D. (1978) Enzymatic inactivation of eukaryotic ribosomes by the pokeweed antiviral protein. *FEBS Lett.* **89,** 257-259.

89. UniProt. (2011) Taxonomy. Phytolacca americana L.

90. NCBI. (2011) Taxonomy Browser. Phytolacca americana.

91. Kraulis, P. (1991) MOLSCRIPT: A program to produce both detailed and schematic plots of protein structure. *J. Appl. Cryst.* **24,** 946-950.

92. Sperti, S., Montanaro, L., Mattioli, A., and Testoni, G. (1975) Relationship between elongation factor I- and elongation factor II- dependent guanosine triphosphatase activities of ribosomes. Inhibition of both activities by ricin. *Biochem. J.* **148,** 447-451.

93. Endo, Y., Mitsui, K., Motizuki, M., and Tsurugi, K. (1987) The mechanism of action of ricin and related toxic lectins on eukaryotic ribosomes. The site and the characteristics of the modification in 28 S ribosomal RNA caused by the toxins. *J. Biol. Chem.* **262,** 5908-5912.

94. Gutell, R. R., and Fox, G. E. (1988) A compilation of large subunit RNA sequences presented in a structural format. *Nucleic Acids Res.* **16 Suppl,** r175-269.

95. Pape, T., Wintermeyer, W., and Rodnina, M. V. (1998) Complete kinetic mechanism of elongation factor Tu-dependent binding of aminoacyl-tRNA to the A site of the E. coli ribosome. *EMBO J.* **17,** 7490-7497.

96. Nissen, P., Hansen, J., Ban, N., Moore, P. B., and Steitz, T. A. (2000) The structural basis of ribosome activity in peptide bond synthesis. *Science* **289,** 920-930.

97. Schmeing, T. M., Seila, A. C., Hansen, J. L., Freeborn, B., Soukup, J. K., Scaringe, S. A., Strobel, S. A., Moore, P. B., and Steitz, T. A. (2002) A pre-translocational intermediate in protein synthesis observed in crystals of enzymatically active 50S subunits. *Nat. Struct. Biol.* **9,** 225-230.

98. Rodnina, M. V., Savelsbergh, A., Katunin, V. I., and Wintermeyer, W. (1997) Hydrolysis of GTP by elongation factor G drives tRNA movement on the ribosome. *Nature* **385,** 37-41.

99. Ramakrishnan, V. (2002) Ribosome structure and the mechanism of translation. *Cell* **108,** 557-572.

100. Andersen, G. R., Nissen, P., and Nyborg, J. (2003) Elongation factors in protein biosynthesis. *Trends Biochem. Sci.* **28,** 434-441.

101. Joseph, S. (2003) After the ribosome structure: how does translocation work? *RNA* **9,** 160-164.

102. Osborn, R. W., and Hartley, M. R. (1990) Dual effects of the ricin A chain on protein synthesis in rabbit reticulocyte lysate. Inhibition of initiation and translocation. *Eur. J. Biochem.* **193,** 401-407.

103. Brigotti, M., Rambelli, F., Zamboni, M., Montanaro, L., and Sperti, S. (1989) Effect of alpha-sarcin and ribosome-inactivating proteins on the interaction of elongation factors with ribosomes. *Biochem. J.* **257,** 723-727.

104. Mansouri, S., Nourollahzadeh, E., and Hudak, K. A. (2006) Pokeweed antiviral protein depurinates the sarcin/ricin loop of the rRNA prior to binding of aminoacyl-tRNA to the ribosomal A-site. *RNA* **12,** 1683-1692.

105. Tumer, N. E., Parikh, B. A., Li, P., and Dinman, J. D. (1998) The pokeweed antiviral protein specifically inhibits Ty1-directed +1 ribosomal frameshifting and retrotransposition in Saccharomyces cerevisiae. *J. Virol.* **72,** 1036-1042.

106. Hudak, K. A., Hammell, A. B., Yasenchak, J., Tumer, N. E., and Dinman, J. D. (2001) A C-terminal deletion mutant of pokeweed antiviral protein inhibits programmed +1 ribosomal frameshifting and Ty1 retrotransposition without depurinating the sarcin/ricin loop of rRNA. *Virology* **279,** 292-301.

107. Robertus, J. D., and Monzingo, A. F. (2004) The structure of ribosome inactivating proteins. *Mini Rev. Med. Chem.* **4,** 477-486.

108. Chen, X. Y., Link, T. M., and Schramm, V. L. (1998) Ricin A-chain: kinetics, mechanism, and RNA stem-loop inhibitors. *Biochemistry* **37,** 11605-11613.

109. Tanaka, K. S., Chen, X. Y., Ichikawa, Y., Tyler, P. C., Furneaux, R. H., and Schramm, V. L. (2001) Ricin A-chain inhibitors resembling the oxacarbenium ion transition state. *Biochemistry* **40,** 6845-6851.

110. Vater, C. A., Bartle, L. M., Leszyk, J. D., Lambert, J. M., and Goldmacher, V. S. (1995) Ricin A chain can be chemically cross-linked to the mammalian ribosomal proteins L9 and L10e. *J. Biol. Chem.* **270,** 12933-12940.

111. Hudak, K. A., Dinman, J. D., and Tumer, N. E. (1999) Pokeweed antiviral protein accesses ribosomes by binding to L3. *J. Biol. Chem.* **274,** 3859-3864.

112. Di, R., and Tumer, N. E. (2005) Expression of a truncated form of ribosomal protein L3 confers resistance to pokeweed antiviral protein and the Fusarium mycotoxin deoxynivalenol. *Mol. Plant Microbe Interact.* **18,** 762-770.

113. Endo, Y., Gluck, A., and Wool, I. G. (1991) Ribosomal RNA identity elements for ricin A-chain recognition and catalysis. *J. Mol. Biol.* **221,** 193-207.

114. Tan, Q. Q., Dong, D. X., Yin, X. W., Sun, J., Ren, H. J., and Li, R. X. (2009) Comparative analysis of depurination catalyzed by ricin A-chain on synthetic 32mer and 25mer oligoribonucleotides mimicking the sarcin/ricin domain of the rat 28S rRNA and E. coli 23S rRNA. *J. Biotechnol.* ***139,*** 156-162.

115. Zamboni, M., Brigotti, M., Rambelli, F., Montanaro, L., and Sperti, S. (1989) High-pressure-liquid-chromatographic and fluorimetric methods for the determination of adenine released from ribosomes by ricin and gelonin. *Biochem. J.* **259,** 639-643.

116. Barbieri, L., Ferreras, J. M., Barraco, A., Ricci, P., and Stirpe, F. (1992) Some ribosome-inactivating proteins depurinate ribosomal RNA at multiple sites. *Biochem. J.* **286 (Pt 1),** 1-4.

117. Barbieri, L., Valbonesi, P., Bonora, E., Gorini, P., Bolognesi, A., and Stirpe, F. (1997) Polynucleotide:adenosine glycosidase activity of ribosome-inactivating proteins: effect on DNA, RNA and poly(A). *Nucleic Acids Res.* **25,** 518-522.

118. Rajamohan, F., Venkatachalam, T. K., Irvin, J. D., and Uckun, F. M. (1999) Pokeweed antiviral protein isoforms PAP-I, PAP-II, and PAP-III depurinate RNA of human immunodeficiency virus (HIV)-1. *Biochem. Biophys. Res. Commun.* **260,** 453-458.

119. Rajamohan, F., Kurinov, I. V., Venkatachalam, T. K., and Uckun, F. M. (1999) Deguanylation of human immunodeficiency virus (HIV-1) RNA by recombinant pokeweed antiviral protein. *Biochem. Biophys. Res. Commun.* **263,** 419-424.

120. Uckun, F. M., Rajamohan, F., Pendergrass, S., Ozer, Z., Waurzyniak, B., and Mao, C. (2003) Structure-based design and engineering of a nontoxic recombinant pokeweed antiviral protein with potent anti-human immunodeficiency virus activity. *Antimicrob. Agents Chemother.* **47,** 1052-1061.

121. Chen, Z., Antoniw, J. F., and White, R. F. (1993) A possible mechanism for the antiviral activity of pokeweed antiviral protein. *Physiol. Mol. Plant Path.* **42,** 249-258.

122. Ussery, M. A., Irvin, J. D., and Hardesty, B. (1977) Inhibition of poliovirus replication by a plant antiviral peptide. *Ann. N Y Acad. Sci.* **284,** 431-440.

123. Aron, G. M., and Irvin, J. D. (1980) Inhibition of herpes simplex virus multiplication by the pokeweed antiviral protein. *Antimicrob. Agents Chemother.* **17,** 1032-1033.

124. Tomlinson, J. A., Walker, V. M., Flewett, T. H., and Barclay, G. R. (1974) The inhibition of infection by cucumber mosaic virus and influenza virus by extracts from Phytolacca americana. *J. Gen. Virol.* **22,** 225-232.

125. Picard, D., Kao, C. C., and Hudak, K. A. (2005) Pokeweed antiviral protein inhibits brome mosaic virus replication in plant cells. *J. Biol. Chem.* **280,** 20069-20075.

126. Uckun, F. M., Rustamova, L., Vassilev, A. O., Tibbles, H. E., and Petkevich, A. S. (2005) CNS activity of Pokeweed anti-viral protein (PAP) in mice infected with lymphocytic choriomeningitis virus (LCMV). *BMC Infect. Dis.* **5,** 9.

127. Hudak, K. A., Wang, P., and Tumer, N. E. (2000) A novel mechanism for inhibition of translation by pokeweed antiviral protein: depurination of the capped RNA template. *RNA* **6,** 369-380.

128. Kurinov, I. V., Rajamohan, F., Venkatachalam, T. K., and Uckun, F. M. (1999) X-ray crystallographic analysis of the structural basis for the interaction of pokeweed antiviral protein with guanine residues of ribosomal RNA. *Protein Sci.* **8,** 2399-2405.

129. Rajamohan, F., Pugmire, M. J., Kurinov, I. V., and Uckun, F. M. (2000) Modeling and alanine scanning mutagenesis studies of recombinant pokeweed antiviral protein. *J. Biol. Chem.* **275,** 3382-3390.

130. Hudak, K. A., Bauman, J. D., and Tumer, N. E. (2002) Pokeweed antiviral protein binds to the cap structure of eukaryotic mRNA and depurinates the mRNA downstream of the cap. *RNA* **8,** 1148-1159.

131. Baldwin, A. E., Khan, M. A., Tumer, N. E., Goss, D. J., and Friedland, D. E. (2009) Characterization of pokeweed antiviral protein binding to mRNA cap analogs: competition with nucleotides and enhancement by translation initiation factor iso4G. *Biochim. Biophys. Acta* **1789,** 109-116.

132. Vivanco, J. M., and Tumer, N. E. (2003) Translation Inhibition of Capped and Uncapped Viral RNAs Mediated by Ribosome-Inactivating Proteins. *Phytopathology* **93,** 588-595.

133. Wang, M., and Hudak, K. A. (2006) A novel interaction of pokeweed antiviral protein with translation initiation factors 4G and iso4G: a potential indirect mechanism to access viral RNAs. *Nucleic Acids Res.* **34,** 1174-1181.

134. Allen, M. L., Metz, A. M., Timmer, R. T., Rhoads, R. E., and Browning, K. S. (1992) Isolation and sequence of the cDNAs encoding the subunits of the isozyme form of wheat protein synthesis initiation factor 4F. *J. Biol. Chem.* **267,** 23232-23236.

135. Browning, K. S. (1996) The plant translational apparatus. *Plant Mol. Biol.* **32,** 107-144.

136. Sperti, S., Brigotti, M., Zamboni, M., Carnicelli, D., and Montanaro, L. (1991) Requirements for the inactivation of ribosomes by gelonin. *Biochem. J.* **277 (Pt 1),** 281-284.

137. Carnicelli, D., Brigotti, M., Montanaro, L., and Sperti, S. (1992) Differential requirement of ATP and extra-ribosomal proteins for ribosome inactivation by eight RNA *N*-glycosidases. *Biochem. Biophys. Res. Commun.* **182,** 579-582.

138. Carnicelli, D., Brigotti, M., Alvergna, P., Pallanca, A., Sperti, S., and Montanaro, L. (1997) Cofactor requirement of ribosome-inactivating proteins from plants. *J. Exp. Bot.* **48,** 1519-1523.

139. Brigotti, M., Keith, G., Pallanca, A., Carnicelli, D., Alvergna, P., Dirheimer, G., Montanaro, L., and Sperti, S. (1998) Identification of the tRNAs which up-regulate agrostin, barley RIP and PAP-S, three ribosome-inactivating proteins of plant origin. *FEBS Lett.* **431,** 259-262.

140. Pallanca, A., Mazzaracchio, R., Brigotti, M., Carnicelli, D., Alvergna, P., Sperti, S., and Montanaro, L. (1998) Uncompetitive inhibition by adenine of the RNA-*N*-glycosidase activity of ribosome-inactivating proteins. *Biochim. Biophys. Acta* **1384,** 277-284.

141. Sandvig, K., and van Deurs, B. (2000) Entry of ricin and Shiga toxin into cells: molecular mechanisms and medical perspectives. *EMBO J.* **19,** 5943-5950.

142. Van Damme, E. J., Peumans, W. J., Barre, A., and Rouge, P. (1998) Plant lectins: a composite of several distinct families of structurally and evolutionary related proteins with diverse biological roles. *Crit. Rev. Plant Sci.* **17,** 575-692.

143. Tumer, N. E., Hudak, K., Di, R., Coetzer, C., Wang, P., and Zoubenko, O. (1999) Pokeweed antiviral protein and its applications. *Curr. Top. Microbiol. Immunol.* **240,** 139-158.

144. Wang, P., and Tumer, N. E. (2000) Virus resistance mediated by ribosome inactivating proteins. *Adv. Virus Res.* **55,** 325-355.

145. Irvin, J. D. (1983) Pokeweed antiviral protein. *Pharmacol. Ther.* **21,** 371-387.

146. Smirnov, S., Shulaev, V., and Tumer, N. E. (1997) Expression of Pokeweed Antiviral Protein in Transgenic Plants Induces Virus Resistance in Grafted Wild-Type Plants Independently of Salicylic Acid Accumulation and Pathogenesis-Related Protein Synthesis. *Plant Physiol.* **114,** 1113-1121.

147. Zoubenko, O., Uckun, F., Hur, Y., Chet, I., and Tumer, N. (1997) Plant resistance to fungal infection induced by nontoxic pokeweed antiviral protein mutants. *Nat. Biotechnol.* **15,** 992-996.

148. Tumer, N. E., Hwang, D. J., and Bonness, M. (1997) C-terminal deletion mutant of pokeweed antiviral protein inhibits viral infection but does not depurinate host ribosomes. *Proc. Natl. Acad. Sci. U S A* **94,** 3866-3871.

149. Ferreras, J. M., Barbieri, L., Girbes, T., Battelli, M. G., Rojo, M. A., Arias, F. J., Rocher, M. A., Soriano, F., Mendez, E., and Stirpe, F. (1993) Distribution and properties of major ribosome-inactivating proteins (28 S rRNA *N*-glycosidases) of the plant Saponaria officinalis L. (Caryophyllaceae). *Biochim. Biophys. Acta* **1216,** 31-42.

150. Stirpe, F., Barbieri, L., Battelli, M. G., Soria, M., and Lappi, D. A. (1992) Ribosome-inactivating proteins from plants: present status and future prospects. *Biotechnology (N Y)* **10,** 405-412.

151. Roberts, L. M., and Lord, J. M. (2004) Ribosome-inactivating proteins: entry into mammalian cells and intracellular routing. *Mini Rev. Med. Chem.* **4,** 505-512.

152. Craig, H. L., Alderks, O. H., Corwin, A. H., Dieke, S. H., and Karel, C. L. (1952) Preparation of toxic ricin. *US Patent Office* **3,060,165.**

153. Smallshaw, J. E., Firan, A., Fulmer, J. R., Ruback, S. L., Ghetie, V., and Vitetta, E. S. (2002) A novel recombinant vaccine which protects mice against ricin intoxication. *Vaccine* **20,** 3422-3427.

154. Mayor, S. (2003) UK doctors warned after ricin poison found in police raid. *BMJ* **326,** 126.

155. Kataoka, J., Habuka, N., Masuta, C., Miyano, M., and Koiwai, A. (1992) Isolation and analysis of a genomic clone encoding a pokeweed antiviral protein. *Plant Mol. Biol.* **20,** 879-886.

156. Monzingo, A. F., Collins, E. J., Ernst, S. R., Irvin, J. D., and Robertus, J. D. (1993) The 2.5 A structure of pokeweed antiviral protein. *J. Mol. Biol.* **233,** 705-715.

157. Chen, Z. C., Antoniw, J. F., Lin, Q., and White, R. F. (1993) Expression of pokeweed (*Phytolacca americana*) antiviral protein cDNA in *Escherichia coli* and its antiviral activity. *Physiol. Mol. Plant Path.* **42,** 237-247.

158. Xu, J., Meng, A. X., Hefferon, K. L., Ivanov, I. G., and Abouhaidar, M. G. (1998) Effect of N-terminal deletions on the activity of pokeweed antiviral protein expressed in E. coli. *Biochimie* **80,** 1069-1076.

159. (1960) The collected papers of Paul Ehrich. Pergamon Press, New York.

160. Fracasso, G., Bellisola, G., Castelletti, D., Tridente, G., and Colombatti, M. (2004) Immunotoxins and other conjugates: preparation and general characteristics. *Mini Rev. Med. Chem.* **4,** 545-562.

161. Bolognesi, A., and Polito, L. (2004) Immunotoxins and other conjugates: pre-clinical studies. *Mini Rev. Med. Chem.* **4,** 563-583.

162. Parikh, B. A., and Tumer, N. E. (2004) Antiviral activity of ribosome inactivating proteins in medicine. *Mini Rev. Med. Chem.* **4,** 523-543.

163. Lappi, D. A., and Wiley, R. G. (2004) Immunotoxins and neuropeptide-toxin conjugates experimental applications. *Mini Rev. Med. Chem.* **4,** 585-595.

164. Jansen, B., Kersey, J. H., Jaszcz, W. B., Gunther, R., Nguyen, D. P., Chelstrom, L. M., Tuel-Ahlgren, L., and Uckun, F. M. (1993) Effective immunochemotherapy of human t(4;11) leukemia in mice with severe combined immunodeficiency (SCID) using B43 (anti-CD19)-pokeweed antiviral protein immunotoxin plus cyclophosphamide. *Leukemia* **7,** 290-297.

165. Uckun, F. M., Haissig, S., Ledbetter, J. A., Fidler, P., Myers, D. E., Kuebelbeck, V., Weisdorf, D., Gajl-Peczalska, K., Kersey, J. H., and Ramsay, N. K. (1992) Developmental hierarchy during early human B-cell ontogeny after autologous bone marrow transplantation using autografts depleted of CD19+ B-cell precursors by an anti-CD19 pan-B-cell immunotoxin containing pokeweed antiviral protein. *Blood* **79,** 3369-3379.

166. Uckun, F. M., Chelstrom, L. M., Finnegan, D., Tuel-Ahlgren, L., Manivel, C., Irvin, J. D., Myers, D. E., and Gunther, R. (1992) Effective immunochemotherapy of CALLA+C mu+ human pre-B acute lymphoblastic leukemia in mice with severe combined immunodeficiency using B43 (anti-CD19) pokeweed antiviral protein immunotoxin plus cyclophosphamide. *Blood* **79,** 3116-3129.

167. Uckun, F. M., Chelstrom, L. M., Irvin, J. D., Finnegan, D., Gunther, R., Young, J., Kuebelbeck, V., Myers, D. E., and Houston, L. L. (1992) In vivo efficacy of B43 (anti-CD19)-pokeweed antiviral protein immunotoxin against BCL-1 murine B-cell leukemia. *Blood* **79,** 2649-2661.

168. Uckun, F. M., Manivel, C., Arthur, D., Chelstrom, L. M., Finnegan, D., Tuel-Ahlgren, L., Irvin, J. D., Myers, D. E., and Gunther, R. (1992) In vivo efficacy of B43 (anti-CD19)-pokeweed antiviral protein immunotoxin against human pre-B cell acute lymphoblastic leukemia in mice with severe combined immunodeficiency. *Blood* **79,** 2201-2214.

169. Erice, A., Balfour, H. H., Jr., Myers, D. E., Leske, V. L., Sannerud, K. J., Kuebelbeck, V., Irvin, J. D., and Uckun, F. M. (1993) Anti-human immunodeficiency virus type 1 activity of an anti-CD4 immunoconjugate containing pokeweed antiviral protein. *Antimicrob. Agents Chemother.* **37,** 835-838.

170. Zarling, J. M., Moran, P. A., Haffar, O., Sias, J., Richman, D. D., Spina, C. A., Myers, D. E., Kuebelbeck, V., Ledbetter, J. A., and Uckun, F. M. (1990) Inhibition of HIV replication by pokeweed antiviral protein targeted to CD4+ cells by monoclonal antibodies. *Nature* **347,** 92-95.

171. Preiss, T., and M, W. H. (2003) Starting the protein synthesis machine: eukaryotic translation initiation. *Bioessays* **25,** 1201-1211.

172. Klann, E., and Dever, T. E. (2004) Biochemical mechanisms for translational regulation in synaptic plasticity. *Nat. Rev. Neurosci.* **5,** 931-942.

173. Kozak, M. (1991) Structural features in eukaryotic mRNAs that modulate the initiation of translation. *J. Biol. Chem.* **266,** 19867-19870.

174. Dever, T. E. (2002) Gene-specific regulation by general translation factors. *Cell* **108,** 545-556.

175. Gallie, D. R. (2002) Protein-protein interactions required during translation. *Plant Mol. Biol.* **50,** 949-970.

176. Gingras, A. C., Raught, B., and Sonenberg, N. (1999) eIF4 initiation factors: effectors of mRNA recruitment to ribosomes and regulators of translation. *Annu. Rev. Biochem.* **68,** 913-963.

177. Marcotrigiano, J., and Burley, S. K. (2002) Structural biology of eIF4F: mRNA recognition and preparation in eukaryotic translation initiation. *Adv. Protein. Chem.* **61,** 269-297.

178. Haghighat, A., and Sonenberg, N. (1997) eIF4G dramatically enhances the binding of eIF4E to the mRNA 5'-cap structure. *J. Biol. Chem.* **272,** 21677-21680.

179. Kahvejian, A., Roy, G., and Sonenberg, N. (2001) The mRNA closed-loop model: the function of PABP and PABP-interacting proteins in mRNA translation. *Cold Spring Harb. Symp. Quant. Biol.* **66,** 293-300.

180. Sachs, A. B., and Varani, G. (2000) Eukaryotic translation initiation: there are (at least) two sides to every story. *Nat. Struct. Biol.* **7,** 356-361.

181. Pestova, T. V., Kolupaeva, V. G., Lomakin, I. B., Pilipenko, E. V., Shatsky, I. N., Agol, V. I., and Hellen, C. U. (2001) Molecular mechanisms of translation initiation in eukaryotes. *Proc. Natl. Acad. Sci. U S A* **98,** 7029-7036.

182. Carrington, J. C., Kasschau, K. D., Mahajan, S. K., and Schaad, M. C. (1996) Cell-to-Cell and Long-Distance Transport of Viruses in Plants. *Plant Cell* **8,** 1669-1681.

183. Gale, M., Jr., Tan, S. L., and Katze, M. G. (2000) Translational control of viral gene expression in eukaryotes. *Microbiol. Mol. Biol. Rev.* **64,** 239-280.

184. van Regenmortel, M. H., Fauquet, C. M., Bishop, D. H., Carstens, E. B., Estes, M. K., Lemon, S. M., Maniloff, J., Mayo, M. A., McGeoch, D. J., Pringle, C. R., and Wickner, R. B. (2000) *Virus Taxonomy: Seventh report of the Interanational Committee on Taxonomy of Viruses.* Academic Press, San Diego.

185. Bushell, M., and Sarnow, P. (2002) Hijacking the translation apparatus by RNA viruses. *J. Cell Biol.* **158,** 395-399.

186. Murphy, J. F., Rychlik, W., Rhoads, R. E., Hunt, A. G., and Shaw, J. G. (1991) A tyrosine residue in the small nuclear inclusion protein of tobacco vein mottling virus links the VPg to the viral RNA. *J. Virol.* **65,** 511-513.

187. Goodfellow, I., Chaudhry, Y., Gioldasi, I., Gerondopoulos, A., Natoni, A., Labrie, L., Laliberte, J. F., and Roberts, L. (2005) Calicivirus translation initiation requires an interaction between VPg and eIF 4 E. *EMBO Rep.* **6,** 968-972.

188. Leonard, S., Plante, D., Wittmann, S., Daigneault, N., Fortin, M. G., and Laliberte, J. F. (2000) Complex formation between potyvirus VPg and translation eukaryotic initiation factor 4E correlates with virus infectivity. *J. Virol.* **74,** 7730-7737.

189. Daughenbaugh, K. F., Fraser, C. S., Hershey, J. W., and Hardy, M. E. (2003) The genome-linked protein VPg of the Norwalk virus binds eIF3, suggesting its role in translation initiation complex recruitment. *EMBO J.* **22,** 2852-2859.

190. Urcuqui-Inchima, S., Haenni, A. L., and Bernardi, F. (2001) Potyvirus proteins: a wealth of functions. *Virus Res.* **74,** 157-175.

191. Pettit Kneller, E. L., Rakotondrafara, A. M., and Miller, W. A. (2006) Cap-independent translation of plant viral RNAs. *Virus Res.* **119,** 63-75.

192. Walsh, J. A., and Jenner, C. E. (2002) Turnip mosaic virus and the quest for durable resistance. *Mol. Plant Pathol.* **3,** 289-300.

193. Suehiro, N., Natsuaki, T., Watanabe, T., and Okuda, S. (2004) An important determinant of the ability of Turnip mosaic virus to infect Brassica spp. and/or Raphanus sativus is in its P3 protein. *J. Gen. Virol.* **85,** 2087-2098.

194. Riechmann, J. L., Lain, S., and Garcia, J. A. (1992) Highlights and prospects of potyvirus molecular biology. *J. Gen. Virol.* **73 (Pt 1),** 1-16.

195. Daros, J. A., Schaad, M. C., and Carrington, J. C. (1999) Functional analysis of the interaction between VPg-proteinase (NIa) and RNA polymerase (NIb) of tobacco etch potyvirus, using conditional and suppressor mutants. *J. Virol.* **73,** 8732-8740.

196. Fellers, J., Wan, J., Hong, Y., Collins, G. B., and Hunt, A. G. (1998) In vitro interactions between a potyvirus-encoded, genome-linked protein and RNA-dependent RNA polymerase. *J. Gen. Virol.* **79 (Pt 8),** 2043-2049.

197. Hong, Y., Levay, K., Murphy, J. F., Klein, P. G., Shaw, J. G., and Hunt, A. G. (1995) A potyvirus polymerase interacts with the viral coat protein and VPg in yeast cells. *Virology* **214,** 159-166.

198. Li, X. H., Valdez, P., Olvera, R. E., and Carrington, J. C. (1997) Functions of the tobacco etch virus RNA polymerase (NIb): subcellular transport and protein-protein interaction with VPg/proteinase (NIa). *J. Virol.* **71,** 1598-1607.

199. Wittmann, S., Chatel, H., Fortin, M. G., and Laliberte, J. F. (1997) Interaction of the viral protein genome linked of turnip mosaic potyvirus with the translational eukaryotic initiation factor (iso) 4E of Arabidopsis thaliana using the yeast two-hybrid system. *Virology* **234,** 84-92.

200. Schaad, M. C., Jensen, P. E., and Carrington, J. C. (1997) Formation of plant RNA virus replication complexes on membranes: role of an endoplasmic reticulum-targeted viral protein. *EMBO J.* **16,** 4049-4059.

201. Lellis, A. D., Kasschau, K. D., Whitham, S. A., and Carrington, J. C. (2002) Loss-of-susceptibility mutants of Arabidopsis thaliana reveal an essential role for eIF(iso)4E during potyvirus infection. *Curr. Biol.* **12,** 1046-1051.

202. Duprat, A., Caranta, C., Revers, F., Menand, B., Browning, K. S., and Robaglia, C. (2002) The Arabidopsis eukaryotic initiation factor (iso)4E is dispensable for plant growth but required for susceptibility to potyviruses. *Plant J.* **32,** 927-934.

203. Borgstrom, B., and Johansen, I. E. (2001) Mutations in pea seedborne mosaic virus genome-linked protein VPg after pathotype-specific virulence in Pisum sativum. *Mol. Plant Microbe Interact.* **14,** 707-714.

204. Johansen, I. E., Lund, O. S., Hjulsager, C. K., and Laursen, J. (2001) Recessive resistance in Pisum sativum and potyvirus pathotype resolved in a gene-for-cistron correspondence between host and virus. *J. Virol.* **75,** 6609-6614.

205. Keller, K. E., Johansen, I. E., Martin, R. R., and Hampton, R. O. (1998) Potyvirus genome-linked protein (VPg) determines pea seed-borne mosaic virus pathotype-specific virulence in Pisum sativum. *Mol. Plant Microbe Interact.* **11,** 124-130.

206. Masuta, C., Nishimura, M., Morishita, H., and Hataya, T. (1999) A single amino Acid change in viral genome-associated protein of potato virus y correlates with resistance breaking in 'virgin a mutant' tobacco. *Phytopathology* **89,** 118-123.

207. Nicolas, O., Pirone, T. P., and Hellmann, G. M. (1996) Construction and analysis of infectious transcripts from a resistance-breaking strain of tobacco vein mottling potyvirus. *Arch. Virol.* **141,** 1535-1552.

208. Rajamaki, M. L., and Valkonen, J. P. (1999) The 6K2 protein and the VPg of potato virus A are determinants of systemic infection in Nicandra physaloides. *Mol. Plant Microbe Interact.* **12,** 1074-1081.

209. Schaad, M. C., Lellis, A. D., and Carrington, J. C. (1997) VPg of tobacco etch potyvirus is a host genotype-specific determinant for long-distance movement. *J. Virol.* **71,** 8624-8631.

210. Leonard, S., Viel, C., Beauchemin, C., Daigneault, N., Fortin, M. G., and Laliberte, J. F. (2004) Interaction of VPg-Pro of turnip mosaic virus with the translation initiation factor 4E and the poly(A)-binding protein in planta. *J. Gen. Virol.* **85,** 1055-1063.

211. Miyoshi, H., Suehiro, N., Tomoo, K., Muto, S., Takahashi, T., Tsukamoto, T., Ohmori, T., and Natsuaki, T. (2006) Binding analyses for the interaction between plant virus genome-linked protein (VPg) and plant translational initiation factors. *Biochimie* **88,** 329-340.

212. Vegetable MD Online. Cornell University, New York.

213. Khan, M. A., Miyoshi, H., Ray, S., Natsuaki, T., Suehiro, N., and Goss, D. J. (2006) Interaction of genome-linked protein (VPg) of turnip mosaic virus with wheat germ translation initiation factors eIFiso4E and eIFiso4F. *J. Biol. Chem.* **281,** 28002-28010.

214. Khan, M. A., Miyoshi, H., Gallie, D. R., and Goss, D. J. (2008) Potyvirus genome-linked protein, VPg, directly affects wheat germ in vitro translation: interactions with translation initiation factors eIF4F and eIFiso4F. *J. Biol. Chem.* **283,** 1340-1349.

215. Purcifull, D. E., and Hiebert, E. (1982) Descriptions of Plant Viruses: Tobacco etch virus.
216. Dreher, T. W., and Miller, W. A. (2006) Translational control in positive strand RNA plant viruses. *Virology* **344,** 185-197.

217. Zeenko, V., and Gallie, D. R. (2005) Cap-independent translation of tobacco etch virus is conferred by an RNA pseudoknot in the 5'-leader. *J. Biol. Chem.* **280,** 26813-26824.

218. Ray, S., Yumak, H., Domashevskiy, A., Khan, M. A., Gallie, D. R., and Goss, D. J. (2006) Tobacco etch virus mRNA preferentially binds wheat germ eukaryotic initiation factor (eIF) 4G rather than eIFiso4G. *J. Biol. Chem.* **281,** 35826-35834.

219. Zitter, A. T. (1973) Reaction of susceptible and tolerant pepper varients to the pepper virus complex in south florida. *Proc. Fla. St. Hort. Soc.* **84,** 146-152.

220. Carrington, J. C., and Freed, D. D. (1990) Cap-independent enhancement of translation by a plant potyvirus 5' nontranslated region. *J. Virol.* **64,** 1590-1597.

221. Gallie, D. R., Tanguay, R. L., and Leathers, V. (1995) The tobacco etch viral 5' leader and poly(A) tail are functionally synergistic regulators of translation. *Gene* **165,** 233-238.

222. Niepel, M., and Gallie, D. R. (1999) Identification and Characterization of the Functional Elements within the Tobacco Etch Virus 5' Leader Required for Cap-Independent Translation. *J. Virol.* **73,** 9080-9088.

223. Gallie, D. R. (2001) Cap-independent translation conferred by the 5' leader of tobacco etch virus is eukaryotic initiation factor 4G dependent. *J. Virol.* **75,** 12141-12152.

224. Khan, M. A., Yumak, H., Gallie, D. R., and Goss, D. J. (2008) Effects of poly(A)-binding protein on the interactions of translation initiation factor eIF4F and eIF4F·4B with internal ribosome entry site (IRES) of tobacco etch virus RNA. *Biochimica et Biophysica Acta (BBA) - Gene Regulatory Mechanisms* **1779,** 622-627.

225. Jahn, M. Sol genomics netweok.

226. Bradford, M. M. (1976) A rapid and sensitive method for the quantitation of microgram quantities of protein utilizing the principle of protein-dye binding. *Anal. Biochem.* **72,** 248-254.

227. Mayberry, L. K., Dennis, M. D., Leah Allen, M., Ruud Nitka, K., Murphy, P. A., Campbell, L., and Browning, K. S. (2007) Expression and purification of recombinant wheat translation initiation factors eIF1, eIF1A, eIF4A, eIF4B, eIF4F, eIF(iso)4F, and eIF5. *Methods Enzymol.* **430,** 397-408.

228. van Heerden, A., and Browning, K. S. (1994) Expression in Escherichia coli of the two subunits of the isozyme form of wheat germ protein synthesis initiation factor 4F. Purification of the subunits and formation of an enzymatically active complex. *J. Biol. Chem.* **269,** 17454-17457.

229. Huang, Z., and Waxman, D. J. (1999) High-Performance Liquid Chromatographic-Fluorescent Method to Determine Chloroacetaldehyde, a Neurotoxic Metabolite of the Anticancer Drug Ifosfamide, in Plasma and in Liver Microsomal Incubations. *Anal. Biochem.* **273,** 117-125.

230. Krzyzosiak, W. J., Biernat, J., Ciesiolka, J., Gulewicz, K., and Wiewiorowski, M. (1981) The reaction of adenine and cytosine residues in tRNA with chloroacetaldehyde. *Nucleic Acids Res.* **9,** 2841-2851.

231. Vanderkooi, J. M., Weiss, C. J., and Woodrow, G. V., 3rd. (1979) Fluorescent derivatives of nucleotides. Metal ion interactions and pH dependency. *Biophys. J.* **25,** 263-275.

232. Ren, J., and Goss, D. J. (1996) Synthesis of a fluorescent 7-methylguanosine analog and a fluorescence spectroscopic study of its reaction with wheatgerm cap binding proteins. *Nucleic Acids Res.* **24,** 3629-3634.

233. Hiratsuka, T. (1983) New ribose-modified fluorescent analogs of adenine and guanine nucleotides available as substrates for various enzymes. *Biochim. Biophys. Acta* **742,** 496-508.

234. PierceBiotechnology (2010) *Pierce NHS-Fluoresceine Antibody Labeling Kit Manual*.

235. Lakowicz, J. R. (2006) *Principles of Fluorescence Spectroscopy.* Third ed., Springer Science.

236. Firpo, M. A., Connelly, M. B., Goss, D. J., and Dahlberg, A. E. (1996) Mutations at two invariant nucleotides in the 3'-minor domain of Escherichia coli 16 S rRNA affecting translational initiation and initiation factor 3 function. *J. Biol. Chem.* **271,** 4693-4698.

237. Khan, M. A., and Goss, D. J. (2004) Phosphorylation states of translational initiation factors affect mRNA cap binding in wheat. *Biochemistry* **43,** 9092-9097.

238. Levine, R. (1977) Fluorescence-quenching studies of the binding of bilirubin to albumin. *Clin. Chem.* **23,** 2292-2301.

239. Zhang, Y., Geiger, J. D., and Lautt, W. W. (1991) Improved high-pressure liquid chromatographic-fluorometric assay for measurement of adenosine in plasma. *Am. J. Physiol.* **260,** G658-664.

240. Miura, K., Okumura, M., Yukimura, T., and Yamamoto, K. (1991) Fluorometric determination of plasma adenosine concentrations using high-performance liquid chromatography. *Anal. Biochem.* **196,** 84-88.

241. Fenton, R. A., and Dobson, J. G. (1992) Fluorometric quantitation of adenosine concentration in small samples of extracellular fluid. *Anal. Biochem.* **207,** 134-141.

242. Rost, B., Yachdav, G., and Liu, J. (2004) The PredictProtein server. *Nucleic Acids Res.* **32,** W321-326.

243. Weber, G. (1975) Energetics of ligand binding to proteins. *Adv. Protein Chem.* **29,** 1-83.

244. Goss, D. J., Parkhurst, L. J., Mehta, A. M., and Wahba, A. J. (1984) Cooperative interactions in the system ribosomes-ribosomal protein S1-polynucleotide triplets. *Biochemistry* **23,** 6522-6529.

245. Carberry, S. E., and Goss, D. J. (1991) Interaction of wheat germ protein synthesis initiation factors eIF-3, eIF-(iso)4F, and eIF-4F with mRNA analogues. *Biochemistry* **30,** 6977-6982.

246. Sambrook, J., and Russell, D. W. (2001) *Molecular Cloning: A Laboratory Manual.* **Vol. 1,** 3 ed., Cold Spring Harbor Laboratory Press, New York.

247. QIAGEN (2003) *QIAGEN Plasmid Purification Handbook.* 2 ed., QIAGEN.

248. Hoefer (2001) *SDS Polyacrylamide Gel Electrophoresis and Isoelectric Focusing Handbook.* Hoefer, Inc.